technische universität
dortmund

Dissertation zur Erlangung des akademischen Grades
Doctor rerum naturalium

Cosmic Neutrinos and Gravity: Probing Spacetime Structure with Neutrino Oscillations

Dominik Hellmann
geboren in Hagen

1996

Lehrstuhl für Theoretische Physik III - Arbeitsgruppe Päs
Fakultät Physik
Technische Universität Dortmund

Erstgutachter:	Prof. Dr. Heinrich Päs
Zweitgutachter:	Prof. Dr. Gudrun Hiller
Externer Gutachter:	Prof. Dr. Frank Deppisch
Vorsitzender der Prüfungskomission:	Prof. Dr. Marc Aßmann
Mitglied der Prüfungskomission:	Dr. Bärbel Siegmann
Abgabedatum:	23. April 2025
Datum der mündlichen Prüfung:	26. Juni 2025

Veröffentlichte und genehmigte Dissertation an der Fakultät Physik der Technischen Universität Dortmund.

Abstract

We explore the potential of neutrino flavour oscillations to constrain and probe new physics models in various settings. First, we show that a coupling between an axion like dark matter candidate and a sterile neutrino with altered dispersion relations can be used to reconcile the sterile flavour with cosmological bounds. The allowed model parameter space is determined by comparing the predicted values for a set of central quantities to those extracted from experiment.

Moreover, we discuss how astrophysical and atmospheric neutrinos can be utilised to probe effective low energy models of quantum gravity. We propose that if quantum gravity violates global quantum numbers, neutrino oscillations provide new possibilities to study the hypothetical fermionic dark sector. We perform a thorough statistical analysis to estimate the sensitivity of atmospheric oscillation experiments, like IceCube, to the considered class of models.

Finally, we discuss potential effects of classical gravity on the neutrino flavour dynamics and the respective implications for current and near-future neutrino experiments. In the course of this, we derive a formula for the amplitude of neutrino flavour transitions in curved spacetimes.

Kurzfassung

Wir untersuchen die Anwendbarkeit von Neutrino-Flavour-Oszillationen zur Einschränkung und Erforschung neuer Physikmodelle in verschiedenen Szenarien. Zunächst zeigen wir, dass eine Kopplung zwischen einem axionartigen Dunkle-Materie-Kandidaten und einem sterilen Neutrino mit veränderten Dispersionsrelationen genutzt werden kann, um die sterile Flavour-Komponente mit kosmologischen Messungen in Einklang zu bringen. Der zulässige Parameterraum des Modells wird bestimmt, indem die vorhergesagten Werte zentraler Größen mit experimentell extrahierten Werten verglichen werden.

Darüber hinaus diskutieren wir, wie astrophysikalische und atmosphärische Neutrinos zur Untersuchung effektiver niedrigenergie Modelle der Quantengravitation genutzt werden können. Wir schlagen vor, dass Neutrino-Oszillationen neue Möglichkeiten zur Erforschung eines hypothetischen fermionischen Dunkle-Materie-Sektors bieten, falls die Quantengravitation globale Quantenzahlen verletzt. Eine umfassende statistische Analyse wird durchgeführt, um die Sensitivität atmosphärischer Oszillationsexperimente wie IceCube gegenüber dieser Klasse von Modellen abzuschätzen.

Schließlich untersuchen wir mögliche Effekte der klassischen Gravitation auf die Neutrino-Flavour-Dynamik und deren Implikationen für aktuelle sowie zukünftige Neutrinoexperimente. Im Zuge dessen leiten wir eine Formel für die Amplitude von Neutrino-Flavour-Übergängen in gekrümmten Raumzeiten her.

Acknowledgements

First and foremost, I would like to thank Prof. Dr. Päs for giving me the opportunity to pursue my PhD in his research group at TU Dortmund. His support has been very helpful, providing creative research ideas and constructive criticism while also fostering a culture of initiative and independent thinking within the group. Moreover, I would like to thank Prof. Dr. Hiller for serving as the second reviewer of this thesis, as well as for hosting the BSM seminar. The BSM seminar provides a valuable platform for sharing and discussing our research within the group, and to prepare for talks at conferences and workshops.

My infinite gratitude goes to all members of the Hiller, Päs, and Stamou working groups, who have managed to create what is probably the best working environment one could ever wish for. It is truly a shame to know that the future will hardly be able to surpass this time. Coming to work with joy every Monday morning and knowing that the weekdays will be in no way inferior to the weekend is something truly special. Even outside of university, it has been (and hopefully will continue to be in the future!!) an absolute privilege and a joy to spend my free time with you. From pool parties/nights at Lara's or Tim's to intense forest walks with Kai or pedal boat fun with Daniel, Carl, and Musti at Fredenbaum Park, you have given me many unforgettable memories. The fact that one can rely on your help and professional advice just as much as one can have fun with you has once again been proven by your willingness to read and critique this thesis.

Special thanks also go, of course, to my office colleagues Tim Brune and Sara Krieg, who have endured me in their immediate surroundings for years and have always been ready for engaging discussions——both about physics and beyond. I would especially like to thank Sara for the fantastic collaboration on three truly wonderful projects. Like any good PhD project, all three naturally had their own unique highs and lows, but we always went through and overcame them together. Furthermore, Carl Schultze should not be forgotten either, with whom I had the pleasure of sharing an office for a short but unforgettable time. In fact, the boundaries of our office have become increasingly blurred over the years, and I am very grateful to have been able to welcome, among others, Patrick Adolf as a regular guest worker in P1-O4-311. But also, the almost nightly visits from Kai Sieja, Daniel Wendler, and Dominik Suelmann often marked the perfect ending to the workday.

However, my deepest gratitude at this point goes to Dr. Mustafa "Musti" Tabet, whose constant advice and support have been invaluable in the creation of this work and the results it contains. Every day, he manages to shine not only as a great friend but also as a mentor with remarkable excellence. Our regular discussions have helped me grow not only as a physicist but also as a person. Thank you, Brudi, you truly are the next step of evolution!

Furthermore, it was the greatest stroke of luck that Musti and Jordi moved from the water-damage office to the neighboring office on our side of the hallway. The 4 pm *break* time that developed over the past years/months became a daily highlight that significantly helped me endure the struggles of writing.

Outside of university, from my first semester to the final months of my PhD, my fiancée Anne and my parents have always supported me and stood by my side through both difficult and good times. Without you, I wouldn't have been able to do this, and I am incredibly grateful to always know you by my side. Thank you, above all, for always lending me your ear when I was stuck in my work and for always believing in me!

Last but not least, I would also like to thank my friends—above all, Jean, Leytschek, Philipp, Ronneburg, and Timon, as well as the entire B.Ö.S.E.E.V.—for the same kind of support, e.V.! The annual *Bollerwagen* tours, *Sach ma kennst du eigentlich Mathe?!*, countless shared *Zwiebelkuchen*, and meetups at the Shof have helped me tremendously in getting through my PhD and never losing hope. Thank you, homies!

Contents

List of Publications

The work presented in this thesis is mostly based on the following publications:

[1] D. Hellmann, H. Päs, and E. Rani, "Searching new particles at neutrino telescopes with quantum-gravitational decoherence," *Phys. Rev. D*, vol. 105, no. 5, p. 055 007, 2022. DOI: 10.1103/PhysRevD.105.055007. arXiv: 2103.11984 [hep-ph].

[2] D. Hellmann, H. Päs, and E. Rani, "Quantum gravitational decoherence in the three neutrino flavor scheme," *Phys. Rev. D*, vol. 106, no. 8, p. 083 013, 2022. DOI: 10.1103/PhysRevD.106.083013. arXiv: 2208.11754 [hep-ph].

[3] D. Hellmann and H. Päs, "Light sterile neutrinos in the early universe: effects of altered dispersion relations and a coupling to axion-like dark matter," *JCAP*, vol. 11, p. 056, 2023. DOI: 10.1088/1475-7516/2023/11/056. arXiv: 2307.12118 [hep-ph].

[4] D. Hellmann, S. Krieg, H. Päs, and M. Tabet, "Neutrino oscillations as a gravitational wave detector?" *JCAP*, vol. 05, p. 075, 2025. DOI: 10.1088/1475-7516/2025/05/075. arXiv: 2405.05000 [hep-ph].

[5] A. Domi, T. Eberl, D. Hellmann, S. Krieg, and H. Päs, "Potential of neutrino telescopes to detect quantum gravity-induced decoherence in the presence of dark fermions," *JCAP*, vol. 01, p. 063, 2025. DOI: 10.1088/1475-7516/2025/01/063. arXiv: 2409.12633 [hep-ph].

The majority of the results presented in Chapter 5 is still to be published at the time of writing.

List of Figures

List of Tables

List of Acronyms

ADR	altered dispersion relation
ANTARES	Astronomy with a Neutrino Telescope and Abyss Environmental Research Project
ALP	axion-like particle
BSM	beyond the Standard Model
BBN	big bang nucleosynthesis
CC	charged current
CL	confidence level
CMB	cosmic microwave background
CνB	cosmic neutrino background
ΛCDM	cosmological-constant-cold-dark-matter
KM3NeT	Cubic Kilometre Neutrino Telescope
DE	dark energy
DESI	Dark Energy Spectroscopic Instrument
DM	dark matter
DOF	degree of freedom
DHS	Dolgov–Hansen–Semikoz
EM	electromagnetic
FASER	Forward Search Experiment
FLRW	Friedmann–Lemaître–Robertson–Walker
GR	general relativity
GW	gravitational wave
IR	infrared
KATRIN	Karlsruhe Tritium Neutrino
LIGO	Laser Interferometer Gravitational-Wave Observatory
LSZ	Lehmann–Symanzik–Zimmerman
LSND	Liquid Scintillator Neutrino Detector
LBL	long baseline
MicroBooNE	Micro Booster Neutrino Experiment
MSW	Mikheyev–Smirnov–Wolfenstein
MiniBooNE	Mini Booster Neutrino Experiment
MC	Monte Carlo
NANOGrav	North American Nanohertz Observatory for Gravitational Waves
ONB	orthonormal basis
P-ONE	Pacific Ocean Neutrino Experiment
PSDM	phase space density matrix
PMNS	Pontecorvo–Maki–Nakagawa–Sakata
PTOLEMY	Princeton Tritium Observatory for Light, Early Universe, Massive Neutrino Yield
PTA	pulsar timing array
QFT	quantum field theory

QG	quantum gravity
QKE	quantum kinetic equation
QM	quantum mechanics
SND@LHC	Scattering and Neutrino Detector at the Large Hadron Collider
SBL	short baseline
SSB	spontaneous symmetry breaking
SM	Standard Model
SGWB	stochastic gravitational wave background
SNO	Sudbury Neutrino Observatory
2PI	Two-Particle Irreducible
VEV	vacuum expectation value
WP	wave packet

1 Introduction

From the first cave men discovering how to utilise fire, to today scientists probing the inner workings of nature under enormous experimental and theoretical efforts, humanity always pushed the frontiers of their knowledge out of insatiable curiosity. This centuries long scientific journey has brought forth two remarkably elegant and robust theories of the description of nature: The Standard Model (SM) of particle physics and the theory of general relativity (GR). While the SM describes the behaviour and dynamics of all known matter to an unprecedented degree of accuracy, GR gives insights into the fundamental structure of spacetime itself and how it is inevitably linked to the distribution of matter moving within it. This interaction between matter and the curvature of spacetime gives rise to the phenomenon of gravity. Despite the tremendous successes of both theories in describing and predicting experimental observations in their respective domains of validity, one—if not the biggest—of their shortcomings is that it has not been possible yet to combine both theories into one unified framework. The SM is formulated as a quantum field theory (QFT), and therefore, represents a fully probabilistic description of nature, whereas GR is a classical, deterministic theory. Since matter, described by the SM, and the dynamics of spacetime are deeply intertwined there must exist one theory based on the same fundamental principles allowing for a unified description. Due to the great success of quantum theory it is usually believed that this should be the framework for such a unified description usually referred to as quantum gravity (QG). There already exist multiple contenders for such a theory but lack of experimental evidence makes it impossible to falsify any of them.

This is mainly due to the weakness of gravity compared to the other fundamental forces of nature. Thus, hypothetical quantum effects of gravity become important at length and energy scales impossible to be probed directly using currently available experimental methods. Therefore, it is necessary to come up with new approaches to test these models indirectly and wrest a hint about the theory of QG from nature.

Besides the quest for a quantum description of spacetime, there are also numerous other open questions, problems and puzzles suggesting the need for extensions of the SM. One area of research where already clear evidence for the incompleteness of the SM has been found is the neutrino sector. Since their discovery and the formulation of the theory of electroweak interactions these particles have been thought to be massless and purely left-chiral fermion fields. However, it has been confirmed that neutrinos can change their flavour during propagation, a phenomenon best explained if the known neutrino states indeed have (different) masses. This raises further questions how these masses are generated and if there also exist right-chiral complementary fields as it is the case for every other SM fermion. These new states would then fully decouple from the SM interactions and are hence often called sterile neutrinos.

A puzzle arising in this context is why neutrino masses are so much smaller compared to those of the other SM particles and if there is a fundamental reason behind this circumstance.

In addition to the blank spots present in the theoretical description of the neutrino sector, there is an even more astounding discrepancy between observations and the SM: Several different astrophysical and cosmological observations over the last decades have shown that most of the gravitating matter in the Universe cannot be accounted for by SM matter. This is usually accounted to a new particle species that only interacts weakly, if at all, with known particles and among themselves. These new particles are categorised under the term dark matter (DM) and it is far from clear what their properties are.

This list of open questions of modern physics is of course not exhaustive but it represents the main topics relevant to this thesis. The main objective of this work is to investigate to what extent neutrinos and their flavour dynamics can be utilised to search for new physics beyond the SM and GR and gain new clues about the problems discussed above. To do so, we consider neutrino flavour transitions within multiple different settings ranging from the hot and dense early Universe over neutrinos travelling vast distances through the vacuum to Earth, up to atmospheric neutrino experiments. To prepare for these investigations we first lay the theoretical foundations with a special focus on neutrino oscillations in Chapter 2.

At short baseline (SBL) experiments, evidence for anomalous neutrino flavour transitions has been found that could in principle be explained by the presence of a light sterile neutrino. This explanation is, however, in conflict with other data from neutrino experiments and cosmology. In particular, a new light degree of freedom (DOF) contributes significantly to the radiation energy density in the early Universe, causing a faster cosmic expansion rate than suggested by cosmic microwave background (CMB) and big bang nucleosynthesis (BBN) measurements. Indeed, the Hubble rate at formation of the CMB, as well as the cosmic helium abundance generated during BBN, are in good agreement with the respective SM and cosmological-constant-cold-dark-matter (ΛCDM) predictions. Hence, resolving the SBL anomalies with light sterile neutrino models requires a mechanism suppressing the population of the sterile neutrino species at early times. Thus, in Chapter 3, we discuss how the existence of light sterile neutrinos can be reconciled with cosmological observations by virtue of a DM candidate field as well as by altered dispersion relations (ADRs). The latter is, for example, motivated by extensions of GR including extra dimensions accessible to the sterile neutrino. Another motivation of ADR-models that we consider in this work are the discrepancies between observations made in SBL, long baseline (LBL) and atmospheric neutrino oscillation experiments. In contrast to SBL experiments, neutrino oscillation patterns at LBL and atmospheric neutrino experiments match the standard three-neutrino-flavour-expectation. Altering the dispersion relation of the sterile neutrino can resolve this discrepancy by introducing an additional energy-dependence into the effective neutrino masses and mixing.

In Chapter 4, we consider how neutrinos travelling large distances between their source and the detector might provide clues about the nature of QG as well as DM. The general idea behind this conjecture is that any quantum system travelling through a quantised spacetime will inevitably become entangled with the hypothetical quantum DOFs of the spacetime.

This in turn leads to decoherence in the considered system that might be observable. If QG violates global quantum numbers, these interactions with quantum spacetime may even lead to transitions between neutrino and DM states that would otherwise be forbidden under non-gravitational interactions. Consequently, signatures of these effects are discussed for astrophysical as well as atmospheric neutrino oscillation experiments.

We return to the study of effects of classical GR on neutrino flavour transitions in Chapter 5. In particular, we discuss whether they are observable in current neutrino experiments. These effects are especially relevant for the field of multimessenger astronomy combining the detection of neutrinos, electromagnetic (EM) signals as well as gravitational waves (GWs) in order to analyse the most extreme environments in the Universe. For example, if neutrino flavour ratios are already influenced by classical gravitational effects, this would have major implications for exotic decoherence searches using astrophysical neutrinos as the one described in Chapter 4. Moreover, we also address the question if neutrino oscillations can be utilised to search for GW signals.

Finally, we summarise our findings in Chapter 6 and place them in the broader context of this thesis. Moreover, we provide an outlook on potential implications for future experiments and theoretical considerations.

2 Theoretical Foundations

In order to lay the foundations for the studies and considerations presented in this thesis, we first introduce the main theoretical concepts we frequently draw from, later in the text. We start with a brief break down of the Standard Model (SM) of particle physics describing the interactions between all known particles within the framework of quantum field theory (QFT). Then, we proceed to discuss the theory of general relativity (GR) describing how matter and energy cause a curvature of spacetime that, in turn, influences the dynamics of particles. Moreover, a brief introduction into the history of the Universe and modern cosmology is presented.

We close this introductory chapter with an in-depth discussion on the subject of neutrino oscillations. This already represents an extension of the SM, as neutrinos are considered to be massless within the SM, since the source of neutrino masses still remains unknown to date. As all later Chapters of this thesis revolve around the topic of neutrino oscillations, this section is of major importance, and hence, constitutes the main part of the theoretical introduction.

2.1 The Standard Model of Particle Physics

The SM is the currently accepted theory describing all known interactions between elementary particles besides gravity. In the following, we briefly review those aspects of the SM that are most important to the content and matter of this thesis: neutrinos and the electroweak interaction. For a more complete introduction into the subject, we refer the reader to References [1–4].

The core framework in which the SM is formulated is QFT on a flat, four dimensional spacetime manifold equipped with the Minkowski metric η. Here, we choose the "mostly minus" convention, i.e. $\eta_{\mu\nu} = \mathrm{diag}(1, -1, -1, -1)$ in Cartesian coordinates. The SM is constructed such that all interactions respect the continuous spacetime symmetries described by the proper, orthochronous Lorentz group $\mathrm{SO}^{\uparrow}(1,3)$ and the spacetime translation group. Therefore, the SM complies, by design, with the fundamental principles of special relativity (SR).

2.1.1 The Gauge Sector

All SM particles interact with each other via the strong or electroweak interactions and the strength of the respective interaction channel is parametrised by the associated charge. The strong interaction couples to the so-called colour charge, while the electroweak interaction

couples to weak isospin as well as the hypercharge Y of the particles. As all charges and their associated currents are exactly conserved, this hints towards the existence of a symmetry of the system for each interaction. Meaning, that in addition to the external spacetime symmetries, all fundamental quantum fields are required to transform under an irreducible representation of the so-called internal gauge group of the SM,

$$\mathcal{G}_{\mathrm{SM}} := \mathrm{SU}(3)_c \times \mathrm{SU}(2)_L \times \mathrm{U}(1)_Y, \tag{2.1}$$

and that all interactions and physical states of the underlying Fock space must be invariant under the corresponding gauge transformations. Here, (S)U(n) denotes the (special) unitary group of degree n and the subscripts indicate the charge quantum numbers associated with the respective symmetry group. Hence, the strong force is associated with $\mathrm{SU}(3)_c$ [5–8] and the electroweak force corresponds to the group $\mathrm{SU}(2)_L \times \mathrm{U}(1)_Y$ [9–12].

Each gauge interaction is mediated by massless spin-1 fields transforming in the vector representation of the Lorentz group, as well as in the adjoint representation of the associated gauge group. In the SM these gauge vector fields are called the gluon, W and B fields denoted by

$$G = G_{c\mu}\tau^{c}_{\mathfrak{su}(3)}\mathrm{d}x^{\mu} \qquad \longleftrightarrow \qquad \mathrm{SU}(3)_c\,, \tag{2.2}$$

$$W = W_{l\mu}\tau^{l}_{\mathfrak{su}(2)}\mathrm{d}x^{\mu} \qquad \longleftrightarrow \qquad \mathrm{SU}(2)_L\,, \tag{2.3}$$

$$B = B_{\mu}\mathrm{d}x^{\mu} \qquad \longleftrightarrow \qquad \mathrm{U}(1)_Y, \tag{2.4}$$

respectively. There always exists a local representation of the gauge fields in terms of a basis $\tau^{a}_{\mathfrak{su}(n)}$ of the Lie algebra $\mathfrak{su}(n)$ and the coordinate one form basis $\mathrm{d}x^{\mu}$ in which they are equivalent to $d = n^2 - 1$ ordinary co-vector fields.

The dynamics of all quantum fields contained in the SM are governed by the principle of stationary action $\delta S_{\mathrm{SM}} = 0$ where the action is given by

$$S_{\mathrm{SM}} = \int \mathrm{d}^4x \mathcal{L}_{\mathrm{SM}}(\Phi_i(x), \partial\Phi_i(x))\,, \tag{2.5}$$

where $\Phi_i(x)$ generically denote all quantum fields present in the theory. The SM Lagrangian[1] $\mathcal{L}_{\mathrm{SM}}$ can be divided into four main sectors, i.e.

$$\mathcal{L}_{\mathrm{SM}} = \mathcal{L}_{\mathrm{gauge}} + \mathcal{L}_{\mathrm{matter}} + \mathcal{L}_{\mathrm{Higgs}} + \mathcal{L}_{\mathrm{Yukawa}}\,. \tag{2.6}$$

Here, $\mathcal{L}_{\mathrm{gauge}}$ contains only the terms describing the dynamics of the gauge vector fields in the vacuum. This part of the Lagrangian is given by

$$\mathcal{L}_{\mathrm{gauge}} = -\frac{1}{4}F_{G_{c\mu\nu}}F_{G_c}{}^{\mu\nu} - \frac{1}{4}F_{W_{l\mu\nu}}F_{W_l}{}^{\mu\nu} - \frac{1}{4}F_{B_{\mu\nu}}F_{B}{}^{\mu\nu}\,, \tag{2.7}$$

[1] To be precise, the SM Lagrangian also contains gauge fixing and ghost terms for each interaction, but we omit them here as these terms are of no significance for this thesis. For more details we refer the reader to References [1–4].

where we have introduced the local representations of the field strength tensors F_X of the gluon ($X = G$), W and B fields ($X = W, B$), respectively. In the geometrical picture of gauge field theory these field strength tensors are the abstract gauge curvature forms related to the gauge fields by

$$F_V := \mathrm{d}V + V \wedge V = \left(\partial_\mu V_{a\nu} - \partial_\nu V_{a\mu} + g f_{bca} V_{b\mu} V_{c\nu}\right) \tau^a_{\mathfrak{su}(n)} \mathrm{d}x^\mu \otimes \mathrm{d}x^\nu \,, \tag{2.8}$$

where f_{abc} are the totally antisymmetric structure constants of the Lie algebra, g is the gauge coupling and $\wedge$ denotes the antisymmetric wedge product. The term $V \wedge V$ is only present for non-abelian gauge groups and results in self interactions among the corresponding gauge bosons.

2.1.2 The Matter Sector

Next, we discuss the matter sector of the SM consisting of several spin-1/2, i.e. fermion, fields. Since the electroweak interaction only acts on left-chiral matter fields, it is maximally parity violating. Due to this special property it would be most natural to formulate the SM in terms of the chiral, two-component Weyl fields transforming in the left- or right-chiral spin-1/2 representation of the Lorentz group. For the sake of a unified notation, however, we exclusively use the four-component spinor formulation in this thesis and employ the respective left- and right-chiral projectors, P_L and P_R, whenever chiral fields appear in the expressions.

The matter sector can further be subdivided into the quark sector and the leptonic sector. Quark fields interact via the strong and electroweak interaction, whereas leptonic fields only interact via the electroweak interaction. Both sectors contain three generations or flavours of left-chiral $\mathrm{SU}(2)_L$ doublets containing an up-type and a down-type component. Moreover, for each component of the left-handed quark doublets q_L there exist right-handed up-type and down-type partner fields, u_R and d_R. The three up-type flavours are called the up (u), charm (c) and top (t) quarks, while the three down-type flavours are termed the down (d), strange (s) and bottom (b) quarks. The situation in the lepton sector is analogous with the exception that there exist no right-handed up-type leptons. Moreover, the down-type leptons are called the electron e, muon μ and tau τ, respectively, whereas the up-type leptons are known as the electron neutrino (ν_e), the muon neutrino (ν_μ) and the tau neutrino (ν_τ). The gauge sector of the SM acts universally on all generations and only the Higgs sector gives physical meaning to the distinction between the different particle flavours.

The structure of the interactions of the matter fields is described by the Lagrangian

$$\mathcal{L}_{\text{matter}} := \mathcal{L}_{\text{matter},L} + \mathcal{L}_{\text{matter},R} \,, \tag{2.9}$$

$$\mathcal{L}_{\text{matter},L} := i\overline{q_L}^j \gamma^\mu D_\mu(R(q_L)) q_L^j + i\overline{\ell_L}^j \gamma^\mu D_\mu(R(\ell_L)) \ell_L^j \,, \tag{2.10}$$

$$\mathcal{L}_{\text{matter},R} := i\overline{u_R}^j \gamma^\mu D_\mu(R(u_R)) u_R^j + i\overline{d_R}^j \gamma^\mu D_\mu(R(d_R)) d_R^j + i\overline{e_R}^j \gamma^\mu D_\mu(R(e_R)) e_R^j \,, \tag{2.11}$$

where ℓ_L^j denotes the left-chiral lepton doublet of flavour j, e_R^j are the associated right-chiral down-type leptons and u_R^j (d_R^j) are the right-chiral up-type (down-type) quark fields.

Table 2.1: Representations and hypercharges Y of all matter fields under the SM gauge group. The notation is such that $R = (R_{\mathrm{SU}(3)_c}, R_{\mathrm{SU}(2)_L}, Y)$, where $R_{\mathrm{SU}(n)}$ denotes the dimension of the representation, i.e. 1 = singlet, 2 = doublet, ... The gauge sector acts universally on all flavours since the representations are the same across all generations.

Quarks			Leptons	
q_L	u_R	d_R	ℓ_L	e_R
$\left(3, 2, \frac{1}{3}\right)$	$\left(3, 1, \frac{4}{3}\right)$	$\left(3, 1, -\frac{2}{3}\right)$	$(1, 2, -1)$	$(1, 1, -2)$

Furthermore, we introduce the 4×4 Dirac matrices γ^μ fulfilling the Clifford algebra relation[2] $\{\gamma^\mu, \gamma^\nu\} = 2\eta^{\mu\nu}\mathbb{1}$. A bar over a fermion ψ denotes Dirac conjugation $\bar{\psi} := \psi^\dagger\gamma^0$ and the subscripts L and R indicate the chirality of the respective field that is projected out using the corresponding projectors $P_L = (\mathbb{1} - \gamma_5)/2$ and $P_L = (\mathbb{1} + \gamma_5)/2$, i.e. $\psi_{L/R} = P_{L/R}\psi$. The fifth Dirac matrix $\gamma_5 := i\gamma^0\gamma^1\gamma^2\gamma^3$ measures the chirality of a spin-1/2 fermion.

All interactions of the SM are described by the gauge covariant derivative,

$$\begin{aligned} D_\mu(R(\psi)) = \partial_\mu &- ig_s G_{c\mu}\tau^c_{\mathfrak{su}(3)}(R_{\mathrm{SU}(3)_c}(\psi)) \\ &- igW_{l\mu}\tau^l_{\mathfrak{su}(2)}(R_{\mathrm{SU}(2)_L}(\psi)) - i\frac{g'}{2}B_\mu Y(\psi)\,, \end{aligned} \tag{2.12}$$

depending on the representation $R(\psi)$ of the corresponding fermion field ψ. Usually the collection of representations is denoted by $R = (R_{\mathrm{SU}(3)_c}, R_{\mathrm{SU}(2)_L}, Y)$ and it contains information about the representations of the generators τ appearing in the covariant derivative. For completeness and a better overview of the different fields we list all representations in Table 2.1. Finally, g_s denotes the strong coupling constant, g is the $\mathrm{SU}(2)_L$ coupling and g' represents the $\mathrm{U}(1)_Y$ coupling constant.

All particles transforming non-trivially under $\mathrm{SU}(3)_c$, i.e. quarks and gluons, are subject to *colour confinement* forcing them to form colour-less bound states called hadrons at low momentum transfers between the constituents. At higher momentum transfers, in contrast, the coupling strength of non-abelian gauge groups decreases monotonically if the number of participating particle flavours is not too large. In the SM this applies to the strong interaction and quarks and gluons can be considered as *asymptotically free* particles in high energy collisions.

2.1.3 The Higgs and Yukawa Sectors

Lastly, we discuss the Higgs sector centered around the scalar Higgs field ϕ transforming in the $(1, 2, 1)$ representation of $\mathcal{G}_{\mathrm{SM}}$. The Higgs field has two key functions in the SM: On the one

[2]The Clifford algebra relation ensures that fermion fields obeying the Dirac equation fulfil the relativistic energy–momentum relation.

hand, its vacuum state spontaneously breaks [13–16] the electroweak symmetry, generating gauge covariant mass terms for the matter and weak boson fields in the process. On the other hand, it gives rise to the flavour structure of the SM by virtue of its Yukawa couplings to the matter fields. To understand the mechanism behind electroweak symmetry breaking, we first have to introduce the Higgs Lagrangian,

$$\mathcal{L}_{\text{Higgs}} = (D_\mu \phi)^\dagger D^\mu \phi - V(\phi)\,, \tag{2.13}$$

containing the minimal coupling of ϕ to the gauge sector and the self interaction potential

$$V(\phi) = \mu \phi^\dagger \phi + \lambda (\phi^\dagger \phi)^2\,. \tag{2.14}$$

The values of the constants μ and λ determine the shape of the Higgs potential and the location of its ground state. To be precise, what really determines the ground state of the field ϕ is the so-called quantum action Γ. This quantity accounts for the presence of quantum fluctuations and reduces to the classical action S in the classical limit. The quantum action Γ generates the equations of motion for the vacuum expectation value (VEV) $\langle\phi\rangle := \langle 0|\,\phi\,|0\rangle$ minimising the quantum corrected Higgs potential. In addition to the quantum fluctuations, also thermal corrections modify the shape of the effective potential. During the evolution of the universe from a hot, dense state to the cold vacuum today, the thermally and quantum corrected parameter μ changes its sign from positive to negative. Consequently, the effective Higgs potential obtains a set of degenerate minima. All minima belong to the same gauge orbit and correspond to suitable, degenerate vacuum states of the QFT. By picking one such ground state, the $\mathrm{SU}(2)_L \times U(1)_Y$ symmetry is said to be spontaneously broken and the whole process is called spontaneous symmetry breaking (SSB). Of course the underlying theory is still fully gauge invariant but the perturbative spectrum of states does not explicitly exhibit this gauge invariance anymore.

In the chosen vacuum state the Higgs field acquires a non-zero VEV and thus has to be reparametrised in terms of new fields with zero VEV. This way one ensures that the field theory can be properly quantised perturbatively and that the particle spectrum only contains particles with physical masses. A common choice of parametrisation of the Higgs doublet reads

$$\phi(x) = \frac{1}{\sqrt{2}} \begin{pmatrix} 0 \\ v \end{pmatrix} + \begin{pmatrix} \phi^+(x) \\ \phi^0(x) \end{pmatrix}\,, \tag{2.15}$$

where $v := \sqrt{2}|\langle\phi\rangle|$. Substituting this parametrisation back into the Higgs Lagrangian $\mathcal{L}_{\text{Higgs}}$ results in mass terms for the electroweak gauge bosons. Furthermore, one usually expresses the fields ϕ^0 and ϕ^+ in terms of real scalar fields

$$\phi^0 =: \frac{1}{\sqrt{2}}(H^0 + i\chi_1)\,, \qquad\qquad \phi^+ =: \frac{1}{\sqrt{2}}(\chi_2 + i\chi_3)\,, \tag{2.16}$$

where only the real Higgs field H_0 gives rise to massive, physical excitations, while χ_k are massless Goldstone bosons. By an appropriate choice of gauge, the Goldstone bosons [13,

17] χ_k can be reinterpreted as the longitudinal polarisation modes of the now massive vector boson fields. In order to identify the boson fields with well-defined masses, the respective mass terms in $\mathcal{L}_{\text{Higgs}}$ need to be diagonalised leading to

$$\mathcal{L}_{\text{Higgs}} \supset m_W^2 W_\mu^+ W^{-\mu} + \frac{m_Z^2}{2} Z_\mu Z^\mu \,, \tag{2.17}$$

where we introduce the physical, massive weak bosons

$$W^{\pm\mu} := \frac{W_1^\mu \mp i W_2^\mu}{\sqrt{2}} \,, \qquad Z^\mu := \cos(\theta_W) W_3^\mu - \sin(\theta_W) B^\mu \,, \tag{2.18}$$

and we define the weak mixing angle θ_W and the weak boson masses via

$$m_W := \frac{vg}{2} \,, \qquad m_Z := \frac{m_W}{\cos(\theta_W)} \,, \qquad \cos(\theta_W) := \frac{g}{\sqrt{g^2 + g'^2}} \,. \tag{2.19}$$

The fourth physical boson field,

$$A^\mu := \cos(\theta_W) B^\mu + \sin(\theta_W) W_3^\mu \,, \tag{2.20}$$

remains massless after SSB and is called the photon field. The photon field corresponds to the remaining, explicit $U(1)_{\text{EM}}$ symmetry and acts as the mediator particle of the electromagnetic (EM) interaction. The charge corresponding to the EM interaction in terms of the z component of the weak isospin T_3 and the weak hypercharge Y is $Q := T_3 + Y/2$.

In addition to the generation of the masses of the weak gauge bosons $W^\pm$ and Z, the Higgs field also is responsible to give masses to (almost) all matter fields. This is because the Higgs field ϕ does not only interact with itself and the gauge sector but also with all matter fields via a Yukawa interaction described by the Lagrangian,

$$\mathcal{L}_{\text{Yukawa}} = -y_{ij}^D \overline{q_L}^i \phi d_R^j - y_{ij}^U \overline{q_L}^i \phi^c u_R^j - y_{ij}^E \overline{\ell_L}^i \phi e_R^j + \text{h.c.} \,, \tag{2.21}$$

$$\phi^c := i\sigma^2 \phi^* \,, \tag{2.22}$$

where σ^2 is the second Pauli matrix. Thus, after introducing the Higgs parametrisation shown in Equation (2.15) this Lagrangian gives rise to gauge invariant, fermionic mass terms for all types of quarks and for the electrically charged, down-type leptons. The neutral, up-type leptons ν_L^i—the so-called neutrinos—do not have masses in the SM due to the lack of right-handed partners ν_R^j. The main reason why ν_R^j are not included into the SM is that for a long time neutrinos were considered massless and hypothetical ν_R^j fields would be singlets under $\mathcal{G}_{\text{SM}}$, and hence, decouple from the theory.

Note, that the Yukawa couplings y_{ij}^X carry flavour indices i, j and,hence, are the only structures in the SM distinguishing between different flavours. This gives rise to a rich phenomenology in the quark flavour sector of the SM since the up- and down-type Yukawa couplings are not diagonal and also not diagonalisable by the same transformations. This leads to a misalignment between the weak interaction (flavour) and mass eigenstates, and hence, allows for transitions

between different generations. Although in this thesis we are mainly concerned with neutrino physics and especially with neutrino oscillations, it is still worthwhile to discuss quark-mixing in more detail. The main reason for this is that in the SM no mixing phenomenon arises in the lepton sector, but the underlying mechanism inducing neutrino mixing in beyond the Standard Model (BSM) theories is a generalisation of the simple scenario of quark-mixing. Therefore, understanding quark-mixing first, gives a good intuition of how leptonic mixing works.

Consider that part of the Yukawa Lagrangian inducing the quark masses, i.e.

$$\mathcal{L}^{q\text{ mass}}_{\text{Yukawa}} = -\frac{y^D_{ij} v}{\sqrt{2}} \overline{d_L}^i d^j_R - \frac{y^U_{ij} v}{\sqrt{2}} \overline{u_L}^i u^j_R + \text{h.c.}\,. \tag{2.23}$$

The terms in Equation (2.23) have the structure of non-diagonal Dirac mass terms where the masses are given by $m^{U/D}_{ij} = v y^{U/D}_{ij}/\sqrt{2}$. We obtain the physical, massive quark fields by applying a singular value decomposition of the form

$$m^U = (V^U_L)\tilde{m}^U (V^U_R)^\dagger\,, \qquad\qquad m^D = (V^D_L)\tilde{m}^D (V^D_R)^\dagger\,, \tag{2.24}$$

with unitary matrices $V^{U/D}_{L/R}$ and real valued, diagonal mass matrices $\tilde{m}^{U/D}$. Defining the massive quark fields as

$$\tilde{u}^j_{L/R} := [V^{U\dagger}_{L/R}]_{jk} u^k_{L/R}\,, \qquad\qquad \tilde{d}^j_{L/R} := [V^{D\dagger}_{L/R}]_{jk} d^k_{L/R}\,, \tag{2.25}$$

yields the diagonal mass Lagrangian

$$\mathcal{L}^{q\text{ mass}}_{\text{Yukawa}} = -\sum_{i=1}^{3} m^U_i \bar{\tilde{u}}^i \tilde{u}^i - \sum_{i=1}^{3} m^D_i \bar{\tilde{d}}^i \tilde{d}^i\,, \tag{2.26}$$

where $m^{U/D}_i$ are the diagonal entries of $\tilde{m}^{U/D}$. In this expression, the advantage of the four-component spinor notation after SSB becomes apparent since now left- and right-handed up- and down-type fields behave as the left- and right-handed components of the same Dirac field. Consequently, they can be combined into Dirac spinors of the form $\psi = \psi_L + \psi_R$ with $\psi \in \{\tilde{u}^j, \tilde{d}^j\}$.

Apart from the Yukawa interaction terms, all right-handed quark fields only appear in terms that are an identity matrix in flavour space, and no couplings between down- and up-type fields exist. Thus, the transformations $V^{U/D}_R$ fully disappear from the SM Lagrangian formulated in terms of the $\tilde{u}$ and $\tilde{d}$ fields. For the left-handed fields the situation is different because of the weak interaction Lagrangian. In particular, the terms coupling together up- and down-type fields, called the charged current (CC) interaction terms, explicitly contain the left-handed transformation matrices after the field redefinition, i.e.

$$\mathcal{L}^q_{\text{matter},CC} := \frac{g}{\sqrt{2}} \left(\bar{\tilde{d}} \left[V^D_L V^{U\dagger}_L \right] \gamma^\mu W^-_\mu P_L \tilde{u} + \text{h.c.} \right)\,, \tag{2.27}$$

where we have defined the mass eigenstate vectors $\tilde{u} = (\tilde{u}^1, \tilde{u}^2, \tilde{u}^3)$ and $\tilde{d} = (\tilde{d}^1, \tilde{d}^2, \tilde{d}^3)$. Since the unitary rotation matrices appear only in the combination $V^D_L V^{U\dagger}_L$ in $\mathcal{L}^q_{\text{matter},CC}$ and

completely vanish from the remaining Lagrangian, we give it its own name, i.e. $U_{\mathrm{CKM}} = V_L^D V_L^{U\dagger}$ after Cabbibo [18], Kobayashi and Maskawa [19]. The matrix U_{CKM} is also refered to as the quark-mixing matrix and gives rise to flavour non-diagonal transitions in CC interactions after redefining the generations in terms of fields with well-defined masses.

2.2 General Relativity and Cosmology

So far, we have discussed the physics of elementary particles valid on small distance and time scales, or in flat spacetime where gravity is not relevant. If we now also want to describe the physics of macroscopic, and hence, classical objects on large distance and time scales including gravitational interactions, the best description we have available today is Einstein's theory of GR [20]. Especially, since we also study the evolution of our Universe as a whole in this work, we want to introduce the most important concepts needed for our considerations. For more details on the theory of GR see, for example, References [21–23].

In the theory of GR, spacetime is described by a four dimensional, smooth, Lorentzian[3] manifold $(\mathcal{M}, g)$, i.e. a manifold equipped with a metric tensor g enabling us to measure distances and proper time intervals and to define a causal structure. Furthermore, spactime is endowed with the uniquely determined Levi–Civita connection ∇ defining a notion of coordinate invariant differentiation (covariant derivative) of tensor fields. This is necessary since in order to define the derivative of, say, a vector field one needs to be able to write down the difference of the vector field evaluated at two different points on $\mathcal{M}$. Since the resulting vectors are members of different tangent spaces it is far from clear how to define this difference and the covariant derivative ∇ is used to establish exactly this *connection* in a well-defined, coordinate invariant way.

One important application of the covariant derivative is the description of the motion of classical point-like particles. In flat spacetime, free particles move along straight lines, i.e. trajectories with constant velocity. Although an arbitrary manifold is generally curved and may not contain any straight lines[4], we can still extend the concept of free motion to general curved spacetimes. To this end, we pick up on the notion of vanishing acceleration using the covariant derivative, i.e.

$$\frac{\nabla}{\mathrm{d}\tau} U(\tau) \equiv 0\,, \tag{2.28}$$

where $U(\tau)$ is the velocity vector of the particle trajectory c and $\nabla/\mathrm{d}\tau$ denotes covariant differentiation along c. A curve fulfilling Equation (2.28) is called a *geodesic* and in any local

[3] The metric being Lorentzian means that its signature is that of the Minkowski metric, i.e. that it has one negative and $(n-1)$ positive eigenvalues on an n dimensional manifold. This is also what gives rise to the causal structure since it enables us to distinguish timelike, lightlike (null), and spacelike curves.

[4] If we embed it into a higher dimensional flat space.

coordinate chart Equation (2.28) reads

$$\frac{\mathrm{d}^2 c^\mu}{\mathrm{d}\tau^2} + \Gamma^\mu_{\rho\sigma} \frac{\mathrm{d}c^\rho}{\mathrm{d}\tau} \frac{\mathrm{d}c^\sigma}{\mathrm{d}\tau} = 0\,, \tag{2.29}$$

with the Christoffel symbols $\Gamma^\mu_{\rho\sigma}$ defining the connection ∇ in local coordinates and the coordinate representation of the curve $c^\mu(\tau)$. In the presence of forces f^μ, the geodesic Equation (2.29) becomes

$$\frac{\mathrm{d}^2 c^\mu}{\mathrm{d}\tau^2} + \Gamma^\mu_{\rho\sigma} \frac{\mathrm{d}c^\rho}{\mathrm{d}\tau} \frac{\mathrm{d}c^\sigma}{\mathrm{d}\tau} = f^\mu(x(\tau))\,. \tag{2.30}$$

generalising Newtons second law from classical, non-relativistic mechanics.

The inherent curvature of a manifold given a connection ∇ is quantified by the Riemann curvature tensor defined by

$$R(X,Y)Z := \nabla_Y \nabla_X Z - \nabla_X \nabla_Y Z + \nabla_{[X,Y]} Z\,, \qquad X, Y, Z \in \mathfrak{X}(\mathcal{M})\,. \tag{2.31}$$

The Riemann tensor *measures* how the second covariant derivative of a vector field Z changes when interchanging the directions X and Y along which we take these derivatives. Therefore, $R(X,Y)Z$ can be interpreted as the difference vector between the infinitesimal parallel transports of Z first along Y and then X and the parallel transport of Z first along X and then Y. If the space would not be curved there should be no difference in how to go along any closed curve but in a curved space the results differ in general. The last term in Equation (2.31) involves the Lie bracket $[X,Y]$ of the vector fields X and Y, and ensures that the full quantity indeed transforms as a tensor under coordinate transformations. Geometrically it corresponds to the infinitesimal parallel transport of Z along a third direction accounting for the possibility that the parallelogram defined by X and Y does not close. This third direction closes the gap. In local coordinates the Riemann tensor reads

$$R^\mu{}_{\nu\lambda\rho} = \partial_\rho \Gamma^\mu_{\lambda\nu} - \partial_\lambda \Gamma^\mu_{\rho\nu} + \Gamma^\mu_{\rho\sigma}\Gamma^\sigma_{\lambda\nu} - \Gamma^\mu_{\lambda\sigma}\Gamma^\sigma_{\rho\nu}\,. \tag{2.32}$$

From this the Ricci tensor and curvature scalar are defined as

$$R_{\mu\nu} := R^\lambda{}_{\mu\lambda\nu}\,, \qquad R := g^{\mu\nu} R_{\mu\nu}\,. \tag{2.33}$$

Since the Levi–Civita connection is uniquely determined by the metric tensor g also the Riemann tensor is directly related to g and its derivatives.

So far we have stated that in GR spacetime is mathematically represented by a general four dimensional manifold and that freely falling particles follow geodesics in that spacetime, but we have not come up with any argument why we need this extra degree of complication. While these statements are also true for special relativity, curvature of Minkowski spacetime vanishes everywhere which is why it is also termed *flat spacetime*. The reason why it is not sufficient to keep spacetime flat is the strong equivalence principle. It states that locally a particle immersed in a gravitational field behaves the same as in an accelerated frame of

reference with equivalent acceleration. From special relativity we already know that coordinate transformations into accelerated frames of reference lead to non-vanishing Christoffel symbols describing the inertial forces acting within that frame. Consequently, also gravitational forces need to be encoded within the Christoffel symbols. It is, however, in general not possible to get rid of gravitational forces by applying a simple coordinate transformation, and hence, gravity must be related to some tensor field of actual physical significance. From considerations of the Newtonian law of gravitation it can then be derived that gravity is directly related to the curvature of the manifold and that the metric tensor itself becomes a dynamic entity obeying the Einstein equations,

$$R_{\mu\nu} - \frac{1}{2} R g_{\mu\nu} = 8\pi G T_{\mu\nu} \,. \tag{2.34}$$

Equation (2.34) relates the geometry, represented here by the Ricci tensor and curvature scalar, to the energy–momentum tensor $T_{\mu\nu}$ describing the matter content of the Universe. Hence, Wheeler's famous phrase *"Space tells matter how to move; Matter tells space how to curve"* [22] directly referencing the Einstein equations as well as the geodesic equation.

2.2.1 Cosmology

A setting of special interest to parts of this thesis is the hot and dense early Universe as neutrinos contribute a significant portion to the energy density at early times. Any new physics scenario affecting the neutrino sector could, therefore, alter the history of the Universe making cosmology an important testing ground when proposing such new physics models. The prevailing model describing the evolution of the Universe is called Big Bang cosmology. The earliest and most important landmarks of this model are the proposal of a homogeneous and isotropic background of microwaves in 1948 by Alpher and Herman [24] and its later discovery in the 1960's by Penzias and Wilson [25].

In Big Bang cosmology [21] spacetime is assumed to obey the cosmological principle, i.e. to be (almost) perfectly spatially homogeneous and isotropic, implying a metric tensor of the form

$$\mathrm{d}s^2 = \mathrm{d}t^2 - a^2(t) \left(\frac{\mathrm{d}r^2}{1 - \kappa r^2} + r^2 \, \mathrm{d}\Omega^2 \right) , \tag{2.35}$$

where the solid angle element is given by $\mathrm{d}\Omega^2 = \mathrm{d}\theta^2 + \sin^2(\theta)\,\mathrm{d}\phi^2$ and $\kappa \in \{-1, 0, 1\}$ is the spatial curvature parameter. This metric is called the Friedmann–Lemaître–Robertson–Walker (FLRW) metric and is the most general metric fulfilling the required symmetry properties. The so-called scale factor $a(t)$ in front of the spatial part of the metric tensor only depends on cosmic time describing the expansion or contraction of physical lengths everywhere in the Universe. The scale factor furthermore represents the only dynamic quantity in the FLRW metric and its time evolution is governed by the Einstein Equations (2.34) and in turn is

therefore dictated by the energy content of the Universe. In the special case of a FLRW spacetime the Einstein equations reduce to the two Friedmann equations

$$\left(\frac{\dot{a}}{a}\right)^2 = \frac{8\pi G}{3}\rho - \frac{\kappa}{a^2}\,, \tag{2.36}$$

$$\frac{\ddot{a}}{a} = -\frac{4\pi G}{3}\left(\rho + 3P\right)\,, \tag{2.37}$$

where ρ and P are the energy density and pressure of the matter content of the Universe, respectively. Observations have shown [26, 27] that the spatial curvature of the Universe is negligible. Thus, from now on we set $\kappa \equiv 0$ for the remainder of this work if not stated otherwise.

The second Equation (2.37) is usually replaced by the equivalent cosmic continuity equation,

$$\dot{\rho} = -3H(\rho + P)\,, \tag{2.38}$$

where we have introduced the Hubble rate $H := \dot{a}/a$. Equation (2.38) can be derived from the Bianchi identity for the Einstein tensor $G_{\mu\nu}$ implying covariant conservation of the energy–momentum tensor, i.e. $\nabla_\mu T^{\mu\nu} \equiv 0$. Moreover, assuming the matter content to be well approximated by an ideal fluid, we can impose the cosmic equation of state,

$$P = w\rho\,, \tag{2.39}$$

where w is a constant of proportionality. For slowly moving matter pressure is negligible and we get $w = 0$, whereas for relativistic matter one finds $w = 1/3$. Both categories are usually called matter (or dust) and radiation, respectively. In addition to these two kinds of fluids, observations [28, 29] of the cosmos have lead to the conclusion that there exists also a third, more exotic form of energy driving the accelerated expansion of the Universe. An accelerated expansion corresponds to $w < -1/3$ as can be inferred from the second Friedmann Equation (2.37). A possible candidate for this so-called dark energy (DE) could be a constant addition to the Einstein equations,

$$R_{\mu\nu} - \frac{1}{2}g_{\mu\nu}R = 8\pi G T_{\mu\nu} + \Lambda\,, \tag{2.40}$$

referred to as the cosmological constant Λ. This corresponds to energy carried by spacetime itself and implies $w = -1$. Since this type of ubiquitous vacuum energy reminds of the vacuum energy of quantum fields usually also this quantum contribution is added to the Einstein equations in a semiclassical approach [30], i.e.

$$R_{\mu\nu} - \frac{1}{2}g_{\mu\nu}R = 8\pi G\left(T_{\mu\nu} + \langle 0|\,\hat{T}_{\mu\nu}\,|0\rangle\right) + \Lambda\,, \tag{2.41}$$

where $\hat{T}_{\mu\nu}$ is the energy–momentum–tensor of the quantum fields and $T_{\mu\nu}$ is the classical contribution. The total DE density can then be parametrised as [30]

$$\rho_{\mathrm{DE}} = \frac{\Lambda}{8\pi G} + \langle 0|\,\hat{\rho}\,|0\rangle\,, \tag{2.42}$$

with $\hat{\rho} = \hat{T}_{00}$. In the SM this contribution is several orders of magnitude larger than the measured DE density implying a large cancellation between the free parameter Λ of GR and the vacuum energy contribution. This almost exact cancellation between a priori unrelated sectors is usually considered to be *unnatural* [30].

For $\kappa = 0$ the scale factor has a strictly monotonic time-dependence and Equation (2.38) can be solved for ideal fluids yielding

$$\rho(a) = \rho_0 \left(\frac{a}{a_0}\right)^{-3(1+w)} , \tag{2.43}$$

with some arbitrary initial scale factor a_0 and initial energy density ρ_0. The energy densities of the different kinds of fluids discussed above hence depend on the scale factor as follows:

- Radiation or relativistic matter: $\rho \propto a^{-4}$
- Dust or non-relativistic matter: $\rho \propto a^{-3}$
- DE (with $w = -1$): $\rho \equiv \text{const.}$

This scale factor-dependence already enables us to determine in which order each of these different components dominates the energy density of an expanding Universe. At very small scale factors radiation has the most significant impact on the evolution of the Universe followed by the matter density and the DE density if the latter is sufficiently small to allow for a domination era of the former two. This means the Universe has evolved from a radiation dominated state in the very early stages over a matter dominated state into a vacuum dominated state, today. In this thesis, we are mainly interested in the radiation dominated era of the Universe, and hence, focus on the discussion of this time span.

In the early Universe, the energy content is given by ultra-relativistic particles interacting with each other constantly. To be able to predict the evolution of the expansion of the Universe it is therefore necessary to trace the evolution of the different particle species. At lowest order in cosmological perturbations, the state of these particles is well described by a set of homogeneous, isotropic phase space distribution functions $f_i(p,t)$. Here, p is the absolute value of the momentum of particle species i and t is the cosmic time. The transport of particles and energy, i.e. the time evolution of the phase space distributions, is governed by the so-called Boltzmann equations (see for example Reference [31])

$$\left(\partial_t + pH\partial_p\right) f_i(t,p) = \mathcal{C}_i[t,p,\{f_j\}] \,. \tag{2.44}$$

The left hand side of this equation describes how the expansion of the Universe affects the distribution functions f_i while the right hand side encodes the effect of microscopic collisions of particles in the plasma. The collision term $\mathcal{C}_i$ is the sum of the thermal QFT-interaction rates for all processes $\mathcal{P}$ the particle species i can participate in. Furthermore, for each processes there exists also the inverse process and we adopt the convention that the *forward* direction of a process produces a particle, i.e. contains the particle of momentum p and species i in the final state $F_{\mathcal{P}}$, while the *backward* direction of a process contains the particle in the initial state

$I_{\mathcal{P}}$. The full collision term can then be written as the sum over all production, i.e. forward directed, processes as[5]

$$\mathcal{C}_i = \sum_{\mathcal{P}} \mathcal{C}_i(I_{\mathcal{P}} \to F_{\mathcal{P}}) - \mathcal{C}_i(F_{\mathcal{P}} \to I_{\mathcal{P}})\,. \tag{2.45}$$

A particle is said to be in thermal equilibrium with another species if all dominant collision processes proceed rapidly enough in both the forward ($I \to F$) and backward $F \to I$ directions such that they surpass the expansion rate of the Universe H. As soon as all interaction rates become too slow, the particle species drops out of equilibrium and effectively follows the collision-free Boltzmann equation,

$$\left(\partial_t + pH\partial_p\right) f_i(t,p) \approx 0\,, \tag{2.46}$$

implying that the particle number in a comoving volume is conserved, i.e.

$$\frac{\mathrm{d}}{\mathrm{d}t}\left(a^3(t) n_i(t)\right) \equiv 0\,, \tag{2.47}$$

with the particle number density

$$n_i(t) := g_i \int \frac{\mathrm{d}^3\vec{p}}{(2\pi)^3} f_i(p,t)\,, \tag{2.48}$$

of particle species i with g_i, the number of internal degrees of freedom (DOFs) of the particle.

Interestingly, for particles in thermal equilibrium the collision term also effectively vanishes since both the forward and backward reactions proceed at the same rate. The significant difference here is that in thermal equilibrium the temperature of species i remains the same as that of the other species it is in equilibrium with. Furthermore, the phase space distribution functions for fermions and bosons in thermal equilibrium are given by

$$f^F_{\mathrm{eq}}(p) = \frac{1}{e^{-\frac{E_i(p)-\mu_i}{T}} + 1}\,, \qquad f^B_{\mathrm{eq}}(p) = \frac{1}{e^{-\frac{E_i(p)-\mu_i}{T}} - 1}\,, \tag{2.49}$$

where μ_i is the chemical potential of the species i. In the ultra-relativistic limit, i.e. for $T \gg m_i, \mu_i$ the resulting number and energy densities of a particle in thermal equilibrium read

$$n_i^{\mathrm{eq}}(t) = \begin{cases} \frac{3}{4}\frac{\zeta(3)}{\pi^2} g_i T^3(t) & \text{fermions} \\ \frac{\zeta(3)}{\pi^2} g_i T^3(t) & \text{bosons} \end{cases}\,, \qquad \rho_i^{\mathrm{eq}}(t) = \begin{cases} \frac{7}{8}\frac{\pi^2}{30} g_i T^4(t) & \text{fermions} \\ \frac{\pi^2}{30} g_i T^4(t) & \text{bosons} \end{cases}\,. \tag{2.50}$$

Together with Equation (2.47) this implies that for particles in thermal equilibrium the temperature behaves as $T \propto a^{-1}$. The energy density of a particle species is related to its phase space distribution via

$$\rho_i(t) := g_i \int \frac{\mathrm{d}^3\vec{p}}{(2\pi)^3} E_i(p) f_i(p,t)\,. \tag{2.51}$$

[5] For completeness we provide the full expression for the collision term in Appendix A.1.

The total radiation energy density can be expressed as

$$\rho_{\text{tot}}(t) = \frac{\pi^2}{30} g_{\text{eff}}(T) T^4 \,, \tag{2.52}$$

with the effective number of DOFs contributing to the energy density

$$g_{\text{eff}}(T) = \sum_b g_b \left(\frac{T_b}{T}\right)^4 + \frac{7}{8} \sum_f g_f \left(\frac{T_f}{T}\right)^4 \,, \tag{2.53}$$

where

$$T_f := \left[\frac{30}{\pi^2}\frac{8}{7}\int \frac{\mathrm{d}^3\vec{p}}{(2\pi)^3} E_i f_i(p,t)\right]^{\frac{1}{4}} \,, \qquad \text{(Fermions)} \tag{2.54}$$

$$T_b := \left[\frac{30}{\pi^2}\int \frac{\mathrm{d}^3\vec{p}}{(2\pi)^3} E_i f_i(p,t)\right]^{\frac{1}{4}} \,, \qquad \text{(Bosons)} \tag{2.55}$$

are effective temperatures for particle species that have already left thermal equilibrium, i.e. have frozen out, and hence, evolve independently from the rest of the plasma of temperature T. If the freeze-out process occurs fast enough also the out-of-equilibrium particles still follow their equilibrium distributions with the effective temperatures $T_f \propto a^{-1}$.

From the energy density we can directly compute the Hubble rate by virtue of the first Friedmann Equation (2.36),

$$H(t) = \sqrt{\frac{8\pi G}{3}\rho_{\text{tot}}(t)} = \sqrt{\frac{4\pi^3 G}{45} g_{\text{eff}}(T(t))}\, T^2(t) \,. \tag{2.56}$$

Moreover, using the time-dependence of the scale factor for a radiation dominated Universe, with $a(t) \propto \sqrt{t}$, we find

$$H(t) = \frac{1}{2t} \,. \tag{2.57}$$

Putting together both equations yields the time–temperature relation for radiation domination

$$t(T) = \sqrt{\frac{45}{16\pi^3 G}\frac{1}{g_{\text{eff}}(T)}}\frac{1}{T^2} \,. \tag{2.58}$$

In periods of constant g_{eff} this relation can also be inverted analytically.

Another important quantity, that is always conserved in a comoving volume during the evolution of the Universe, is the entropy

$$S \equiv a^3(t)\frac{(\rho + P)}{T} \,, \tag{2.59}$$

If the temperature drops below the mass of a particle species, its annihilation processes dominate the opposing pair-creation processes as the available phase space for the latter reaction shrinks. The affected particle species then drops out of thermal equilibrium and annihilates with its antiparticles. Since the total entropy S is conserved, whenever the contribution of a particle species to S fades due to such an annihilation, the temperature for the remainder of the plasma rises compared to its equilibrium evolution $T \propto a^{-1}$. This phenomenon is called reheating and microscopically the temperature increase is mediated by the collision terms injecting the energy released from the annihilation into the remaining particle species. If there exists a particle–antiparticle asymmetry in the annihilating species, the annihilation does not fully erase the species and its remaining component can get back to thermal equilibrium with the plasma again if its remaining interactions proceed sufficiently rapid. In any other case the annihilated species fully freezes out.

To conclude this section, we give a brief overview over major events happening during temperatures from $T \approx 300\,\mathrm{MeV}$ to $T \approx 0.3\,\mathrm{eV}$ as this temperature span is of major importance for the discussions in Chapter 3. Around the confinement scale of QCD [32] $T_{\mathrm{QCD}} \approx 150\,\mathrm{MeV}$ to $214\,\mathrm{MeV}$ quarks and gluons confine into hadrons representing the physical DOFs at temperatures below T_{QCD}. This leads to a drop in the effective DOFs [32] from $g_{\mathrm{eff}} \sim 61.75$ to $g_{\mathrm{eff}} \sim 17.25$ as all but the lightest hadrons have masses much larger than the masses of the lightest quarks and massless gluons contributing a significant amount to g_{eff} due to their colour DOFs. The predominant interaction between all free particles now is the EM interaction followed by the spontaneously broken weak interaction as well as the Yukawa interaction induced by the confined strong interaction. Moreover, below T_{QCD} the only hadrons in thermal equilibrium are pions, i.e. $\pi^{\pm}$ and π^0, annihilating shortly after at around $T_\pi \approx 130\,\mathrm{MeV}$. Because of the simultaneous drop in effective DOFs each annihilation corresponds to a reheating of the remaining plasma now containing only light leptons, i.e. $\mu^{\pm}$, $e^{\pm}$, ν_j and $\bar{\nu}_j$, and photons.

The next annihilation occurs at around $T_{\mu^{\pm}} \sim 105\,\mathrm{MeV}$ where muons and antimuons annihilate each other up to a small potential particle–antiparticle asymmetry. This asymmetry is shifted to the lighter leptons $e^{\pm}$ and $\nu_j/\bar{\nu}_j$ via muon decay, afterwards. The freeze-out processes discussed so far do not happen because of the force mediating the interactions being too weak but rather due to limited phase space volume of the pair-creation processes and the instability of the respective particles. The opposite applies for neutrino decoupling happening roughly between $T_\nu \approx 0.8\,\mathrm{MeV}$ to $4\,\mathrm{MeV}$ where weak interactions maintaining equilibrium between the neutrinos and the EM plasma become inefficient. From this event on, neutrinos basically act as free streaming particles whose temperature redshifts with a^{-1} and remains approximately equal to the photon temperature until $e^{\pm}$ annihilation at $T \sim 0.511\,\mathrm{MeV}$. Here, another reheating occurs leading to a difference between the photon and effective neutrino temperature which can be estimated from entropy conservation to be $T = \sqrt[3]{11/4}T_\nu$. Indeed only the low energy modes of neutrinos have fully decoupled by this time implying also a slight reheating of the high energy neutrino modes and a subsequent departure from the equilibrium Fermi–Dirac distribution at these energies. Another important event at $T_{\mathrm{BBN}} \sim 0.7\,\mathrm{MeV}$ and below is the freeze-out of neutron–proton reactions and big bang nucleosynthesis (BBN). During BBN the

non-relativistic protons and neutrons present in the plasma combine to form the first atomic nuclei from $p = {}^1\mathrm{H}$ to ${}^7\mathrm{Li}$ and ${}^7\mathrm{Be}$.

The last important event marking the definite end of the radiation domination era is the decoupling of photons and the formation of the cosmic microwave background (CMB) at roughly $T \sim 0.3\,\mathrm{eV}$.

2.2.2 Quantum Field Theory in Curved Spacetime

Although a quantum theory of gravity still seems to be far out of reach, we can nevertheless construct QFT on a classical background manifold $\mathcal{M}$ on which a non-trivial pseudo-Riemannian metric is defined. In the following, we briefly discuss one of the consequences of the absence of global Poincaré symmetry on general manifolds for QFT, namely that the particle concept becomes dependent on the state of motion of the oberserver. For a complete review of QFT in curved spacetime, see for example References [33, 34].

For the usual quantisation procedure of a classical field theory to simply carry over from flat to curved spacetime, we need to assume that the spacetime is globally hyperbolic[6]. That means that there exists a continuous family of spacelike hypersurfaces $\{\Sigma_t\}_{t\in\mathbb{R}}$ foliating the manifold $\mathcal{M}$ and where any maximal causal curve intersects every hypersurface Σ_t exactly once. These hypersurfaces are called Cauchy surfaces and the spacetime is said to be foliated by those Cauchy surfaces if $\mathcal{M} = \bigcup_t \Sigma_t$. The property of global hyperbolicity ensures that the formulation of initial value problems is well-defined and that no closed timelike curves exist. Global hyperbolicity furthermore enables the definition of the conjugate momenta π_a of a classical field ψ_a with Lagrangian density $\mathcal{L}$, i.e.

$$\pi_a = \frac{\partial \mathcal{L}}{\partial(n^\mu \nabla_\mu \psi_a)}\,, \tag{2.60}$$

in a coordinate invariant way by using the timelike normal vectors n_μ of the Cauchy foliation. Using these canonical momenta one can impose the usual (anti-)commutation relations on the field theory. Next, in order to define the notion of particles or field quanta the field is decomposed as

$$\psi_a(x) = \sum_J \left(a_J \xi_{aJ}(x) + b_J^\dagger \epsilon_{aJ}(x) \right)\,, \tag{2.61}$$

in terms of ladder operators $(a_J^{(\dagger)}, b_J^{(\dagger)})$ and a basis of mode functions $\{(\xi_J, \epsilon_J)\}_J$ labelled by the quantum numbers J characterising the state of the associated particle. The mode functions solve the underlying field equations, i.e. for example the Klein–Gordon, Dirac or Maxwell equations in curved spacetime. In this section, we mainly focus on fermions in curved spacetime as we are interested in the behaviour of neutrinos in a curved background in Chapter 5. Of course neutrinos obey the Dirac equation in curved spacetime given by

$$\left(i\gamma^\mu_{ab}(x)[\delta_{bc}\partial_\mu + \Gamma_{bc\mu}(x)] - \delta_{ac} m \right) \psi_c(x) = 0\,, \tag{2.62}$$

[6]For field quantisation in a non-globally hyperbolic spacetime see for example Reference [35].

where $\gamma^\mu(x) = \gamma^\alpha e_\alpha{}^\mu(x)$ are the curved spacetime gamma matrices inherited from flat spacetime by virtue of the frame fields e_α defining an orthonormal frame at every point in spacetime. Moreover, Γ_μ is the so-called spin connection defined by

$$\Gamma_\mu(x) := \frac{1}{8}[\gamma^\alpha, \gamma^\beta] e_\alpha{}^\nu(x) g_{\nu\rho}(x) \nabla_\mu e_\beta{}^\rho(x)\,, \tag{2.63}$$

and the mode functions are chosen such that they form an orthonormal basis (ONB)

$$\langle \xi_J, \xi_K \rangle = \langle \epsilon_J, \epsilon_K \rangle = \delta_{JK}\,, \qquad\qquad \langle \xi_J, \epsilon_K \rangle = 0\,, \tag{2.64}$$

with respect to the scalar product

$$\langle u, v \rangle := \int\limits_{\Sigma_t} \bar{u}(x)\gamma^\mu(x)v(x)\,\mathrm{d}\sigma_\mu(x)\,, \qquad\qquad \mathrm{d}\sigma_\mu(x) := n_\mu(x)\sqrt{|h(x)|}\,\mathrm{d}^3\vec{x}\,, \tag{2.65}$$

on any Cauchy surface Σ_t with metric h_{ij} induced by g. As long as both arguments of the scalar product fulfil the equations of motion of the field, the scalar product is invariant under the change of the Cauchy surface Σ_t.

Because there exists an infinite number of sets of mode solutions, the first question that arises is which set to choose. In Minkowski spacetime one naturally chooses those modes closely associated with the Poincaré symmetry and the usual Cartesian coordinates

$$\xi_{\vec{p}s}(x) = u_s(\vec{p})\frac{e^{-ip_\mu x^\mu}}{\sqrt{(2\pi)^3 2p^0}}\,, \qquad\qquad \epsilon_{\vec{p}s}(x) = v_s(\vec{p})\frac{e^{ip_\mu x^\mu}}{\sqrt{(2\pi)^3 2p^0}}\,, \tag{2.66}$$

with spin s, momentum $\vec{p}$, energy $p^0 = \sqrt{|\vec{p}|^2 + m^2}$ and the basis spinors $u_s(\vec{p})$ and $v_s(\vec{p})$. The modes ξ (ϵ) are said to be positive (negative) frequency since they fulfil the relations

$$\frac{\partial \xi_{\vec{p}s}}{\partial t}(x) = -ip^0 \xi_{\vec{p}s}(x)\,, \qquad\qquad \frac{\partial \epsilon_{\vec{p}s}}{\partial t}(x) = ip^0 \epsilon_{\vec{p}s}(x)\,. \tag{2.67}$$

Positive frequency modes directly correspond to particle excitations of the field whereas negative frequency excitations correspond to antiparticles. The vacuum state of this mode construction is Poincaré-invariant, and hence, all inertial observers agree on the same notion of particles. This means that if one observer measures a fixed number of particles, any other inertial observer will see the same amount of field quanta. In curved spacetime, however, Poincaré symmetry is absent in general and the notions of positive and negative frequencies become observer-dependent in that they depend on the flow of time an observer experiences. This is formalised by the general positive and negative frequency conditions [23]

$$\frac{\nabla \xi_J}{\mathrm{d}\tau}(c(\tau)) = -i\omega_J \xi_J(c(\tau))\,, \qquad\qquad \frac{\nabla \epsilon_J}{\mathrm{d}\tau}(c(\tau)) = -i\omega_J \epsilon_J(c(\tau))\,, \tag{2.68}$$

where the covariant derivative is taken along the world line c of the observer. Here, ω_J is the energy or frequency associated with a single-particle state with quantum numbers J. The

Fock space of any observer would now be constructed from that set[7] of modes fulfilling the conditions in Equations (2.68). Thereby, these relations establish a direct link between the state of motion of an observer and their particle concept. In the absence of any symmetry it is then not guaranteed that two observers following different worldlines will define the same or equivalent notions of particles, as we will see below.

The main reason for the unintuitive nature of the particle concept is that usually one thinks of particles as localised entities that should behave the same way in flat and curved spacetime due to the equivalence principle. This, however, is not true since particles of definite momenta or energy are highly delocalised and are in one-to-one correspondence to the globally defined mode solutions, ξ and ϵ, of the underlying equations of motion of the field. Only as soon as we consider sufficiently localised wave packets (WPs) of particles the global structure of the manifold becomes less important. To construct those WPs, we still need to specify which observer is measuring the particle and two different observers, O and $\tilde{O}$, would in general find differing WPs for the same state, depending on the mode decomposition corresponding to their flow of time.

The translation between two different Fock space constructions of observers, O and $\tilde{O}$, based on the associated modes, (ξ, ϵ) and $(\tilde{\xi}, \tilde{\epsilon})$, is facilitated by a so-called Bogoliubov transformation [36]

$$\xi_J = \sum_\sigma \left[\alpha_{J\sigma}\tilde{\xi}_\sigma + \beta_{J\sigma}\tilde{\epsilon}_\sigma\right] , \tag{2.69}$$

$$\epsilon_J = \sum_\sigma \left[\alpha^*_{J\sigma}\tilde{\epsilon}_\sigma - \beta^*_{J\sigma}\tilde{\xi}_\sigma\right] , \tag{2.70}$$

where α and β are the (fermionic) Bogoliubov coefficients fulfilling the relation

$$\delta_{JK} = \sum_\sigma \left(\alpha_{J\sigma}\alpha^*_{K\sigma} + \beta^*_{J\sigma}\beta_{K\sigma}\right) . \tag{2.71}$$

The decomposition of the same quantum field in terms of two different sets of modes and ladder operators fulfilling the usual (anti-)commutation relations immediately dictates the Bogoliubov transformation properties of the ladder operators, i.e.

$$a_j = \sum_\sigma \left[\alpha^*_{j\sigma}\tilde{a}_\sigma + \beta^*_{j\sigma}\tilde{b}^\dagger_\sigma\right] , \tag{2.72}$$

$$b_j = \sum_\sigma \left[\alpha^*_{j\sigma}\tilde{b}_\sigma - \beta^*_{j\sigma}\tilde{a}^\dagger_\sigma\right] . \tag{2.73}$$

This implies that the vacuum state of observer $\tilde{O}$ is not necessarily free of field quanta in terms of the particle concept of observer O, i.e.

$$\langle\tilde{0}|\, n_j \,|\tilde{0}\rangle = \langle\tilde{0}|\, a^\dagger_j a_j \,|\tilde{0}\rangle = \sum_\sigma |\beta_{j\sigma}|^2 . \tag{2.74}$$

[7] Their still might be several sets of mode functions fulfilling these conditions for the given observer, but they all give rise to the same definition of particles characterised by different, equivalent sets of quantum numbers in the respective constructions.

As already mentioned above, for the simple example of Minkowski spacetime global Poincaré-invariance ensures that the family of inertial observers defines equivalent notions of particles and in particular agrees on the same unique and universal vacuum state. This is because the inertial flow of time is related to the timelike Killing field $T = \partial_t$, and by symmetry, positive and negative frequencies have the same meaning for all inertial observers. However, the situation is already different in flat spacetime when extending the class of considered observers to those accelerated in the x direction, for example. These observers experience a different flow of time defined by the Killing field $\tilde{T} = x\partial_t - t\partial_x$. The field $\tilde{T}$ leads to entirely different mode solutions by virtue of Equation (2.68). Consequently, the notion of particles an accelerated observer would define follows from an inequivalent Fock space construction based on the *non-inertial* modes $\tilde{\xi}_\sigma$ and $\tilde{\epsilon}_\sigma$. The physical consequence of this inequivalence is that even if all inertial observers agree that no particles are present, i.e. the quantum field is in the Minkowski vacuum state, all accelerated observers would see a thermal bath of particles as their vacuum state is different from the Minkowskian one. This is called the Unruh effect [37–39].

In general curved spacetimes it is far from guaranteed that two observers define equivalent notions of particles which is mainly because of the lack of global Poincaré symmetry or any symmetry at all. Especially in spacetimes with strongly time varying gravitational fields, i.e. spacetimes lacking time-like Killing fields, no pair of macroscopically separated observers define the same notions of particles. A possible example of such a scenario is a spacetime going through a phase of inflation. The particles observer $\tilde{O}$ then sees, although observer O experiences an empty Universe, are said to be produced gravitationally.

2.3 Neutrino Oscillations

Now that we have discussed the broad theoretical foundations on which this thesis is based, we narrow down the scope to the more specific topics of this work concerning the theory and applications of neutrino oscillations. The first theoretical considerations of neutrino oscillations date back to 1957 by Pontecorvo [40, 41] who was looking for a phenomenon in the lepton sector similar to neutral kaon oscillations. Later on in 1962 Maki, Nakagawa and Sakata [42] considered the possibility of non-diagonal weak interactions and flavour mixing. Pontecorvo then applied his formalism of neutrino oscillations to the neutrino flavour system [43]. This formalism predicted the phenomenon of a reduced solar electron neutrino flux at Earth that came to be known as the solar neutrino problem. This problem first emerged in the mid 1960's in the Homestake mine experiment conducted by Ray Davis Jr. et al. to measure the flux of solar neutrinos. It was found that roughly only one third of the expected flux of electron neutrinos has been measured in this experiment [44]. The final evidence for neutrino oscillations was brought forward about forty years later by the groups of Kajita and McDonald in the Super-Kamiokande experiment [45] and the Sudbury Neutrino Observatory (SNO) [46], respectively.

This phenomenon can be consistently described if neutrinos indeed are massive particles. Since this has become the accepted explanation for the occurrence of neutrino oscillations, it also

represents direct evidence for the incompleteness of the lepton sector of the SM, as no mass generation mechanism for neutrinos exists within the SM, as already mentioned in Section 2.1. The most general Lagrangian in terms of chiral fields describing neutrino masses can be written as

$$\begin{aligned}\mathcal{L}_{\nu,\text{mass}} = &-\frac{1}{2}\sum_{j=1}^{3}\sum_{k=1}^{3}(\overline{\nu_L^{jc}} m_{a,jk}^{M} \nu_L^k + \overline{\nu_L^j} m_{a,jk}^{M*} \nu_L^{kc}) \\ &- \sum_{j=1}^{n_s}\sum_{k=1}^{n_s}(\overline{\nu_R^{jc}} m_{s,jk}^{M} \nu_R^k + \overline{\nu_R^j} m_{s,jk}^{M*} \nu_R^{kc}) \\ &- \sum_{j=1}^{3}\sum_{k=1}^{n_s}(\overline{\nu_L^j} m_{jk}^{D} \nu_R^k + \overline{\nu_R^k} m_{jk}^{D*} nu_L^j)\,,\end{aligned} \tag{2.75}$$

where we have introduced n_s right-handed, SM singlet fields ν_R^j in addition to the three SM neutrinos ν_L^j and we have written the sum over generation indices explicitly. Moreover, we have introduced the particle–antiparticle conjugation[8] operation

$$\psi^c := \mathcal{C}\bar{\psi}^T\,, \tag{2.76}$$

where the matrix $\mathcal{C}$ can be defined as $\mathcal{C} := i\gamma^2\gamma^0$ in the chiral representation. In contrast to ν_L, the number of ν_R fields is not constrained by demanding the SM to be anomaly free as the ν_R are SM singlets. Hence, they are often also called sterile neutrinos. In the same spirit, the ν_L fields are called active neutrinos, hence the subscripts s and a attached to the respective Majorana mass matrices, m_s^M and m_a^M.

The Lagrangian defined in Equation (2.75) contains two different types of fermion mass terms, Majorana and Dirac mass terms. While Dirac mass terms always include two distinct fermion fields of opposite chiralities, Majorana mass terms can also be written with only a single chiral field. The mass matrices appearing in Equation (2.75) are $m_a^M \in \mathbb{C}^{3\times3}$, $m_s^M \in \mathbb{C}^{n_s\times n_s}$ and $m^D \in \mathbb{C}^{3\times n_s}$, where the first two are complex symmetric and the latter one is an arbitrary complex matrix. A crucial difference between Majorana and Dirac mass terms is that Majorana mass terms, involving only one type of chiral field, explicitly break all $U(1)$ symmetries. Consequently, the affected particles cannot be charged under any gauge interaction with this symmetry group, like e.g. electromagnetism. Furthermore, all mass terms including active neutrinos must be generated during electroweak SSB since otherwise they would break the SM gauge symmetry explicitly.

As in the case of quarks in the SM we need to diagonalise the kinetic term of the neutrino Lagrangian in order to find the propagating, physical states of definite mass. To do so, we collect all left- and right-chiral neutrino fields in the vectors $\vec{\nu}_L$ and $\vec{\nu}_R$, respectively, and combine them into a single left-handed vector $\vec{n}_L := (\vec{\nu}_L, \vec{\nu}_R^c)$. Afterwards, using the properties

[8] Note that this is not the same as charge conjugation since particle–antiparticle conjugation also flips the chirality of a chiral fermion field.

of $\mathcal{C}$, we can rewrite the Lagrangian in Equation (2.75) to the form

$$\mathcal{L}_{\nu,\text{mass}} = \frac{1}{2}\vec{n}_L^T \mathcal{C}^\dagger \hat{M} \vec{n}_L + \frac{1}{2}\vec{n}_L^\dagger \mathcal{C} \hat{M}^* \vec{n}_L^* \,, \qquad \hat{M} := \begin{pmatrix} m_a^M & m_D \\ m_D^T & m_s^M \end{pmatrix} . \tag{2.77}$$

In this formulation the neutrino mass Lagrangian assumes the form of a collection of Majorana mass terms reflecting the fact that a Dirac mass term is only a special case of a Majorana mass term coupling two different chiral fields to each other with the same mass. Again, $\hat{M}$ is complex symmetric and can be brought to a diagonal form using a single unitary transformation $\hat{M}_D = U^T \hat{M} U$, where $\hat{M}_D$ is the diagonal matrix with positive semi-definite diagonal entries m_i^ν. These diagonal entries correspond to the absolute values of the eigenvalues of $\hat{M}$. The neutrino fields of definite mass can, thus, be written as

$$\tilde{\nu}_{Lj} = \sum_{a=1}^{n_f} U_{aj}^* n_{La} \,, \tag{2.78}$$

and we can build the corresponding massive Majorana spinors $\tilde{\nu}_j := \tilde{\nu}_{Lj} + \tilde{\nu}_{Lj}^c$. Here, $n_f = 3 + n_s$ is the total number of chiral flavour states and the leptonic mixing matrix U is called the Pontecorvo–Maki–Nakagawa–Sakata (PMNS) matrix. Finally the Lagrangian in Equation (2.75) becomes

$$\mathcal{L}_{\nu,\text{mass}} = -\frac{1}{2}\sum_{k=1}^{n_f} m_k^\nu \bar{\tilde{\nu}}_k \tilde{\nu}_k \,. \tag{2.79}$$

Here, we see that in the general Dirac *and* Majorana mass scenario, we get as many mass eigenfields as we have chiral flavour eigenfields, i.e. $3 + n_s$. In the limit of vanishing Majorana masses and if $n_s = 3$, one can combine the six Majorana mass eigenfields $\tilde{\nu}_j$ into three Dirac fields. Only in this scenario will neutrino mass eigenstates be of the Dirac type.

As an explanation of the smallness of the three lightest neutrino masses, there exist several so-called seesaw models [47–50] featuring a sterile Majorana mass matrix m_s^M with entries several orders of magnitude larger than those of the other mass matrices. As we are primarily interested in the consequences of neutrino masses, rather than in their origin, we will not consider these models in more detail here.

Assuming that we have already brought the charged lepton mass matrices to a diagonal form and have appropriately redefined the active neutrino flavour eigenfields to absorb the charged lepton mixing matrices[9] before transforming the neutrino mass Lagrangian, the weak interaction Lagrangian becomes

$$\begin{aligned} \mathcal{L}_{\text{weak}}^\nu = {} & \frac{g}{2\cos(\theta_W)} Z_\mu \sum_{a=e,\mu,\tau} \sum_{j,k=1}^{3+n_s} U_{ak} U_{aj}^* \bar{\tilde{\nu}}_j \gamma^\mu P_L \tilde{\nu}_k \\ & + \frac{g}{\sqrt{2}} \sum_{a=e,\mu,\tau} \sum_{j=1}^{3+n_s} \left(W_\mu^- U_{aj} \bar{e}_a \gamma^\mu P_L \tilde{\nu}_j + W_\mu^+ U_{aj}^* \bar{\tilde{\nu}}_j \gamma^\mu P_L e_j \right) . \end{aligned} \tag{2.80}$$

[9] One can also perform the field redefinitions of charged and neutral leptons simultaneously, as shown for the up- and down-type quarks in Section 2.1. In this case, the PMNS matrix is a combination of U and V_L^e, but the procedure is fully equivalent to the approach discussed here.

Note that if U is a 3×3 matrix, the neutral current interaction is form-invariant under this change of basis, but the CC interaction always contains the leptonic mixing matrix as we have already seen in the quark sector. This is what gives rise to the phenomenon of neutrino flavour oscillations, i.e. the main topic of this thesis: A neutrino produced in CC interactions is in a state of definite flavour $|\nu_a\rangle$ corresponding to a coherent superposition of mass eigenstates. During propagation the mass eigenstates evolve with their individual time evolution phases changing the admixture of the mass eigenstates during propagation. Detection of the neutrino again proceeds via a CC process and the measured flavour can be different from that of the original neutrino. As the flavour transition probabilities oscillate over the length the neutrinos have travelled, this phenomenon is called neutrino (flavour) oscillations.

Using the simple reasoning above, one can quickly derive the standard expression for the flavour transition probabilities in the case of ultra-relativistic neutrinos: The produced and evolved flavour eigenstate is described by:

$$|\nu_a(T)\rangle := e^{-i\hat{H}T}|\nu_a\rangle = \sum_j U^*_{aj} e^{-iE_jT}\big|\nu_j\big\rangle \,, \tag{2.81}$$

where the energy eigenvalues of the free neutrino Hamiltonian are

$$E_j = \sqrt{|\vec{p}|^2 + m_j^2} \approx |\vec{p}| + \frac{m_j^2}{2|\vec{p}|} \,. \tag{2.82}$$

The probability to detect a flavour eigenstate ν_b after a distance $L \sim T$ then reads

$$P_{ab}(L) := \langle \nu_b | \nu_a(L)\rangle = \left| \sum_j U_{bj} e^{-i\frac{m_j^2 L}{2|\vec{p}|}} U^*_{aj} \right|^2 \,. \tag{2.83}$$

Although this expression describes neutrino flavour transitions in vacuum to very high accuracy, the derivation given above can only be regarded as an intuitive way to memorise the oscillation formula as it glosses over several crucial details and inconsistencies that are important to understand under which conditions the standard oscillation formula is actually applicable. Of course there is some truth to the above reasoning as it produces the correct result and also catches the main conceptual points important to neutrino oscillations. The main questions that arise when taking a closer look at the derivation above are:

1. Are neutrino states of definite flavour well-defined?
2. When are neutrinos actually produced and detected as a coherent superposition of mass eigenstates?
3. Under which conditions can we define a universal flavour transition probability that is independent of the details of the neutrino production and detection process?
4. Should we assume the neutrino state to be produced and detected with definite momentum (as assumed above) or definite energy?

5. How can a plane wave (definite momentum state) be localised in space such that the conversion $L \sim T$ is justified?

6. If neutrinos are localised on the other hand: How do the inherent position and momentum space uncertainties of the WPs affect the oscillation formula?

It turns out that in order to answer the first three questions consistently, we have to consider the full neutrino production–propagation–detection process from first principles in a QFT based approach [51–55]. As these questions are of minor importance for this thesis, we only briefly discuss the QFT approach to neutrino oscillations in Section 2.3.1. Assuming that there are situations where a universal flavour oscillation probability is well-defined, it suffices to consider neutrinos as coherent superpositions of freely propagating mass eigenstate WPs in order to answer questions four to six. This is done in Section 2.3.2. Furthermore, in Section 2.3.3, we discuss under which circumstances neutrino flavour transitions are well described by considering the neutrino flavours as a simple quantum mechanical n level system with an $n \times n$ Hamiltonian $\hat{H}$ as used for the naive derivation shown above. In doing so, we also see how this effective Hamiltonian changes as neutrinos traverse a medium, and how other effects, like decoherence due to inelastic scattering, can be described in this framework.

2.3.1 Quantum Field Theory Approach to Neutrino Oscillations

In order to give a meaningful definition of the previously discussed neutrino flavour transition probability, we first need to take a step back and consider how these flavour transitions are studied experimentally. The flavours of the produced and detected neutrinos are determined from the flavours of the charged leptons that accompany the respective CC production or detection process. This is due to the fact that neutrinos themselves are invisible to the detection apparatus, which usually relies on the measurement of an EM signal. Therefore, the most consistent approach to the study of neutrino flavour transitions is considering the total interaction rate of the full production, propagation and detection process, $\mathrm{d}\Gamma_{ab}$.

In the QFT approach, only the external particles producing and detecting the neutrino are considered as initial and final WP states, while the neutrino is treated as an internal mediator particle, cf. Figure 2.1. This is why it is often also called the external WP approach to neutrino oscillations. For example, if a charged lepton ℓ_a^- scatters off of a proton, it may produce a neutron in combination with a neutrino. The neutrino would then escape the production site and travel a macroscopic distance towards a prepared detector. There, the incoming neutrino could interact with a neutron from an atomic nucleus, producing a proton and a charged lepton ℓ_b^- that can be detected via its Cherenkov radiation, i.e.

$$\underbrace{\boxed{p + \ell_a^- \to n}}_{\text{external particles}} + \nu_a \longrightarrow \nu_b + \underbrace{\boxed{n \to p + \ell_b^-}}_{\text{external particles}} . \tag{2.84}$$

In the language of Figure 2.1, Equation (2.84) translates to:

Production Initial State $p_1^{\text{in}} = p$, $p_2^{\text{in}} = \ell_a^-$ and $n_I = 2$

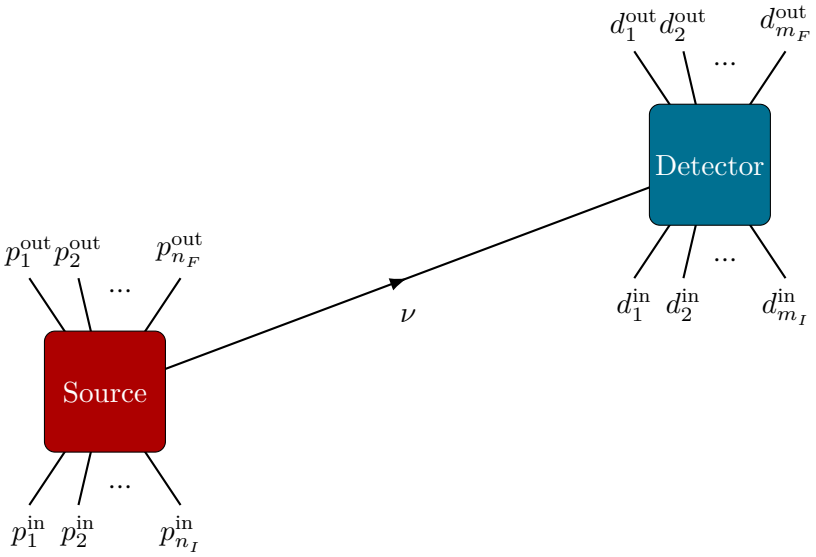

Figure 2.1: Diagrammatic representation of the neutrino production–propagation–detection process.

Production Final State $p_1^{\text{out}} = n$ and $n_F = 1$

Detection Initial State $d_1^{\text{in}} = n$ and $m_I = 1$

Detection Final State $d_1^{\text{out}} = p$, $d_2^{\text{out}} = \ell_b^-$ and $m_F = 2$

If we assume these external particles to be precisely localised in momentum space, i.e. to be well represented by plane waves, the neutrino produced in this reaction would have definite energy *and* momentum, and therefore, also its mass would be precisely determined. It is hence mandatory to take a more realistic but also more complicated approach by defining the external initial and final state particles as WPs.

In the most general case, the full initial and final states of a process, as depicted in Figure (2.1), are given by

$$|I_a, \text{in}\rangle := \prod_{A=1}^{n_I} \underline{a}^\dagger_{\text{in}}(p_A^{\text{in}}, \vec{Q}_A, X_A^{\text{S}_I}) \prod_{B=1}^{m_I} \underline{a}^\dagger_{\text{in}}(d_B^{\text{in}}, \vec{Q}'_B, X_B^{\text{D}_I}) \, |0, \text{in}\rangle \ , \tag{2.85}$$

$$|F_b, \text{out}\rangle := \prod_{C=1}^{n_F} \underline{a}^\dagger_{\text{out}}(p_C^{\text{out}}, \vec{K}_C, X_C^{\text{S}_F}) \prod_{D=1}^{m_F} \underline{a}^\dagger_{\text{out}}(d_D^{\text{out}}, \vec{K}'_D, X_D^{\text{D}_F}) \, |0, \text{out}\rangle \ , \tag{2.86}$$

where we define the effective WP in and out ladder operators as

$$\underline{a}^\dagger_{\text{out/in}}(\psi, \vec{P}, X) := \int \mathrm{d}^3\vec{p} \, \phi_\psi(\vec{p}, \vec{P}) e^{ipX} a^\dagger_{\psi,\text{out/in}}(\vec{p}) \, , \tag{2.87}$$

where the underscore indicates that a WP state instead of a plane wave state is created. The creation operator in Equation (2.87) produces a particle of species ψ at $t \to \pm\infty$ with

momentum space WP ϕ_ψ centered around the mean momentum $\vec{P}$ by acting on the respective in and out vacua $|0, \text{in}\rangle$ and $|0, \text{out}\rangle$. The momentum space WP in the adopted normalisation convention is of the form

$$\phi_\psi(\vec{p}, \vec{P}) = \frac{\varphi_\psi(p, P)}{\sqrt{(2\pi)^3 2E_p}}\,, \tag{2.88}$$

where φ is a Lorentz-invariant form factor normalised such that the WP states have unit norm[10] in any inertial frame of reference. Moreover, we include a spacetime translation phase into the definition of $\underline{a}^\dagger$ such that the position space wave function of the particle is localised at $\vec{X}$ at time X^0. In this way we are able to encode the information of the coordinates of the neutrino source and detector into the states making sure that for example only those particles participating in the neutrino detection overlap in the detector.

The scattering amplitude for the full process is, as usual, simply given by the overlap of the in and out states that we have just defined, i.e.

$$\mathcal{A}_{ab}(X_\text{S}, X_\text{D}) := \langle F_b, \text{out}|I_a, \text{in}\rangle\ . \tag{2.89}$$

Assuming neutrino instead of antineutrino exchange, the general neutrino production–propagation–detection process can be decomposed as (cf. Appendix A.2)

$$\begin{aligned}\mathcal{A}_{ab} = \sum_j U^*_{aj} U_{bj} \iint \mathrm{d}^4 z\, \mathrm{d}^4 y\, \mathbb{V}_\text{D}(z) \mathbb{V}_\text{S}(y) \\ \times \tilde{M}_\text{D}(\{Q'_B\}, \{K'_D\}) S_j(z-y) \tilde{M}_\text{S}(\{Q_A\}, \{K_C\})\,,\end{aligned} \tag{2.90}$$

where $\tilde{M}_\text{S/D}$ are the matrix elements of the neutrino production and detection sub-processes, *without* the neutrino spinors, evaluated at the mean momenta of the external particles and S_j is the propagator of the j-th neutrino mass eigenstate. Furthermore, the overlap volume functions $\mathbb{V}_\text{S/D}$ are given by the products of position space WPs of the external particles, see Appendix A.2 for the explicit expressions. They encode the information about the spacetime regions where the external particles overlap in the source and detector, respectively, and depend on the initial average spacetime coordinates $X_E^{\text{S/D}_{I/F}}$ as well as the mean momenta of the external particles. Therefore, the overlap volumes determine whether the external particles indeed scatter off of each other to produce a neutrino or if they miss each other. Moreover, we define the mean impact points of external particles in the source and detector by

$$X^\mu_\text{S/D} := \int \mathrm{d}^4 x\, \mathbb{V}_\text{S/D}(x) x^\mu\,. \tag{2.91}$$

These points, hence, correspond to the mean production and detection vertices of the neutrino.

Before we continue our discussion, we first briefly comment on neutrino propagation in matter. The QFT formalism we are considering at the moment is not only capable of describing neutrino

[10] This corresponds to the (anti-)commutation relations $[\underline{a}_\text{out/in}(\psi, \vec{P}, X), \underline{a}^\dagger_\text{out/in}(\psi, \vec{P}, X)]_\pm \equiv 1$.

oscillations in vacuum but also in a medium. In the latter case the neutrino propagators appearing in Equation (2.90) need to be replaced by the finite temperature propagators [56] obeying the Schwinger–Dyson equation,

$$\left[\not{\partial}_x - MP_R - M^\dagger P_L\right] S(x,y) - \int \mathrm{d}^4 z\, \Sigma(x,z) S(z,y) = \delta^4(x-y)\mathbb{1}\,, \tag{2.92}$$

in the flavour basis. Here, $\Sigma(x,z)$ is the thermal self energy whose real part corresponds to forward scattering processes in matter giving rise to an altered index of refraction for neutrinos and thereby induces effective masses. The imaginary part of $\Sigma(x,z)$, in contrast, encodes inelastic scattering processes of neutrinos into different particle states or vice versa, and therefore, describes (hypothetical) neutrino decay, neutrino attenuation in matter or neutrino production for example due to the decay of heavy leptons. Moreover, M is the neutrino mass matrix in the flavour basis. In the following, we mainly focus on the QFT treatment of neutrino oscillations in vacuum, but we come back to neutrino oscillations in matter in Section 2.3.3 and discuss the consequences of Equation (2.92) for the effective quantum mechanical model of neutrino oscillations that we develop in this section and Section 2.3.2.

The vacuum neutrino propagator can be expressed in terms of the neutrino and antineutrino mode functions, ξ and ϵ, as

$$S_j(z,y) = \sum_{s=\pm 1/2} \int \mathrm{d}^3\vec{p} \left[\Theta(z^0-y^0)\xi_{j;s\vec{p}}(z)\bar{\xi}^j_{j;s\vec{p}}(y) - \Theta(y^0-z^0)\epsilon^j_{j;s\vec{p}}(y)\bar{\epsilon}^j_{j;s\vec{p}}(z)\right], \tag{2.93}$$

where j is the mass eigenstate index, s is the spin polarisation of the neutrino and $\vec{p}$ its momentum. We use this abstract form of the neutrino propagator, that is also valid in curved spacetime QFT, in order to prepare our considerations of neutrino oscillations in curved spacetime in Chapter 5. Moreover, the propagator representation in Equation (2.93) clearly distinguishes between neutrino and antineutrino contributions and, thus, is especially suitable to motivate the internal WP approach to neutrino oscillations. In contrast to the external WP approach, the flavour transition amplitude in the internal WP approach is derived directly from the overlap of freely propagating, effective neutrino WP states. The *internal* neutrino line in Figure 2.1 is, thus, assumed to become on-shell and the production and detection dynamics are encoded within the corresponding neutrino WPs. As we discuss in more detail in Appendix A.3, this is well justified since the spatially macroscopic separation of the production and detection volumes indeed forces the internal neutrino state to go on-shell, leading to a strong suppression of the antiparticle contribution[11] of the neutrino propagators within the amplitude in Equation (2.90).

Moreover, as discussed in Section 2.2.2 in general an observer chooses a set of modes associated with the flow of time in their own rest frame. Since in the current scenario we deal with two observers, one at the neutrino source (O_S) and one at the neutrino detection site (O_D), using a single mode decomposition as in Equation (2.93) does not give a meaningful representation of

[11] This only holds in case the external particles are such that a neutrino instead of an antineutrino is expected to be exchanged. In the opposite case, the structure of the amplitude in Equation (2.90) reverses and only the antiparticle contribution from the propagator S_j contributes.

the experimental situation as we make the transition to curved spacetime. Instead, we should express the production process and the produced neutrino in terms of the mode functions ξ^{S} used by the source-bound observer O_{S} and, analogously, we should use the respective detection modes ξ^{D} to describe the detection process as well as the detected neutrino state. In the (local) inertial frames $z^{\mu}_{\mathrm{S/D}}$ of these observers, the respective modes should then (approximately) reduce to the usual expressions

$$\xi^{\mathrm{S/D}}_{j;s\vec{p}}(z_{\mathrm{S/D}}) = u_{j;s}(\vec{p})\frac{e^{-ip_{\mu}z^{\mu}_{\mathrm{S/D}}}}{\sqrt{(2\pi)^3 2p^0}}\,, \qquad \epsilon^{\mathrm{S/D}}_{j;s\vec{p}}(z_{\mathrm{S/D}}) = v_{j;s}(\vec{p})\frac{e^{ip_{\mu}z^{\mu}_{\mathrm{S/D}}}}{\sqrt{(2\pi)^3 2p^0}}\,, \tag{2.94}$$

normalised according to Equation (2.64). For inertial observers in Minkowski spacetime the different modes ξ, ξ^{S} and ξ^{D} are of course equivalent. The only difference between them is in which coordinate system they assume the simple form given in Equation (2.94). In case of the simple example of two inertial observers, O_{S} and O_{D}, at rest with respect to each other, the respective source and detector modes become

$$\xi^{\mathrm{S/D}}_{j;s\vec{p}}(x) = u_{j;s}(\vec{p})\frac{e^{-ip_{\mu}(x^{\mu}-X^{\mu}_{\mathrm{S/D}})}}{\sqrt{(2\pi)^3 2p^0}}\,, \tag{2.95}$$

within the arbitrary inertial frame x^{μ} where $X^{\mu}_{\mathrm{S/D}}$ represent the origins of the local inertial coordinate frames $z^{\mu}_{\mathrm{S/D}}$. We have chosen these origins to coincide with the average neutrino production and detection vertices.

Under the assumption of negligible gravitational particle production[12] we can use the completeness relation of the particle modes $\xi^{\mathrm{S/D}}_{j}$ and that particles and antiparticles of different mode constructions do not mix and get (cf. Appendix A.3)

$$\mathcal{A}_{ab} \approx \Theta(X^0_{\mathrm{D}} - X^0_{\mathrm{S}}) \sum_j U^*_{aj}U_{bj} \sum_{ss'} \iint \mathrm{d}^3\vec{p}\,\mathrm{d}^3\vec{p}\,'\, \Phi^{\mathrm{D}*}_{j;s}(\vec{p})\Phi^{\mathrm{S}}_{j;s'}(\vec{p}\,')\langle \xi^{\mathrm{D}}_{j;s\vec{p}}, \xi^{\mathrm{S}}_{j;s'\vec{p}\,'}\rangle\,, \tag{2.96}$$

with the effective neutrino WPs $\Phi^{\mathrm{S}}_{js'}$ and $\Phi^{\mathrm{D}}_{js'}$, that can be written as

$$\Phi^{\mathrm{S}}_{j;s'}(\vec{p}\,') := \int \mathrm{d}^4x\, \mathbb{V}_{\mathrm{S}}(x)\bar{\xi}^{\mathrm{S}}_{j;s'\vec{p}\,'}(x)\tilde{M}_{\mathrm{S}}(\{Q_A\},\{K_C\})\,, \tag{2.97}$$

$$\Phi^{\mathrm{D}*}_{j;s}(\vec{p}) := \int \mathrm{d}^4x\, \mathbb{V}_{\mathrm{D}}(x)\tilde{M}_{\mathrm{D}}(\{Q_A\},\{K_C\})\xi^{\mathrm{D}}_{j;s\vec{p}}(x)\,. \tag{2.98}$$

Apart from the mode decomposition of the neutrino propagator and the transition to the source and detector mode description, our derivation of the amplitude heavily relied on the assumption of a flat background spacetime. Thus, all expressions obtained so far are only strictly valid in Minkowski spacetime for inertial observers, O_{S} and O_{D}. Nevertheless, we expect these expressions to also carry over to curved spacetime since the rules of Lehmann–Symanzik–Zimmerman (LSZ)-reduction are very similar in QFT in curved spacetime compared to QFT in Minkowski spacetime [33]. Moreover, since the overlap functions $\mathbb{V}_{\mathrm{S/D}}$

[12] We discuss this topic in more detail in Chapter 5.

are strongly localised, evaluating the vertex integrals in the local inertial frames at the source and the detector are expected to result in equivalent expressions for the neutrino WPs as we have obtained them here.

Finally, by defining the one particle states for the observers, O_{S} and O_{D}, via the action of the ladder operators $a^{\mathrm{S/D}}_{j;s\vec{p}}$ associated with the $\xi^{\mathrm{S/D}}_{j;s\vec{p}}$ mode constructions on the respective free vacua $|0;\mathrm{S/D}\rangle$, i.e.

$$\left|\nu_j,\vec{p},s;\mathrm{S}\right\rangle := a^{\mathrm{S}\dagger}_{j;s\vec{p}}\,|0;\mathrm{S}\rangle\ , \qquad\qquad \left|\nu_j,\vec{p},s;\mathrm{D}\right\rangle := a^{\mathrm{D}\dagger}_{j;s\vec{p}}\,|0;\mathrm{D}\rangle\ , \tag{2.99}$$

we can express the flavour transition amplitude as

$$\begin{aligned}\mathcal{A}_{ab} \approx \Theta(X^0_{\mathrm{D}} - X^0_{\mathrm{S}}) \sum_j U^*_{aj}U_{bj} \sum_{\sigma,\sigma'} \iint \mathrm{d}^3\vec{p}\,\mathrm{d}^3\vec{p}\,' \\ \times \Phi^{\mathrm{D}*}_{js}(\vec{p})\Phi^{\mathrm{S}}_{js'}(\vec{p}\,')\left\langle\nu_j,\vec{p},s;\mathrm{D}\middle|\nu_j,\vec{p}\,',s';\mathrm{S}\right\rangle\ .\end{aligned} \tag{2.100}$$

Moreover, if source and detector are at rest with respect to each other, the scalar product of single-particle states is spin and momentum diagonal and incorporates the usual oscillation phase

$$\left\langle\nu_j,\vec{p},s;\mathrm{D}\middle|\nu_j,\vec{p}\,',s';\mathrm{S}\right\rangle = \delta_{ss'}\delta^{(3)}(\vec{p}-\vec{p}\,')e^{-ip_\mu(X_{\mathrm{D}}-X_{\mathrm{S}})^\mu}\ . \tag{2.101}$$

This proves the validity of the internal WP approach. We consider this formalism and the further evaluation of Equation (2.100) in more detail in the next section. Before we do so, we answer the first three questions from our list formulated at the end of the preceding section. Afterwards, we turn towards the precise definition of the neutrino flavour transition probability.

We begin by answering the first two questions: Are neutrino flavour states well-defined, and under which conditions are neutrinos produced as a coherent superposition of mass eigenstates? The simple answer to the first question is *no*. Flavour states would have ill-defined mass, and therefore, would not be suitable external states. Instead one can define them as effective states, i.e. as coherent superpositions of mass eigenstates in the sense of Equation (2.100). According to Equation (2.100) the exact admixture of mass eigenstates is *not* universal but depends on the production and detection mechanisms, in general. Only in the limit where all momentum space distributions for all mass eigenstates are approximately equal, i.e. $\Phi^{\mathrm{S/D}}_j \equiv \Phi^{\mathrm{S/D}}$, the commonly used relation,

$$|\nu_a\rangle = \sum_j U^*_{aj}\,|\nu_j\rangle\ , \tag{2.102}$$

is justified. This is the case only if the contributing mass eigenstates have quasi degenerate masses [53] compared to the mean neutrino energy, i.e. $m_j^2 - m_k^2 \ll E^2$, and if the production and detection coherence conditions are fulfilled. If, for example, very heavy neutrino mass eigenstates contribute to the flavour states such that some mass eigenstates are ultra-relativistic and some are non-relativistic, the associated effective neutrino WPs will differ significantly

from each other. Moreover, if the momentum space WPs of the external particles become too narrow, the coherence of the mass eigenstate superposition is strongly suppressed as not all mass eigenstates are allowed to be produced on the mass shell. This could happen, for example, due to precise final state measurements or initial state preparation. In this case, the corresponding effective neutrino WPs vanish as energy–momentum conservation at production and detection cannot be fulfilled.

Next, in order to answer the third question, i.e. to determine under which conditions a universal flavour transition probability P_{ab} can be defined, we need to compute the differential rate $\mathrm{d}\Gamma_{ab}$ of the full process. To this end, we consider the experimental situation again. Usually in neutrino oscillation experiments, many neutrino events are collected over the course of several years of data taking corresponding to many different external particle configurations in the source and the detector. Moreover, many of these external particles, taking part in neutrino production and detection, remain unobserved and often only a subset of the particles in the detector are measured directly to reconstruct the energy of the exchanged neutrino. Therefore, it is necessary to average the amplitude $\mathcal{A}_{ab}$, describing the production and detection of a single neutrino, over all possible external initial states and to sum over all unobserved final states. This procedure is called macroscopic averaging and is discussed in more detail in Appendix A.4 closely following Reference [54]. The key result, however, is simply that given the quasi degeneracy of neutrino masses the total rate can be factorised as [53, 54]

$$\mathrm{d}\Gamma_{ab} = \int \mathrm{d}E \int \mathrm{d}^3\vec{x}_\mathrm{S} \int \mathrm{d}^3\vec{x}_\mathrm{D}\, \frac{\Phi^\mathrm{S}(E,\vec{x}_\mathrm{S})}{4\pi|\vec{x}_\mathrm{D}-\vec{x}_\mathrm{S}|^2} P_{ab}(E,|\vec{x}_\mathrm{D}-\vec{x}_\mathrm{S}|)\,\mathrm{d}\sigma^\mathrm{D}\left(\vec{x}_\mathrm{D},E,\{\vec{K}'_D\}\right), \tag{2.103}$$

where Φ^S is the effective neutrino flux at the source and $\mathrm{d}\sigma^\mathrm{D}$ is the differential detection cross section. If the neutrino mass squared differences were non-negligible, the neutrino production and detection matrix elements as well as the neutrino mean momenta would differ significantly among the different mass eigenstates. In this case the production and detection dynamics can not be factorised out of the sum over the contributions of different mass eigenstate that is contained within the oscillation probability P_{ab}. Consequently, the validity of Equation (2.103) would break down. Therefore, only for quasi degenerate neutrino mass eigenstates and under the assumption of coherent neutrino production and detection, the universal flavour oscillation probability P_{ab} can be defined. In any other case, one needs to consider the full rate $\mathrm{d}\Gamma_{ab}$ in order to describe the probabilities of neutrino flavour transitions.

Finally, note that in the limit where the definition of an oscillation probability is well-defined, there exists a shortcut [53] to obtain an equivalent expression for P_{ab}: Starting with a simple parametrisation for the effective neutrino WPs in terms of the produced and detected mean momenta and the average source and detector coordinates, X_S and X_D, one can obtain P_{ab} by simply integrating the square of the amplitude in Equation (2.100) over the production and detection times, i.e.

$$P_{ab}(E;\vec{X}_\mathrm{S},\vec{X}_\mathrm{D}) = \frac{\int_0^{T_\mathrm{S}}\int_L^{L+T_\mathrm{D}} \mathrm{d}t_\mathrm{S}\,\mathrm{d}t_\mathrm{D}\,|\mathcal{A}_{ab}(E;X_\mathrm{S},X_\mathrm{D})|^2}{\sum_b \int_0^{T_\mathrm{S}}\int_L^{L+T_\mathrm{D}} \mathrm{d}t_\mathrm{S}\,\mathrm{d}t_\mathrm{D}\,|\mathcal{A}_{ab}(E;X_\mathrm{S},X_\mathrm{D})|^2}\,. \tag{2.104}$$

The additional normalisation of the result then enforces the unitarity condition, i.e.

$$\sum_b P_{ab} \equiv 1\,. \tag{2.105}$$

This ad hoc scheme is justified as the full treatment shows that in this case all production and detection related details simply factorise and cancel upon normalisation. With this last insight, we have finally set up everything necessary for the discussion of the internal WP approach in the next section. There we also take a closer look at the different decoherence effects arising due to the separation of neutrino WPs as well as at the precise quantification of the production and detection coherence conditions.

2.3.2 Internal Wave Packet Approach

In case the propagation process is approximately independent of the details of neutrino production and detection the flavour transition probability is well-defined and we can consider the free propagation of effective neutrino mass eigenstate WPs and extract the probability using the shorthand scheme defined by Equation (2.104). The neutrino WPs encode information about the production and detection process in this scenario, but all mass eigenstate WPs have to be approximately equal, as discussed in the last section.

In order to answer the remaining points four to six from our list of questions regarding the subtleties of the theory of neutrino oscillations, we now discuss an explicit example for a simple but robust model of propagating neutrino WPs and the resulting neutrino oscillation formula. We could have answered these questions of course already in the QFT based approach, but it is much more instructive to see the answers arise in the explicit examples in the following. However, we will frequently borrow some insights from the more fundamental QFT approach to keep our discussions on track.

The amplitude for the flavour transition is given in Equation (2.100) and we choose Gaussian momentum space WPs, as it is usually done in the Literature [57–60], for each mass eigenstate, i.e.

$$\phi_j^{\mathrm{S}}(\vec{p},\vec{P}_j) = \left(2\pi\sigma_{\mathrm{S}j}^2\right)^{-\frac{3}{4}} \exp\left(-\frac{1}{4}\frac{(\vec{p}-\vec{P}_j)^2}{\sigma_{\mathrm{S}j}^2}\right)\,, \tag{2.106}$$

$$\phi_j^{\mathrm{D}}(\vec{p},\vec{Q}_j) = \left(2\pi\sigma_{\mathrm{D}j}^2\right)^{-\frac{3}{4}} \exp\left(-\frac{1}{4}\frac{(\vec{p}-\vec{Q}_j)^2}{\sigma_{\mathrm{D}j}^2}\right)\,. \tag{2.107}$$

The neutrino WPs at the source are centered around the mean momentum $\vec{P}_j$ with momentum width $\sigma_{\mathrm{S}j}$, whereas the detected mass eigenstate momentum space WPs peak at $\vec{Q}_j$ with effective width $\sigma_{\mathrm{D}j}$. Moreover, for simplicity, we assume that each spin direction is equally likely and that the WPs are hence independent of the spin quantum number. A crucial point worth noticing here is that Gaussian WPs lead to Lorentz-invariant flavour transition amplitudes as shown, for example, in Reference [59].

Plugging the Gaussian WPs into the amplitude in Equation (2.100) yields

$$\begin{aligned}\mathcal{A}_{ab}(\vec{L},\Delta T;\{\vec{P}_j,\vec{Q}_j\}) = \sum_j U_{aj}^* U_{bj} \left(2\pi\sigma_{\mathrm{S}j}\sigma_{\mathrm{D}j}\right)^{-\frac{3}{2}} \int \mathrm{d}^3\vec{p} \\ \times \exp\left(-\frac{(\vec{p}-\vec{Q}_j)^2}{4\sigma_{\mathrm{D}j}^2} - \frac{(\vec{p}-\vec{P}_j)^2}{4\sigma_{\mathrm{S}j}^2} - i(E_p\Delta T - \vec{p}\vec{L})\right) .\end{aligned} \tag{2.108}$$

Next, Taylor expanding the exponent up to second order around the dominant mean momentum,

$$\bar{\vec{p}}_j := \frac{\sigma_{\mathrm{D}j}^2\vec{P}_j + \sigma_{\mathrm{S}j}^2\vec{Q}_j}{\sigma_{\mathrm{S}j}^2 + \sigma_{\mathrm{D}j}^2} , \tag{2.109}$$

and solving the resulting Gaussian momentum space integral yields, cf. Appendix A.5.2,

$$\begin{aligned}\mathcal{A}_{ab}(\vec{L},\Delta T;\{\vec{P}_j,\vec{Q}_j\}) = \sum_j U_{aj}^* U_{bj} \left(\sigma_{\mathrm{D}j}^3\sigma_{\mathrm{S}j}^3\det(\Sigma_j)\right)^{-\frac{1}{2}} \exp\left(-i(\bar{E}_j T - \bar{\vec{p}}_j\vec{L})\right) \\ \times \exp\left(-\frac{1}{4}\frac{(\vec{P}_j-\vec{Q}_j)^2}{\sigma_{\mathrm{S}j}^2+\sigma_{\mathrm{D}j}^2} - \frac{1}{2}(\bar{\vec{v}}_j\Delta T - \vec{L})^T\Sigma_j^{-1}(\bar{\vec{v}}_j\Delta T - \vec{L})\right) .\end{aligned} \tag{2.110}$$

Here, we define the following mean quantities for the j-th mass eigenstate WP:

$$\bar{E}_j := \sqrt{|\bar{\vec{p}}_j|^2 + m_j^2} , \tag{2.111}$$

$$\bar{\vec{v}}_j := \frac{\bar{\vec{p}}_j}{\bar{E}_j} , \tag{2.112}$$

$$\Sigma_j := \frac{\mathbb{1}}{2}\left(\frac{1}{\sigma_{\mathrm{S}j}^2} + \frac{1}{\sigma_{\mathrm{D}j}^2}\right) + i\frac{\Delta T}{\bar{E}_j}\left(\mathbb{1} - \bar{\vec{v}}_j\otimes\bar{\vec{v}}_j\right) . \tag{2.113}$$

From top to bottom these quantities represent the mean neutrino energy, group velocity, and position space covariance matrix, respectively. The latter quantity Σ_j defines the effective shape and size of the overlap region between the produced and detected neutrino WPs.

The first exponential in Equation (2.110) represents the mean propagation phase giving rise to the typical oscillation pattern obtained in the naive derivation of the oscillation probability. In addition to this, Equation (2.110) also features an exponential function encoding the WP nature of the neutrinos. This factor induces what is called decoherence in the neutrino system since it describes the damping of the quantum interference terms in the final probability. From the first term in the exponent of this suppression factor, we can infer that only source and neutrino configurations with approximately matching mean momenta, i.e.

$$|\vec{P}_j - \vec{Q}_j| \ll \sqrt{2(\sigma_{\mathrm{S}j}^2 + \sigma_{\mathrm{D}j}^2)} , \tag{2.114}$$

contribute to the flavour transition process. Or to put it the other way around: If a neutrino mass eigenstate is detected and projected onto a WP state with mean momentum $\vec{Q}_j$ then we know that it must have been produced with a very similar mean momentum $\vec{P}_j$.

Moreover, from the position space shape function,

$$\Xi_j^2(\vec{L}, \Delta T) := (\bar{\vec{v}}_j \Delta T - \vec{L})^T \Sigma_j^{-1} (\bar{\vec{v}}_j \Delta T - \vec{L}) \,, \tag{2.115}$$

we deduce that the amplitude is only significantly different from zero in a region of the volume $V_X = 1/\sqrt{\det(\mathrm{Re}(\Sigma_j^{-1}))}$ around $\vec{L} = \bar{\vec{v}}_j \Delta T$. In cases where V_X is sufficiently narrow and all coherence damping effects are indeed negligible, the standard oscillation probability is recovered as the ad hoc identification $\vec{L} \sim \Delta T$ is justified. Note, however, this is in contradiction to the plane wave approximation used in the ad hoc approach, as in the plane wave limit $V_X \to \infty$ instead of 0. We now proceed to discuss how a certain hierarchy of approximations solves this apparent paradox.

To this end, we further decompose Σ_j into its eigenvectors and eigenvalues:

$$\Sigma_j = \sigma_{\parallel j}^2 (\vec{s}_\parallel^{\,j} \otimes \vec{s}_\parallel^{\,j}) + \sum_{a=1}^{2} \sigma_{\perp j}^2 (\vec{s}_{\perp,a}^{\,j} \otimes \vec{s}_{\perp,a}^{\,j}) \,, \tag{2.116}$$

where $\vec{s}_\parallel^{\,j} := \bar{\vec{p}}_j / |\bar{\vec{p}}_j|$ is parallel to the neutrino direction and $\vec{s}_{\perp,1}^{\,j}$, $\vec{s}_{\perp,2}^{\,j}$ are two mutually orthonormal, non-zero vectors perpendicular to the average neutrino propagation direction. The effective position space uncertainties in the current scenario are given by:

$$\sigma_{\parallel j}^2 := \frac{1}{2} \left(\frac{1}{\sigma_{\mathrm{S}j}^2} + \frac{1}{\sigma_{\mathrm{D}j}^2} \right) + i \frac{\Delta T}{\bar{E}_j} (1 - |\bar{\vec{v}}_j|^2) \,, \tag{2.117}$$

$$\sigma_{\perp j}^2 := \frac{1}{2} \left(\frac{1}{\sigma_{\mathrm{S}j}^2} + \frac{1}{\sigma_{\mathrm{D}j}^2} \right) + i \frac{\Delta T}{\bar{E}_j} \,. \tag{2.118}$$

Their imaginary part gives rise to the effect of WP spreading which in the case of the parallel eigenvalue is also affected by Lorentz contraction. To keep our discussion simple, we neglect the spreading of WPs from now on and set:

$$\sigma_{\parallel j}^2 \approx \sigma_{\perp j}^2 \approx \frac{1}{2} \left(\frac{1}{\sigma_{\mathrm{S}j}^2} + \frac{1}{\sigma_{\mathrm{D}j}^2} \right) =: \Theta_j^2 \,. \tag{2.119}$$

In terms of these quantities the position space exponent then becomes:

$$\Xi_j^2(\vec{L}, \Delta T; \{\vec{P}_j, \vec{Q}_j\}) \;\approx\; \frac{(\bar{v}_j \Delta T - L_{\parallel j})^2}{\Theta_j^2} + \frac{L_{\perp j}^2}{\Theta_j^2} \,, \tag{2.120}$$

$$L_{\parallel j} := |\vec{s}_\parallel^{\,j} \cdot \vec{L}| \,, \tag{2.121}$$

$$L_{\perp j} := \sqrt{(\vec{s}_{\perp,1}^{\,j} \cdot \vec{L})^2 + (\vec{s}_{\perp,2}^{\,j} \cdot \vec{L})^2} \,. \tag{2.122}$$

As in the QFT approach, we can now reduce the problem to a one dimensional setting since usually the total propagation distance $L := |\vec{L}|$ is much larger than the neutrino WP, i.e. $L \gg \Theta_j$, and since the amplitude is only significantly different from zero if $L_{\perp j} \sim \Theta_j$ we can set $L \approx L_{\parallel j}$ for all mass eigenstates. Furthermore, in the same spirit we define $\bar{v}_j := |\bar{\vec{v}}_j|$, $\bar{p}_j := |\bar{\vec{p}}_j|$ and set $\vec{P}_j =: P_j \vec{\ell}$ and $\vec{Q}_j =: Q_j \vec{\ell}$ from now on where $\vec{\ell} := \vec{L}/|\vec{L}|$.

From this, we finally obtain from Equation (2.110)

$$\begin{aligned}\mathcal{A}_{ab}(L, \Delta T; \{P_j, Q_j\}) \approx \sum_j U_{aj}^* U_{bj} \left(\Theta_j^2 \sigma_{\mathrm{D}j} \sigma_{\mathrm{S}j}\right)^{-\frac{3}{2}} \exp\left(-i(\bar{E}_j T - \bar{p}_j L)\right) \\ \times \exp\left(-\frac{1}{4}\frac{(P_j - Q_j)^2}{\sigma_{\mathrm{S}j}^2 + \sigma_{\mathrm{D}j}^2} - \frac{1}{2}\frac{(\bar{v}_j \Delta T - L)^2}{2\Theta_j^2}\right).\end{aligned} \tag{2.123}$$

Next, in order to arrive at the final oscillation probability, we need to square Equation (2.123) and integrate it with respect to the neutrino production and detection times as instructed by Equation (2.104). As shown in Reference [53] and Appendix A.5.1, for time translation invariant systems, this temporal double integral can be reduced to a simple integral over the propagation time ΔT instead, i.e.

$$P_{ab}(L, \{P_j, Q_j\}) \approx \frac{\int_{-\infty}^{\infty} \mathrm{d}\Delta T |\mathcal{A}_{ab}(L, \Delta T; \{P_j, Q_j\})|^2}{\int_{-\infty}^{\infty} \mathrm{d}\Delta T \sum_b |\mathcal{A}_{ab}(L, \Delta T; \{P_j, Q_j\})|^2}. \tag{2.124}$$

This greatly simplifies the task at hand and amounts to another Gaussian integral over ΔT in our case. We perform the explicit computation in Appendix A.5.3 and find

$$\begin{aligned}P_{ab}(L, p) = \frac{1}{N} \sum_{j,k} U_{aj}^* U_{bj} U_{ak} U_{bk}^* \left(\Theta_j^2 \sigma_{\mathrm{S}j} \sigma_{\mathrm{D}j} \Theta_k^2 \sigma_{\mathrm{S}k} \sigma_{\mathrm{D}k}\right)^{-\frac{3}{2}} \left(\frac{2\pi}{\sigma_{Ejk}^2}\right)^{\frac{1}{2}} \\ \times \exp\left(i \Delta p_{jk} L - i \frac{\Delta E_{jk}}{\bar{v}_{jk}} L - \left(\frac{L}{L_{jk}^{\mathrm{coh}}}\right)^2 - \frac{1}{2}\left(\frac{\Delta E_{jk}}{\sigma_{Ejk}}\right)^2\right) \\ \times \exp\left(-\frac{(P_j - Q_j)^2}{2\sigma_{Pj}^2} - \frac{(P_k - Q_k)^2}{2\sigma_{Pk}^2}\right),\end{aligned} \tag{2.125}$$

with the coherence length L_{jk}^{coh} and the effective energy and momentum resolutions, σ_{Ejk} and σ_{Pj}, respectively, defined by

$$L_{jk}^{\mathrm{coh}} := \sqrt{2} \frac{\sqrt{\Theta_j^2 \bar{v}_k^2 + \Theta_k^2 \bar{v}_j^2}}{|\bar{v}_j - \bar{v}_k|}, \qquad \sigma_{Ejk}^2 := \left(\frac{\bar{v}_j^2}{\Theta_j^2} + \frac{\bar{v}_k^2}{\Theta_k^2}\right), \qquad \sigma_{Pj}^2 := 2(\sigma_{\mathrm{S}j}^2 + \sigma_{\mathrm{D}j}^2). \tag{2.126}$$

Moreover, the energy and momentum differences, ΔE_{jk} and Δp_{jk}, as well as the weighted average velocity of mass eigenstate WPs j and k $\bar{v}_{jk}$ are given by

$$\Delta E_{jk} := \bar{E}_j - \bar{E}_k, \qquad \Delta p_{jk} := \bar{p}_j - \bar{p}_k, \qquad \bar{v}_{jk} := \frac{\Theta_j^2 \bar{v}_k^2 + \Theta_k^2 \bar{v}_j^2}{\Theta_j^2 \bar{v}_k + \Theta_k^2 \bar{v}_j}. \tag{2.127}$$

Until now, we have maintained as much generality as possible but in order for P_{ab} to be actually well-defined it is necessary that the mean momenta P_j as well as the Q_j differ only slightly in the mass index j and that the neutrino masses are very similar to each other compared to the total energy scale. Furthermore, also the shape of each mass eigenstate WP should be similar implying $\sigma_{\mathrm{S}j} \equiv \sigma_{\mathrm{S}}$ and $\sigma_{\mathrm{D}j} \equiv \sigma_{\mathrm{D}}$ for all mass eigenstate indices j.

In the following, we therefore expand all quantities up to first order around a representative squared mass $\bar{m}^2$ that could for example be chosen as the smallest mass square of the neutrino mass eigenstates or as an average of all three squared masses. We then also define the momentum p and energy $E := \sqrt{p^2 + \bar{m}^2}$ a produced or detected neutrino mass eigenstate WP with squared mass $\bar{m}^2$ would have. Here, it is important that one uses this reference mass, momentum and energy when computing the neutrino source flux and detection cross section from Equation (2.103). In the approximation $|m_j^2 - \bar{m}^2| \ll p^2$ and $|P_j - p| \ll p$ and neglecting the differences $P_j - Q_j$, we obtain

$$\Delta E_{jk} \approx \frac{\Delta m_{jk}^2}{2E} + v \Delta p_{jk}\,, \qquad \Delta m_{jk}^2 := m_j^2 - m_k^2\,, \qquad v := \frac{p}{E}\,, \tag{2.128}$$

and the fully approximated oscillation probability reads:

$$\begin{aligned} P_{ab}(L,E) \approx \sum_{jk} U_{aj}^* U_{ak} U_{bj} U_{bk}^* \exp\left(-i \frac{\Delta m_{jk}^2}{2p} L\right) \\ \times \exp\left(-\left(\frac{L}{L_{jk}^{\mathrm{coh}}}\right)^2 - \frac{1}{2}\left(\frac{\Delta E_{jk}}{\sigma_E}\right)^2\right)\,, \end{aligned} \tag{2.129}$$

with

$$L_{jk}^{\mathrm{coh}} \approx \Theta \left| \frac{\Delta m_{jk}^2}{4E^2} - \frac{\bar{m}^2}{2E^2} \frac{\Delta p_{jk}}{p} \right|^{-1}\,, \qquad \sigma_E^2 := \frac{2v^2}{\Theta^2}\,. \tag{2.130}$$

This result also holds if the ultra-relativistic approximation breaks down, i.e. $\bar{m}^2 \gtrsim p^2$, as long as mass degeneracy applies, i.e. $|m_j^2 - \bar{m}^2| \ll p^2$. Still the same oscillation phase $\Phi_{jk}(L,p) = \Delta m_{jk}^2 L/(2p)$ arises as in the ultra-relativistic scenario. We can now easily read off the remaining conditions that have to be fulfilled in order to arrive at the standard oscillation probability.

Production and Detection Coherence The production and detection coherence condition reads

$$|\Delta E_{jk}| = \left| \frac{\Delta m_{jk}^2}{2E} + v \Delta p_{jk} \right| \ll \frac{\sqrt{2} v}{\Theta} = \sigma_E\,. \tag{2.131}$$

It states that the mean production and detection energy resolutions must not be too small such that the energy splittings of the different mass eigenstates can be resolved. For energy

splittings larger than the effective energy resolution σ_E the respective interference terms are damped and the associated oscillations are impeded. The energy resolution σ_E can also be interpreted as the inverse of the temporal resolution of the neutrino experiment. Since $\Theta^2 \propto (\sigma_{\mathrm{S}}^{-2} + \sigma_{\mathrm{D}}^{-2})$ it is dominated by the narrowest momentum width and consequently the same holds for all quantities derived from it, like σ_E.

Propagation Coherence As long as the baseline L is much smaller than the coherence length L_{jk}^{coh}, i.e.

$$L \ll L_{jk}^{\mathrm{coh}}\,, \tag{2.132}$$

the different neutrino mass eigenstate WPs overlap sufficiently during propagation such that the WP decoherence exponential can be neglected.

While the production and detection coherence condition is linked to the temporal localisation $\Theta_T \sim 1/\sigma_E$ of the neutrino system, the propagation coherence condition is associated with the spatial localisation Θ of the WPs. The crucial point now is that the corresponding inequalities compete with each other: While the production and detection coherence suffer from delocalised neutrinos, as this implies a more precise momentum measurement, the propagation coherence increases for large Θ. It is therefore mandatory to check if the given experiment allows for a window in which both effects are negligible. In case of arbitrarily long propagation distances, as they occur for example for astrophysical neutrinos, the coherence length is most likely to be too small to be negligible. Hence, if all other decoherence effects can be neglected, the only modification to the standard expression for P_{ab} comes from the propagation coherence exponential and reads

$$P_{ab}(L,E;\bar{m}^2) \approx \sum_{jk} U_{aj}^* U_{ak} U_{bj} U_{bk}^* \exp\left(-i\frac{\Delta m_{jk}^2}{2p}L\right) \exp\left(-\left(\frac{L}{L_{jk}^{\mathrm{coh}}}\right)^2\right)\,, \tag{2.133}$$

for Gaussian neutrino WPs. Differently shaped neutrino WPs give rise to different damping exponentials like $\exp\left(-L/L_{jk}^{\mathrm{coh}}\right)$ in the case of Lorentzian WPs [59].

To summarise our discussion, we now collect all answers to the remaining questions, four to six, from our list:

4. Should we assume the neutrino state to be produced and detected with definite momentum (as assumed above) or definite energy?

5. How can a plane wave (definite momentum state) be localised in space such that the conversion $L \sim T$ is justified?

6. If neutrinos are localised on the other hand: How do the inherent position and momentum space uncertainties of the WPs affect the oscillation formula?

The answer to question four is that neither is justified, as we have seen that the full mean four-momenta of the mass eigenstate WPs in general differ from each other and either equating their spatial or temporal components introduces errors that actually prevent us from obtaining the correct oscillation phase. Instead one should expand all quantities around a reference mean momentum p and energy E corresponding to a neutrino of mass $\bar{m}^2$. If all mass squared differences are small compared to the average momentum scale p, we obtain the correct oscillation phase $\Phi_{jk} = \Delta m^2_{jk} L/(2p)$.

Next, questions five and six can be answered simultaneously: Neutrinos need to be considered as WP states otherwise exact energy and momentum conservation implies that the mass eigenstate that has been produced or detected could be precisely determined contradicting the assumption of coherent production and detection of flavour eigenstates. Furthermore, only in the WP framework neutrinos can be viewed as (partially) localised in position space and the approximation $L \sim \Delta T$ is justified within the uncertainties of the respective WPs, as has been demonstrated above. To be precise, in order for the oscillation probability to be a well-defined quantity, we need that neutrinos are quasi degenerate in mass $|m_j^2 - \bar{m}^2| \ll p^2$ and that the production and detection coherence condition in Equation (2.131) is satisfied. For purely ultra-relativistic neutrinos, these conditions are fulfilled very naturally since already $m_j^2 \ll p^2$ and $\Delta E_{jk} \ll \sigma_E$ as no current generation experiment can resolve the neutrino masses. If in addition to this also propagation coherence is maintained, i.e.

$$\frac{L}{4\sqrt{2}\sigma_X} \ll \frac{E^2}{|\Delta m^2_{jk}|}\,, \tag{2.134}$$

the standard oscillation probability is obtained. In any other case the WP nature of the neutrino damps the oscillation pattern and yields the constant flavour transition probability,

$$P_{ab}(L,E) \equiv \sum_j |U_{aj}|^2 |U_{bj}|^2\,, \tag{2.135}$$

in the fully decohered regime, which answers question six.

Finally, for ultra-relativistic neutrinos, we can now also approximate $\bar{m}^2 \approx 0$ and get an even simpler expression for the coherence length, i.e.

$$L^{\text{coh}}_{jk} \approx 4\Theta \frac{E^2}{|\Delta m^2_{jk}|} =: 4\sqrt{2}\sigma_X \frac{E^2}{|\Delta m^2_{jk}|}\,, \tag{2.136}$$

where we have used that in the literature the position space width of the neutrino WPs is usually defined by $\Theta =: \sqrt{2}\sigma_X$.

Since both the QFT as well as the quantum mechanics (QM) WP formalisms are rather cumbersome and especially for ultra-relativistic neutrinos at current neutrino experiments the production and detection coherence conditions are satisfied to a high degree, we discuss an effective quantum mechanical model for the theory of neutrino oscillations in the next section. This approach is designed to incorporate the effects of interaction and propagation decoherence while keeping the simplicity of our initial naive *derivation* of the neutrino oscillation probability. One only needs to take care if one of the inequalities above does not hold for the experiment under consideration.

2.3.3 Effective Flavour Space Description of Neutrino Oscillations

As in the last section, we assume that all neutrino mass eigenstates are produced and detected with almost identical momentum space WPs centered around very similar mean momenta with equal width. In this case, neutrino propagation can be considered to be independent from the details of the neutrino production and detection processes and the flavour transition probability is well-defined. Since we have now discussed the range of validity of the standard formula as well as possible modifications to it due to matter effects and the WP nature of neutrinos, we can finally write down an effective quantum mechanical description of neutrino oscillations. In this much simpler and most commonly used formalism, neutrino flavours are considered to be a quantum mechanical n_f level system whose unitary evolution is governed by an effective $n_f \times n_f$ Hamiltonian $\hat{H}$.

First neglecting all sources of coherence damping, like for example the WP separation effect or incoherent scattering with a background matter distribution, the flavour state can be described by a simple QM state vector $|\psi\rangle$. Its time (or length) evolution is driven by the Schrödinger equation,

$$i\frac{\mathrm{d}\,|\psi(x)\rangle}{\mathrm{d}x} = \hat{H}(x)\,|\psi(x)\rangle\ , \qquad \hat{H}(x) = \frac{\hat{M}^2}{2p} + \hat{V}(x)\,, \tag{2.137}$$

where in the mass basis $\hat{M}^2$ is represented by a diagonal matrix with m_j^2 as its j-th diagonal entry and $p := |\vec{p}|$ is the average momentum of the system, as defined in Section 2.3.2. Furthermore, $\hat{V}$ is a potential term induced for example by elastic forward scattering of neutrinos off of background matter or changes in the relativistic dispersion relation as discussed for example in Chapter 3. In case $\hat{V}$ is induced by forward scattering effects, it can be computed from the thermal neutrino self energy Σ_T via:

$$\hat{V}(x) \approx V^0(|\vec{p}|,\vec{p};x) + \frac{\vec{p}}{|\vec{p}|}\cdot\vec{V}(|\vec{p}|,\vec{p};x)\,, \qquad \text{(neutrinos)} \tag{2.138}$$

$$\hat{\bar{V}}(x) \approx -V^0(-|\vec{p}|,\vec{p};x) + \frac{\vec{p}}{|\vec{p}|}\cdot\vec{V}(-|\vec{p}|,\vec{p};x)\,, \qquad \text{(antineutrinos)} \tag{2.139}$$

$$V^\mu(|\vec{p}|,\vec{p};x) = \frac{1}{4}\mathrm{Tr}(\Sigma_T(|\vec{p}|,\vec{p};x)\gamma^\mu)\,, \tag{2.140}$$

as shown for example in Reference [61].

As soon as decoherence cannot be neglected anymore, it is still possible to extend the currently discussed formalism to the framework of open quantum systems, see References [62–64] for a review, that allows for influences of DOFs outside the effective n_f level system and thereby enables the inclusion of non-coherent effects in the neutrino system. Due to the consequent possibility of mixed states it is, however, mandatory to describe the state of the system by the more general density operator $\rho(x)$. Moreover, the Schrödinger equation for $|\psi\rangle$ then needs to be replaced by the evolution equation of $\rho(x)$ given by:

$$\frac{\mathrm{d}\rho(x)}{\mathrm{d}x} = -i[\hat{H},\rho(x)] + \Omega[x,\rho(x)]\,, \tag{2.141}$$

where $\Omega[x, \rho(x)]$ encodes all non-unitary components of the system evolution, i.e. the net coherence damping in the neutrino flavour system. The solution $\rho(x)$ of Equation (2.141) for given initial state $\rho(x_0) = \rho_0$ describes the state of the system at any *greater* length $x > x_0$. Since Ω usually contains irreversible effects Equation (2.141) can, in general, not be used to obtain the state at earlier stages than x_0. In the following, we distinguish two types of contributions to Ω: Those who are of the so-called Lindblad form [63] and those that are not. The Lindbladian contributions to Ω are memoryless, i.e. do not depend on the state of the system, trace preserving and positive and can, therefore, be described by a simple, linear operator D acting on ρ, i.e. $\Omega[x, \rho(x)] = D(x)\rho(x) + \tilde{\Omega}[x, \rho(x)]$, where $\tilde{\Omega}$ represents all non-Lindbladian contributions to Ω. The operator D is called the dissipator in the following.

The probability to find the neutrino system in the state $|\chi\rangle$ in the detector can be computed by acting the projector $\mathrm{Pr}_\chi = |\chi\rangle\langle\chi|$ onto the system state $\rho(x)$ and taking the trace:

$$P_\chi(x) = \mathrm{Tr}\left[\mathrm{Pr}_\chi \rho(x)\right] . \tag{2.142}$$

Of course also mixed final states are allowed and can be easily taken into account by replacing Pr_χ by the corresponding final state density matrix. In the following, we discuss how the different decoherence effects, we have considered so far, enter the effective flavour space formalism.

Production and Detection Coherence If the conditions for production or detection coherence are not sufficiently satisfied such that the corresponding damping factors in the oscillation probability (2.129) cannot be neglected, the flavour transition probability is ill-defined and the formalism under consideration is not applicable.

Wave Packet Decoherence The effect of *propagation decoherence* or *decoherence due to WP separation* is an effect that depends on the distance travelled by the neutrino system, and hence, needs to be included into the operator Ω. More precisely, this is an example for a Lindbladian type of decoherence and the corresponding dissipator, assuming Gaussian neutrino WPs, has the form

$$D^{\mathrm{wp}}(x)\rho(x) = \sum_{j \neq k} d^{\mathrm{wp}}_{jk}(x) \left|\nu_j\right\rangle \left\langle\nu_k\right| \mathrm{Tr}\left[\left|\nu_k\right\rangle \left\langle\nu_j\right| \cdot \rho(x)\right] , \qquad d^{\mathrm{wp}}_{jk} = -\frac{x}{2{L^{\mathrm{coh}}_{jk}}^2} . \tag{2.143}$$

The action of this operator has the net effect of multiplying all off-diagonal elements of ρ in the mass basis by the respective WP decoherence factor $x/(2{L^{\mathrm{coh}}_{jk}}^2)$ and leads to the same exponential damping of the coherence terms as shown in Equation (2.133). For other types of neutrino WPs, slightly different dissipators need to be employed. For Lorentzian WPs, for example, we get $d^{\mathrm{wp}}_{jk} = -1/L^{\mathrm{coh}}_{jk}$ with $L^{\mathrm{coh}}_{jk} = 4\sigma_X E^2/|\Delta m^2_{jk}|$, where $E \approx p$ is the average neutrino energy.

Dissipative Matter Effects Lastly, in the presence of matter effects also inelastic scatterings can occur. Typical processes are neutrino absorption in the ambient matter or the scattering to different energy modes. These kinds of effects enter the more general dissipation terms $\tilde{\Omega}$ as they are possibly not trace preserving due to the reduction of the number of neutrinos in the ensemble or depend on the state of the system itself. The full set of evolution equations for the neutrino and antineutrino density matrices ρ and $\bar{\rho}$, respectively, then reads

$$\begin{aligned}\frac{\partial\rho}{\partial x}(x,E) = -i[\hat{H}(x,E),\rho(x,E)] + D(x,E)\rho(x,E) \\ - \{\Gamma(x,E),\rho(x,E)\} + \mathcal{C}[x,E,\rho,\bar{\rho}]\,,\end{aligned} \tag{2.144}$$

$$\begin{aligned}\frac{\partial\bar{\rho}}{\partial x}(x,E) = -i[\hat{\bar{H}}(x,E),\bar{\rho}(x,E)] + \bar{D}(x,E)\bar{\rho}(x,E) \\ - \{\bar{\Gamma}(x,E),\bar{\rho}(x,E)\} + \bar{\mathcal{C}}[x,E,\bar{\rho},\rho]\,,\end{aligned} \tag{2.145}$$

cf. References [65–72]. We have made the energy-dependence of the system explicit since in general we have one density matrix per energy mode. Here, $\hat{H}$ ($\hat{\bar{H}}$) is the neutrino (antineutrino) Hamiltonian in matter, as described above, and D ($\bar{D}$) encodes all Lindbladian decoherence effects in the neutrino (antineutrino) evolution. All incoherent scattering effects are described by the anticommutator between neutrino (antineutrino) attenuation terms Γ ($\bar{\Gamma}$) and the density matrix as well as by the neutrino (antineutrino) collision terms $\mathcal{C}$ ($\bar{\mathcal{C}}$). The reason to split up the new interaction terms into two distinct contributions is that the first one involving the anticommutator is also linear in ρ and acts only on one single energy mode but it is usually not trace preserving. This term is what describes neutrino absorption or decay in matter. In contrast to this, the collision terms, $\mathcal{C}$ and $\bar{\mathcal{C}}$, in general involve non-linear interactions of neutrinos among themselves as well as scatterings off of background matter. These terms couple the evolution of neutrino and antineutrino densities as well as the evolution of different momentum modes. The exact expressions for the attenuation terms are given in Appendix A.6.

3 Light Sterile Neutrinos with Altered Dispersion Relations Coupling to Axion-Like Dark Matter in the Early Universe

This chapter is based on Reference [73].

In this chapter, we consider the consequences of non-standard active–sterile neutrino oscillations on experimentally constrainable cosmological parameters like the effective number of light DOFs N_{eff} and the helium-4 abundance $Y_{^4\text{He}}$. The particular class of models we discuss features an additional light sterile neutrino generation ν_s subject to an altered dispersion relation (ADR) inducing a linearly energy-dependent potential in the neutrino Hamiltonian. Such potentials, for example, arise in models proposed in References [74–80]. From a phenomenological point of view, introducing a light fourth generation is motivated by the so-called short baseline (SBL) anomalies where anomalous neutrino oscillations have been observed that could be interpreted as an oscillation over a fourth light neutrino mass eigenstate $m_4 = \mathcal{O}(\text{eV})$. These anomalies have been observed in several experiments with short neutrino propagation distances $L \sim 10\,\text{km}$ to $100\,\text{km}$, starting with results from the Liquid Scintillator Neutrino Detector (LSND) collaboration [81] in the (anti-)$\nu_\mu \to$ (anti-)ν_e channel in the early 2000s and later supplemented by the reactor [82] and gallium [83] anomalies reporting anomalous (anti-)ν_e disappearance. In more recent years, the Mini Booster Neutrino Experiment (MiniBooNE) collaboration reported results in the same (anti-)$\nu_\mu \to$ (anti-)ν_e channel, supporting the LSND results [84, 85]. Together, the results from both experiments yield a combined statistical significance of $6.1\,\sigma$ for a deviation from the standard three-neutrino-paradigm. In contrast to the SBL results, atmospheric [86–88] and long baseline (LBL) accelerator experiments [89–91] do not report analogous discrepancies with the three-neutrino-paradigm. Since some of these experiments operate at much higher energies E and propagation lengths L but similar values of L/E, this places stringent constraints on the mass and mixing parameters of the plain sterile neutrino extension. This discrepancy motivates the introduction of ADRs for the additional sterile neutrino introducing terms into the standard oscillation probability that explicitly depend on the neutrino energy suppressing oscillations over the fourth mass eigenstate at higher energies. The most recent results from the Micro Booster Neutrino Experiment (MicroBooNE) collaboration [92–95], however, disfavour the ν_e appearance excess observed in the MiniBooNE experiment. Nevertheless, as has been shown in Reference [96], even the MicroBooNE data hint towards the existence of an eV scale sterile neutrino at $2.95\,\sigma$ significance. Hence, light sterile neutrinos remain an interesting extension of the lepton sector and are expected to persist as an active area of research in the following decades as discussed in Reference [97].

In addition to this phenomenological motivation, also on the theory side there are reasons to assume that sterile neutrinos are subject to ADRs. For example in models with asymmetrically warped extra dimensions, all gauge charged particles may be bound to the four dimensional SM-submanifold (brane), while gauge singlets—like sterile neutrinos—are allowed to enter the bulk. Consequently, when considering the dispersion relation of these singlet states restricted to the SM-brane, the dispersion relation gains new terms compared to non-singlet states as has been extensively discussed in References [74–80]. There also exist other scenarios motivated e.g. by quantum gravitational theories where Lorentz violating terms alter the usual dispersion relation $p^2 = m^2$, see Reference [98] for a recent review.

Light sterile neutrinos mixing with the active neutrino sector do not only have an impact on terrestrial neutrino oscillation experiments but would also leave their imprint in cosmological parameters. The most prominent examples are the number of light DOFs N_{eff} shortly before last scattering, the effective sterile neutrino mass parameter m_s^{eff} that can be derived from CMB power spectra and the helium-4 abundance $Y_{^4\text{He}}$ generated during BBN. An additional ultra-relativistic species in equilibrium with the SM plasma would contribute a full new DOF increasing the expansion rate of the Universe compared to the standard cosmological-constant-cold-dark-matter (ΛCDM) model. Furthermore, due to the relatively large mass of ν_4 compared to the masses of the three lightest neutrino mass eigenstates, ν_4 can have a significant impact on structure formation. This impact is parametrised by the effective sterile mass parameter m_s^{eff} [29]. Lastly, the cosmic helium abundance is influenced by the number of free neutrons present in the plasma during BBN, and the weak interactions keeping protons and neutrons in thermal equilibrium are catalysed by the abundance of electron neutrinos at that time. Therefore, we are interested in the evolution of neutrino phase space densities in the early Universe, taking into account all important thermal and quantum effects like elastic and inelastic scattering of neutrinos with the background plasma, as well as neutrino flavour oscillations.

We have already considered the presented class of models in an earlier work [99]. There, we have also estimated the effective number of light DOFs and the consequences of the presence of the light sterile neutrino for BBN in a simple framework. In this framework, we have approximated the phase space densities of the SM neutrinos by the respective equilibrium distributions. The distribution of the sterile neutrino has then been determined using the phase space densities of the active neutrinos in combination with the active–sterile oscillation probability and interaction rates. As a result, we have obtained that there exist parameter configurations for which the thermalisation of the sterile neutrino is indeed suppressed. This motivates to employ a more sophisticated approach in order to check if these interesting findings persist. Thus, in contrast to the heuristic approach used in Reference [99], combining neutrino oscillations and scattering processes in an ad hoc manner, we now adopt a first principles framework to achieve a consistent description of both effects and their influence on the neutrino densities. This is done using the phase space density matrix (PSDM) formalism, describing the population of the neutrino mass eigenstates, as well as possible quantum correlations between them arising due to oscillations. In particular, this new approach improves our previous work [99] by taking into account oscillation damping due to fast collisions, collective neutrino

oscillations [69] and scattering processes between different energy modes.

To keep this analysis simple and focused on the interplay of the active and sterile sectors, we consider a one active plus one sterile neutrino toy model. The active neutrino is taken to be the electron neutrino and we approximate the densities of the other SM neutrino species by the ν_e distribution, if needed. This approximation is justified here, since we are mainly interested in the question whether the considered extensions of the plain light sterile neutrino scenario can indeed lead to a significant suppression of the population of ν_s in the early Universe. In order to perform a precision estimation of cosmological parameters like N_{eff}, one needs to also take into account active–active neutrino oscillations, finite temperature QED corrections, as well as the different interaction channels available for ν_e, ν_μ and ν_τ in different phases of the early Universe, see for example References [100–102].

In addition to the ADRs, we also introduce a hypothetical ultra-light scalar field ϕ, feebly coupling to the sterile neutrino. This new field ϕ is assumed to be produced non-thermally and to form a coherent Bose–Einstein condensate throughout the history of the Universe. It belongs to the class of axion-like particles (ALPs) and may also contribute to the dark sector since it does not couple directly to SM particles. The feeble Yukawa coupling λ between the ALP-condensate and the sterile neutrino leads to a time-dependent mass contribution for ν_s, suppressing the mixing between the active and sterile sector at early times. In contrast to other models [103–109] featuring couplings between dark bosons and sterile neutrinos, refractive effects on the neutrino sector induced by scatterings off of background particles are negligible in the scenario under consideration due to the smallness of the coupling λ. This furthermore ensures that ϕ does not thermalise via indirect interactions with the SM plasma and does not add yet another contribution to N_{eff}. Models with ALPs, feebly coupled to sterile neutrinos, have already been extensively discussed in the literature [110–120] in cosmological as well as non-cosmological applications. In this context, our work represents the first study in which this mechanism is considered in the PSDM formalism and in combination with ADRs.

The chapter is organised as follows: We start with a detailed discussion of the models under consideration in Section 3.1. Afterwards, in Section 3.2, we define the central cosmological quantities N_{eff}, m_s^{eff} and the helium-4 abundance $Y_{^4\text{He}}$ and how we use them to estimate if a given model configuration is in tension or agreement with cosmological data. In Section 3.3, we briefly discuss the equations of motion for the neutrino PSDM in the early Universe and the implementation of the models in this framework. From the neutrino PSDM we predict the values of all cosmological parameters of interest for each given model configuration. The corresponding results are presented in Section 3.4. Finally, we summarise and conclude this segment of the thesis in Section 3.5.

3.1 Model Definition

The effective flavour space Hamiltonian governing neutrino flavour oscillations at momentum $p \equiv |\vec{p}|$ in the early Universe can be written as

$$\hat{H}_0(p,T) = \frac{\hat{M}^2}{2p} + \hat{V}_{\text{matter}}(p,T)\,, \tag{3.1}$$

where the first term is just the usual vacuum Hamiltonian, as introduced in Section 2.3.3, and the latter term describes the effective potential induced by forward scattering interactions of neutrinos with the background plasma at temperature T as discussed in Section 2.3.3. It can be shown that the matter potential takes the form [121]

$$\hat{V}_{\text{matter}}(p,T) = V_e(p,T)\mathbb{P}_e\,, \tag{3.2}$$

$$V_e(p,T) = \pm\sqrt{2}G_{\text{F}}(n_{e^-}(T) - n_{e^+}(T)) - \frac{8\sqrt{2}G_{\text{F}}p}{3}\left(\frac{\rho_{e^\pm}(T)}{m_W^2} + \frac{\rho_{\nu_e}(T)}{m_Z^2}\right)\,, \tag{3.3}$$

with the Fermi coupling G_{F} and the number and energy densities n_α and ρ_α of particle species α, respectively. The first term in V_e constitutes the common Mikheyev–Smirnov–Wolfenstein (MSW) potential, carrying a positive sign for neutrinos and a negative one for antineutrinos while the second term is a higher order correction in the W and Z boson masses to the standard low energy four fermion approximation of the weak interaction. Assuming the lepton asymmetry of the Universe to be of the order of the baryon asymmetry of the Universe—which we do in the following in accordance with References [100, 101]—the usual MSW term is actually negligible over the correction term. Moreover, we have introduced the electron flavour projector $\mathbb{P}_e$, whose matrix elements in flavour space are given by $(\mathbb{P}_e)_{ij} = \delta_{ie}\delta_{je}$.

In the simple $(1+1)$ neutrino scenario under consideration, the neutrino mass matrix assumes the form

$$\hat{M} = \begin{pmatrix} m_{ee} & m_{es}^* \\ m_{es} & m_{ss} \end{pmatrix}\,. \tag{3.4}$$

In accordance with Reference [113], as well as with neutrino mass and mixing fits to SBL data, we choose the mass matrix elements to be given by $m_{ee} \approx 0\,\text{eV}$, $m_{es} \approx 0.12\,\text{eV}$, $m_{ss} \approx 1.1\,\text{eV}$. This is equivalent to a vacuum mixing angle θ fulfilling $\sin(2\theta) \approx 0.21$. In the following, we discuss how the Hamiltonian in Equation (3.1) changes in the presence of the ADR effect and the coupling of ν_s to the ALP field. In case of the ALP extension this amounts to an effective contribution to the mass matrix $\hat{M}$, but since the modified mass matrix reduces to the *bare* one at late times it is still reasonable to estimate the bare mass parameters in Equation (3.4) using fits to SBL data.

3.1.1 Sterile Neutrinos with Altered Dispersion Relations

Changing the relativistic dispersion relation of sterile neutrinos also influences the vacuum Hamiltonian of the neutrino system. It can be shown [78] that in the common ultra-relativistic

approximation this effect amounts to an effective potential for the sterile neutrino. In the following, we parametrise this sterile or ADR potential as

$$\hat{V}_{\mathrm{ADR}}(p) = V_s(p)\mathbb{P}_s\,, \qquad V_s(p) = -\frac{bp}{2}\mathbb{P}_s\,, \tag{3.5}$$

matching the parametrisations discussed e.g. in References [74, 78, 79]. The strength of the ADR effect is specified by the free ADR parameter b and the sterile neutrino projector $\mathbb{P}_s$ ensures that the ADR potential only affects the sterile species.

3.1.2 Sterile Neutrinos Coupling to Axion-Like Dark Matter

The second modification to the plain sterile neutrino extension we consider here, is a feeble Yukawa coupling of ν_s to an ultra-light, real, scalar field ϕ. The corresponding ALP Lagrangian reads

$$\mathcal{L}(\phi, \partial_\mu\phi) = \frac{1}{2}(\partial_\mu\phi)(\partial^\mu\phi) - \frac{m_\phi^2}{2}\phi^2 - \frac{\lambda}{2}\phi\left(\bar{\nu}_s^c\nu_s + \bar{\nu}_s\nu_s^c\right)\,, \tag{3.6}$$

with $\lambda > 0$. The only requirements we impose on the scalar field ϕ are $m_\phi \ll 1\,\mathrm{eV}$ and that it is produced non-thermally in the early Universe such that it forms a homogeneous, coherent condensate. This condensate then behaves like a classical scalar field, obeying the Klein–Gordon equation in an FLRW spacetime. Therefore, its cosmic time evolution reads [113]

$$\phi(t) = \phi_0\eta(t)\,, \qquad \eta(t) := N_\eta\frac{J_{\frac{1}{4}}(m_\phi t)}{\sqrt[4]{m_\phi t}}\,, \tag{3.7}$$

and is fully specified by the scalar mass m_ϕ and the amplitude ϕ_0 at $t \to 0$. Here, $J_\nu(z)$ denotes the Bessel functions of the first kind and order $\nu \in \mathbb{R}$, and the normalisation $N_\eta \approx 1.08$ is chosen such that $\eta(0) = 1$.

We assume the feeble coupling, i.e. $\lambda \ll 1$, between the scalar ϕ and sterile neutrino ν_s to be sufficiently small such that scattering effects of ν_s with potential background quanta of ϕ can be safely neglected. Furthermore, this also ensures that ϕ does not thermalise if ν_s does via oscillations. Otherwise, the scalar field would yet yield another unwanted contribution to the radiation energy density. Nevertheless, if the amplitude ϕ_0 is sufficiently large, the coupling can still have a significant effect on the sterile neutrino by inducing an additional time-dependent mass term

$$\Delta m_{ss}(t) = \lambda\phi_0\eta(t) =: m_{s0}\eta(t)\,. \tag{3.8}$$

By virtue of the time–temperature relation in the early Universe discussed in Section 2.2, we can rewrite the time-dependence of the additional mass term in terms of the temperature of the

primordial plasma. Hence, the net effect of this extension on the Hamiltonian in Equation (3.1) is the following replacement of the mass matrix M:

$$\hat{M} \to \hat{M}(T) = \begin{pmatrix} m_{ee} & m_{es}^* \\ m_{es} & m_{ss} + \Delta m_{ss}(T) \end{pmatrix} , \tag{3.9}$$

and since $\eta(t) \to 0$ for $t \gg 1/m_\phi$, we get $\hat{M}(T(t)) \to \hat{M}_{\text{bare}}$ at late times as already pointed out above.

While the ALP does not contribute to the radiation energy density of the Universe, it does yield a potentially significant contribution to the dark matter (DM) energy density [113] under the assumptions outlined above. Assuming, for example, that ϕ contributes a significant amount to the DM density measured today, the following order-of-magnitude estimate holds [113]:

$$\phi_0 \sim 10^{15}\,\text{GeV} \left(\frac{10^{-15}\,\text{eV}}{m_\phi} \right)^{\frac{1}{4}} . \tag{3.10}$$

Consequently, even for very feeble couplings $\lambda \sim 10^{-21}$ and for scalar masses $m_\phi \sim 10^{-10}\,\text{eV}$ the effective sterile neutrino mass amplitude m_{s0} can be as large as $m_{s0} \sim 100\,\text{eV}$. This shows that even in case of very feeble couplings a sizeable additional sterile mass contribution is possible without the need to assume absurdly large ϕ_0 leading to an overproduction of DM.

Since $\eta(t) \approx 1$ at early times $t \lesssim 1/m_\phi$ this mechanism can yield a significant suppression of active–sterile oscillations in the early Universe, while allowing for this oscillation channel at later times when $\eta \to 0$ at $t \gg 1/m_\phi$. Therefore, this extension to the plain sterile neutrino model offers a promising opportunity to suppress sterile neutrino thermalisation in the early Universe without invalidating the sterile neutrino solution to the SBL anomalies today. This comes at the cost of effectively two new model parameters m_ϕ and m_{s0} that, together with the ADR parameter b, represent the three dimensional parameter space of the full model we consider here.

3.1.3 Active–Sterile Neutrino Mixing and Resonance Structure

The total Hamiltonian of the model under consideration now reads

$$\hat{H}(p,T) = \frac{\hat{M}^2(T)}{2p} + \hat{V}_{\text{matter}}(p,T) + \hat{V}_{\text{ADR}}(p) , \tag{3.11}$$

and can be diagonalised by an SO(2) transformation

$$U(\theta(p,T)) := \begin{pmatrix} \cos(\theta(p,T)) & \sin(\theta(p,T)) \\ -\sin(\theta(p,T)) & \cos(\theta(p,T)) \end{pmatrix} , \tag{3.12}$$

with $\theta(p,T) \in [0,\pi]$, without loss of generality. The mixing angle defined by this procedure then must fulfil the following relation:

$$\tan(2\theta(p,T)) = \frac{2m_{es}(m_{ee} + m_{ss} + \Delta m_{ss}(T))}{((m_{ss} + \Delta m_{ss}(T))^2 - m_{ee}^2) + 2p(|V_e(p,T)| - |V_s(p)|)} . \tag{3.13}$$

On the one hand, for a very large effective sterile mass term, i.e.

$$(m_{ss} + \Delta m_{ss}(T))^2 \gg 2p\big||V_e(p,T)| - |V_s(p)|\big|\,, \tag{3.14}$$

we see that $\theta(p,T) \to 0$ and oscillations are strongly suppressed. On the other hand, also if $2pV_s$ becomes very large compared to all other terms in the denominator, mixing is strongly suppressed. The latter scenario particularly affects the high energy modes, and hence, a more thorough analysis is needed to estimate the impact of the ADR potential on sterile neutrino thermalisation at lower temperatures in the early Universe.

Contrarily to mixing suppression, the ADR potential can also enhance mixing between the active and sterile states up to the point where the so-called resonance condition

$$\begin{aligned}((m_{ss} + \Delta m_{ss}(T))^2 - m_{ee}^2) + 2p(|V_e(p,T)| - |V_s(p)|) \to 0^{\pm} \\ \Leftrightarrow |\tan(2\theta(p,T))| \to \infty\,.\end{aligned} \tag{3.15}$$

is fulfilled. In this case, the mass eigenstates are an equal admixture of the active and sterile neutrinos and the gap between the effective mass eigenvalues is minimal. We can now define the resonance momentum value $p_{\mathrm{res}}(T)$ at which the resonance condition in Equation (3.15) is fulfilled.

In summary, this shows that the interplay between the matter potential, the ADR potential and the time- or temperature-dependent mass determines the effective neutrino mixing in the primordial plasma. This mixing is a crucial ingredient to understand the evolution of neutrino densities in the early Universe.

3.2 Analysis Strategy and Parameter Space

The presence of new light DOFs can have significant impact on the evolution of the Universe and on cosmological observables. Two important quantities that can be extracted from cosmological measurements are the radiation energy density ρ_{tot} shortly before last scattering and the primordial helium abundance $Y_{^4\mathrm{He}}$ after BBN. The SM and ΛCDM predictions of these quantities are in good agreement with the most recent fits to cosmological data [29, 122], meaning that any extension or modification of either theory needs to be thoroughly tested if they have the potential to significantly alter the respective predictions. Moreover, when extending the SM by a light sterile neutrino, the effective sterile neutrino mass m_s^{eff} can be defined to parametrise the impact of the new heavier neutrino state on structure formation. This parameter in turn can also be constrained by fits to cosmological data.

3.2.1 Central Quantities of the Analysis

In order to be able to quantify the changes introduced by the light sterile neutrino, ADR and ALP extension of the SM we introduce the following quantities in the early Universe:

1. The effective number of ultra-relativistic DOFs N_{eff}
2. The effective sterile neutrino mass m_s^{eff}
3. The helium mass fraction $Y_{^4\text{He}}$

The first quantity is used to estimate the influence of ultra-relativistic DOFs not contained in the SM on the radiation energy density between electron–positron annihilation and last scattering ρ_{tot}, while the second one parametrises the impact of the free streaming of the sterile neutrino on matter power spectra as neutrinos cool to non-relativistic temperatures. Moreover, $Y_{^4\text{He}}$ represents the amount of helium produced during BBN for the given model.

In accordance with References [29, 102], we define the effective number of additional ultra-relativistic DOFs via

$$\rho_{\text{rad}} =: N_{\text{eff}} \frac{7}{8} \left(\frac{4}{11}\right)^{\frac{4}{3}} \rho_\gamma + \rho_\gamma \,, \tag{3.16}$$

where ρ_γ is the photon energy density. The factor 7/8 in this definition accounts for the fact that in the SM the only contributions to the radiation energy density can be caused by neutrinos which are fermionic particles. Moreover, the factor $(4/11)^{4/3}$ accounts for the reheating of the photon temperature due to electron–positron annihilation, assuming fully decoupled neutrinos. According to the latest predictions [102], assuming three SM neutrinos with the addition of the standard mass and mixing parameters yields $N_{\text{eff}}^{\text{std}} = 3.044$. The deviation from $N_{\text{eff}} = 3$, even in the standard case, is explained by the fact that neutrinos are not fully decoupled during electron–positron annihilation as well as by the impact of finite temperature QED effects. In order to isolate the influence of the sterile neutrino, we also define the number of *additional* ultra-relativistic DOFs as

$$\Delta N_{\text{eff}} := N_{\text{eff}} - 3.046 \,, \tag{3.17}$$

where we choose a slightly different value for $N_{\text{eff}}^{\text{std}}$ to be able to directly compare our results to fits obtained in Reference [29]. Note that when using N_{eff} to constrain light sterile neutrino models, it is implicitly assumed that the sterile DOF is ultra-relativistic roughly until last scattering at sub-eV temperatures. For $m_4 = 1.1\,\text{eV}$ this is not exactly true, but in accordance with the literature (see e.g. References [29, 101, 113]), we neglect small corrections due to the finite neutrino mass in the very low temperature regime.

As soon as neutrinos become non-relativistic, their free streaming has an impact on structure formation and matter power spectra imprinted within the CMB. Especially when adding a light sterile neutrino to the model whose mass is larger than that of the SM neutrinos, it is important to also estimate the impact of the sterile mass. To this end, we define the effective sterile mass m_s^{eff} by [29]

$$m_s^{\text{eff}} = \Omega_s h^2 \times 94.1\,\text{eV} \,, \tag{3.18}$$

where $\Omega_s = \rho_s^0/\rho_{\text{c}}$ is the energy fraction of the sterile neutrino today and h is the Hubble rate today in units of $100\,\text{km}/(\text{s}\,\text{Mpc})$. Note that in our model extension including the ALP,

the fourth mass eigenvalue m_4 itself becomes time and temperature-dependent. In order to maintain the ultra-relativistic approximation for ν_s, however, we only consider model configurations for that $m_4 \approx 1.1\,\mathrm{eV}$ well after electron–positron annihilation. As described in Reference [29], in our model m_s^{eff} can be estimated by

$$m_s^{\mathrm{eff}} \approx \Delta N_{\mathrm{eff}} m_4 \,, \tag{3.19}$$

as the properties of the sterile neutrino in our model approximately match with those of a Dodelson–Widrow neutrino [123], since it is produced via mixing effects only.

Finally, the helium abundance is usually estimated [29] using the helium mass fraction

$$Y_{^4\mathrm{He}} := \frac{4 n_{\mathrm{He}}}{n_{\mathrm{B}}} \,, \tag{3.20}$$

corresponding to the number density of baryons bound into ^{4}He nuclei normalised to the total baryon number density. The experimentally accessible value of $Y_{^4\mathrm{He}}$ corresponds to that at the time directly after BBN since, afterwards, $Y_{^4\mathrm{He}}$ remains constant. Similarly after electron–positron annihilation also the effective number of neutrino species N_{eff} remains constant as the neutrinos fully decouple around this time. It is therefore possible to compute all values of interest within the era of radiation domination although some of their values, in principle, need to be known at last scattering or even later.

3.2.2 Definition of the Parameter Space

In the analysis presented in the following we calculate the quantities ΔN_{eff}, $m_s^{\mathrm{eff}}$and $Y_{^4\mathrm{He}}$ for several model parameter configurations and compare them to their experimentally estimated values. The sterile neutrino ADR and ALP model is parametrised by three independent parameters: The ALP mass m_ϕ, the amplitude of the ALP-induced sterile neutrino mass contribution m_{s0} and, finally, the ADR parameter b. We restrict the range of ALP masses to $m_\phi \in [10^{-20}, 10^{-14}]\,\mathrm{eV}$. By excluding ALP masses smaller than $10^{-20}\,\mathrm{eV}$, we ensure that the heaviest mass eigenstate ν_4 remains ultra-relativistic for all times and that its mass reduces to $m_4 = 1.1\,\mathrm{eV}$ long before last scattering. At ALP masses above $m_\phi \sim 10^{-14}\,\mathrm{eV}$ the ALP VEV $\phi_0\eta$ starts to vanish too early in order to yield a significant contribution to the sterile neutrino mass. For the parameter m_{s0} we choose a range of $m_{s0} \in [10, 250]\,\mathrm{eV}$ in agreement with Reference [113].

Finally, although we assume the ADR model to be compatible with the results from SBL experiments, we do not strictly set $b \sim 10^{-17}$ as obtained as a promising value in Reference [79]. Instead, we only choose the ADR parameter to be non-negative, i.e. $b \in [0, \infty)$, to allow for a variation of b during the cosmic evolution between the early stages of the Universe and today. In extra dimensional models, for example, such a variation can occur if the curvature of the extra dimension changes over time. Then, however, this mechanism needs to predict the evolution of the ADR parameter towards SBL compatible values today, in order to ensure consistency with results from SBL experiments.

3.3 Evolution of Neutrino Densities in the Early Universe

Since all central quantities discussed in the last section depend on neutrino phase space densities, it is crucial to be able to estimate them reliably. This is achieved by employing the so-called PSDM approach that consistently takes into account scattering processes in the early Universe as well as neutrino flavour transitions. Therefore, this approach resembles a generalisation of the Boltzmann transport equations usually employed to determine the phase space densities of particles in the primordial plasma. The PSDM ϱ_{jk} is defined as the thermal average of neutrino mass eigenstate creation and annihilation operators [121, 124]

$$(2\pi)^3\delta^3(\vec{p}-\vec{q})\varrho_{jk}(\vec{p}) := \langle a_k(\vec{p})^\dagger a_j(\vec{q})\rangle := \mathrm{Tr}(\hat{\Pi} a_k(\vec{p})^\dagger a_j(\vec{q}))\,, \tag{3.21}$$

where $\hat{\Pi}$ is the density operator representing the state of the primordial plasma. According to this definition the diagonal elements of $\varrho_{jj}(\vec{p})$ are the regular neutrino phase space densities we are interested in, whereas the off-diagonal elements encode information about quantum correlations between different neutrino mass eigenstates due to neutrino oscillations. Taking into account these off-diagonal elements is the main difference to the usual Boltzmann approach and enables the consistent treatment of oscillations and collisions [125] in a thermal environment.

Since we are interested in the phase space densities of neutrino interaction eigenstates, we transform the PSDM from the mass basis to the flavour basis, employing the neutrino mixing matrix U, i.e.

$$\varrho^f_{jk} = \sum_{l,m} U_{jl}\varrho_{lm}(U^\dagger)_{mk}\,. \tag{3.22}$$

Moreover, we omit the superscript f in the following by renaming $\varrho^f \to \varrho$.

3.3.1 Quantum Kinetic Equations for the Density Matrix

The PSDM can be extracted from the two-point correlation function, i.e. the thermal propagator, of neutrino fields. In particular, the PSDM is encoded in the statistical part

$$F_{jk}(x^\mu, y^\mu) = \langle[\nu_j(x^\mu), \bar{\nu}_k(y^\mu)]\rangle\,, \tag{3.23}$$

of the thermal propagator encoding the particle occupation numbers [124]. As we have already mentioned in Section 2.3.1, the thermal propagator obeys the Schwinger–Dyson Equations (2.92) that can be obtained from the Two-Particle Irreducible (2PI) effective action. From this, equations of motion for the statistical correlator F_{jk} can be derived. Then, the statistical correlator and its equations of motion are transformed to phase space by employing a so-called Wigner transform, i.e. a partial Fourier transform applied to the relative coordinate, resulting in $\tilde{F}_{jk}(X^\mu, p^\mu)$, where $X^\mu = (x^\mu + y^\mu)/2$ is the absolute coordinate and p^μ is the four-momentum. Afterwards, the transformed equations of motion need to be expanded in small quantities, namely neutrino masses, weak couplings and spacetime derivatives divided

by the neutrino energy. From this procedure the Boltzmann-like equations of motion for the PSDM, called the quantum kinetic equation (QKE), can be obtained [100, 101, 121, 124, 126]

$$(\partial_t - pH\partial_p)\varrho(t,p) = -i[\hat{H}(t,p), \varrho(t,p)] + \mathcal{C}[t,p,\varrho]\,, \tag{3.24}$$

where H is the Hubble rate, $\hat{H}$ is the neutrino Hamiltonian given in Equation (3.1), p is the modulus of the neutrino three momentum, and $\mathcal{C}$ is the collision term describing incoherent scattering of neutrinos among themselves and with the background particles. The derivative operator $(\partial_t - pH\partial_p)$ describes the effect of the expansion of the Universe on the neutrino system.

The above procedure actually results in two coupled equations for the neutrino and antineutrino PSDMs, ϱ and $\bar{\varrho}$, but as argued already before in Section 3.1, we assume the lepton asymmetry to be negligible compared to the total neutrino density. Therefore, we approximate $\varrho \approx \bar{\varrho}$ and only need to consider the equations of motion for ϱ.

Finally, the collision term is assembled from all individual neutrino scattering processes

$$\mathcal{C}[t,p,\varrho] = \sum_{k\in\mathcal{P}} \mathcal{C}_k[t,p,\varrho]\,, \tag{3.25}$$

where $\mathcal{P}$ is the set of all interaction channels in our $1+1$ scenario:

1. $\nu_e e^- \longleftrightarrow \nu_e e^-$
2. $\nu_e e^+ \longleftrightarrow \nu_e e^+$
3. $\nu_e \bar{\nu}_e \longleftrightarrow e^- e^+$
4. $\nu_e \mu^- \longleftrightarrow \nu_e \mu^-$
5. $\nu_e \mu^+ \longleftrightarrow \nu_e \mu^+$
6. $\nu_e \bar{\nu}_e \longleftrightarrow \mu^- \mu^+$
7. $\nu_e \nu_e \longleftrightarrow \nu_e \nu_e$
8. $\nu_e \bar{\nu}_e \longleftrightarrow \nu_e \bar{\nu}_e$

Also neutrino–nucleon scattering should be included in this list, but since at the temperatures of interest nucleons are non-relativistic their number densities follow Boltzmann statistics and are strongly suppressed. Therefore, we neglect these contributions. Moreover, also contributions from neutrino–neutrino scattering can be omitted as they only represent a sub-leading contribution, see e.g. References [100, 101].

All collision terms can be calculated using methods presented in Reference [126]. For the first process, for example, we get

$$\begin{aligned}\mathcal{C}_1[t,p,\varrho] = \frac{32G_F^2}{p}\int \frac{\mathrm{d}^3\vec{p}_1}{(2\pi)^3 2E_1}\frac{\mathrm{d}^3\vec{p}_2}{(2\pi)^3 2E_2}\frac{\mathrm{d}^3\vec{p}_3}{(2\pi)^3 2E_3}(2\pi)^4\delta^4(p^\mu + p_1^\mu - p_2^\mu - p_3^\mu) \\ \times \left\{g_R^2(p_\alpha p_3^\alpha)(p_{1\beta}p_2^\beta) + g_L^2(p_\alpha p_1^\alpha)(p_{2\beta}p_3^\beta) - g_L g_R(p_\alpha p_2^\alpha)m_e^2\right\} \\ \times \Phi_1(t,p^\mu,p_1^\mu,p_2^\mu,p_3^\mu)\,,\end{aligned} \tag{3.26}$$

where we define the effective couplings $g_L = 1/2 + \sin^2(\theta_W)$ and $g_R = \sin^2(\theta_W)$. For the remaining collision terms relevant to the integration of the QKEs, see Appendix B.1. The

statistical factor Φ_1 encodes how many electrons and neutrinos are available for each direction of the reaction, and is given by

$$\Phi_1(t, p^\mu, p_1^\mu, p_2^\mu, p_3^\mu) := \Phi_1^+(t, p^\mu, p_1^\mu, p_2^\mu, p_3^\mu) - \Phi_1^-(t, p^\mu, p_1^\mu, p_2^\mu, p_3^\mu)\,, \tag{3.27}$$

with

$$\Phi_1^+(t, p^\mu, p_1^\mu, p_2^\mu, p_3^\mu) := [1 - f_{e^-}(t, p_1)] f_{e^-}(t, p_3) \{\mathbb{P}_e \varrho(t, p_2) \mathbb{P}_e, \mathbb{1} - \varrho(t, p)\}\,, \tag{3.28}$$

$$\Phi_1^-(t, p^\mu, p_1^\mu, p_2^\mu, p_3^\mu) := f_{e^-}(t, p_1)[1 - f_{e^-}(t, p_3)] \{\mathbb{P}_e [\mathbb{1} - \varrho(t, p_2)] \mathbb{P}_e, \varrho(t, p)\}\,. \tag{3.29}$$

Here, f_{e^-} denotes the electron phase space distribution assumed to follow its equilibrium value where the $e^\pm$ temperature is equal to the photon temperature. The functions $\phi_1^\pm$ are the statistical factors of the forward and backward directions of the first process and contain the appropriate Pauli blocking factors $1 - f$ for final state fermions. These factors explicitly take into account the Pauli exclusion principle and suppress a reaction if the respective final state is already occupied.

Now that we have specified how to obtain the evolution of the neutrino and antineutrino PSDMs we also have to consider the back reaction of changes in the neutrino density on the remaining particle species in the primordial plasma. Since apart from (anti-)neutrinos the only particle species relevant to the dynamics of the scale factor and the evolution of neutrino densities at the temperatures of interest are light (anti-)leptons and photons that are in kinetic equilibrium with each other, the remaining free physical quantity is the temperature T_γ of the EM plasma. The time evolution of T_γ can be derived from the cosmic continuity Equation (2.38) by plugging in the equilibrium distribution for all electromagnetically interacting particles parametrised by T_γ and solving for the derivative $\dot{T}_\gamma$. Therefore, the central task of this project is the simultaneous integration of the differential equations for T_γ and ϱ as all quantities of interest, i.e. ΔN_{eff} and $Y_{^4\text{He}}$ can be computed from this information.

3.3.2 Solution of the Quantum Kinetic Equations

The differential equations governing the time evolution of the PSDM and photon temperature are non-linear and coupled and cannot be solved analytically for given initial conditions. Therefore, we need to employ numerical methods that are described in the following.

To simplify the solution of our set of evolution equations, we introduce the new variables[1]

$$x(t, p) := a(t)\,, \qquad y(t, p) := a(t)\frac{p}{\Lambda}\,. \tag{3.30}$$

The variable x plays the role of the new *time* variable and is just given by the scale factor a. Furthermore, the scale factor is normalised such that $a(t_0) = x_0 = \Lambda / T_\gamma(t_0)$ at the initial time t_0 to be specified below, where $\Lambda = 1\,\text{MeV}$ is a suitable energy scale for the problem.

[1] Note that this choice of new variables slightly differs from the choice in Reference [73] as we assume the scale factor to be dimensionless, here.

The new dimensionless momentum variable can be interpreted as follows: Neglecting effects of scattering and oscillations, i.e. setting $\mathcal{C} \equiv 0$ and $\hat{H} \equiv 0$, an initial phase space distribution is only redshifted by the convectional derivative in Equation (3.24). That means the value of ϱ obtained for a fixed momentum $p^\star$ at initial time t_0 will, at some later time $t > t_0$, correspond to the redshifted momentum $p^\star a(t_0)/a(t)$. Defining the new momentum $y \propto pa(t)$ accounts for this effect and leads to a constant PSDM if oscillations and collisions can be neglected. This can be shown by transforming the QKEs into the set of new variables yielding

$$x\tilde{H}(x)\frac{\partial\tilde{\varrho}}{\partial x}(x,y) = -i[\hat{\tilde{H}}(x,y),\tilde{\varrho}(x,y)] + \tilde{\mathcal{C}}[x,y,\tilde{\varrho}(x,y)]\,. \tag{3.31}$$

If the right hand side of this equation vanishes, the PSDM in the new variables indeed remains constant. In the following, we omit the tildes above all quantities since we always express them in terms of the new variables.

Moreover, the photon temperature evolution equation can be written as

$$T'_\gamma(x) = -\frac{T_\gamma(x)}{x}\frac{3[\rho_{\text{tot}}(x)+P_{\text{tot}}(x)]+x\rho'_{\nu,\text{tot}}}{\Xi(x)}\,, \tag{3.32}$$

$$\Xi(x) \coloneqq 4\rho_\gamma + \sum_{\alpha\in\{e,\mu\}}\frac{g_\alpha}{2\pi^2}\int_0^\infty \mathrm{d}p\; p^2\frac{E_\alpha^2}{T_\gamma}\frac{e^{\frac{E_\alpha}{T_\gamma}}}{\left(1+e^{\frac{E_\alpha}{T_\gamma}}\right)^2} \tag{3.33}$$

$$= T_\gamma\left(\frac{\mathrm{d}\rho_\gamma}{\mathrm{d}T_\gamma} + \sum_{\alpha\in\{e,\mu\}}\frac{\mathrm{d}\rho_\alpha}{\mathrm{d}T_\gamma}\right)\,, \tag{3.34}$$

where the prime denotes the derivative with respect to x, $\rho_{\nu,\text{tot}}$ is the total neutrino energy density and all other appearing quantities are introduced in Section 2.2.1. As we show in Appendix B.2, if all particle species contributing to ρ_{tot} are in thermal equilibrium with each other and are ultra-relativistic, the solution of Equation (3.32) is $T_\gamma(x) = T_\gamma(x_0)x_0/x$. Using the definition of x, we see that indeed $x = \Lambda/T_\gamma(x)$ in this simple case. Therefore, to be consistent we need to choose the initial time x_0 such that this equilibrium conditions applies. Furthermore, the inverse of x can be interpreted as the temperature of a particle species that decouples instantaneously at x_0. We will, therefore, call this quantity the comoving temperature $\bar{T} \coloneqq \Lambda/x$ and it approximately coincides with the photon temperature before electron–positron annihilation. Moreover, $\bar{T}$ also approximately coincides with the effective electron neutrino temperature.

Initial Conditions Before specifying the initial PSDM $\varrho(x_0,y)$, we need to determine a suitable starting point for the integration of the QKEs and the photon temperature. For the study of sterile neutrino thermalisation, it is sufficient to consider temperatures of $T_\gamma \approx \mathcal{O}(100\,\text{MeV})$, see e.g. Reference [101]. At these temperatures collisions damp the oscillation terms and active neutrinos are in thermal equilibrium with the rest of the primordial plasma. Moreover, since in the considered class of models sterile neutrino states can only be populated

via oscillations, we can assume that the total energy density only contains contributions from SM particles $\rho_{\text{tot}} = \rho_{\text{tot,SM}}$. Of course there could be an initial population of sterile neutrinos, but since ν_s does not interact with the SM plasma itself, its density is negligible to the SM neutrino densities due to the numerous reheating processes occurring in the early Universe due to the annihilation processes of SM particles. Thus, for simplicity, we assume the initial sterile neutrino density to vanish.

For our purposes we find $T_\gamma(x_0) = 100\,\text{MeV}$, i.e. $x = 0.01$, to be sufficient, see Appendix B.3 for more details. To achieve a precision estimate of all central quantities of our analysis, we would need to start the integration of the system of differential equations earlier [101] at about $T_\gamma(x_0) = 500\,\text{MeV}$. Moreover, it would also be necessary to take all active neutrino flavours and active–active flavour oscillations into account. Since we are only interested in the potential[2] of the ADR and ALP extensions of the plain sterile neutrino model to suppress the population of ν_s in the early Universe, it is, however, still sufficient to use the starting point $T_\gamma(x_0) = 100\,\text{MeV}$.

The main argument for this, discussed in Appendix B.3, is that if oscillations are unsuppressed at $x_0 < 0.01$ then they are even less suppressed afterwards as the strength of the collisions monotonically decreases with time. In this case, assuming the initial sterile phase space density to vanish at $x_0 = 0.01$ is wrong, but we find that the thermalisation of the sterile species proceeds sufficiently rapidly such that final densities do not depend strongly on the initial conditions. In the contrary case, where oscillations are suppressed until $x_0 = 0.01$, the assumptions of vanishing sterile densities and active–sterile correlations represent a good approximation. Furthermore, SM neutrinos and the EM plasma are still in thermal equilibrium at this initial time. Therefore, the starting point $T_\gamma(x_0) = 100\,\text{MeV}$ is sufficient to estimate whether the sterile species reaches thermal equilibrium with the SM plasma.

The main reason to choose $x_0 = 0.01$, despite the mentioned disadvantages, is that scattering and energy density contributions of muons are strongly Boltzmann suppressed, and hence, can be safely neglected after $x_0 = 0.01$, leading to a tremendous simplification of our calculations. Ultimately, our initial conditions thus read

$$\varrho(x_0, y) \equiv f_\nu^{\text{eq}}(y)\mathbb{P}_e\,, \qquad f_\nu^{\text{eq}}(y) := (\exp(y) + 1)^{-1}\,, \tag{3.35}$$

and $T_\gamma = 100\,\text{MeV}$ at $x_0 = 0.01$.

End of the Time Evolution We extract the neutrino phase space densities at $x_{\text{fin}} = 50$, corresponding to $T_\gamma(x_{\text{fin}}) \approx 28\,\text{keV}$, because we find that at these temperatures ϱ has reached its asymptotic value. Furthermore, in this stage of the Universe neutrino interactions have fully frozen out, the helium abundance reached its final value, the relativistic approximation of the neutrino dispersion relation is still valid and the Universe is still radiation dominated.

[2]Although we are only performing a proof-of-principle analysis here, it is still important to treat oscillations and collisions in a unified framework, i.e. to thoroughly solve the QKEs, since sterile neutrinos can only be populated via oscillations.

Numerical Methodology The last step before solving the QKEs and the evolution equation for T_γ is choosing a proper discretisation of the dimensionless momentum space $\Omega_y = [0, \infty)$. To this end, we pick $N_y = 109$ equidistant momentum nodes between the low and high momentum cutoffs, $y_{\min} = 10^{-4}$ and $y_{\max} = 20$. Unfortunately, we cannot choose $y_{\min} = 0$ as at this value the ultra-relativistic approximation definitely breaks down and our QKE are not suitable to describe the corresponding low energy modes. This only introduces a small error since these low energy modes only constitute a negligible contribution to the energy densities and all other quantities we are interested in. Moreover, the high momentum cutoff is chosen such that we are already in the exponential suppression regime of the solution to Equation (3.31) meaning $\varrho(x, y_{\max}) \sim (\exp(20) + 1)^{-1} \sim 10^{-9}$. The total relative error introduced into the calculation of the neutrino energy density is on the order of 10^{-6}.

In summary, we have transformed Equations (3.31) and (3.32) into $4N_y + 1$ real, coupled ordinary differential equations between $x_0 = 0.01$ and $x_{\text{fin}} = 50$ with initial conditions $\varrho(x_0, y_k) = f_\nu^{\text{eq}}(y_k)\mathbb{P}_e$ and $T_\gamma(x_0) = 100\,\text{MeV}$. Here, we use that the PSDM at each momentum node has four real, independent parameters. For more details on the numerical procedure see Appendix B.4.

3.3.3 Calculating the Helium Abundance

Lastly, we present how the helium mass fraction is calculated from the neutrino PSDM, obtained using the procedure described before. This section closely follows the textbook [127] on kinetic theory in the early Universe. In order to simplify our analysis we will only estimate the neutron abundance using the appropriate Boltzmann equations, but we do not solve the set of kinetic equations describing the detailed conversion of neutrons into helium nuclei. We rather use the fact that at the end of BBN approximately all neutrons are bound into ^{4}He nuclei and only a small fraction is contained in Deuterium, ^{3}He and heavier elements. Therefore, we get that

$$Y_{^4\text{He}} = \frac{4n_{^4\text{He}}}{n_\text{B}} \approx 2\frac{n_n}{n_\text{B}} =: 2X_n\,, \tag{3.36}$$

and that it is sufficient to estimate the neutron fraction $X_n = n_n/n_\text{B}$.

The time evolution of X_n is easily obtained from the Boltzmann equations for n_n. Using that the baryon number in a comoving volume is conserved at temperatures of the order $\mathcal{O}(\Lambda = 1\,\text{MeV})$ we find the evolution equations for X_n to be [127]

$$\frac{\mathrm{d}X_n(x)}{\mathrm{d}x} = \frac{\lambda_{pn}(x)}{xH}(1 - X_n(x)) - \frac{\lambda_{np}(x)}{xH}X_n(x)\,, \tag{3.37}$$

where λ_{pn} and λ_{np} are the thermal interaction rates corresponding to the processes

$$n + e^+ \leftrightarrow p + \bar{\nu}_e\,, \qquad n + \nu_e \leftrightarrow p + e^-\,, \qquad n \leftrightarrow p + \bar{\nu}_e + e^-\,. \tag{3.38}$$

Here, λ_{pn} corresponds to the $\leftarrow$-direction, whereas λ_{np} corresponds to the $\rightarrow$-direction. For more details on the definition and properties of the interaction rates see Appendix B.5.

The differential Equation (3.37) is solved between $x_0^\star$ and $x_{\mathrm{fin}}^\star$ that are defined such that

$$T_\gamma(x_0^\star) = 5\,\mathrm{MeV} \qquad \text{and} \qquad t(x_{\mathrm{fin}}^\star) = 300\,\mathrm{s} \qquad \Leftrightarrow \qquad T_\gamma(x_{\mathrm{fin}}^\star) \approx 0.07\,\mathrm{MeV}\,, \tag{3.39}$$

lying within the integration interval of the QKEs for all model configurations. The end point of the integration is chosen according to a fixed value of cosmic time instead of a fixed value of the photon temperature since the time–temperature relation changes depending on the influence of ν_s on the Hubble rate. However, the end of BBN is determined by the condition that the respondible nuclear interaction rates are negligible compared to the Hubble rate that is directly related to the cosmic time via Equation (2.57). This relation does not change under the influence of the sterile species as it only depends on the radiation domination assumption.

The solution of the photon temperature in terms of x is used in order to find $x_0^\star$ and $x_{\mathrm{fin}}^\star$ and the neutrino PSDM enters the calculation of the interaction rates $\lambda_{np(pn)}$. For this purpose, we interpolate our solutions for ϱ on the (x, y)–grid defined in the previous section.

Unfortunately, the approximation $Y_{^4\mathrm{He}} \approx 2X_n$ is rather rough and it is not appropriate to compare our results for $Y_{^4\mathrm{He}}$ to actual measurements like those presented in Reference [122]. Nevertheless, we can still compare the model predictions to the SM prediction in our computation scheme and see if the difference exceeds the experimentally obtained uncertainties stated in Reference [122].

For completeness, we summarise all differential equations in terms of the dimensionless variables in Appendix B.6.

3.4 Effective Number of Light Degrees of Freedom and Helium Abundance

Now that we have outlined the details of the analysis strategy, we can finally evaluate our central quantities ΔN_{eff}, m_s^{eff} and $Y_{^4\mathrm{He}}$ on several benchmark points in our parameter space that we have chosen in order to fit the proof-of-principle paradigm of this analysis. To this end, we first consider the ADR- and ALP-only cases where we only switch on one of these new physics effects. Afterwards, we consider certain interesting parameter configurations in the ADR + ALP scenario. For each configuration we estimate the additional number of light DOFs ΔN_{eff}, the effective sterile neutrino mass m_s^{eff} as well as the final helium abundance $Y_{^4\mathrm{He}}$. The values obtained for ΔN_{eff} and m_s^{eff} are then compared to recent measurements by the Planck collaboration [29] summarised in Table 3.1. Furthermore, our predictions for $Y_{^4\mathrm{He}}$ are compared to the corresponding SM prediction in our approximation and it is investigated if the difference of both predictions exceeds the respective experimental uncertainties $\sigma_{Y_{^4\mathrm{He}}} = 0.004$ (68 % CL) or $2\sigma_{Y_{^4\mathrm{He}}} = 0.008$ (95 % CL) presented in Reference [122].

Table 3.1: Upper limits on N_{eff} and m_s^{eff} obtained at 95 % confidence level (CL) by the Planck collaboration in Reference [29] in a combined fit assuming different priors on the physical sterile neutrino mass m_4, as can be inferred from References [29, 128].

Measurement	N_{eff}	ΔN_{eff}	m_s^{eff} / eV
TT, TE, EE + lowE + lensing + BAO ($m_4 < 20\,\text{eV}$)	3.29	0.24	0.65
TT, TE, EE + lowE + lensing + BAO ($m_4 < 4\,\text{eV}$)	3.34	0.29	0.23

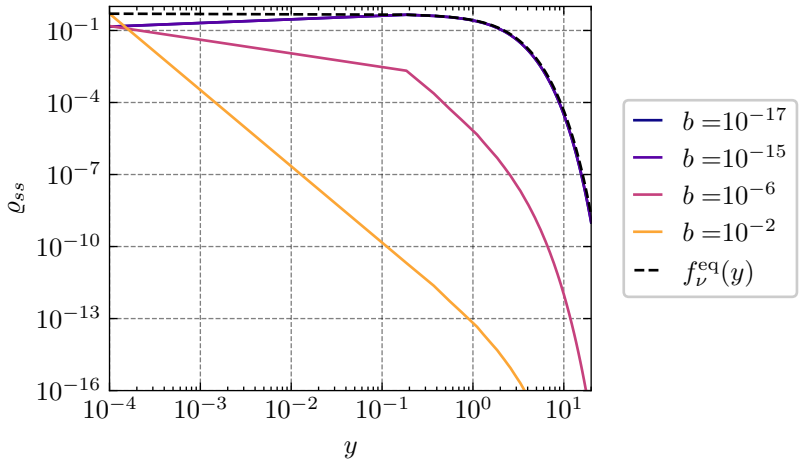

Figure 3.1: Final ($x = 50$) ν_s phase space distributions (solid) as a function of the comoving momentum y for various ADR parameters $b \in \{10^{-17}, 10^{-15}, 10^{-6}\}$ compared to the equilibrium density f_ν^{eq} (dashed).

3.4.1 Predictions for the Central Quantities in the ADR-only Scenario

The final values for ΔN_{eff}, m_s^{eff} and $Y_{^4\text{He}}$ are shown in Table 3.2. It is clear that for small ADR parameters b sterile neutrinos equilibrate with the EM plasma and contribute a full new DOF. At much larger ADR parameter values roughly around $b \sim 10^{-6}$ the ADR effect leads to an effective suppression of the production of sterile neutrinos and all values of ΔN_{eff} and m_s^{eff} are within the 95% CL intervals obtained by the Planck collaboration. In Figure 3.1, we show the final sterile neutrino phase space distributions to support our interpretation. The thermal development of the PSDM can be explained by considering the effective mixing between ν_e and ν_s below $T_\gamma \sim 100\,\text{MeV}$. Especially the evolution of the dimensionless resonance momentum $y_{\text{res}}(\bar{T})$ determines which momentum modes experience vacuum-like mixing, resonant enhancement or mixing suppression. Other than in SBL experiments there is no fixed value for the resonance but it evolves with temperature since the matter potential depends on the comoving temperature $\bar{T}$ and directly enters the resonance condition (3.15). The temperature evolution of y_{res} for each parameter configuration from Table 3.2 is shown in Figure 3.2. For each curve individually, Figure 3.2 can be subdivided into three regions:

Table 3.2: Estimated additional light DOFs ΔN_{eff}, effective sterile mass m_s^{eff} and helium abundance at $x = 50$ for different ADR parameters b.

b	ΔN_{eff}	m_s^{eff} / eV	$Y_{^4\text{He}} - Y_{^4\text{He}}^{\text{SM}}$
0	1.31	1.44	0.008
10^{-17}	1.31	1.44	0.008
10^{-15}	1.31	1.44	0.008
10^{-12}	1.33	1.46	0.008
10^{-6}	0.01	0.01	0.000
10^{-4}	0.01	0.01	0.000
10^{-2}	0.01	0.01	0.000

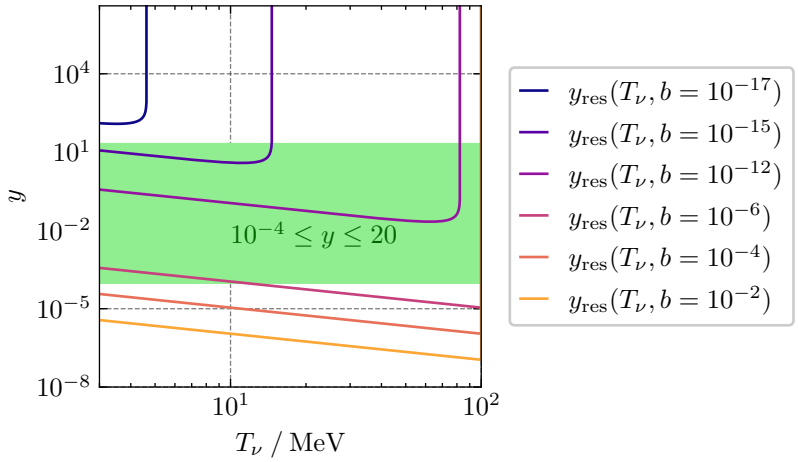

Figure 3.2: Resonance momentum evolution in terms of the comoving temperature $\bar{T} = \Lambda/x$ for different ADR parameters $b \in \{10^{-17}, 10^{-15}, 10^{-12}, 10^{-6}, 10^{-4}, 10^{-2}\}$. The green shaded region indicates the momentum range relevant for the computation of the central quantities of this analysis ΔN_{eff}, m_s^{eff} and $Y_{^4\text{He}}$.

1. Vacuum-like mixing
2. Resonant enhancement
3. Mixing suppression

The first region contains all momentum and temperature configurations for which the matter and ADR potential are negligible compared to the sterile mass and $\tan 2\theta(x, y) \approx \tan 2\theta_{\text{vac}}$. This is the case below each resonance curve, i.e. at small momenta compared to y_{res}. The second region is given by the resonance curve itself and a small band around it. In this region we have $|\tan 2\theta(x, y)| \gg 1$ and mixing is close to maximal. At much higher momenta $y \gg y_{\text{res}}$ the ADR potential dominates the mixing and $|\tan 2\theta(x, y)| \ll 1$ implying[3] $\nu_e \approx \nu_4$

[3]Note that, although, we consider a $1 + 1$ neutrino model, we still need to account for the presence of the other active neutrinos, e.g. when computing the radiation energy density. Thus, we denote the heaviest

and $\nu_s \approx \nu_1$, as the system has passed the level crossing. In addition to this, for each parameter configuration exists a threshold temperature above that no resonance can occur as the active neutrino potential is too large to be surpassed by the ADR potential. In this region to the right of each resonance curve the transition from vacuum-like mixing to mixing suppression is smooth.

Small ADR Parameters Using this discussion as our main tool, we can infer from Figure 3.2 that for very small ADR parameters, i.e. $b < 10^{-15}$, the resonance curves are located well above the relevant momentum region. Consequently, the effective mixing is close to the (large) vacuum-like mixing at small momenta and matter effect modified mixing at higher momenta from the green region in Figure 3.2. Due to the constant supply of ν_e from weak interactions in the plasma, sterile neutrinos are copiously produced via oscillations at small ADR parameters and temperatures above neutrino freeze-out, and hence, lead to $\Delta N_{\text{eff}}(x_{\text{fin}}) \approx 1$.

Intermediate ADR Parameters The reasoning seems to be somewhat more involved for ADR parameter configurations corresponding to resonance curves within the region of relevant momenta. As one of these momentum modes passes through the resonance the active–sterile oscillations are enhanced and sterile neutrinos are produced. This phase of resonant enhancement, however, holds on only for a short period of time. While this might cause an increase of the sterile neutrino distribution in this mode, the long term mixing behaviour is much more important. In all cases where the resonance curve reaches into the region of momenta relevant to the calculation of ΔN_{eff}, the effective mixing in the resonance-less temperature region is already close to the large vacuum mixing and all relevant momentum modes have already been equilibrated. This also shows that our chosen initial conditions $\varrho_{ss}(x_0) \equiv 0$ are rather inaccurate for intermediate and small ADR parameter configurations. The resulting, final PSDM, however, is independent of this choice as it is quickly driven towards thermal equilibrium shortly after x_0.

Large ADR Parameters In contrast to the former cases, at very large ADR parameters, i.e. $b \gtrsim 10^{-6}$, the initial condition $\varrho \equiv f_\nu^{\text{eq}} \mathbb{P}_e$ is sufficiently accurate since all relevant momentum modes are subject to large mixing suppression either because the resonance curve is located beneath all relevant momenta or because of collision induced oscillation damping at very high temperatures where no resonance exists. Thus, all sterile momentum modes remain unpopulated until neutrino freeze-out at arond $T_\nu \sim 3\,\text{MeV}$ and the total number of neutrinos is conserved afterwards. Therefore, the resulting ΔN_{eff} is close to zero and in agreement with the SM prediction.

In addition to ΔN_{eff} and m_s^{eff}, we also need to consider the impact of each model configuration on $Y_{^4\text{He}}$ as compatibility of the prediction for the former two quantities with measurements does not imply the same for $Y_{^4\text{He}}$. This is mainly because in addition to a faster expansion rate

mass eigenstate by ν_4, even though it should actually be called ν_2 in our framework.

of the Universe, indicated by ΔN_{eff}, also the depletion of electron neutrinos due to oscillations into the sterile state can influence the time evolution of the neutron fraction X_n, and hence, also the resulting helium abundance $Y_{^4\text{He}}$. While scenarios with $\Delta N_{\text{eff}} \sim 1$ will certainly lead to a discrepancy as neutron freeze-out occurs earlier than for $\Delta N_{\text{eff}} \sim 0$, also a decreased electron neutrino density leads to smaller interaction rates $\lambda_{np(pn)}$ than in the SM. Both effects would lead to a larger neutron fraction and helium abundance. The difference between the cases of the electron neutrino depletion and greater overall ΔN_{eff} is that ΔN_{eff} remains approximately constant after neutrino freeze-out since the total neutrino density in a comoving volume is conserved then, but oscillations can still alter the flavour composition.

The results for the final helium abundance at $t \approx 300\,\text{s}$—corresponding to a photon temperature of about $T_\gamma \approx 0.07\,\text{MeV}$—are also presented in Table 3.2. There, we report the differences between the model prediction and our SM prediction $Y^{\text{SM}}_{^4\text{He}} = 0.227$ that can be compared to the one and two sigma uncertainties $\sigma_{Y_{^4\text{He}}} = 0.004$ and $2\sigma_{Y_{^4\text{He}}} = 0.008$ of the experimental measurement, respectively. As expected for all parameter cases yielding $\Delta N_{\text{eff}} \sim 1$, also the helium abundance deviates significantly from the SM prediction exceeding the SM prediction by two sigma. Only for very large ADR parameters, the predictions are in agreement with $Y^{\text{SM}}_{^4\text{He}} = 0.227$ within one sigma of the experimental uncertainties. Here, the same arguments apply as for ΔN_{eff} since for very large ADR the resonance curve is still well below or at least at the lower boundary of the relevant momentum region. As low energy neutrinos do not contribute significantly to the neutron–proton interaction rates, depletion of electron neutrinos in these modes do not affect the final helium abundance. This can also be checked by inspecting Figure 3.3, where the temperature evolution of the relative deviation of the neutron fraction from the SM prediction is shown for ADR parameters $b = 10^{-17}$ and $b = 10^{-4}$. Here, we see that around the temperatures $T_\gamma = 2\,\text{MeV}$ to $4\,\text{MeV}$ all curves, including the SM prediction, depart from equilibrium. As $X_n(b = 10^{-17})$ leaves equilibrium slightly earlier than $X_n^{\text{SM}} \approx X_n(b = 10^{-4})$, it freezes out at a higher temperature, and hence, yields a larger helium abundance in the end. In contrast to that, the large ADR configuration $b = 10^{-4}$ corresponds to a negligible sterile neutrino density and to near-to SM neutron–proton interaction rates.

3.4.2 Predictions for the Central Quantities in the ALP-only Scenario

Next, we turn to the class of ALP-only models where the ADR potential is switched off, i.e. $b = 0$, but the coupling of ν_s to the ALP field ϕ is switched on. The corresponding free parameters in these scenarios are the additional sterile neutrino mass amplitude m_{s0} and the ALP mass m_ϕ. Since we assume the coupling between ν_s and ϕ to be feeble, and hence, resulting scattering processes to be negligible, the only effect of the sterile neutrino–ALP coupling is the additional sterile mass contribution. Therefore, the only modification of the model class under consideration, compared to the plain sterile neutrino scenario, is the replacement of the m_{ss} mass matrix element in the Hamiltonian (3.1) to $m_{ss} + m_{s0}\eta(t, m_\phi)$, cf. Equation (3.7). The time-dependence of the VEV η is solely controlled by the ALP mass m_ϕ as shown in Figure 3.4. At times $t \ll 1/m_\phi$ the time-dependence η of the scalar VEV is effectively constant and begins to decrease and oscillate after $t \gtrsim 1/m_\phi$. This and the fact that

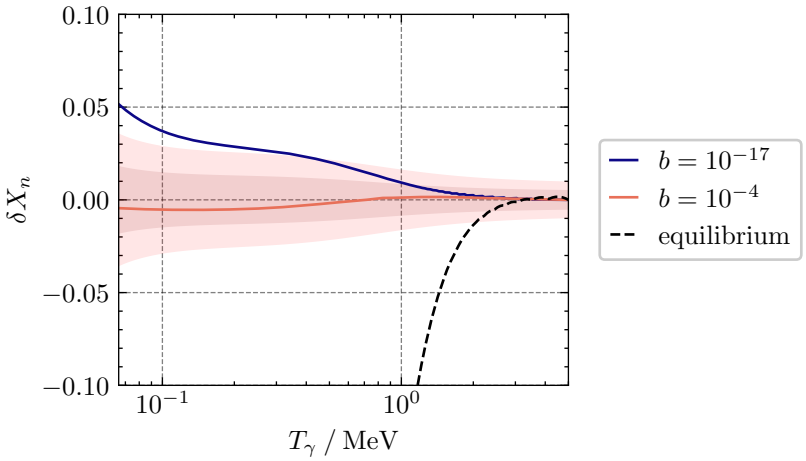

Figure 3.3: Evolution of the relative deviation of the neutron abundance $\delta X_n := (X_n - X_n^{\mathrm{SM}})/X_n^{\mathrm{SM}}$ with respect to the photon temperature T_γ for two different ADR parameters, i.e. $b \in \{10^{-17}, 10^{-4}\}$, after neutron freeze-out. The dashed black curve represents the relative deviation of the equilibrium curve from the SM expectation while the two solid curves correspond to the relative deviations in the two benchmark scenarios, respectively. The red shaded regions indicate the one (dark red) and two sigma (light red) uncertainty bands of the SM prediction.

m_{s0} determines the amplitude of the additional sterile mass contribution are the key points for the understanding of the behaviour of sterile neutrino densities, and consequently, also key points for the understanding of the behaviour of the central observables in this analysis.

The final values for the effective number of additional light DOFs ΔN_{eff}, the effective sterile neutrino mass m_s^{eff} as well as the final helium abundance $Y_{^4\mathrm{He}}$ for a grid of parameter values are shown in Table 3.3. From these results we infer that smaller m_ϕ and larger m_{s0} are favoured by experimental data. This can be explained straightforwardly using our discussion of the parameter-dependence of the full sterile mass matrix element $m_{ss}(t)$, and the dependence of the effective mixing angle on $m_{ss}(t)$ shown in Equation (3.13). Especially during the phase where η is constant, larger m_{s0} yield larger sterile masses, implying smaller effective mixing according to Equation (3.13). In particular, only the benchmark configurations $(m_{s0} = 250\,\mathrm{eV}, m_\phi = 10^{-20}\,\mathrm{eV})$ and $(m_{s0} = 250\,\mathrm{eV}, m_\phi = 10^{-16}\,\mathrm{eV})$ are compatible with almost all Planck bounds from Table 3.1. The only exception is the most stringent bound obtained for m_s^{eff}, i.e. $m_s^{\mathrm{eff}} < 0.23\,\mathrm{eV}$. This last bound, according to our findings above, would also be fulfilled when slightly increasing the additonal sterile mass amplitude to $m_{s0} > 250\,\mathrm{eV}$.

We further stress this argument by plotting $\tan 2\theta(\bar{T}, y)$ for different values of m_{s0} in Figure 3.5 while the ALP mass is kept fixed at $m_\phi = 10^{-20}\,\mathrm{eV}$ ensuring that $\eta \equiv \mathrm{const}$ during the integration of the QKEs. The resulting temperature-dependence of the effective mixing angle, shown in Figure 3.5, is thus only induced by the matter potential V_e. As discussed in the last section, the size of the effective mixing angle crucially determines how much ν_s is populated in the early Universe. We can see that this is indeed the case by considering the left panel

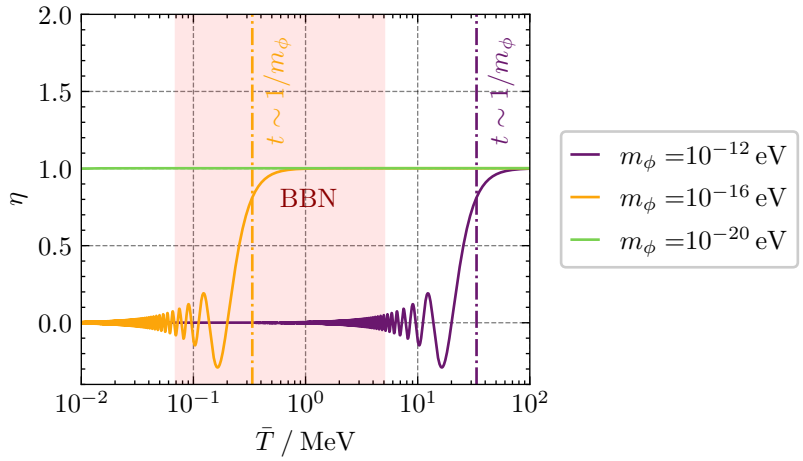

Figure 3.4: Behaviour of the normalised scalar VEV η for different ALP mass parameters m_ϕ at comoving temperatures $\bar{T}$ in the integration range of the QKEs. The dash dotted lines mark the temperatures at which $t \sim m_\phi$ where m_ϕ has the value corresponding to the solid curve in the same colour. Furthermore, the red shaded region indicates the approximate range of temperatures during which BBN takes place.

of Figure 3.6 where the temperature evolution of the sterile neutrino phase space density is shown for the same parameters used for the mixing plots in Figure 3.5.

Increasing the ALP mass to larger values leads to an earlier decrease of the effective mixing angle, and therefore, also to stronger population of the sterile neutrino momentum modes as can be seen in the right panel of Figure 3.6. Especially for $m_\phi > 10^{-16}\,\text{eV}$ the sterile mass decreases while neutrinos are still in thermal equilibrium with the remaining primordial plasma, and hence, electron neutrino states converted into ν_s are refilled leading to the thermalisation of all neutrino species and $\Delta N_{\text{eff}} \sim 1$.

Based on the values of the final helium abundance listed in Table 3.3, we see exactly the same picture as for ΔN_{eff} and m_s^{eff}: Experimental measurements of the helium abundance from BBN also prefer smaller m_ϕ and larger m_{s0}. For scalar masses $m_\phi \gtrsim 10^{-18}\,\text{eV}$ the additional sterile mass contribution starts decreasing already before BBN, giving rise to active–sterile oscillations, and hence, a potential depletion of the electron neutrino density. However, we find that $Y_{^4\text{He}}$ seems to be insensitive to this effect as there is no difference in $Y_{^4\text{He}}$ between the $m_\phi = 10^{-20}\,\text{eV}$ and $m_\phi = 10^{-16}\,\text{eV}$ at least within the significant digits dictated by $\sigma_{Y_{^4\text{He}}} = 0.004$. As shown in Figure 3.7, the electron neutrino density indeed decreases as expected, but the impact of this effect on the neutron–proton interaction rates is negligible. Finally, in Figure 3.8 we compare the evolution of the neutron fractions X_n for the configurations from Table 3.3 that are most and least compatible with the SM prediction. While the most compatible curve stays close to the SM baseline, the least compatible one departs from equilibrium much earlier leading to a larger neutron and, thus, also to a larger helium abundance.

Table 3.3: Estimated additional light DOFs $\Delta N_{\rm eff}$, effective sterile mass $m_s^{\rm eff}$ and helium abundance at $x = 50$ for different ALP parameters, m_{s0} and m_ϕ.

m_{s0} / eV	m_ϕ / eV	$\Delta N_{\rm eff}$	$m_s^{\rm eff}$ / eV	$Y_{^4\rm He}$
50	10^{-20}	1.18	1.30	0.007
50	10^{-16}	1.17	1.29	0.007
50	10^{-12}	1.25	1.38	0.008
100	10^{-20}	0.75	0.83	0.005
100	10^{-16}	0.75	0.83	0.005
100	10^{-12}	0.88	0.97	0.006
250	10^{-20}	0.21	0.23	0.002
250	10^{-16}	0.21	0.23	0.002
250	10^{-12}	0.25	0.28	0.002

3.4.3 Predictions for the Central Quantities in the Combined ADR and ALP Scenario

The consideration of the ALP only scenario in the last section has shown that for vanishing ADR parameters a sterile neutrino with masses in the $m_4 \sim 1\,\text{eV}$ range, today, can be reconciled with cosmological data. This also carries over to small ADR parameters in the range interesting for a resolution of the SBL anomalies, i.e. $b \lesssim 10^{-15}$. At these small ADR parameter values the sterile potential is effectively negligible compared to the modified sterile mass and the matter potential dominating the mixing. This can be seen by inspecting the denominator of $\tan 2\theta$ in Equation (3.13). Since the mixing structure ultimately determines whether the sterile neutrino thermalises in the early Universe, we expect that the results for the smallest ADR parameters under consideration effectively coincide with those for a vanishing ADR potential. Indeed this is also what we find, i.e.

$$\Delta N_{\rm eff}(m_\phi = 10^{-20}\,\text{eV}, m_{s0} = 250\,\text{eV}, b = 10^{-17}) = 0.21\,, \tag{3.40}$$

$$m_s^{\rm eff}(m_\phi = 10^{-20}\,\text{eV}, m_{s0} = 250\,\text{eV}, b = 10^{-17}) = 0.23\,\text{eV}\,, \tag{3.41}$$

$$Y_{^4\rm He}(m_\phi = 10^{-20}\,\text{eV}, m_{s0} = 250\,\text{eV}, b = 10^{-17}) = 0.002\,, \tag{3.42}$$

and similarly for $b = 10^{-15}$. Here, we have chosen to consider the most promising benchmark scenario from Section 3.4.2, i.e. $(m_\phi = 10^{-20}\,\text{eV}, m_{s0} = 250\,\text{eV})$, with $b \neq 0$ and $b \ll 1$. We find that almost all cosmological bounds, but the most stringent one for $m_s^{\rm eff}$, i.e. $m_s^{\rm eff} < 0.23\,\text{eV}$, are fulfilled. Again according to our previous findings, slightly increasing the mass amplitude m_{s0} would also lead to agreement of the current scenario with the tightest constraint on $m_s^{\rm eff}$.

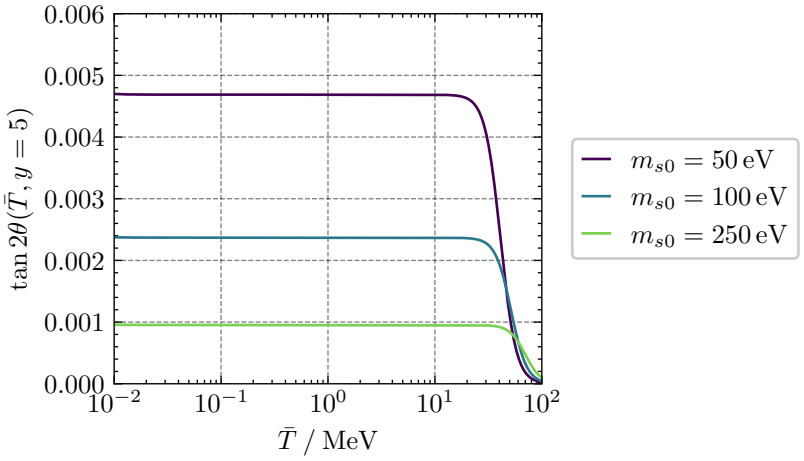

Figure 3.5: Effective $\tan 2\theta$ for different values of m_{s0} at temperatures in the integration range of the QKEs. Here, we fixed $m_\phi = 10^{-20}\,\mathrm{eV}$ such that η remains constant for all temperatures of interest.

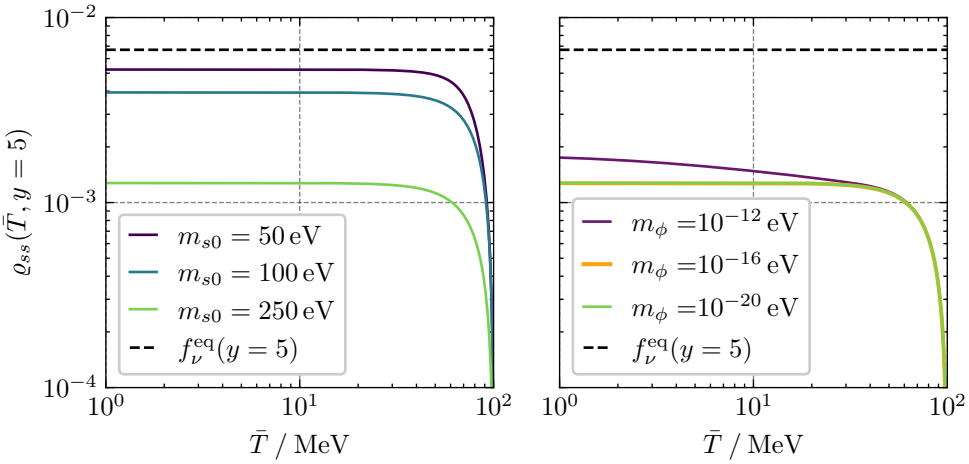

Figure 3.6: Temperature evolution of ϱ_{ss} at $y = 5$ compared to the equilibrium value (black, dashed line). The left panel shows parameter configurations with $m_\phi = 10^{-20}\,\mathrm{eV}$ and varying m_{s0}, whereas the right panel shows the curves corresponding to $m_{s0} = 250\,\mathrm{eV}$ and varying m_ϕ.

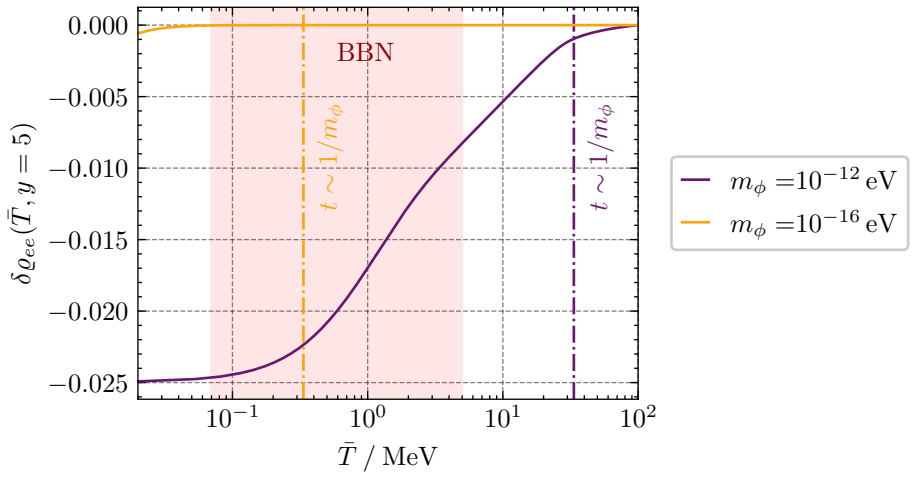

Figure 3.7: Comoving temperature evolution of the relative deviation of the electron neutrino density from its equilibrium value $\delta\varrho_{ee} := (\varrho_{ee} - f_\nu^{\mathrm{eq}})/f_\nu^{\mathrm{eq}}$ at $y = 5$. Shown are two parameter configurations with different m_ϕ and $m_{s0} = 250\,\mathrm{eV}$. The dashed lines indicate the onset of the oscillation of the scalar field VEV η corresponding to the different scalar mass values. Furthermore, the temperature span of BBN is indicated by the red shaded region.

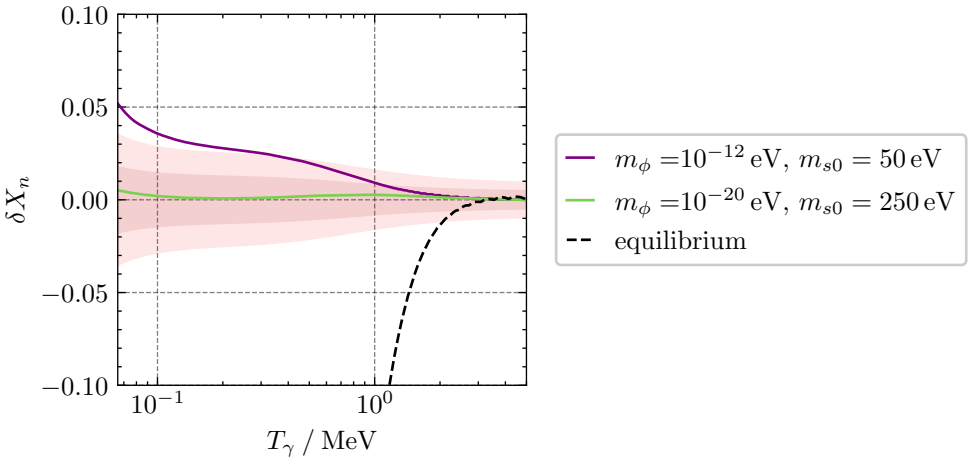

Figure 3.8: As Figure 3.3 for ALP-only scenarios after neutron freeze-out.

3.5 Summary and Conclusion

In this chapter, we have studied the consequences of a light, strongly mixed sterile neutrino in combination with ADRs and couplings to an ALP on cosmological parameters. It turns out that for both additions to the plain sterile neutrino model, there exist parameter configurations such that the predictions for the cosmological quantities under consideration are in agreement with the respective experimental bounds. In particular, we consider the effective number of additional light DOFs ΔN_{eff}, the effective sterile neutrino mass m_s^{eff}, as well as the amount of helium-4 produced during BBN $Y_{^4\text{He}}$. The most stringent bounds on ΔN_{eff} and m_s^{eff} have been determined to be $\Delta N_{\text{eff}} < 0.24$ and $m_s^{\text{eff}} < 0.23\,\text{eV}$, respectively, cf. Reference [29]. Furthermore, the helium-4 abundance has been shown [122] to agree with the SM prediction to within the margin of error $\sigma_{Y_{^4\text{He}}} = 0.004$.

For the ADR-only model, we conclude that parameter configurations motivated by their potential to solve the SBL anomalies, i.e. $b \sim 10^{-17}$, are not sufficient to prevent the thermalisation of the light sterile neutrino. These scenarios lead to

$$\Delta N_{\text{eff}}(b = 10^{-17}) \approx 1.31\,, \tag{3.43}$$
$$m_s^{\text{eff}}(b = 10^{-17}) \approx 1.44\,\text{eV}\,, \tag{3.44}$$
$$Y_{^4\text{He}}(b = 10^{-17}) - Y_{^4\text{He}}^{\text{SM}} \approx 0.008\,, \tag{3.45}$$

exceeding the bounds on ΔN_{eff}, m_s^{eff} as well as resulting in a 95 % CL deviation from $Y_{^4\text{He}}^{\text{SM}} \approx 0.227$ representing the SM prediction for the helium abundance obtained within our approximation scheme.

In contrast, increasing the ADR parameter b to much larger values $b \gtrsim 10^{-6}$ leads to excellent agreement with experimentally determined values for all three quantities:

$$\Delta N_{\text{eff}}(b \gtrsim 10^{-6}) \approx 0.01\,, \tag{3.46}$$
$$m_s^{\text{eff}}(b \gtrsim 10^{-6}) \approx 0.01\,\text{eV}\,, \tag{3.47}$$
$$Y_{^4\text{He}}(b \gtrsim 10^{-6}) - Y_{^4\text{He}}^{\text{SM}} = 0.000\,. \tag{3.48}$$

This is due to the sizeable active–sterile mixing suppression between all neutrino momentum modes relevant for our calculations. Consequently, the sterile neutrino does not thermalise and its phase space distribution stays close to zero. Since the time evolution of the ADR parameter might be tied to the cosmic evolution, assuming large ADR parameters in the early Universe does not contradict the initial motivation of the ADR model as a possible solution the SBL anomalies.

Adding a feeble Yukawa coupling between an ultra-light ALP-field ϕ and ν_s introduces a time varying sterile neutrino mass $m_{ss} \to m_{ss} + m_{s0}\eta(t, m_\phi)$, and therefore, also leads to a variable mixing angle. This additional source of mixing suppression can be used to bring very small ADR parameter values in agreement with experimental data. For an ALP-mass

$m_\phi = 10^{-20}\,\mathrm{eV}$ and additional mass amplitude $m_{s0} = 250\,\mathrm{eV}$, for example, we obtain

$$\Delta N_{\mathrm{eff}}(m_\phi = 10^{-20}\,\mathrm{eV}, m_{s0} = 250\,\mathrm{eV}, b = 10^{-17}) = 0.21\,, \tag{3.49}$$

$$m_s^{\mathrm{eff}}(m_\phi = 10^{-20}\,\mathrm{eV}, m_{s0} = 250\,\mathrm{eV}, b = 10^{-17}) = 0.23\,\mathrm{eV}\,, \tag{3.50}$$

$$Y_{^4\mathrm{He}}(m_\phi = 10^{-20}\,\mathrm{eV}, m_{s0} = 250\,\mathrm{eV}, b = 10^{-17}) = 0.002\,. \tag{3.51}$$

Here, only the prediction for m_s^{eff} coincides with the strictest upper limit obtained by the Planck collaboration and, strictly speaking, can hence not be considered to be in full agreement with all bounds. Nevertheless, for slightly larger values of m_{s0}, corresponding to larger active–sterile mixing suppression, also the ALP-only as well as the small ADR + ALP scenario can be brought into full agreement with *all* experimentally obtained bounds.

As this analysis is merely a proof-of-principle study to show that the SM extensions under consideration are indeed suitable to suppress the thermalisation of sterile neutrino species in the early Universe, we have accommodated a number of approximations. Potential future analyses aimed at a precision calculation of ΔN_{eff}, m_s^{eff}, $Y_{^4\mathrm{He}}$ and possible other cosmological parameters would especially need to improve in the following ways:

1. Include all SM neutrino generations
2. Start the QKE integration earlier at $T_\gamma \sim 500\,\mathrm{MeV}$
3. Include finite temperature QED effects on scattering rates and the evolution of the photon temperature

The current study has been carried out for one active (electron flavour) and one sterile neutrino generation. We justify this simplifying approximation by the fact that the main effect, i.e. the missing suppression due to active–sterile decoupling above the resonance, is a generic effect that has been found to also occur in the presence of more neutrino generations [79]. Hence, our main findings still hold in, for example, a $3 + 1$ neutrino generation framework. Moreover, in case of the ALP extension the mechanism suppressing sterile neutrino equilibration is the increase of the corresponding mass matrix element due to the additional mass contribution. Also in higher dimensional flavour spaces this leads to mixing suppression if all diagonal entries of the sterile mass matrix become very large compared to all other matrix elements.

Regarding the second point, we stress that in this analysis we are mainly interested in parameter configurations leading to an unpopulated sterile species. For these cases it has been shown to be sufficient to start the integration of the QKEs at $T_\gamma(x_0) = 100\,\mathrm{MeV}$. All other parameter configurations, in principle, need a more sophisticated treatment to achieve a precision estimate of any observable and require $T_\gamma(x_0) \sim 500\,\mathrm{MeV}$. This, however, will not change the result that $\Delta N_{\mathrm{eff}} \sim 1$ but could only potentially further increase this value.

Finally, accounting for finite temperature QED corrections can make a significant difference in the prediction of cosmological parameters, as has been shown in Reference [102]. In the case of ΔN_{eff} they can lead to an increase of $\Delta N_{\mathrm{eff}} \sim 0.1$. Nevertheless, for the present analysis it is sufficient to neglect these effects as they only play a sub-leading role for the thermalisation

of the sterile neutrino species since it can only thermalise via oscillations that are not strongly influenced by finite temperature QED corrections.

The main statement of this analysis, therefore, is that SM extensions including light sterile neutrinos can be reconciled with cosmological observations by adding ADRs or a coupling to an ALP condensate, representing a possible DM candidate. For the ADR-only scenario one would need ADR parameters on the order of $b \sim 10^{-6}$ or larger, while in the ALP-only case the experimentally preferred parameter configurations are $m_\phi \lesssim 10^{-14}\,\mathrm{eV}$ and $m_{s0} \gtrsim 100\,\mathrm{eV}$. The combination of both extensions can help bringing the small ADR parameter scenarios into agreement with cosmological data representing a possibility to account for the resolution of SBL anomalies using the ADR model without introducing a time-dependence for the ADR parameter b.

4 Quantum Gravitational Decoherence in Neutrino Flavour Oscillations

This chapter is based on References [129–131].

One of the fundamental open questions in physics is if gravity is quantised similarly to all other forces of nature and if so, how this theory of quantum gravity (QG) needs to be formulated. If at the fundamental level gravity is indeed described by a quantum theory, spacetime itself would be subject to quantum fluctuations [132, 133] (see e.g. Reference [134] for a recent review). These quantum fluctuations are commonly referred to as *spacetime foam* and correspond to geometric perturbations such as virtual black holes [135]. Moreover, any particle system propagating within spacetime would hence encounter and interact with the spacetime foam [136–139], leading to an increasing degree of entanglement between the particle and QG DOFs.

Typically one assumes that at energies far below the Planck scale these interactions would be strongly suppressed, and hence, be practically not observable e.g. at accelerators. However, due to the large distances neutrinos travel between their source and the detector, these QG effects could in principle build up to a measurable effect. In this regard, especially atmospheric and cosmic neutrinos seem to be very promising candidates to observe this elusive effect.

In the context of neutrino oscillations, the entanglement between the spacetime state and the neutrino state leads to an additional source of quantum decoherence [140–145]. As in any experimental setup, the QG DOFs would not be accessible, and hence, need to be traced over in the theoretical description. Therefore, it is mandatory to describe the propagating neutrino system in the framework of open quantum systems to account for the hypothetical interaction with the spacetime foam while omitting the description of the QG DOFs itself. For LBL, atmospheric and solar neutrinos there already exist several analyses of non-standard decoherence effects, see e.g. References [146–150].

As has been shown by Israel, Hawking and Page, see e.g. References [151–153], classical black holes are fully described by mass, energy, angular momentum and charge. If a particle crosses the event horizon, only these properties are conserved for an observer on the outside of the horizon. Extrapolating this property of classical black holes to virtual horizons appearing in the spacetime foam, it is usually assumed that QG violates the conservation of quantum numbers associated with global symmetries [154, 155], such as (lepton) flavour, so that only unbroken gauge charges are preserved. This has also gained recent support in the context of the AdS/CFT correspondence [156]. Assuming this property, also transitions between different propagating mass eigenstates sharing the same unbroken gauge quantum numbers would be

allowed. We, hence, propose that in the presence of fermionic DM, or more generally, in the presence of fermionic $\mathrm{SU}(3)_c \times U(1)_{\mathrm{EM}}$ singlets, the flavour violating property of QG implies that also transitions between neutrinos and these dark fermions can occur. Consequently, the overall probability of detecting a neutrino is reduced due to these transitions into the dark sector, possibly enabling the simultaneous search for DM and QG effects at neutrino experiments. However, the overall probability of detecting any fermionic particle remains conserved under this new effect.

This chapter is structured as follows: In Section 4.1 we give a detailed description of how we model this QG effect and also compute the modified vacuum oscillation probability and discuss its asymptotic behaviour for a general number n_f of neutrino / dark fermion generations. Next, in Section 4.2, we consider the case of cosmic neutrinos and the impact of the QG effect on the total neutrino flux and neutrino flavour ratios for an exemplary QG parameter configuration at neutrino telescopes. Furthermore, we compare the commonly employed simple power law neutrino flux parametrisation to a more sophisticated approach, taking into account the effects of finite lifetimes of primary particles producing the neutrinos. After considering astrophysical neutrinos, we estimate the potential of atmospheric neutrino oscillation experiments to constrain the QG parameter space including the number of fermions n_f. To this end we perform a statistical analysis on a publicly available Monte Carlo (MC) data set provided by IceCube [157]. Finally, we conclude in Section 4.4.

4.1 Modelling Quantum Gravity Effects

The theoretical framework of open quantum systems allows for the description of a quantum subsystem S that is coupled to an environment E even if the details of the theory describing this environment are not known. This makes it the most suitable foundation for the description of neutrino oscillations in a quantum spacetime as long as we are able to specify the average effect of the QG DOFs on the neutrino flavour evolution.

As already discussed in Section 2.3 the quantum state in this framework is described by the density operator ρ_S. Assuming the interactions between the environment and the subsystem to be memory-less, i.e. independent of ρ_S, the time evolution of the density operator is governed by the so-called Lindblad equation

$$\frac{\mathrm{d}\rho_S}{\mathrm{d}x}(x) = -i[\hat{H}_S(x), \rho_S(x)] + D[\rho_S(x)]\,, \tag{4.1}$$

where the first term is the well known commutator term from the von Neumann equation describing the unitary part of the time evolution, whereas the second term includes all memory-less dissipative effects, and encodes the non-unitary impact of the environment on the time evolution of ρ_S. The linear operator $D[\rho_S]$ is hence often called the dissipator of the (sub-)system. For the case of high energy neutrinos travelling through matter, we also have to include the corresponding incoherent scattering terms discussed in Section 2.3.3 which may not be entirely memory-less. This extends Equation (4.1) to Equation (2.144). Furthermore, if

we also want to describe the propagation of antineutrinos, we also have to solve the respective Equation (2.145) for the antineutrino density operator. From now on, we drop the subscript S since we only consider the subsystem density operator $\rho_S \to \rho$ in the following. Moreover, for the remainder of this section we focus on the modification of neutrino oscillations in vacuum caused by the presence of QG effects in order to not obscure the discussion. Adding matter effects back in is then straight forward as we only have to include the coherent scattering potentials into the Hamiltonian $\hat{H}$ and add the incoherent scattering terms to Equation (4.1).

System Hamiltonian For the simple case of neutrino oscillations in vacuum, the system Hamiltonian $\hat{H}$ in the mass basis is just the diagonal $n_f \times n_f$-matrix of energy eigenvalues for a given average momentum $p \equiv |\vec{p}|$, i.e.

$$\langle \psi_i | \, \hat{H}(p) \, | \psi_j \rangle := E_i \delta_{ij} \,, \qquad\qquad E_i = \sqrt{p^2 + m_i^2} \,. \tag{4.2}$$

Here, $|\psi_j\rangle$ denotes the j-th mass eigenstate, where we assign the first three to be the three SM neutrino mass eigenstates while the remaining $|\psi_j\rangle$ correspond to hypothetical sterile neutrinos or other fermionic $\mathrm{SU}(3)_c \times U(1)_{\mathrm{EM}}$ singlets. We generically call these additional singlet states dark fermions in the following. As usual, the mass basis is connected to the flavour basis by a unitary transformation U, where we assume U to be approximately block diagonal, i.e.

$$U = U_{\mathrm{PMNS}}^{3\times 3} \oplus U_{\mathrm{dark}}^{(n_f-3)\times(n_f-3)} \,. \tag{4.3}$$

This corresponds to the assumption of negligible mixing between the three SM neutrino flavours and the dark sector, justified by the close-to-unitarity [158, 159] of the 3×3 PMNS matrix. Moreover, since we are only interested in active–active flavour transitions in the following, the details of the dark sector mixing matrix are irrelevant.

A potential complication arises when we consider dark fermion states whose mass is much larger than that of the active neutrinos. In a Poincaré-invariant theory, transitions from these light neutrinos to heavy dark fermions far outside the mass uncertainty of the initial neutrino beam would be strongly suppressed due to four-momentum conservation. Consequently, the system would effectively reduce to the standard three neutrino scenario, although transitions to the dark sector would technically be allowed by the structure of the interactions. This problem, however, can be alleviated if Poincaré-invariance would be violated as the system energy approaches the Planck scale, allowing for transitions between states with masses much smaller than the energy scale, i.e. $m_i, m_j \ll p$, even if these masses are not within the mass uncertainty of the initial neutrino beam. Therefore, as the beam energy increases, heavier dark sector species would be allowed to appear in the beam, gradually enlarging the system.

In contrast, if it turns out that even in a full theory of QG, four-momentum is sufficiently conserved such that transitions outside the mass uncertainty of the beam are forbidden, only very light dark fermions are allowed to contribute to the system S.

In either case, we can employ the ultra-relativistic approximation for the Hamiltonian, i.e.

$$\hat{H} = \sum_i \sqrt{p^2 + m_i^2}\, |\psi_i\rangle \langle\psi_i| \approx \mathbb{1}E + \frac{\hat{M}^2}{2E}\,, \tag{4.4}$$

where $E = p$ is the energy of a neutrino with vanishing mass. In the following, we omit the term proportional to the identity from the Hamiltonian, as it only appears inside of the commutator, and hence, does not contribute to the evolution of the system.

Dissipator Parametrisation The dissipator in this scenario can be divided into a standard term describing the impact of WP separation on the system and one term parametrising the net QG effect on the propagating system, i.e.

$$D[\rho(x)] = D_{\mathrm{WP}}[\rho(x)] + D_{\mathrm{QG}}[\rho(x)]\,, \tag{4.5}$$

$$D_{\mathrm{WP}}[\rho(x)] = -\sum_{j\neq k} \frac{\mathrm{d}\Gamma_{jk}^{\mathrm{WP}}(x)}{\mathrm{d}x} \mathbb{P}_j \rho(x) \mathbb{P}_k\,, \tag{4.6}$$

where $\mathbb{P}_j = |\psi_j\rangle \langle\psi_j|$ is the projector onto the j-th mass eigenstate and

$$\Gamma_{jk}^{\mathrm{WP}}(x) = \left(\frac{x}{L_{jk}^{\mathrm{coh}}}\right)^2\,, \qquad\qquad L_{jk}^{\mathrm{coh}} = 4\sqrt{2}\sigma_X \frac{E^2}{|\Delta m_{jk}^2|}\,, \tag{4.7}$$

is the decoherence function for Gaussian neutrino WPs, as has been shown in Section 2.3.3. Here, σ_X denotes the position space WP width, and $\Delta m_{jk}^2 = m_j^2 - m_k^2$ are the squared mass differences of the neutrinos. In contrast to the standard contribution of WP separation to the dissipator, the QG effect cannot be derived from a more fundamental description since no widely accepted theory of QG exists yet. Therefore, we need to employ a systematic, phenomenological approach to determine the parametrisation of D_{QG}. To this end, we make use of the fact that the density operator and the system Hamiltonian are hermitian $(n_f \times n_f)$ matrices, and hence, can be decomposed into a basis of n_f^2 hermitian matrices $\{\lambda_A : A = 0, \ldots, n_f^2 - 1\}$. For $A > 1$ we take λ_A to be proportional to the respective generator of $\mathrm{SU}(n_f)$ and λ_0 to be proportional to the identity matrix. Furthermore, we define the scalar product on the space of hermitian matrices $\mathbb{H}(n_f)$ to be given by

$$\langle A, B\rangle := 2\mathrm{Tr}[A \cdot B]\,, \qquad\qquad \forall A, B \in \mathbb{H}(n_f)\,, \tag{4.8}$$

and choose the normalisation of λ_A such that they form an ONB with respect to this scalar product. For more details on the choice of the basis matrices and their properties see Appendix C.1. Using this decomposition, the density operator and dissipator can be written as

$$\rho(x) = \rho^A(x)\lambda_A\,, \qquad\qquad \rho^A(x) = \langle\lambda_A, \rho(x)\rangle\,, \tag{4.9}$$

$$D[\rho] = \mathcal{D}^A{}_B \rho^B(x)\,, \qquad\qquad \mathcal{D}^A{}_B = \langle\lambda_A, D[\lambda_B]\rangle\,. \tag{4.10}$$

For the QG effect, we assume that it does not induce any particle loss, i.e. it conserves the total probability of the system. This is reflected by setting $\mathcal{D}^0{}_A \equiv \mathcal{D}^A{}_0 \equiv 0$. For the remaining matrix elements, we adopt a parametrisation of the form [137–146, 160–164]

$$[\mathcal{D}_{\mathrm{QG}}]^A{}_B = -\gamma^A{}_B \left(\frac{E}{E_0}\right)^n , \tag{4.11}$$

where $\gamma^A{}_B$ are constants and E_0 is a reference energy. Moreover, in order for the QG effect to be maximally flavour violating as discussed before, the submatrix $\gamma^A{}_B$ must not have any zero eigenvalues [129, 130]. This restriction alone suffices to ensure that the vacuum oscillation probability approaches a uniform flavour distribution in the asymptotic limit $x \to \infty$.

Model Assumptions and Fermion Number Violation For the sake of clarity, we now briefly summarise the assumptions we impose on the class of QG models under consideration:

1. QG maximally violates global charges
2. QG conserves unbroken gauge charges
3. QG conserves the total probability of the system
4. QG conserves spin and angular momentum
5. QG conserves the direction of propagation

Furthermore, we allow for the possibility that QG violates energy conservation as the system energy E approaches the Planck scale. Note that especially the first three assumptions are commonly employed in low energy effective descriptions of QG, cf. References [136–138, 154–156], while the latter two depend on the assumed degree of Poincaré-invariance-violation. Since QG violates global charges, also fermion number is not conserved[1]. In principle, this also leads to transitions between neutrinos ν_a and antineutrinos ν_b^c, so that we would need to combine the density operators of particles and antiparticles into one common density operator. Moreover, also the evolution equation and mixing matrix would need to be adjusted to account for the oscillations and WP decoherence of antineutrinos. However, since we consider the ultra-relativistic limit, the chirality and helicity of the propagating particles coincide. Due to the assumed conservation of spin and the direction of the momentum, helicity also is a conserved quantity under QG interactions. Therefore, the probability for the transition of an initially left-handed active neutrino into a right-handed particle, like $\nu_a \to \nu_b^c$, is strongly suppressed and will be neglected in the following.

From now on, we choose the quantum gravitational dissipator to be diagonal, i.e. to be of the form

$$\mathcal{D}_{\mathrm{QG}} = -\mathrm{diag}\left(0, \gamma_1, \dots, \gamma_{n_f^2-1}\right) \left(\frac{E}{E_0}\right)^n =: -\mathrm{diag}\left(0, \Gamma_1, \dots, \Gamma_{n_f^2-1}\right) , \tag{4.12}$$

[1] This may for example induce Majorana masses for uncharged particles after integrating out QG DOFs.

for simplicity. This constitutes only a mild restriction to the generality of our results, as these only rely on the asymptotic uniformness of the flavour probability distribution. Multiple experimental analyses [146, 150, 165, 166] have already been conducted involving similar models using the parametrisation (4.11). The resulting upper limits imply that ${\gamma^A}_B$ has to be very small, as expected. The most recent IceCube analysis [150] on that subject concludes ${\gamma^A}_B < 10^{-15}\text{eV}$ for $n \geq 0$ and $E_0 = 1\,\text{TeV}$. Finally, we note that for a diagonal dissipator the details of the sub-Hamiltonian of the dark sector are not relevant for the active–active transitions we consider in this work.

Vacuum Oscillation Probability The probability for a neutrino of initial flavour ν_a to be measured as a neutrino of flavour ν_b after a propagation distance L reads

$$P_{ab}(L) = \text{Tr}[\Pi_b \cdot \rho(L)] = \frac{1}{2}\langle \Pi_b, \rho(L)\rangle\,, \qquad \rho(0) = \Pi_a\,, \tag{4.13}$$

where Π_a is the projector on the a-th flavour eigenstate. In vacuum, the oscillation probability in the presence of QG effects then becomes [130]

$$\begin{aligned}
P_{ab}(L) = \frac{1}{n_f} &+ \sum_{k=3}^{n_f-1} \frac{e^{-\Gamma_{n_f(n_f-1)+k}L}}{k(k+1)} \\
&+ \frac{e^{-\Gamma_{n_f(n_f-1)+1}L}}{2}\left(|U_{a1}|^2 - |U_{a2}|^2\right)\left(|U_{b1}|^2 - |U_{b2}|^2\right) \\
&+ \frac{e^{-\Gamma_{n_f(n_f-1)+1}L}}{6}\left(|U_{a1}|^2 + |U_{a2}|^2 - 2|U_{a3}|^2\right)\left(|U_{b1}|^2 + |U_{b2}|^2 - 2|U_{b3}|^2\right) \\
&+ 2\sum_{k>j=1}^{3} \text{Re}(U^*_{ak}U_{bk}U_{aj}U^*_{bj}) e^{-\left(\frac{L}{L^{\text{coh}}_{jk}}\right)^2 - \bar{\Gamma}_{I_{jk}+1,I_{jk}}L} \cos\!\left(\omega_{jk}L\right) \\
&+ 2\sum_{k>j=1}^{3} \text{Re}(U^*_{ak}U^*_{bk}U_{aj}U_{bj}) \frac{\Delta\Gamma_{I_{jk}+1,I_{jk}}}{\omega_{jk}} e^{-\left(\frac{L}{L^{\text{coh}}_{jk}}\right)^2 - \bar{\Gamma}_{I_{jk}+1,I_{jk}}L} \sin\!\left(\omega_{jk}L\right) \\
&- 2\sum_{k>j=1}^{3} \text{Im}(U^*_{ak}U_{bk}U_{aj}U^*_{bj}) \frac{\Delta E_{jk}}{\omega_{jk}} e^{-\left(\frac{L}{L^{\text{coh}}_{jk}}\right)^2 - \bar{\Gamma}_{I_{jk}+1,I_{jk}}L} \sin\!\left(\omega_{jk}L\right),
\end{aligned} \tag{4.14}$$

which is one of the main results of this chapter. For a detailed derivation see Appendix C.2. Here, we have introduced several abbreviations for better readability.

Firstly, the mean and reduced difference of two decoherence functions are denoted by:

$$\bar{\Gamma}_{A,B} := \frac{\Gamma_A + \Gamma_B}{2}\,, \qquad \Delta\Gamma_{A,B} := \frac{\Gamma_A - \Gamma_B}{2}\,, \tag{4.15}$$

respectively. Furthermore, the usual and the modified oscillation frequencies are given by:

$$\Delta E_{jk} := \frac{\Delta m^2_{jk}}{2E}\,, \qquad \omega_{jk} := \sqrt{(\Delta E_{jk})^2 - (\Delta\Gamma_{I_{jk}+1,I_{jk}})^2}\,. \tag{4.16}$$

Lastly, the index mapping function I_{jk} translates mass eigenstate indices into the corresponding indices of the basis matrices, i.e.

$$I_{jk} = \begin{cases} 1\,, & j = 1 \wedge k = 2 \\ 3\,, & j = 1 \wedge k = 3 \\ 2n_f - 1\,, & j = 2 \wedge k = 3 \end{cases}\,, \tag{4.17}$$

which is fixed by the chosen ordering of basis matrices discussed in Appendix C.1. In the simplest possible case where all QG decoherence functions coincide, the oscillation formula (4.14) reduces to:

$$\begin{aligned} P_{ab}(L) = \frac{1}{n_f} &+ e^{-\Gamma L}\left[\sum_{j=1}^{3} |U_{aj}|^2 |U_{bj}|^2 - \frac{1}{n_f}\right] \\ &+ 2e^{-\Gamma L}\sum_{k>j=1}^{3} \mathrm{Re}(U_{ak}^* U_{bk} U_{aj} U_{bj}^*) e^{-\left(\frac{L}{L_{jk}^{\mathrm{coh}}}\right)^2} \cos\left(\frac{\Delta m_{jk}^2 L}{2E}\right) \\ &- 2e^{-\Gamma L}\sum_{k>j=1}^{3} \mathrm{Im}(U_{ak}^* U_{bk} U_{aj} U_{bj}^*) e^{-\left(\frac{L}{L_{jk}^{\mathrm{coh}}}\right)^2} \sin\left(\frac{\Delta m_{jk}^2 L}{2E}\right)\,. \end{aligned} \tag{4.18}$$

This simplified formula enables a much simpler discussion of the asymptotic limits of P_{ab}.

Asymptotic Limits of the Oscillation Formula The asymptotic behaviour of the flavour transition probability P_{ab} can be analysed in two different ways:

(i) Fixing a certain energy E while varying the baseline L

(ii) Fixing the baseline L and varying the neutrino energy E

First we consider the case of a varying baseline. At small baselines $L \ll L_{jk}^{\mathrm{coh}} \ll \Gamma^{-1}$ the standard oscillation probability is recovered as all decoherence effects are negligible. Increasing the baseline beyond the onset of WP separation $L_{jk}^{\mathrm{coh}} \ll L \ll \Gamma^{-1}$ yields $\exp(-\Gamma L) \approx 1$, and $\exp\left(-(L/L_{jk}^{\mathrm{coh}})^2\right) \approx 0$, leading to

$$P_{ab}(L) \approx \sum_{j=1}^{3} |U_{aj}|^2 |U_{bj}|^2\,. \tag{4.19}$$

This represents the WP decoherence limit. At even larger propagation distances $L_{jk}^{\mathrm{coh}} \ll \Gamma^{-1} \ll L$, all decoherence damping factors essentially vanish and the QG limit yields

$$P_{ab}(L) \approx \frac{1}{n_f}\,. \tag{4.20}$$

As expected, the fully decohered flavour transition probability is independent of the travel distance L and represents a completely uniform flavour distribution. We demonstrate the

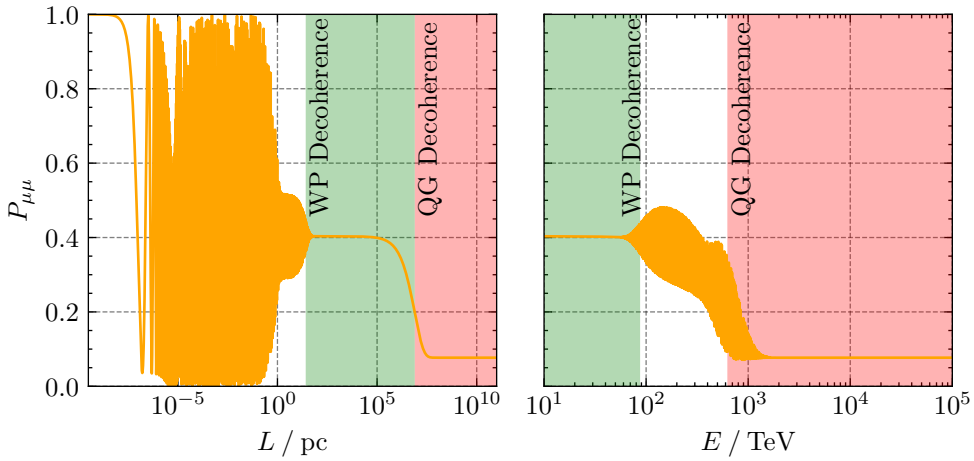

Figure 4.1: The $\nu_\mu \to \nu_\mu$ oscillation probability as a function of the neutrino base length (left panel) and the neutrino energy (right panel). The green shaded regions indicate the lengths and energies at which WP decoherence dominates whereas the red shaded regions indicate the QG decoherence domination regime. For demonstration purposes, we choose $E = 10\,\text{TeV}$ (left panel) and $L = 2\text{pc}$ (right panel) and we set the QG parameters to be $n_f = 13$, $n = 2$, $E_0 = 1\,\text{TeV}$ and $\gamma_1, \ldots, \gamma_{n_f^2-1} = 8.2 \times 10^{-33}\,\text{eV}$. We choose the remaining neutrino oscillation parameters as displayed in Table 4.1.

length-dependent oscillation probability and the corresponding asymptotic limits for an exemplary parameter configuration in the left panel of Figure 4.1.

Changing the point of view and considering $P_{ab}(E)$ as a function of energy, one can also define two energy scales corresponding to the different limits discussed for the distance-dependent case: The WP coherence energy E_{jk}^{WP} and the QG coherence energy E^{QG}. For Gaussian WPs we get

$$E_{jk}^{\text{WP}} = \sqrt{\frac{|\Delta m_{jk}^2| L}{4\sqrt{2}\sigma_x}}\,, \tag{4.21}$$

and since the WP coherence exponential decreases for decreasing energy, we infer that oscillations are strongly damped at $E < E_{jk}^{\text{WP}}$. The QG energy scale is only well-defined for $n \neq 0$ and in this case reads

$$E^{\text{QG}} = \frac{E_0}{(\gamma L)^{\frac{1}{n}}}\,. \tag{4.22}$$

For $n < 0$, the behaviour of the QG decoherence effect is similar to that of WP decoherence, i.e. decoherence increases at small energies. Moreover, due to the smallness of γ in this case, we have $E^{\text{QG}} \ll E_{jk}^{\text{WP}}$. In the opposite scenario, i.e. $n > 0$, QG induced decoherence occurs at very high energies $E \gg E^{\text{QG}} \gg E_{jk}^{\text{WP}}$. This is the class of scenarios we focus on in the

Table 4.1: Neutrino masses and mixing parameters from nuFit v5.3 [167] assuming normal ordering. The exemplary WP width is taken from Reference [168].

Parameter	Value	Reference
Δm^2_{21}	$7.41^{+0.21}_{-0.20} \times 10^{-5}\,\mathrm{eV}^2$	[167]
Δm^2_{32}	$2.511^{+0.027}_{-0.027} \times 10^{-3}\,\mathrm{eV}^2$	[167]
$\sin^2(\theta_{12})$	$0.307^{+0.012}_{-0.011}$	[167]
$\sin^2(\theta_{13})$	$0.02203^{+0.00056}_{-0.00058}$	[167]
$\sin^2(\theta_{23})$	$0.572^{+0.018}_{-0.023}$	[167]
σ_x	$10^{-13}\,\mathrm{m}$	[168]

following. The right panel of Figure 4.1 shows the energy-dependent behaviour of P_{ab} and the corresponding asymptotic limits are indicated by the green and red shaded regions.

Both graphs shown in Figure 4.1 exhibit an oscillatory behaviour in the length and energy regions where decoherence effects are negligible. These oscillations, however, can only be observed if the energy resolution ΔE of the experiment fulfils

$$\frac{\Delta E}{E} \lesssim \frac{2E}{\Delta m^2_{jk} L}\,, \tag{4.23}$$

and if the size of the neutrino production region Σ_S is much smaller than the oscillation lengths, i.e. $\Sigma_\mathrm{S} \ll L^\mathrm{osc}_{jk}$.

4.2 Quantum Gravitational Decoherence in Astrophysical Neutrinos

As shown in the last section, QG effects become stronger as the system travels over large distances and at high energies, depending on the particular model. Therefore, it is well motivated to consider cosmic neutrinos in the very high energy range to search for QG effects. Neutrino telescopes like IceCube, Astronomy with a Neutrino Telescope and Abyss Environmental Research Project (ANTARES), Cubic Kilometre Neutrino Telescope (KM3NeT) or the proposed Pacific Ocean Neutrino Experiment (P-ONE) [169] in the western pacific offer promising future prospects in this regard. So far, IceCube has observed the diffuse astrophysical neutrino flux originating from multiple cosmic neutrino sources [170–174]. While in principle it is possible to already utilise these measurements for the study of hypothetical QG decoherence effects, it is very impractical at the moment since a precise modelling of the population and properties of neutrino sources is needed to draw conclusions on the allowed QG parameter space. Furthermore, the onset of QG induced decoherence would be blurred since the neutrino source are located at various different distances, leading to various different QG energies. Therefore, it would be more practical if sufficient neutrino data from point-like cosmic sources are accumulated at current or future neutrino experiments.

In the following, we further pursue this line of thought and compare two different approaches to model neutrino fluxes from such a point-like astrophysical neutrino source, in order to estimate to which extent a flux model-independent analysis of the QG parameter space is possible. To this end, we apply both flux models to compute two interesting quantities in which we expect QG decoherence and the additional numbers of dark fermions to be observable: Summed neutrino fluxes and neutrino flavour ratios. While flavour ratios are expected to be driven towards a democratic distribution, i.e.

$$\left(\Phi_e : \Phi_\mu : \Phi_\tau\right) \equiv \left(\frac{1}{3} : \frac{1}{3} : \frac{1}{3}\right) , \tag{4.24}$$

due to QG effects, summed neutrino fluxes are expected to be especially interesting since they would decrease in the QG limit depending on the number of fermions n_f, present in the system. Hence, summed neutrino fluxes would exhibit a dip at high energies that is absent under the standard hypothesis.

The first flux model represents a simple estimation involving only the oscillation probability and the flux of neutrinos emerging directly from the source. The neutrino flux of flavour ν_b at Earth is in this case usually modelled by (see e.g. Reference [175])

$$\phi_b^{\oplus}(E) = \sum_{a=e,\mu,\tau} \frac{\Phi_a^{\mathrm{S}}(E)}{4\pi L_{\mathrm{S}}^2} P_{ab}(L_{\mathrm{S}}, E) , \tag{4.25}$$

where Φ_a^{S} is the integrated total flux of ν_a per unit time and energy coming from the source S, $\phi_b^{\oplus}(E)$ is the flux of ν_b per unit area, time and energy at Earth, and L_{S} is the distance between the Earth $\oplus$ and the source S. Here, we implicitly assume that neutrinos are emitted directly and isotropically from the source.

The second flux model we consider here is more general in that it takes into account the possibility that neutrinos usually occur as secondary particles, e.g. as byproducts of decays of particles the source has primarily emitted. A pulsar, for example, regularly ejects charged particles like protons interacting with photons from its surface or with material from the surrounding supernova remnant. The mesons, e.g. pions and kaons, produced in these processes then decay into neutrinos travelling vast distances until they are eventually detected at Earth. There are of course also other mechanisms producing, for example, neutrons, see e.g. Reference [160], that also decay into neutrinos leading to different initial flavour ratios. Since we are interested in high energy ($E \gtrsim 1\,\mathrm{TeV}$) cosmic neutrinos, the primary particles must also have been ultra-relativistic. Consequently, the lifetime of these particles is dilated by a large Lorentz factor leading to significant travel distances before they decay into neutrinos. Hence, the distances the secondary neutrinos have to propagate before they potentially reach Earth vary significantly. This has direct impact on the observation of QG effects since the energy at which these decoherence effects arise depends on the propagation distance of the neutrino system.

In total, the ν_b flux per unit time and energy in this more general scenario is given by[2]

$$\phi_b^{\oplus}(E) = \sum_{\eta\in\mathrm{S}} \sum_{a=e,\mu,\tau} \int_{m_\eta}^{\infty} \int_0^{L_\mathrm{S}} \frac{\Phi_\eta^\mathrm{S}(E)}{4\pi L_\mathrm{S}^2} \frac{m_\eta e^{-\frac{m_\eta \ell}{p_\eta \tau_\eta}}}{p_\eta \tau_\eta} \pi_{\eta a}(E_\eta, E) P_{ab}(E, L_\mathrm{S} - \ell)\, \mathrm{d}\ell\, \mathrm{d}E_\eta \ , \tag{4.26}$$

where η is the primary particle produced isotropically in the vicinity of the source with total flux Φ_η^S, energy E_η and mean lifetime τ_η. For the detailed derivation and discussion of this formula see Appendix C.3. The spectral probability for the primary particle η to decay into a neutrino ν_a of energy E is denoted by $\pi_{\eta a}(E_\eta, E)$. It is given by

$$\pi_{\eta a}(E_\eta, E) = \frac{1}{\Gamma'_\eta} \int_0^{E_\nu^{\max}} \frac{\mathrm{d}\Gamma'_{\eta a}}{\mathrm{d}E'}(m_\eta, E') \int_{-1}^{1} \delta\left(E - \frac{E_\eta E'}{m_\eta}(1 + \cos\theta')\right) \frac{\mathrm{d}\cos\theta'}{2}\, \mathrm{d}E' \ , \tag{4.27}$$

where $\mathrm{d}\Gamma'_{\eta a}$ is the differential decay rate of η in its rest frame. Here, we integrate over the neutrino energy E' and the angle θ' between the neutrino emission and the direction of the boost into the lab frame. The delta constraint enforces equality of the boosted η-rest frame energy E' of the neutrino and its lab frame energy E. For a discussion of the properties of $\pi_{\eta a}$ see Appendix C.3. Finally, also the exponential decay distribution as well as the neutrino oscillation probability P_{ab} need to be included into Equation (4.26). The former describes the overall probability for the primary particle to decay in the first place, while the latter represents the probability for ν_a to oscillate into ν_b over the remaining distance $L_\mathrm{S} - \ell$.

By combining all quantities in Equation (4.26) related to the production of the initial neutrino flavour into an effective differential neutrino source flux,

$$\frac{\mathrm{d}\Phi_a^\mathrm{S}}{\mathrm{d}\ell}(E, \ell) = \sum_{\eta\in\mathrm{S}} \int_{m_\eta}^{\infty} \Phi_\eta^\mathrm{S}(E_\eta) \frac{e^{-\frac{\ell}{v_\eta \tau_\eta}}}{v_\eta \tau_\eta} \pi_{\eta a}(E_\eta, E)\, \mathrm{d}E_\eta \ , \tag{4.28}$$

we can show that the general flux model can be formulated equivalently to Equation (4.25):

$$\phi_a^{\oplus}(E) = \sum_{a=e,\mu,\tau} \int_0^{L_\mathrm{S}} \frac{1}{4\pi L_\mathrm{S}^2} \frac{\mathrm{d}\Phi_a^\mathrm{S}}{\mathrm{d}\ell}(E, \ell) P_{ab}(E, L_\mathrm{S} - \ell)\, \mathrm{d}\ell \ . \tag{4.29}$$

The crucial difference here is that the neutrino source cannot be considered as point-like anymore. If the source produces neutrinos directly or if the primaries decay very quickly, i.e. $\mathrm{d}\Phi_a^\mathrm{S}/\mathrm{d}\ell \propto \delta(\ell)$, Equation (4.29) reduces to Equation (4.25).

[2] Equation (4.26) is a generalised version of the flux formulas presented in References [160, 176].

4.2.1 Summed Astrophysical Neutrino Fluxes

The first quantity we consider in terms of the discussed flux models is the summed neutrino flux,

$$\Phi^{\oplus}_{\mathrm{tot}}(E) := \sum_{b=e,\mu,\tau} \Phi^{\oplus}_{b}(E)\,, \tag{4.30}$$

at Earth. Note that we only sum over measurable flavours in the beam, i.e. ν_e, ν_μ and ν_τ and assume an idealised 100% identification rate. Therefore, at energies $E \gg E^{\mathrm{QG}}$ and if $n_f > 3$, the summed flux decreases to

$$\phi^{\oplus}_{\mathrm{tot}}(E) = \sum_{a=e,\mu,\tau} \int_0^{L_{\mathrm{S}}} \frac{1}{4\pi L_{\mathrm{S}}^2} \frac{\mathrm{d}\Phi^{\mathrm{S}}_a}{\mathrm{d}\ell}(E,\ell) \sum_{b=e,\mu,\tau} \underbrace{P_{ab}(E, L_{\mathrm{S}}-\ell)}_{\to 1/n_f}\,\mathrm{d}\ell \to \frac{3}{n_f}\frac{\Phi^{\mathrm{S}}_{\mathrm{tot}}}{4\pi L_{\mathrm{S}}^2}\,, \tag{4.31}$$

whereas for $n_f = 3$, the QG modified flux coincides with the standard expectation, since in this case the summed oscillation probability always yields 1. In the presence of additional dark fermions, the summed flux therefore exhibits a dip around E^{QG}, indicating, if observed, not only the onset of QG decoherence enabling a fit of the QG parameters, but also hints towards the existence of dark fermions.

In the following, we investigate in how far the location of the dip depends on the underlying neutrino flux model. This is important since for any analysis of the QG parameter space, the dip location and shape are what determines the QG parameters. We expect that especially for long lived primary particles, like neutrons, the chosen flux model can have a significant impact on the location of the dip and that a precise modelling of the processes in the source is mandatory in order to be able to draw reliable conclusions on the QG model parameters. To see that, note that the QG coherence energy (4.22) indicating the location of the hypothesised flux dip is length-dependent and that in the generalised setting of Equation (4.29), neutrinos may be emitted throughout the entire path between the primary particle source and the Earth. Therefore, we first define a generalised QG decoherence energy via the comparison of the standard and QG modified flux predictions. In the simplest scenario of an effectively point-like neutrino source, the ratio of standard and QG flux predictions fulfils:

$$\frac{\Phi^{\oplus}_{\mathrm{tot}}(E_{\mathrm{QG}}, L)}{\Phi^{\oplus}_{\mathrm{tot,std}}(E_{\mathrm{QG}}, L)} \equiv p_{\mathrm{QG}} := \frac{3}{n_f} + 3\sum_{k=3}^{n_f-1} \frac{\exp\left(-\frac{\gamma_{n_f(n_f-1)+k}}{\gamma_{\min}}\right)}{k(k+1)}\,, \tag{4.32}$$

where we implicitly define the location of the dip to be such that all QG decoherence inducing exponentials have at least decayed to $1/e$. In case of a point-like source this happens at:

$$E^{\mathrm{simple}}_{\mathrm{QG}}(L) := \max_{A\in\{1,\ldots,n_f^2-1\}} \frac{E_0}{(\gamma^A L)^{\frac{1}{n}}} =: \frac{E_0}{(\gamma_{\min} L)^{\frac{1}{n}}}\,. \tag{4.33}$$

For the generalised scenario we instead use Equation (4.32) as a defining relation. For promptly decaying primaries, like pions, the general flux reduces to the simple formula (4.25), and hence, also $E^{\mathrm{general}}_{\mathrm{QG}}$ converges towards $E^{\mathrm{simple}}_{\mathrm{QG}}$.

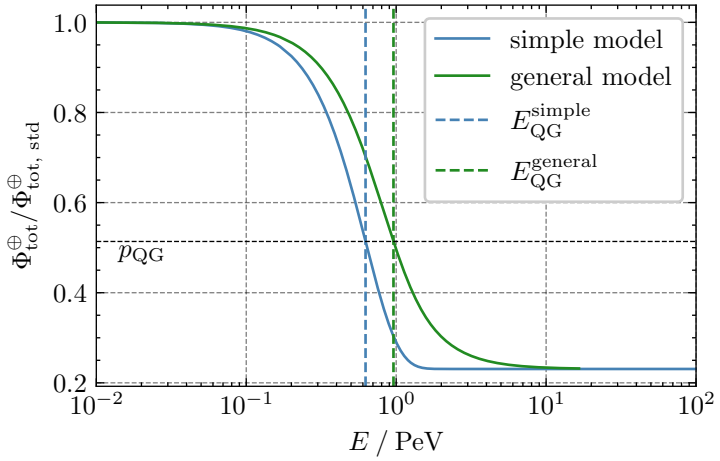

Figure 4.2: Comparison of the resulting total neutrino fluxes at Earth as a function of neutrino energy assuming the simple flux model (blue line) versus the more general model taking into account the finite lifetime of the primary particles (green line). We assume a distance of $L_{\mathrm{S}} = 2\,\mathrm{kpc}$ between source and detector, we set the QG parameters to be $n_f = 13$, $n = 2$, $E_0 = 1\,\mathrm{TeV}$ and $\gamma^A \equiv 8.2 \times 10^{-33}\,\mathrm{eV}$. The remaining neutrino oscillation parameters are given in Table 4.1.

In the opposite case, e.g. when the primaries are neutrons, the onset of the dip can be delayed or smeared significantly, as one can infer from Figure 4.2, where we compare the QG to standard total flux ratios in the simple and the general flux models. Here, we assume a cosmic neutron source at a distance of $L_{\mathrm{S}} = 2\,\mathrm{kpc}$, roughly corresponding to the distance to Cygnus OB2 that has been identified as a potentially interesting cosmic neutrino source in Reference [160]. The oscillation and standard decoherence parameters used for this plot are displayed in Table 4.1. For the QG decoherence parameters we choose $n = 2$, motivated by string theory [177–179], $E_0 = 1\,\mathrm{TeV}$ and $\gamma^A \equiv \gamma = 8.2 \times 10^{-33}\,\mathrm{eV}$, which is in agreement with the latest bounds on QG parameters [150]. For demonstration purposes, we choose the number of fermions to be $n_f = 3 + 10$. Furthermore, in case of the simple flux model we assume an energy spectrum,

$$\Phi_e^{\mathrm{S}}(E) = \Phi_0 E^{-\gamma_\nu}\,, \tag{4.34}$$

with $\gamma_\nu = 2.5$, cf. References [173, 174]. This corresponds to the blue line in Figure 4.2, where we indeed observe a dip towards $3/n_f$ times the standard flux expectation around the coherence energy $E_{\mathrm{QG}}^{\mathrm{simple}}(L_{\mathrm{S}})$.

For the curve of the more accurate flux prediction displayed in green in Figure 4.2, we see that the dip is smeared out compared to the simple scenario as the primary neutrons may

travel significant distances before they decay. We obtain a total neutrino flux of:

$$\begin{aligned}\Phi_{\mathrm{tot}}^{\oplus}(E) = &\int_{E_n^{\min}}^{E_n^{\max}} \mathrm{d}E_n \, \frac{\Phi_n^{\mathrm{S}}(E_n)}{4\pi L_{\mathrm{S}}^2} \pi_{ne}(E_n, E) \\ &\times \left\{ \frac{3}{n_f} - \frac{n_f - 3}{n_f} \frac{e^{-\Gamma L_{\mathrm{S}}}}{\Gamma\lambda_n - 1} + \frac{n_f - 3\Gamma\lambda_n}{n_f} \frac{e^{-\frac{L_{\mathrm{S}}}{\lambda_n}}}{\Gamma\lambda_n - 1} \right\} .\end{aligned} \tag{4.35}$$

Here, π_{ne} is the well known neutrino energy distribution induced by the β decay of the neutron. For completeness, we derive and discuss it in Appendix C.4. Moreover, $\lambda_n = u_n \tau_n$ is the mean free path of the decaying neutrons in the lab frame and their flux density is parametrised as:

$$\Phi_n^{\mathrm{S}}(E) = \Phi_0 E^{-\gamma_n} , \tag{4.36}$$

with $\gamma_n = 3.1$ as suggested in Reference [160].

In a real world experiment, only the neutrino flux corresponding to the model realised in nature can be observed, and hence, computing the flux ratios for different models purely from experimental data, as shown in Figure 4.2, is impossible. Of course one can divide the data by the simulated standard expectation, but the parameters entering this simulated curve need to be determined by fitting the curve to the data. In general, these fit parameters differ for different models and thus the data-to-simulation ratio would not have the same meaning as the ratios shown in Figure 4.2, for which the same underlying flux parameters are assumed. It is therefore more meaningful to consider the absolute fluxes in order to draw conclusions about the potential of any experiment to constrain the QG parameter space. Given the precise knowledge about all processes producing the primary particles η in the source, the neutrino flux model would be perfectly determined and the only free parameters are the QG model parameters that can then be fitted directly. Such an ideal scenario, however, is highly unrealistic and in addition to the QG parameters we are interested in, also several parameters related to systematic uncertainties of the experiment and the flux model of the source need to be fitted to the data simultaneously. As can be seen in Figure 4.3, the shape of the total neutrino flux spectrum at Earth depends strongly on the underlying model. In the left panel of the Figure, we show the simple flux model using the same parameter configuration as above, whereas the right panel displays the total neutrino flux spectrum assuming the general model, again for a cosmic neutron source. This strong dependence of the shape reduces the statistical discrimination power of any realistic experiment between the standard and QG models, especially when multiple primary particle species lead to multiple neutrino flux components. A flux model-independent analysis of total neutrino fluxes alone is therefore difficult to achieve at current and future neutrino telescopes assuming a single point-like source. If several sources of the same type producing equivalent fluxes of primary particles could be identified, a simultaneous fit could reduce this problem as the varying distances to these sources would change the impact of QG effects while the flux parameters remain the same across all sources.

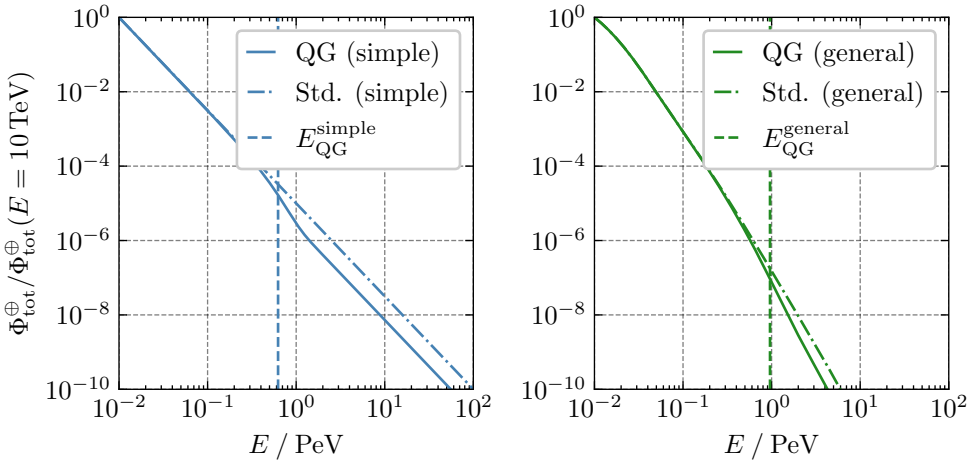

Figure 4.3: Comparison of the resulting neutrino flux shapes at Earth as a function of neutrino energy assuming the simple flux model (left panel) versus the more general model taking into account the finite lifetime of the primary particles (right panel). We assume a distance of $L_S = 2\,\mathrm{kpc}$ between source and detector, we set the QG parameters to be $n_f = 13$, $n = 2$, $E_0 = 1\,\mathrm{TeV}$ and $\gamma^A \equiv 8.2 \times 10^{-33}\,\mathrm{eV}$. The remaining neutrino oscillation parameters are given in Table 4.1.

If, however, too few point-like sources are known as it is the case today, also taking neutrino flavour ratios into account can alleviate some of these difficulties. The reason for this is that flavour ratios depend more strongly on the QG parameters than on the underlying flux parameters, because per construction the shape-dependence of the neutrino energy spectrum mostly drops out of these observables.

4.2.2 Flavour Ratios at Neutrino Telescopes

Neutrino flavour ratios are the summed fluxes of neutrinos and antineutrinos of a given flavour divided by the total fluxes, i.e.

$$R^{\oplus}(E) := \left(R_e^{\oplus}(E) : R_\mu^{\oplus}(E) : R_\tau^{\oplus}(E)\right) , \tag{4.37}$$

$$R_a^{\oplus}(E) := \frac{\Phi_a^{\oplus}(E) + \bar{\Phi}_a^{\oplus}(E)}{\Phi_{\mathrm{tot}}^{\oplus}(E) + \bar{\Phi}_{\mathrm{tot}}^{\oplus}(E)} , \qquad a = e, \mu, \tau \tag{4.38}$$

where the bar indicates the antineutrino fluxes. In the QG limit, all ratios tend towards a democratic $(1/3 : 1/3 : 1/3)$ distribution, as all flavours appear with the same probability in the beam regardless of the number of fermions n_f and of the initial flavour composition. Therefore, the $R_a^{\oplus}(E)$ are insensitive to the total number of fermions, but, as discussed already in the preceding section, only weakly depend on the underlying neutrino energy spectrum. Thus, the combination of the total neutrino flux and neutrino flavour ratios is a promising set of observables for QG searches at neutrino telescopes. In the following, we consider the

different initial flavour compositions for astrophysical neutrinos and compare the predictions for their resulting flavour ratios in the detector with and without the QG effect.

The most commonly discussed initial flavour compositions are [160, 175]:

- Pion source: $R^{\text{in}}(E) = (1/3 : 2/3 : 0)$
- Muon damped pion source: $R^{\text{in}}(E) = (0 : 1 : 0)$
- Neutron source: $R^{\text{in}}(E) = (1 : 0 : 0)$

In case of the pion source, two muon antineutrinos and one electron antineutrino are generated in the decay chain of the pion and the daughter muon. If this muon is absorbed or deflected due to ambient material surrounding the source, only the original muon antineutrinos are detected at Earth. This is called the muon damped neutrino source in the following. Lastly, the neutron decay only generates an electron antineutrino, and hence, leads to an initial flavour ratio of $R^{\text{in}}(E) = (1 : 0 : 0)$.

In the following, we also compare the predicted fluxes for the three different sources to a measurement [180] of astrophysical neutrino flavour ratios performed by the IceCube collaboration. In particular, we present the best fit point as well as the respective 68% and 95% confidence regions obtained within the IceCube analysis. Since the underlying data set contains neutrinos from the diffuse astrophysical neutrino flux, our predictions can not be compared directly to the measurement as we predict the flavour ratios for a single point-like neutrino source. The reason why we do not use data from identified point-like sources is that there are no flavour ratio analyses for these kinds of sources available, yet. It is, however, still instructive to show the comparison to get an idea of the expected statistical discrimination power of neutrino telescopes between the standard and QG scenarios for the different sources.

Pion Source Figure 4.4 shows the final flavour ratios for the QG and standard scenarios, respectively. The left panel shows the mean flavour ratios across all energies considered, whereas the right panel shows the high energy limit $E \geq E_{\text{QG}}$. Since the standard prediction for an initial flavour ratio of $R^{\text{in}}(E) = (1/3 : 2/3 : 0)$ is very close to the democratic ratios $R^{\oplus}(E) = (1/3 : 1/3 : 1/3)$ predicted by the QG model, neutrinos from a pion source are not favourable for QG decoherence searches utilising neutrino flavour ratios. This is because higher statistics and better control over systematic uncertainties are needed in order to significantly distinguish the standard and QG scenarios compared to other initial flavour compositions. As can be judged from Figure 4.4, the confidence regions are too large to differentiate between the two theory predictions, even if a number of events can be accumulated from a single pion source comparable to the number of events that has entered the analysis presented in Reference [180]. Note that this analysis used neutrino events originating from a multitude of astrophysical sources.

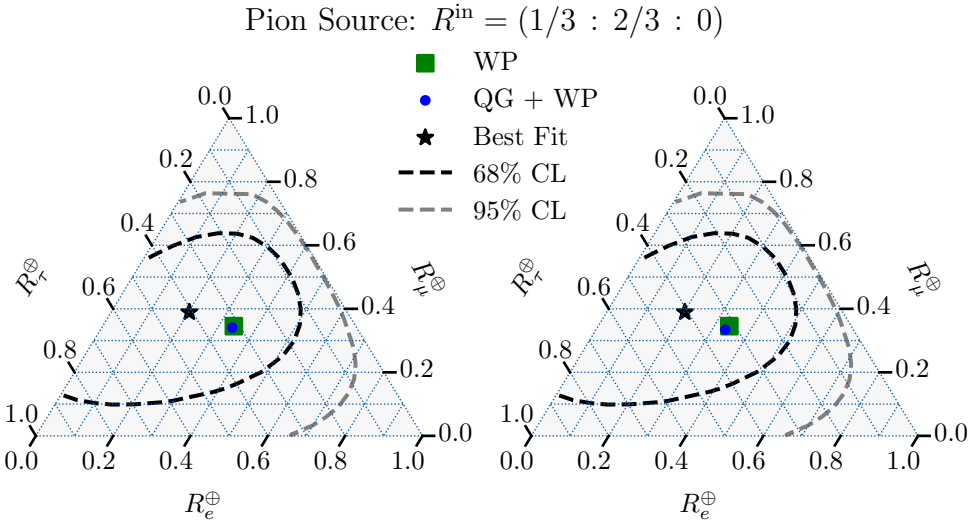

Figure 4.4: Average neutrino flavour ratios for neutrinos from a pion source. For the left panel we average the flavour ratios over the full available energy range, whereas in the right panel the averaging is only applied to the high energy neutrino events, i.e. $E \geq E_{\text{QG}}$. The square green marker indicates the standard WP decoherence expectation, while the blue dot represents the prediction including the QG decoherence effects. All model parameters are chosen as in Figure 4.2. Both panels also report the best fit point (star shaped marker), the 68 % CL contour (dashed black line) as well as the 95 % CL contour (dashed grey line) obtained from the flavour ratio analysis performed in Reference [180] on the diffuse astrophysical neutrino background.

Muon Damped Source For a pion source where the daughter muons from the pion decay are stopped or deflected in the surrounding material, leading to an initial flavour ratio $R^{\text{in}}(E) = (0 : 1 : 0)$, the situation at first seems more promising as the distance between the democratic center and the standard prediction increases. Especially in the large E limit, the opportunities to distinguish the QG and standard scenarios are improved compared to a conventional pion source, as can be seen in Figure 4.5. However, factoring in the confidence regions obtained in Reference [180], we see that both predictions are in agreement with the best fit point and it is not possible to distinguish between the different theory predictions.

Neutron Source Finally, assuming a neutron source emitting only $\bar{\nu}_e$, i.e. $R^{\text{in}} = (1 : 0 : 0)$, we see that the standard and QG scenarios can be best distinguished among the considered scenarios, which is mainly due to $\theta_{13} \ll 1$. This is especially true at energies above E^{QG}, where the QG ratios are almost fully in the democratic decoherence limit as can be seen in Figure 4.6. Here, the distance between the WP and QG scenarios becomes comparable to the size of the 1σ region around the best fit point. We need to stress again that a direct comparison between the best fit point and the theory predictions is meaningless, as multiple different sources with potentially multiple different initial flavour ratios have contributed to the measured neutrino

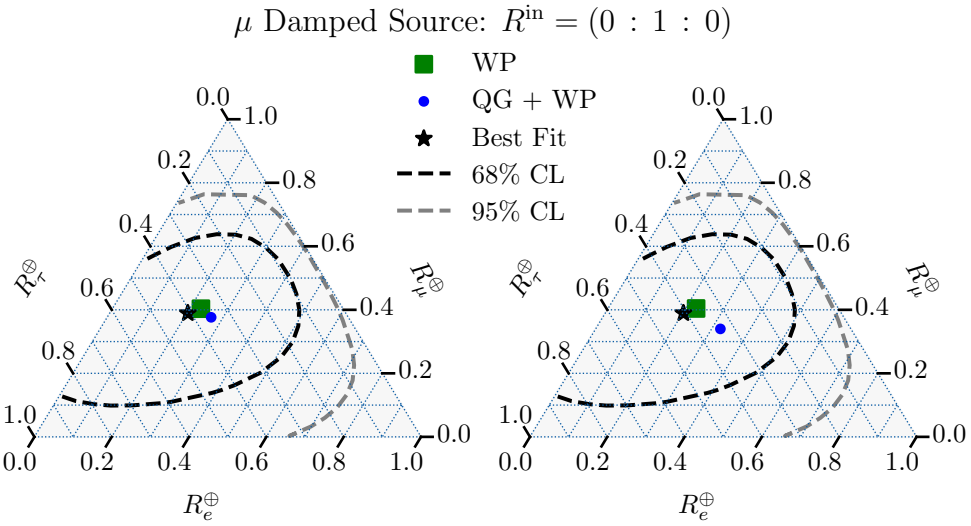

Figure 4.5: As Figure 4.4 for a muon damped pion source.

events and thus entered the best fit point. Still, the size of the confidence regions provide a rough estimate of what to expect for the statistical discrimination power as soon as flavour ratio data from single astrophysical neutrino sources is available.

In conclusion, sources whose main neutrino production mechanism is neutron decay seem to be the most favourable ones. Since we advocate the consideration of the combination of total neutrino fluxes and flavour ratios in order to improve sensitivity to the QG parameter space, the situation is slightly more complicated due to the long lifetimes of the neutrons. As we have seen in the previous section, long lived primary particles induce a smearing of the QG dip, making a precise estimation of the QG parameters more difficult. It is therefore evident that a compromise between the lifetime of the primary particles and an optimal initial flavour composition is inevitable.

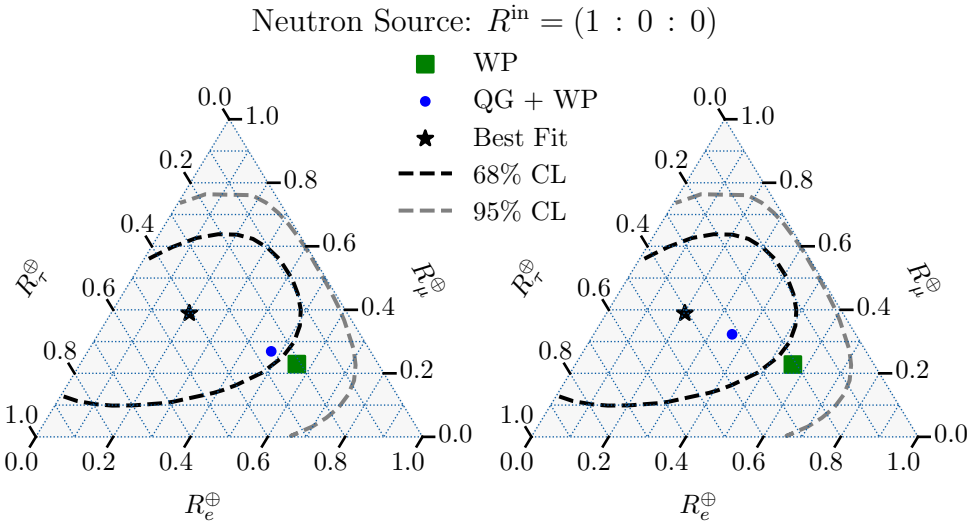

Figure 4.6: As Figure 4.4 for a neutron source.

4.3 Quantum Gravitational Decoherence in Atmospheric Neutrinos

Since at the moment astrophysical decoherence searches are rather difficult due to the lack of statistics from identified point-like neutrino sources [181], the most promising way to search for long distance, non-standard decoherence effects in neutrino oscillations is to utilise atmospheric neutrinos. While even recent searches could only constrain the available parameter space for certain classes of QG models, it is still important to see how the various models lead to different bounds on the parameters. We are, therefore, especially interested in the explicit bounds atmospheric experiments can draw given the model assumptions discussed above and how a varying number of fermions affects these constraints. Moreover, we estimate the extent to which these bounds can realistically be expected to improve in the near future by combining measurements from different experiments.

When considering high energy atmospheric neutrinos, it is mandatory to include coherent as well as incoherent matter effects into the description of neutrino oscillations. To this end, we employ the numerical library `nuSQuIDS` [72] implementing the full set of density operator evolution equations discussed in Section 4.1 and 2.3.3. In order to provide a realistic estimate of the bounds atmospheric neutrino experiments can draw on the QG parameter γ, we explicitly consider IceCube as the underlying experimental setup and use a public MC data set [157] as well as the associated, pre-computed scale factor distributions parametrising the systematic effects of the set up on neutrino event counts and reconstruction. Moreover, we use a reference energy $E_0 = 1\,\text{TeV}$ roughly representing the peak energy of the IceCube neutrino flux, different energy power-laws $n \in \{0, 1, 2\}$ and different numbers of fermions $n_f \in \{3, 4, 5, 6\}$. These numbers are motivated, for example, by the hypothetical existence of (possibly light) sterile

neutrinos that would be suitable candidates matching our definition of dark fermions.

4.3.1 Modelling of Neutrino Fluxes and Detector Response at IceCube

We model the initial conventional and prompt atmospheric neutrino fluxes using the publicly available `nuflux` library [182] and employ the implemented `H3a SIBYLL23C` hadronic interaction model split into conventional and prompt atmospheric flux components. The astrophysical component is estimated using a simple power law spectrum,

$$\Phi_a^{\text{astro}}(E) = \Phi_0 \left(\frac{E}{10^5\,\text{GeV}} \right)^{-2.5} , \qquad \Phi_0 = 0.787 \times 10^{-18}\, \frac{1}{\text{GeV}\,\text{sr}\,\text{cm}^2\,\text{s}} \tag{4.39}$$

as suggested in References [157, 183]. All fluxes are propagated through the atmosphere and the Earth using our own implemented decoherence model as well as all pre-implemented matter effects, as described in detail in Section 2.3.3, such as coherent forward scattering, neutrino absorption, tau neutrino regeneration and neutrino energy degradation using the `nuSQuIDS` package. We repeat this procedure for a grid of several different QG decoherence parameter configurations and for different numbers of fermions. For the QG parameter γ, we consider the range $\gamma \in [10^{-20}, 10^{-14}]\,\text{eV}$ motivated by previous QG analyses, see e.g. Reference [150]. Afterwards, we perform a one dimensional interpolation of the resulting neutrino fluxes on the discretely spaced γ values for each (n_f, n) configuration and convert these idealised fluxes into actual neutrino events in the IceCube neutrino observatory using the publicly available MEOWS MC sample.

The MC sample contains track-like ν_μ and $\bar{\nu}_\mu$ events in the energy region $500\,\text{GeV} \leq E \leq 10\,\text{TeV}$ and zenith angle range $-1.0 \leq \cos\theta_{\text{zenith}} \leq 0.0$. Moreover, it contains a total of 4902627 unweighted neutrino events translating to 305735 events when summing up the corresponding nominal MC weights modelling the detector response. This corresponds to a livetime of $T = 7.6\,\text{yr}$. The different events contain information about the true and reconstructed neutrino energies and zenith angles. The energy and angular resolutions of the reconstruction amount to $\sigma_{\log_{10}(E/\text{GeV})} \sim 0.3$ and $\sigma_{\cos\theta_{\text{zenith}}} \sim 0.005$ to 0.015 [184]. We compute the nominal, reconstructed event counts [150, 184] by evaluating the interpolated true neutrino flux distributions obtained from `nuSQuIDS` on the true energies and cosine zenith angle values contained in the MC sample and by multiplying the resulting fluxes with the associated nominal MC weights and the livetime T. Afterwards, all weights belonging to events falling into the same energy and cosine zenith bin are added together.

In order to also account for systematic effects accustom to the experimental conditions at the IceCube neutrino observatory, we apply the following rescaling procedure to the nominal MC weights $\bar{w}$:

$$w_{lj}(\vec{\eta}) = \prod_{i=1}^{n_{\text{sys}}} \alpha_{lj}^i(\eta_i) \bar{w}_{lj} \,, \tag{4.40}$$

Table 4.2: Collection of nuisance parameters η_j, their nominal values $\bar{\eta}_j$, standard deviations σ_{η_j}, and box constraints taken into account in this analysis. For more details see References [150, 184].

Parameter η_j	Nominal Value $\bar{\eta}_j$	Standard Deviation σ_{η_j}	Box Constraint
DOM Efficiency	0.97	0.1	$[0.94, 1.03]$
Bulk Ice Gradient 0	0.0	1.0	$\mathbb{R}$
Bulk Ice Gradient 1	0.0	1.0	$\mathbb{R}$
Forward Hole Ice (p_2)	-1.0	10.0	$[-5, 3]$
Normalisation ($\Phi_{\text{conv.}}$)	1.0	0.4	$\mathbb{R}$
Spectral shift ($\Delta\gamma_{\text{conv.}}$)	0.00	0.03	$\mathbb{R}$
Atm. Density	0.0	1.0	$\mathbb{R}$
Barr WM	0.0	0.40	$[-0.5, 0.5]$
Barr WP	0.0	0.40	$[-0.5, 0.5]$
Barr YM	0.0	0.30	$[-0.5, 0.5]$
Barr YP	0.0	0.30	$[-0.5, 0.5]$
Barr ZM	0.0	0.12	$[-0.25, 0.5]$
Barr ZP	0.0	0.12	$[-0.2, 0.5]$
Normalisation (Φ_{astro})	0.787	0.36	$\mathbb{R}$
Spectral Shift ($\Delta\gamma_{\text{astro}}$)	0.0	0.36	$\mathbb{R}$
Cross Section σ_{ν_μ}	1.00	0.03	$[0.5, 1.5]$
Cross Section $\sigma_{\bar{\mu}_\mu}$	1.000	0.075	$[0.5, 1.5]$
Kaon Energy Loss σ_{KA}	0.0	1.0	$\mathbb{R}$

where $\bar{w}_{lj}$ is the nominal weight of the j-th MC event in bin l, α^i_{lj} is the associated scale factor corresponding to the i-th systematic effect and the w_{lj} are the final, rescaled MC weights. Furthermore, we introduce a set of so-called nuisance parameters η_i for each partial systematic effect parametrising its impact on the number of event counts. The systematic effects we take into account are described in detail in References [150, 184] and correspond to the collection of nuisance parameters shown in Table 4.2. Table 4.2 also shows the nominal values $\bar{\eta}_i$ of the nuisance parameters as well as their standard deviations σ_{η_i} and the box constraints indicating the allowed range of values for each η_i. Evaluating the systematic scale factors α^i_{lj}, extracted from the above mentioned public data release, at the nominal values of the nuisance parameters always yields $\alpha^i_{lj}(\bar{\eta}_i) = 1$. Hence, in this case the rescaling procedure simply results in the nominal MC weights.

4.3.2 Statistical Treatment

In order to estimate the discriminating power of the IceCube neutrino observatory between the standard and QG oscillation scenarios, we perform a likelihood ratio test on the estimated binned event counts obtained from the procedure described in the last section. The full set of

parameters of our decoherence model is given by the number of fermions $n_f \in \{3, 4, 5, 6\}$, the QG energy power-law $n \in \{0, 1, 2\}$ and the decoherence parameter $\gamma \in [0, \infty)$. Because n_f as well as n assume values in discrete spaces, the full parameter space Ξ can be decomposed into a collection of disjoint parameter subspaces, i.e.

$$\Xi := \bigcup_{n_f=3}^{6} \bigcup_{n=0}^{2} \Theta(n_f, n)\,, \qquad \Theta(n_f, n) := \{n_f\} \times \{n\} \times [0, \infty)\,. \tag{4.41}$$

Therefore, each configuration of n_f and n defines a separate model category that corresponds to a simply connected parameter subspace $\Theta(n_f, n)$. The only overlap of these different categories is the point $\gamma = 0$ for which the standard oscillation formula for $n_f = 3$ is obtained.

Since we consider a simple counting experiment with an MC based theory prediction, we employ the effective likelihood function [185],

$$\mathcal{L}_{\text{bin}}(n_f, n, \gamma, \vec{\eta}|\vec{X}) := \prod_{l=1}^{n_{\text{bins}}} \mathcal{L}_{\text{eff}}(N_l(n_f, n, \gamma, \vec{\eta}), \sigma_l^2(n_f, n, \gamma, \vec{\eta})|X_l)\,, \tag{4.42}$$

$$\mathcal{L}_{\text{eff}}(N, \sigma^2|X) := \frac{\beta^\alpha \Gamma(X + \alpha)}{X!(1 + \beta)^{X+\alpha}\Gamma(\alpha)}\,, \quad \alpha = 1 + \frac{N^2}{\sigma^2}\,, \quad \beta = \frac{N}{\sigma^2}\,, \tag{4.43}$$

for the distribution of bin counts. Here, X_l, $N_l(n_f, n, \gamma, \vec{\eta})$ and $\sigma_l^2(n_f, n, \gamma, \vec{\eta})$ denote the measured event count, the event count predicted by the model and the associated MC error in bin l, respectively. The latter two quantities are computed from the MC weights as follows:

$$N_l(n_f, n, \gamma, \vec{\eta}) = \sum_{j=1}^{n_l^{\text{MC}}} w_{lj}\,, \qquad \sigma_l^2(n_f, n, \gamma, \vec{\eta}) = \sum_{j=1}^{n_l^{\text{MC}}} w_{lj}^2\,, \tag{4.44}$$

where n_l^{MC} is the number of MC events in bin l.

As we are interested in constraints on the model parameters n_f, n and γ in the presence of multiple nuisance parameters associated with the systematic effects of the underlying experiment, we define the profile likelihood function of our statistical analysis as

$$\mathcal{L}_{\text{profile}}(n_f, n, \gamma) := \sup_{\vec{\eta} \in U_{\text{sys}}} \mathcal{L}_{\text{bin}}(n_f, n, \gamma, \vec{\eta}|\vec{X}) \cdot \mathcal{L}_{\text{sys}}(\eta)\,, \tag{4.45}$$

in which we maximise the full likelihood consisting of the bin-count likelihood $\mathcal{L}_{\text{bin}}$ and the systematic likelihood

$$\mathcal{L}_{\text{sys}}(\eta) := \prod_{i=1}^{n_{\text{sys}}} \frac{e^{-\frac{(\eta_i - \bar{\eta}_i)^2}{2\sigma_{\eta_i}^2}}}{\sqrt{2\pi\sigma_{\eta_i}^2}}\,, \tag{4.46}$$

over the allowed range of values for the nuisance parameters U_η, specified by the box constraints given in Table 4.2. In using the systematic likelihood (4.46), we assume that the nuisance parameters follow uncorrelated Gaussian distributions centered around the respective nominal

values [150, 184]. Indeed, the Bulk Ice Gradient as well as the astrophysical normalisation and spectral shift nuisance parameter pairs should each follow a two dimensional correlated Gaussian distribution, but due to the lack of information about the associated correlations in the literature [150, 157, 184], we neglect these correlations in this analysis.

We perform the likelihood ratio test for each model category, i.e. n_f–n configuration, individually, in order for the underlying parameter set to be simply connected. As our *pseudo data set*, we use the standard prediction $X_l = N_l(n_f, n, 0, \vec{\eta}) =: N_l^{\text{std}}$. The null hypothesis parameter space then corresponds to the parameter configuration we wish to test, i.e.

$$\Theta_0(n_f, n, \gamma) := \{n_f\} \times \{n\} \times \{\gamma\}\,, \tag{4.47}$$

and therefore, is zero dimensional. Consequently, our test statistics becomes:

$$\ln(\Lambda)(n_f, n, \gamma) = -2 \ln \left(\frac{\sup_{\vec{p} \in \Theta_0(n_f,n,\gamma)} \mathcal{L}_{\text{profile}}(\vec{p}|\vec{X})}{\sup_{\vec{p} \in \Theta(n_f,n)} \mathcal{L}_{\text{profile}}(\vec{p}|\vec{X})} \right)\,, \tag{4.48}$$

where we collect the model parameters in one parameter vector $\vec{p} = (n_f, n, \gamma)$ for convenience of notation.

In the limit of very large bin counts, our test statistics $\ln(\Lambda)$ converges to the following simplified χ^2 test statistics,

$$\chi^2(n_f, n, \gamma) = \inf_{\vec{\eta} \in U_\eta} \left[\sum_{l=1}^{n_{\text{bins}}} \frac{(N_l(\vec{p}, \vec{\eta}) - N_i^{\text{std}})^2}{N_l(\vec{p}, \vec{\eta}) + \sigma_l^2(\vec{p}, \vec{\eta})} + \sum_{i=1}^{n_{\text{sys}}} \frac{(\eta_i - \bar{\eta}_i)^2}{\sigma_{\eta_i}^2} \right]_{\vec{p}=(n_f,n,\gamma)}\,. \tag{4.49}$$

According to Wilk's theorem, this test statistics follows a χ^2 distribution with $\dim(\Theta(n_f, n)) - \dim(\Theta_0(n_f, n, \gamma)) = 1$ DOF. Using $\chi^2(n_f, n, \gamma)$, we finally determine the upper bounds on γ for each n_f–n configuration for a given CL.

4.3.3 Estimated Sensitivities at IceCube

The resulting upper limits on the QG parameter at 90% CL for the chosen benchmark scenarios described in the former sections are displayed in Table 4.3. In addition to the upper limits for γ obtained using the statistics from our pseudo data set and taking into account the systematic effects relevant at IceCube, Table 4.3 also shows upper limits on γ for an idealised scenario without any systematics and only taking into account statistical limitations as well as the effects of energy and directional reconstruction. These upper bounds are roughly one order of magnitude stronger, demonstrating the potential sensitivity current atmospheric neutrino experiments would in principle be able to reach when reducing the impact of systematic effects. This can, for example, be achieved by combining measurements from many different experiments like KM3NeT, IceCube and potential future neutrino telescopes. Moreover, Figure 4.7 shows the corresponding values of the χ^2 test statistics depending on γ as well as the χ^2 values associated with the 68 %, 90 % and 95 % CLs. The results obtained for $n_f = 3$

Table 4.3: Upper limits for the QG parameter γ at 90% CL for the different model configurations. The values in parentheses represent the 90% CL bounds obtained in an idealised statistics-only approach, i.e. without taking into account the systematic uncertainties of the experimental setup.

n_f	γ / 10^{-16} eV		
	$n = 0$	$n = 1$	$n = 2$
3	1.35×10^{1} (1.52)	3.54 (5.20×10^{-1})	1.60×10^{-1} (2.76×10^{-2})
4	1.18×10^{1} (1.33)	2.83 (4.37×10^{-1})	1.16×10^{-1} (2.11×10^{-2})
5	1.09×10^{1} (1.24)	2.51 (3.99×10^{-1})	9.68×10^{-2} (1.81×10^{-2})
6	1.04×10^{1} (1.18)	2.32 (3.76×10^{-1})	8.63×10^{-2} (1.65×10^{-2})

are in very good agreement with the ones obtained in Reference [150] for the state selection scenarios corresponding to our model assumptions. Increasing the number of fermions for a given power-law, the bounds become stricter which is expected as in the decoherence limit, the oscillation probabilities deviate stronger from the standard one for increasing n_f. This behaviour can also be seen by inspecting Figure 4.8. Moreover, increasing the power-law n also results in stricter bounds since at the verge of the decoherence limit the oscillation probability departs much stronger from the standard prediction for higher n. Therefore, the QG coherence energy needs to be shifted to much higher values such that no significant effects appear in the data. However, for $n > 0$ the largest deviations clearly originate from the high energy region where statistics are low and systematic uncertainties are larger compared to the lower energy region, reducing the sensitivity of atmospheric neutrino experiments compared to an idealised scenario with equally high statistics in all energy regions.

In order to cross check the validity of our results and to estimate in which energy and cosine zenith regions we expect the highest sensitivities, we consider the following three bin-wise defined quantities:

$$\text{signed}\chi_l^2(n_f, n, \gamma) := \frac{|N_l(n_f, n, \gamma, \vec{\eta}^*) - N_l^{\text{std}}|(N_l(n_f, n, \gamma, \vec{\eta}^*) - N_l^{\text{std}})}{N_i(n_f, n, \gamma, \vec{\eta}^*)}\,, \tag{4.50}$$

$$\text{signed}\bar{\chi}_l^2(n_f, n, \gamma) := \frac{|N_l(n_f, n, \gamma, \vec{\bar{\eta}}) - N_l^{\text{std}}|(N_l(n_f, n, \gamma, \vec{\bar{\eta}}) - N_l^{\text{std}})}{N_l(n_f, n, \gamma, \vec{\bar{\eta}})}\,, \tag{4.51}$$

$$\text{signed}X_l^2(n_f, n, \gamma) := \frac{|\Phi_l(n_f, n, \gamma) - \Phi_l^{\text{std}}|(\Phi_l(n_f, n, \gamma) - \Phi_l^{\text{std}})}{\Phi_l(n_f, n, \gamma)}\,, \tag{4.52}$$

where $\vec{\eta}^*$ is the best fit value for the nuisance parameters given the set of model parameters, $\vec{\bar{\eta}}$ is the vector of nominal values for the nuisance parameters and Φ_l is the integrated true neutrino flux in bin l. Consequently, the first quantity signedχ_l^2 estimates the sensitivity contribution from each bin to the final χ^2 value including statistical as well as systematic effects while the latter two quantities exclude any impact due to the systematic rescaling procedure. Comparing signedχ_l^2 and signed$\bar{\chi}_l^2$ therefore allows for an assessment of the effect of the systematic scale

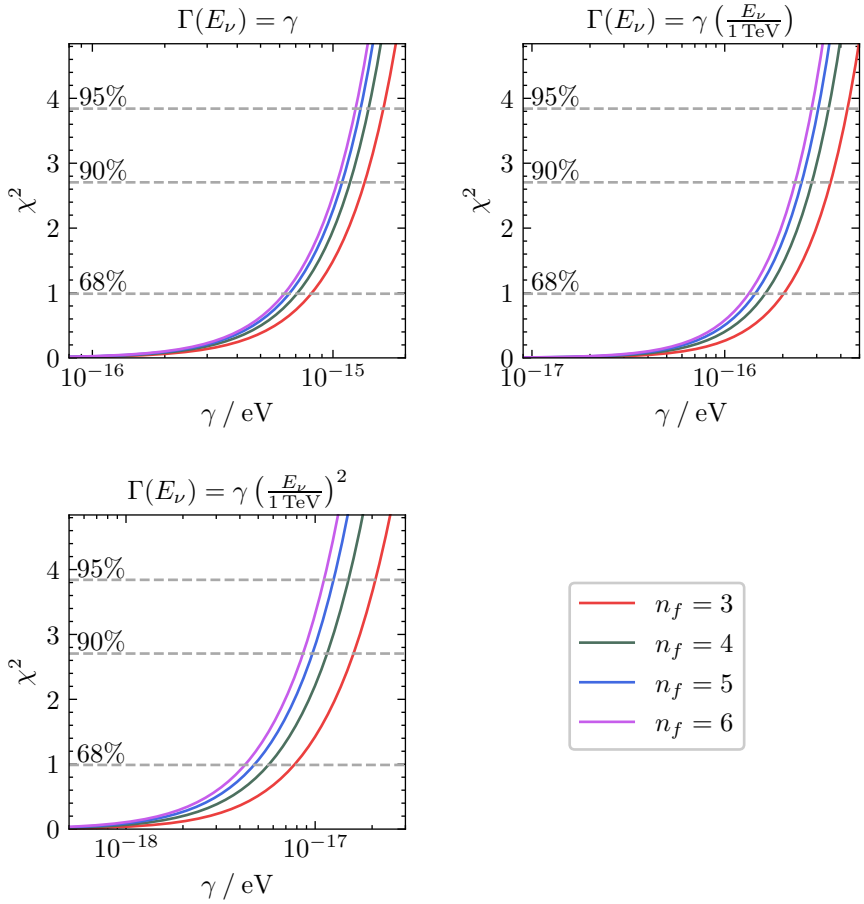

Figure 4.7: Dependence of the χ^2 test statistics on the QG parameter γ for the different decoherence models under consideration. The χ^2 threshold values for the 68 %, 90 % and 95 % CLs are indicated by dashed lines.

factors at $\vec{\eta}^*$, while comparing signed$\bar{\chi}^2_l$ and signedX^2_l provides information about the impact of energy and directional reconstruction.

In Figure 4.9, we show the quantity signedX^2_l in the true energy and cosine zenith plane for $n_f = 4$ scaled such that the lowest values of signedX^2_l coincide with those of signed$\bar{\chi}^2_l$. For the energy-independent decoherence model ($n = 0$), we see that neutrinos with lower energies and larger travel distances would be expected to be most sensitive to this model category. This is because the decoherence effect in this scenario only depends on the travel distance, i.e. cosine zenith, and neutrino fluxes are higher in the low energy bins. Factoring in the effects of energy reconstruction and detector response by considering the signed$\bar{\chi}^2_l$ in the reconstructed energy and cosine zenith plane presented in Figure 4.10 for $n_f = 4$ shows that the naive expectation from the model persists since the region of highest sensitivity is only slightly deformed to higher energies and higher cosine zenith values. In contrast to that, the impact of the energy and directional reconstruction for the linearly energy-dependent decoherence model ($n = 1$)

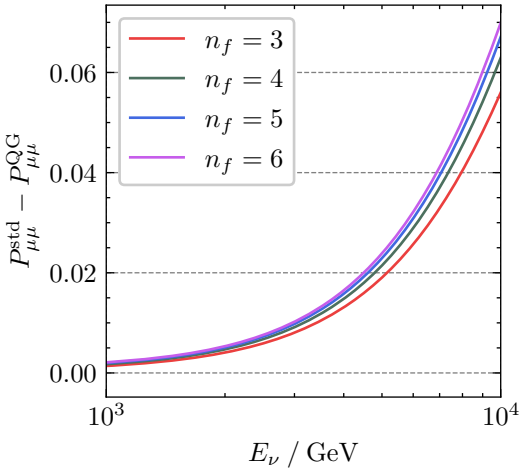

Figure 4.8: Shown is the energy-dependence of the difference between the standard and QG predictions for the $P_{\mu\mu}$ probability for various numbers of fermions and $n = 2$, at the 95 % CL bound $\gamma = 2.08 \times 10^{-17}\,\text{eV}$ for $n_f = 3$ and $n = 2$. The neutrino travel distance is chosen to be the full Earth diameter, i.e. $\cos\theta_{\text{zenith}} = -1$.

appears to be larger when comparing the right most panels in the top rows of Figures 4.9 and 4.10. While the naive model expectation predicts the regions of largest sensitivity to be located at low to intermediate energies and large propagation distances, after applying the event reconstruction also higher reconstructed energy and $\cos(\theta_{\text{zenith}})$ bins significantly contribute to the overall sensitivity.

Next, considering the quadratically energy-dependent decoherence model ($n = 2$), we see in the panel in the bottom row of Figure 4.9 that due to the increasing decoherence effect at high energies, the naive expectation is that high energy bins and upgoing ($\cos(\theta_{\text{zenith}}) \sim -1$) neutrinos contribute most to the overall sensitivity. After applying the energy reconstruction, cf. the panel in the bottom row in Figure 4.10, this remains true, however, the sensitivity region is shifted to larger $\cos(\theta_{\text{zenith}})$ values.

Finally, also applying the systematic scaling procedure at the best fit value $\vec{\eta}^*$ of the nuisance parameters transforms Figure 4.9 into Figure 4.11. Across all decoherence models, the minimisation of χ^2 with respect to the nuisance parameters naturally results in much smaller values of signedχ^2_l compared to signed$\bar{\chi}^2_l$. For $n = 0$, the region of highest sensitivity still remains in place, but the systematic scaling causes another region to appear next to it. The latter is located at higher cosine zenith values and indicates a positive deviation from the standard case instead of a negative one as we would expect form the decoherence model. Moreover, for the linearly energy-dependent model, i.e. $n = 1$, the sensitivity region is further smeared across all energy and cosine zenith bins. Lastly, considering the bottom panel of Figure 4.11 we see that for $n = 2$, the sensitivity region again remains largely intact when compared to the respective panel in Figure 4.10.

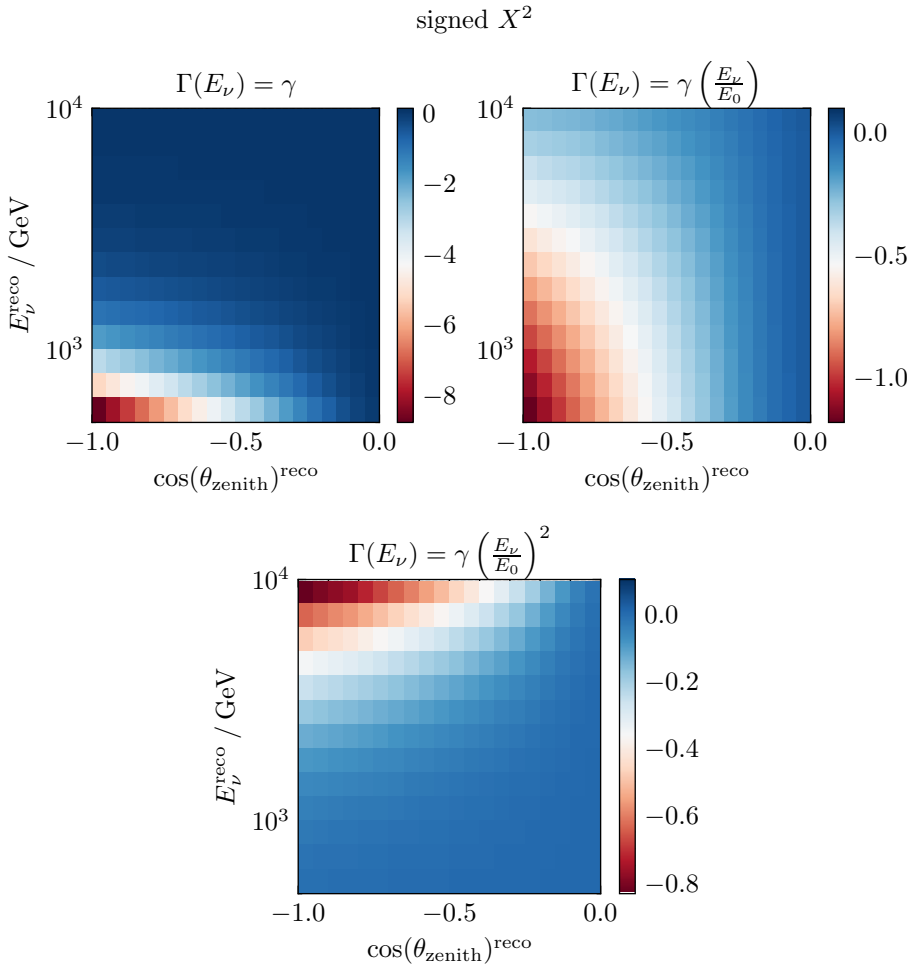

Figure 4.9: The binned quantity signedX_l^2 computed from the true neutrino fluxes in the true cosine zenith and energy plane for $n_f = 4$ and the considered decoherence models at the respective 95 % CL γ values: $\gamma \in \{1.41 \times 10^{-15}, 3.46 \times 10^{-16}, 1.50 \times 10^{-17}\}$ eV (from left to right, top to bottom). We scale signedX_l^2 such that its lowest values coincide with the respective signed$\bar{\chi}_l^2$ determined from the reconstructed event counts.

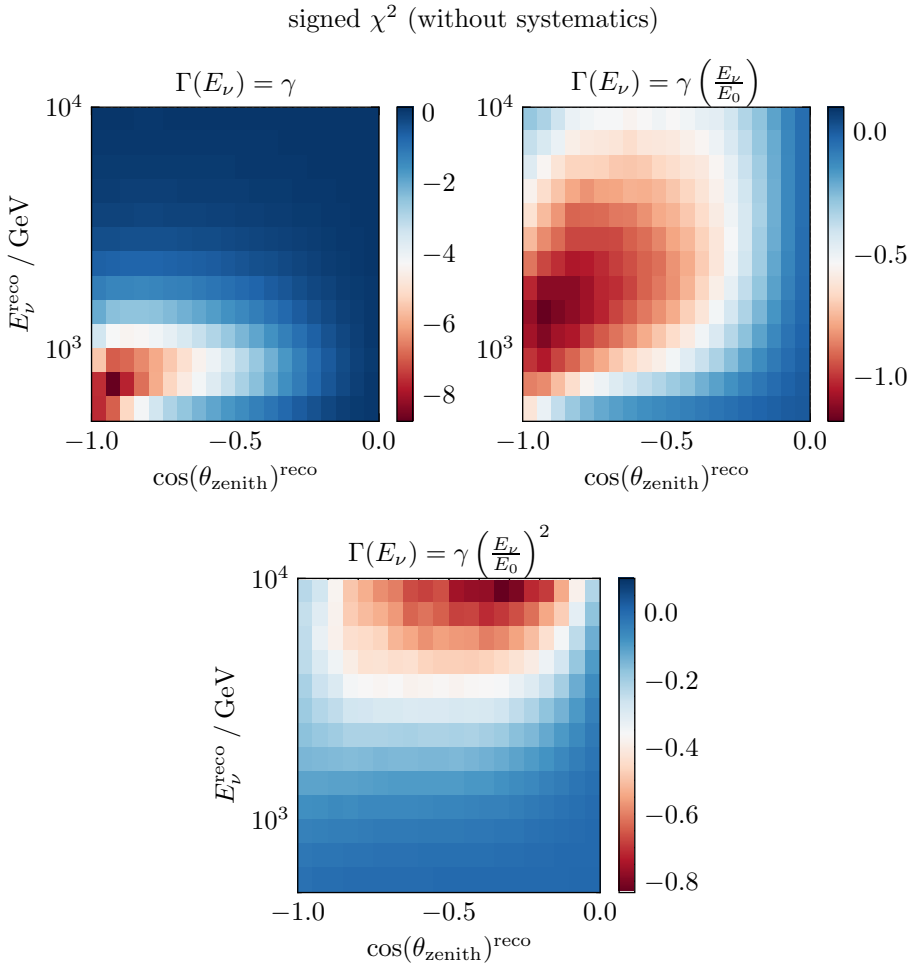

Figure 4.10: The binned quantity signed$\bar{\chi}_l^2$ (i.e. *without* systematic effects) in the reconstructed cosine zenith and energy plane for $n_f = 4$ and the considered decoherence models at the respective 95% CL γ values: $\gamma \in \{1.41 \times 10^{-15}, 3.46 \times 10^{-16}, 1.50 \times 10^{-17}\}$ eV (from left to right, top to bottom).

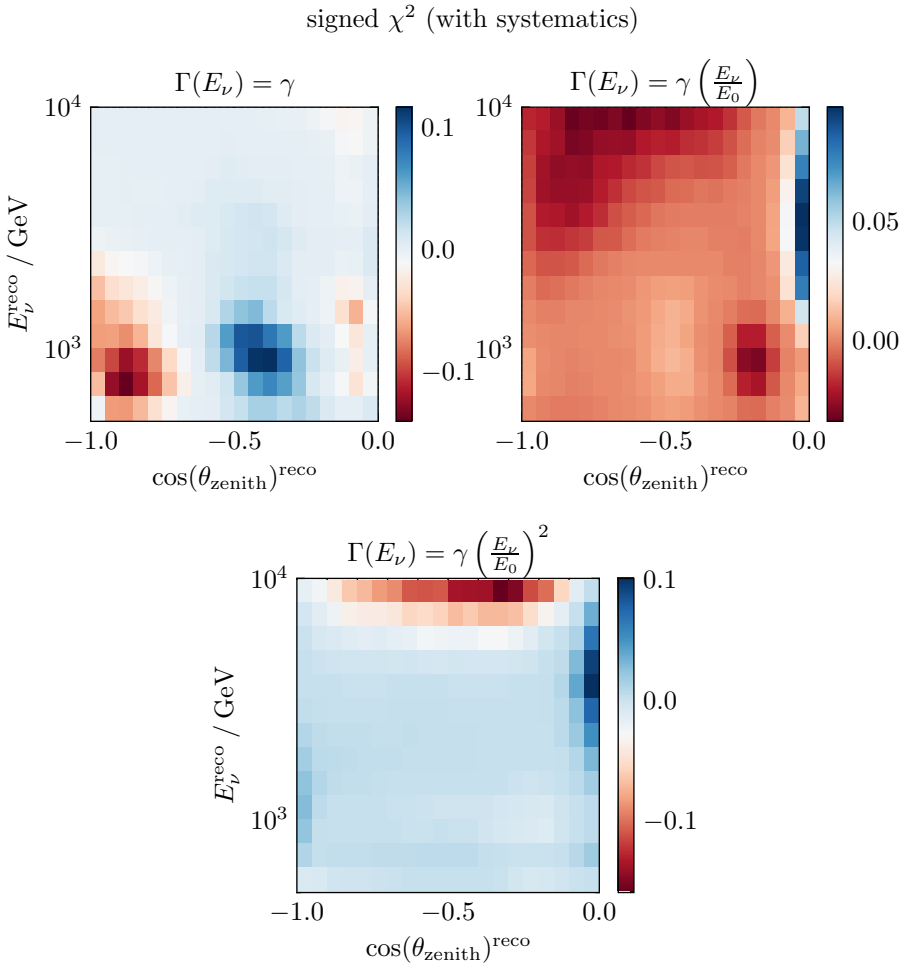

Figure 4.11: The binned quantity signedχ^2_l (i.e. with systematic effects) in the reconstructed cosine zenith and energy plane for $n_f = 4$ and the considered decoherence models at the respective 95% CL γ values: $\gamma \in \{1.41 \times 10^{-15}, 3.46 \times 10^{-16}, 1.50 \times 10^{-17}\}$ eV (from left to right, top to bottom).

4.4 Summary and Conclusion

In this chapter, we have proposed and analysed a phenomenological model describing the impact of QG DOFs on neutrino oscillations. Via entanglement between the neutrino flavour and QG DOFs, decoherence is induced in the neutrino system. This decoherence effect gives rise to several damping terms of the form $e^{-\Gamma(E)L}$ in the oscillation probability $P_{ab}(L, E)$ that we parametrise in terms of the neutrino energy using a common power-law, i.e. $\Gamma(E) \propto \gamma E^n$. Moreover, we assume the QG effects to maximally violate the conservation of charges associated with global symmetries and to only conserve unbroken gauge charges, angular momentum, the direction of propagation as well as the total probability of the fermion system. This implies that the oscillation probability approaches a uniform flavour distribution, i.e. $P_{ab} \to 1/n_f$, in the QG decoherence limit, where n_f is the total number of flavours. In the presence of hypothetical dark fermions, such as sterile neutrinos [186], WIMPs [187] or FIMPs [188], n_f may even be extended to $n_f > 3$, providing a link to the fermionic dark sector.

First, we have applied this model to cosmic neutrinos representing the potentially most interesting candidates to consider in this framework as the QG decoherence function grows in strength at increasing propagation distances. We find that in models where the decoherence effect also increases with growing neutrino energy, i.e. $n > 0$, a dip in the total neutrino flux spectrum occurs after a certain energy E_{QG} if $n_f > 3$. The strength of this dip directly depends on the number of fermions that are allowed to appear in the initially pure neutrino beam. Finding such a dip at future neutrino telescopes enables a direct fit of the model parameters and an estimation of the number of dark fermions. The prominence and location of the dip change if the neutrinos are not originating form the same source but rather a distribution of sources, as in the case of the already measured diffuse astrophysical neutrino flux. Moreover, we have shown that the same happens if long lived, highly Lorentz boosted particles are produced as primary particles in the cosmic source and the neutrinos only emerge as decay products of these particles. In both cases, the neutrino ensemble propagates a distribution of baselines, and hence, experiences different degrees of QG decoherence. This complicates a fit to future neutrino data as more parameters accounting for the variety of different flux models need to be fitted to the data simultaneously. To partially circumvent this issue, we propose to take neutrino flavour ratios as well as total neutrino fluxes into account since flavour ratios have a weaker dependence on the underlying flux model. Also considering neutrinos from multiple sources that produce equivalent neutrino spectra can lead to an improved sensitivity to the QG parameters. In the QG decoherence limit, all flavour ratios tend to a democratic $(1/3 : 1/3 : 1/3)$ distribution and thus provide a cross check of the QG hypothesis. In contrast to total fluxes, neutrino flavour ratios are insensitive to the total number of fermions in the system. Thus, even if $n_f = 3$ and no dip occurs in the total neutrino flux spectrum, the QG effect always leads to a uniform flavour distribution, especially in the high energy bins $E > E_{\mathrm{QG}}$. This in itself is an interesting signature to search for at current and future neutrino telescopes such as IceCube and KM3NeT. However, currently such an analysis is not feasible as it would suffer from limited statistics.

In the second part of this chapter, we have performed a statistical analysis using publicly

available MC data in order to estimate the sensitivity of IceCube to the QG decoherence parameter γ for energy dependencies $n \in \{0, 1, 2\}$ and numbers of fermions in the range $n_f \in \{3, 4, 5, 6\}$. We have found that sensitivity to a given QG decoherence parameter γ increases as the number of fermion species in the beam grows. This is due to the larger deviation of P_{ab} from the standard probability as the QG limit is reached. The analysis has been performed using realistic initial neutrino flux models that are propagated from the atmosphere into the detector using the widely adopted neutrino oscillation software `nuSQuIDS`, extended by the model under consideration. Lastly, we have accounted for systematic and detector effects using the MC sample in order to reweight the true neutrino events into reconstructed ones. Moreover, we estimate the regions of energies and cosine zenith angles in which IceCube would be most sensitive to the new decoherence effect. This provides further discriminating power from other potential decoherence effects that exhibit a different sensitivity pattern.

Future analyses using combined data from different neutrino telescopes, as for example IceCube and KM3NeT, can provide even more interesting insights into the nature of QG due to larger event samples and different systematic uncertainties. Ultimately, this may contribute to a better theoretical understanding of the fundamental properties of spacetime.

5 Neutrino Oscillations in Curved Spacetime

In this chapter, Section 5.4 is based on Reference [189].

Multimessenger astronomy is one of the most important and promising areas of ongoing research since it offers the possibility to study the most distant phenomena like the collisions of black holes and neutron stars, the inner workings of supernovae and particle production around compact stellar objects (for an excellent review see e.g. Reference [190]). This is made possible by combining the analysis of EM, neutrino and gravitational wave (GW) signals from the cosmos and opens the window for new physics searches impossible to conduct in a laboratory. In this work, we mainly focus on the neutrino component of multimessenger astronomy.

Apart from energy and directional information, neutrinos can also provide insights into the physical processes that produced them by analysing the final flavour composition in neutrino telescopes. On their way to Earth, neutrinos are not deflected by galactic EM fields making them an important complementary component to EM signals in, for example, the study of supernovae, and cosmic particle accelerators like pulsars and blazars. However, just like EM signals, neutrinos also pass through non-trivial gravitational potential landscapes. Depending on their exact origin, neutrinos may even encounter strong gravitational fields, and the expansion of the Universe may be non-negligible. It is therefore imperative to understand the influence of the curvature of spacetime not only on the neutrino path but also on the flavour dynamics.

There already exist numerous studies on neutrino flavour and spin transitions in gravitational fields in different degrees of approximation ranging from semiclassical considerations [191–201], based on the Hamilton–Jacobi equation, up to more fundamental approaches [202, 203] using the framework of QFT in curved spacetime. For example, the commonly used Stodolsky phase [191], generalising the oscillation phase to neutrinos propagating along geodesics, is based on the action of a classical particle in curved spacetime. In contrast to this, in the approach presented e.g. in Reference [202], the oscillation probability is derived from the evolution of the lepton flavour operator in QFT in curved spacetime. In most approaches, neutrino oscillations are treated in the effective plane wave formalism and no rigorous extension of the WP formalism to curved backgrounds have been undertaken yet. Effects due to the WP nature of neutrinos are at most taken into account via an ad hoc implementation of the Stodolsky phase [200, 201]. Since the Stodolsky phase only involves the mean momentum of a WP, integrated along the corresponding geodesic, this raises the questions if other modes, contributing to the neutrino WP, are accounted for consistently in this treatment. Thus, to address this issue, we derive a formula from first principles in QFT in curved spacetime,

accounting for the fact that propagating neutrino states are produced as WPs. We show that for strongly peaked momentum space WPs, i.e. close-to plane wave states, the Stodolsky phase treatment indeed represents a good approximation.

Due to the subtleties arising when formulating QFT on general manifolds, it is important to carefully consider the physical conditions applying to an experiment studying neutrino flavour transitions within the theoretical formalism. The most important subtlety, for the purposes of this work, is the observer-dependence of the particle concept and the associated phenomenon of gravitational or Unruh-like particle production [37–39, 152, 204, 205]. We start our analysis by discussing under what circumstances this additional particle production can be neglected and how well defined a universal flavour transition probability, and the internal WP picture, is in curved spacetimes. From these considerations, we then derive a general formula for the neutrino flavour transition amplitude that is valid as long as gravitational particle production is negligible at the energy scale of the detected neutrino events. This is done in Section 5.1. Since it is difficult to further simplify the obtained expression under general conditions, we consider scenarios where all neutrino mass eigenstate geodesics remain close to each other and curvature effects are negligible on the scale of the neutrino WP at any given time, in Section 5.2. Afterwards, in Section 5.3, we apply the resulting formula to the scenario of linearised gravity including the special cases of Newtonian fields as well as GW spacetimes. Moreover, we consider the application of neutrino oscillations in GW spacetimes in more detail in Section 5.4. Here, we also formulate several criteria that need to be fulfilled in order to observe an effect induced by GWs in neutrino flavour transitions. Lastly in Section 5.5, we apply these criteria to discuss why—apart from exotic scenarios—neither current nor near-future neutrino experiments will possibly be sensitive to any gravitational influence on the neutrino oscillation pattern. Finally, we conclude in Section 5.6.

5.1 Neutrino Oscillations in the Absence of Gravitational Particle Production and Related Effects

As extensively discussed in Section 2.3, any neutrino flavour oscillation experiment is comprised of two main components: the neutrino source and the detector. Both occupy a certain region in spacetime that can be considered to be macroscopic compared to the much smaller volume in which the neutrino production and detection processes happen, respectively. We denote the average spacetime event of neutrino production taking place at proper time $\mathcal{T}_{\mathrm{S}}$ of the source by $X_{\mathrm{S}}(\mathcal{T}_{\mathrm{S}})$, and in close analogy we write $X_{\mathrm{D}}(\mathcal{T}_{\mathrm{D}})$ for the event of neutrino detection in dependence of the proper time $\mathcal{T}_{\mathrm{D}}$ of the detector. For a unified notation, we assume in the following that both neutrino production and detection are observed by two hypothetical observers, O_{S} and O_{D}, respectively. Usually the term *observer* refers to some kind of measurement apparatus where in the case of O_{D} the most obvious choice would be the neutrino detector itself, while in case of the source, especially when considering neutrinos of astrophysical origin, the production may even go completely unmeasured. We still pretend, in the following, that a source-bound

observer O_{S} exists and, similar to the macroscopic averaging procedure discussed at the end of Section 2.3.1, simply average and sum over all unmeasured quantities in the end.

According to our discussion in Section 2.2.2, the definition of the particle concept in curved spacetime is unavoidably tied to the state of motion of an observer itself. In this light, we now reconsider the neutrino production, propagation and detection process in curved spacetime. The most fundamental approach would be to extend the external WP formalism [51–55], discussed in Section 2.3.1, to curved spacetime. In case gravitational particle production is non-negligible due to significant discrepancies between the notions of particles the observers at the source and detector define, the only correct treatment is to consider the production–propagation–detection process as a whole since the single sub-processes cannot be disentangled from each other, in general. This is because gravitationally[1] produced particles may interact with the propagating neutrino or the external states in the detector and add more possible diagrams with topologies different from the one shown in Figure 2.1. This invalidates the single-particle picture of neutrino propagation and possibly prevents the factorisation of the production, propagation and detection sub-processes. Consequently, the universal oscillation probability would be inherently ill-defined. From now on, we restrict ourselves to the more common case where gravitational particle production can be neglected for the energy modes of interest. In this case, the external and internal WP approaches to neutrino oscillations become equivalent again and the propagating neutrino can be viewed as a free particle, just as in flat spacetime.

This restriction does not pose a strong constraint due to the weakly interacting nature of neutrinos, enabling efficient measurements roughly starting at $\mathcal{O}(\mathrm{keV})$ energies. Especially, in contexts where gravitational particle production may become important, i.e. for neutrinos of astrophysical origin, typical neutrino energies are even larger. The required Unruh temperature (or the gravitational equivalent thereof) would, hence, need to be of similar magnitude, implying the presence of regions with extremely strong spacetime curvature in the vicinity of the neutrino path. Therefore, the expressions derived in the following are only invalid for the consideration of such extreme conditions.

Let $(\xi^{\mathrm{S}}_{j;J}, \epsilon^{\mathrm{S}}_{j;J})$ be the set of mode solutions to the Dirac equation with neutrino mass m_j chosen by observer O_{S} and $(\xi^{\mathrm{D}}_{j;\sigma}, \epsilon^{\mathrm{D}}_{j;\sigma})$ those chosen by the detection observer O_{D}. The corresponding ladder operators, creating a (anti-)neutrino mass eigenstate j with quantum numbers J and σ, are $(a^{(\dagger)}_{\mathrm{S}j;J}, b^{(\dagger)}_{\mathrm{S}j;J})$ and $(a^{(\dagger)}_{\mathrm{D}j;\sigma}, b^{(\dagger)}_{\mathrm{D}j;\sigma})$, respectively. Consequently, the neutrino WPs the observers at the source and detector define are

$$|\nu_a, X_{\mathrm{S}}\rangle = \sum_j U^*_{aj} \sum_J \phi^{\mathrm{S}}_j(J) a^\dagger_{\mathrm{S}j;J} |0, \mathrm{S}\rangle \ , \tag{5.1}$$

$$|\nu_b, X_{\mathrm{D}}\rangle = \sum_j U^*_{bj} \sum_\sigma \phi^{\mathrm{D}}_j(\sigma) a^\dagger_{\mathrm{D}j;\sigma} |0, \mathrm{D}\rangle \ , \tag{5.2}$$

[1] From here on, we simply refer to gravitational particle production whenever we discuss the particles produced due to different definitions of the particle concepts of two observers.

where $\phi_j^{\mathrm{S/D}}$ are the WPs specifying the probability to measure the quantum numbers J and σ in the respective state and $|0,\mathrm{S/D}\rangle$ are the vacua of the source and detector observers, respectively. Choosing for example an explicit parametrisation in terms of momenta $\vec{p}$ and spins s, i.e. $J=\sigma=(\vec{p},s)$, these states become

$$|\nu_a, X_{\mathrm{S}}\rangle = \sum_j U_{aj}^* \sum_{s=\pm 1/2} \int \mathrm{d}^3\vec{p}\, \phi_j^{\mathrm{S}}(\vec{p},s) a^\dagger_{\mathrm{S}j;\vec{p}s} \,|0,\mathrm{S}\rangle \ , \tag{5.3}$$

$$|\nu_b, X_{\mathrm{D}}\rangle = \sum_j U_{bj}^* \sum_{s=\pm 1/2} \int \mathrm{d}^3\vec{p}\, \phi_j^{\mathrm{D}}(\vec{p},s) a^\dagger_{\mathrm{D}j;\vec{p}s} \,|0,\mathrm{D}\rangle \ . \tag{5.4}$$

Finally, the neutrino flavour transition amplitude is defined by the overlap of both states, i.e.

$$\mathcal{A}_{ab}(X_{\mathrm{S}}, X_{\mathrm{D}}) := \langle \nu_b, X_{\mathrm{D}} | \nu_a, X_{\mathrm{S}}\rangle = \sum_j U_{aj}^* U_{bj} \sum_{J\sigma} \phi_j^{\mathrm{D}*}(\sigma)\phi_j^{\mathrm{S}}(J)\, \langle 0,\mathrm{D}|\, a_{\mathrm{D}j;\sigma} a^\dagger_{\mathrm{S}j;J}\,|0,\mathrm{S}\rangle \ . \tag{5.5}$$

In general, the VEV $\langle 0,\mathrm{D}|\, a_{\mathrm{D}j;\sigma} a^\dagger_{\mathrm{S}j;J}\,|0,\mathrm{S}\rangle$ evaluates to

$$\langle 0,\mathrm{D}|\, a_{\mathrm{D}j;\sigma} a^\dagger_{\mathrm{S}j;J}\,|0,\mathrm{S}\rangle = \alpha^{\mathrm{SD}}_{J\sigma}\, \langle 0,\mathrm{D}|0,\mathrm{S}\rangle + \sum_\rho \beta^{\mathrm{SD}}_{J\rho} \underbrace{\langle 0,\mathrm{D}|\, a_{\mathrm{D}j;\sigma} b_{\mathrm{D}j;\rho}\,|0,\mathrm{S}\rangle}_{=\langle \nu_{j;\sigma}\bar{\nu}_{j;\rho},\mathrm{D}|0,\mathrm{S}\rangle}, \tag{5.6}$$

where $\alpha^{\mathrm{SD}}_{J\sigma}$ and $\beta^{\mathrm{SD}}_{J\sigma}$ are the Bogoliubov coefficients translating between the source and detector Fock space constructions. Moreover, the matrix element in the last term represents the amplitude for the gravitational production of a neutrino–antineutrino (detection) state from the source vacuum. As shown in Reference [206] for the case of scalar fields, these vacuum to many-particle amplitudes can also be related to the Bogoliubov coefficients. From Equation (5.5), we can now infer an explicit criterion for the negligibility of gravitational particle production in the modes of interest, i.e.

$$0 \approx \sum_\rho \beta^{\mathrm{SD}}_{J\rho}\, \langle \nu_{j;\sigma}\bar{\nu}_{j;\rho},\mathrm{D}|0,\mathrm{S}\rangle \ , \qquad \forall J,\sigma : \phi_j^{\mathrm{S}}(J) > \delta \quad \wedge \quad \phi_j^{\mathrm{D}}(\sigma) > \delta \, , \tag{5.7}$$

where δ is an apriori chosen accuracy parameter determining when to consider contributions from the WPs to be negligible as the corresponding quantum number configurations rarely occur in the given experiment.

Equation (5.7) represents a rather formal requirement and especially the accuracy parameter δ is hardly accessible in experiments. Thus, it is preferable to rephrase it in terms of the experimentally accessible quantum number, e.g. momentum, distributions: Given the quantum number distribution of neutrinos in an experiment, Equation (5.7) states that the production of neutrino–antineutrino pairs need to be negligible in those configurations appearing with significant probability in the experiment. If this is the case, the one-particle picture is valid and the flavour transition amplitude (5.5) is well-defined. Lastly, we can also relate the amplitude to the scalar products of source and detection mode functions via

$$\boxed{\mathcal{A}_{ab}(X_{\mathrm{S}}, X_{\mathrm{D}}) := \langle 0,\mathrm{D}|0,\mathrm{S}\rangle \sum_j U_{aj}^* U_{bj} \sum_{J\sigma} \phi_j^{\mathrm{D}*}(\sigma)\phi_j^{\mathrm{S}}(J) \langle \xi^{\mathrm{D}}_{j;\sigma}, \xi^{\mathrm{S}}_{j;J}\rangle \, ,} \tag{5.8}$$

which exhibits the same structure as the flat spacetime formula for the internal WP approach. This is the main result of this section. The information about the location and state of motion of the observers as well as which quantum numbers of the neutrino system they measure is encoded within the mode functions $\xi^{\mathrm{S/D}}$. The most important examples, we consider in the following sections, are freely falling observers, measuring the neutrino momenta and helicities within their respective local inertial frames. In this special case, the mode functions reduce to their flat spacetime form given in Equation (2.66), i.e.

$$\xi^{\mathrm{S/D}}_{j;\vec{p}s}(z) = u_{j;s}(p)\frac{e^{-ip_\mu z^\mu}}{\sqrt{(2\pi)^3 2E_j}}\,, \tag{5.9}$$

at lowest order in the normal coordinate expansion about the origin ($z = 0$) of the local inertial frame.

In order to compute the neutrino oscillation probability from the amplitude (5.8), we need to apply the same treatment as discussed in Sections 2.3.1 and 2.3.2, i.e. integrating over the worldlines of the neutrino source and detector, respectively, and normalising the result appropriately, i.e.

$$P_{ab}(\mathrm{S},\mathrm{D}) = \frac{\int_{\mathcal{T}_{\mathrm{S1}}}^{\mathcal{T}_{\mathrm{S2}}} \mathrm{d}\mathcal{T}_{\mathrm{S}} \int_{\mathcal{T}_{\mathrm{D1}}}^{\mathcal{T}_{\mathrm{D2}}} \mathrm{d}\mathcal{T}_{\mathrm{D}}\, |\mathcal{A}_{ab}(X_{\mathrm{S}}(\mathcal{T}_{\mathrm{S}}), X_{\mathrm{D}}(\mathcal{T}_{\mathrm{D}}))|^2}{\int_{\mathcal{T}_{\mathrm{S1}}}^{\mathcal{T}_{\mathrm{S2}}} \mathrm{d}\mathcal{T}_{\mathrm{S}} \int_{\mathcal{T}_{\mathrm{D1}}}^{\mathcal{T}_{\mathrm{D2}}} \mathrm{d}\mathcal{T}_{\mathrm{D}} \sum_b |\mathcal{A}_{ab}(X_{\mathrm{S}}(\mathcal{T}_{\mathrm{S}}), X_{\mathrm{D}}(\mathcal{T}_{\mathrm{D}}))|^2}\,. \tag{5.10}$$

Here, we formulate the integral in terms of the proper times, $\mathcal{T}_{\mathrm{S}}$ and $\mathcal{T}_{\mathrm{D}}$, instead of coordinate times in order to achieve a coordinate-independent description. Moreover, we define the livetime intervals of source and detector as $[\mathcal{T}_{\mathrm{S1}}, \mathcal{T}_{\mathrm{S2}}]$ and $[\mathcal{T}_{\mathrm{D1}}, \mathcal{T}_{\mathrm{D2}}]$, respectively. Equation (5.10) indeed simplifies to Equation (2.104) if source and detector move along straight world lines. Due to the normalisation procedure the global factor $\langle 0, \mathrm{D}|0, \mathrm{S}\rangle$ will drop out and we can as well redefine the amplitude (5.8) to leave it out from the start.

To close this section, we discuss the difficulties of applying Equation (5.8) to real world examples. In any case, the mode solutions $\xi^{\mathrm{S/D}}$, linked to the flow of proper time of the observers, relevant for the neutrino experiment have to be known globally or at least on a large patch of the manifold. Solving the Dirac equation, even in coordinate systems associated with the isometries of a spacetime, is often already difficult. Especially appealing for this task are time-like isometries corresponding to time-like Killing fields in order to be able to define a common particle concept for a large class of observers. If the flow of time of the considered observers then doesn't even coincide with the Killing time, the task of solving the Dirac equation becomes even more challenging. One simple example, where this is indeed possible, is the case of inertial observers in Minkowski spacetime, where we obtain a simple oscillation phase from the scalar product of mode solutions, i.e.

$$\mathcal{A}^{\mathrm{flat}}_{ab}(X_{\mathrm{S}}, X_{\mathrm{D}}) = \sum_j U^*_{aj} U_{bj} \sum_{s=\pm 1/2} \int \mathrm{d}^3\vec{p}\, \phi^{\mathrm{D}*}_j(\vec{p}, s)\phi^{\mathrm{S}}_j(\vec{p}, s) e^{-ip_\mu (X_{\mathrm{D}} - X_{\mathrm{S}})^\mu}\,, \tag{5.11}$$

which is the standard result. The modes only differ in that they are defined with respect to the local (and therefore also global) inertial frames with origin at the events X_{S} and X_{D}, respectively. Therefore, when evaluating the scalar product $\langle \xi^{\mathrm{D}}_{j;\vec{q}s}, \xi^{\mathrm{S}}_{j;\vec{p}r} \rangle$ only a phase factor arises. By virtue of the equivalence principle, when considering sufficiently localised[2] neutrino WPs such that curvature effects can be neglected on the region containing the neutrino WPs at any given instant in time, we should expect a similar relation as (5.11) to apply. In these scenarios, we expect the only modifications to be caused by the global curvature of the neutrino geodesics.

5.2 Neutrino Oscillations in Weak Gravitational Fields

In most cases of interest, gravitational fields are rather weak and lead to a sub-leading modification of the neutrino flavour transition mechanism. Therefore, commonly gravitational effects are entirely neglected when studying neutrino oscillations in experiments ranging from SBL and LBL collider set-ups over solar neutrino experiments to neutrino telescopes observing galactic and extra-galactic neutrinos. Only in the latter case, the expansion of the Universe is usually taken into account by modifying the derivative operator in the effective Schrödinger equation for the neutrino flavour system. In the following, we derive a modified formula for the neutrino flavour transition amplitude taking into account the lowest order curvature effects.

As already motivated in the last section, from now on, we assume the neutrino to be sufficiently localised such that there exists a simply connected region $U_\nu \subset \mathcal{M}$ that contains the world tubes of all neutrino mass eigenstate WPs, such that the local curvature is negligible on any intersection of U_ν with a Cauchy surface Σ_t, i.e. at any instant in time. Moreover, we consider a freely falling neutrino source and detector where the natural set of quantum numbers labelling the source and detection modes are the neutrino momenta and spins. In this formulation, the localisation condition is equivalent to the requirement that only sufficiently short wave lengths, that are not probing the global structure of the manifold, contribute to the neutrino WP. Therefore, the mode solutions, associated to these wave lengths, can be well approximated by the flat spacetime modes (2.66) on the scale of the neutrino WPs. Indeed, this last requirement can in principle be relaxed in order to also take possible spin precession effects into account by expanding the Dirac equation up to second order in the local inertial frame. We, however, are interested in the non-trivial lowest order gravitational influence in this work, and therefore, neglect these effects.

The derivation presented in the following is based on the fact that all strongly localised mass eigenstate WPs on average follow classical geodesics c_j, uniquely determined by their mean initial coordinate and four-velocity. We then apply Equation (5.8) and propagate the initial neutrino WP from the production vertex X_{S} to the detection vertex X_{D}. In general, there exist multiple geodesics connecting X_{S} and X_{D}, and these geodesics in general also differ from the

[2]Sufficiently localised means if on any Cauchy surface Σ_t the width of and the distance between the coordinate space WPs is much smaller than the minimal curvature radius of the manifold within the region of neutrino propagation.

average neutrino paths c_j. This is especially true when considering production and detection events with space-like separation. However, as shown in Appendix (A.3), the amplitude $\mathcal{A}_{ab}$ vanishes for space-like distances between source and detector. Therefore, in the following, we only focus on production and detection events that are causally connected. In this case, we perform the propagation in a step-by-step manner along the geodesic c, connecting X_{S} and X_{D}, that is closest[3] to all mass eigenstate geodesics c_j.

In each step $\tau \to \tau + \Delta\tau$ along the curve c, we compute the new momentum space wave function in terms of locally inertial modes at the time $\tau + \Delta\tau$ in terms of the momentum space WP at τ. This next local inertial frame with origin at $c(\tau + \Delta\tau)$ is assumed to be such that its coordinate tangent vectors coincide with the parallel transport of those at the last point $c(\tau)$. In this sense, we parallel transport the initial local inertial frame from the source to the detector. After the propagation procedure, we take the limit $\Delta\tau \to 0$ and match the transported frame onto the detection frame. This matching is facilitated by a simple local Lorentz transformation. The combined operation of parallel transport and transforming into the detection system then encodes the gravitational influence on the initial neutrino momentum, such as gravitational redshift. In addition to that, it also encodes redshift effects due to a potential relative motion of source and detector that would also be present in Minkowski spacetime.

We start by defining the position space neutrino mass eigenstate WPs at production and detection by

$$\psi_j^{\mathrm{S}}(x) \coloneqq \sum_{s=\pm 1/2} \int \mathrm{d}^3\vec{p}\, \phi_j^{\mathrm{S}}(\vec{p}, s) \xi^{\mathrm{S}}_{j;\vec{p}s}(x)\,, \qquad \psi_j^{\mathrm{D}}(x) \coloneqq \sum_{s=\pm 1/2} \int \mathrm{d}^3\vec{p}\, \phi_j^{\mathrm{D}}(\vec{p}, s) \xi^{\mathrm{D}}_{j;\vec{p}s}(x)\,, \tag{5.12}$$

and express the amplitude in Equation (5.8) in terms of these quantities as

$$\mathcal{A}_{ab}(X_{\mathrm{S}}, X_{\mathrm{D}}) = \sum_j U^*_{aj} U_{bj} \langle \psi_j^{\mathrm{D}}, \psi_j^{\mathrm{S}} \rangle\,. \tag{5.13}$$

Since we neglect gravitational particle production as before, we can now insert an identity on the space of positive frequency solutions of the form

$$\mathbb{1}[\cdot]\big|_{\text{pos. freq.}} = \sum_{s=\pm 1/2} \int \mathrm{d}^3\vec{p}\, \xi^{X_{\mathrm{S}} \to X_{\mathrm{D}}}_{j;\vec{p}s} \langle \xi^{X_{\mathrm{S}} \to X_{\mathrm{D}}}_{j;\vec{p}s}, \cdot \rangle\,, \tag{5.14}$$

and get

$$\mathcal{A}_{ab}(X_{\mathrm{S}}, X_{\mathrm{D}}) = \sum_j U^*_{aj} U_{bj} \sum_{s=\pm 1/2} \int \mathrm{d}^3\vec{p}\, \langle \psi_j^{\mathrm{D}}, \xi^{X_{\mathrm{S}} \to X_{\mathrm{D}}}_{j;\vec{p}s} \rangle \langle \xi^{X_{\mathrm{S}} \to X_{\mathrm{D}}}_{j;\vec{p}s}, \psi_j^{\mathrm{S}} \rangle\,. \tag{5.15}$$

Here and in the following, we denote by $\xi^{X_{\mathrm{S}} \to X}$ those modes that reduce to the flat spacetime form (2.66) in the vicinity of $X = c(\tau)$ in the local inertial frame with origin at X emerging from the parallel transport of the source frame in the sense discussed above. From now on, we also call these mode functions the parallel transported modes. Therefore, we have reduced

[3] We explain this criterion in more detail at a later point in the derivation.

the task of computing the scalar product of coordinate space WPs to the evaluation of the simpler quantities

$$\phi_j^{\mathrm{prop}}(\vec{p},s) := \langle \xi_{j;\vec{p}s}^{X_{\mathrm{S}}\to X_{\mathrm{D}}}, \psi_j^{\mathrm{S}} \rangle \,, \tag{5.16}$$

$$\phi_j^{\mathrm{match}}(\vec{p},s) := \langle \xi_{j;\vec{p}s}^{X_{\mathrm{S}}\to X_{\mathrm{D}}}, \psi_j^{\mathrm{D}} \rangle \,. \tag{5.17}$$

The first scalar product represents the momentum space WP of the produced neutrino state in terms of the transported modes at the detector, whereas the latter scalar product is the detected momentum space WP in terms of the same set of modes. It will turn out that ϕ_j^{prop} is especially suitable to perform the propagation from X_{S} to X_{D}, while ϕ_j^{match} will be responsible for the matching of the parallel transported, locally inertial modes at the detector and the original detection modes, hence their names. For simplicity, we suppress the mass eigenstate index j in the following as all computation steps proceed in an analogous way for all mass eigenstate WPs.

5.2.1 Propagation of the Produced Neutrino Wave Packet

We compute the propagated momentum space WP by applying the step-by-step procedure sketched at the beginning of this section. To this end, let

$$\tau_{\mathrm{S}} = \tau_0 < \tau_1 < \ldots < \tau_n = \tau_{\mathrm{D}} \,, \qquad\qquad n \in \mathbb{N} \,, \tag{5.18}$$

be an equidistant partition of the proper time interval of the geodesic c with $\Delta\tau := (\tau_{\mathrm{D}} - \tau_{\mathrm{S}})/n = \tau_i - \tau_{i-1}$ for all $i = 1, \ldots, n$ and define $X_i := c(\tau_i)$. Furthermore, let $E_\mu(\tau)$ be the set of four unique parallel transported basis vectors coinciding at τ_{S} with the orthonormal coordinate basis of the local inertial source frame, i.e.

$$E_\mu(\tau_{\mathrm{S}}) = \frac{\partial}{\partial z_{\mathrm{S}}^\mu}(c(\tau_{\mathrm{S}})) \,, \tag{5.19}$$

and choose a frame field $\{e_\alpha\}_{\alpha=0}^3$ that also coincides with the E_μ along the geodesic c. By definition $E_\mu(\tau_i)$ is thus also identical with the coordinate bases $\partial/\partial z_i^\mu(X_i)$ of all *parallel transported* local inertial frames along the geodesic and the frame field therefore fulfils ${e_\alpha}^\mu(X_i) = {\delta_\alpha}^\mu$ within the i-th parallel transported inertial frame.

The core ingredient of the step-by-step propagation procedure is to be able to relate the momentum space WP in terms of the transported modes at X_{i+1} to the WP defined with respect to those modes transported to the previous point X_i

$$\phi^{\mathrm{S}\to i+1}(\vec{p},s) := \langle \xi_{\vec{p},s}^{X_{\mathrm{S}}\to X_{i+1}}, \psi^{\mathrm{S}} \rangle = \int\limits_{\Sigma} \mathrm{d}^3\sigma_\mu(x)\, \bar{\xi}_{\vec{p},s}^{X_{\mathrm{S}}\to X_{i+1}}(x)\gamma^\mu(x)\psi^{\mathrm{S}}(x) \,. \tag{5.20}$$

To accomplish this task, we first choose the spacelike hypersurface $\Sigma = \Sigma_i$ such that it contains the point X_i, as illustrated in Figure 5.1, and also take the coordinate system in which we

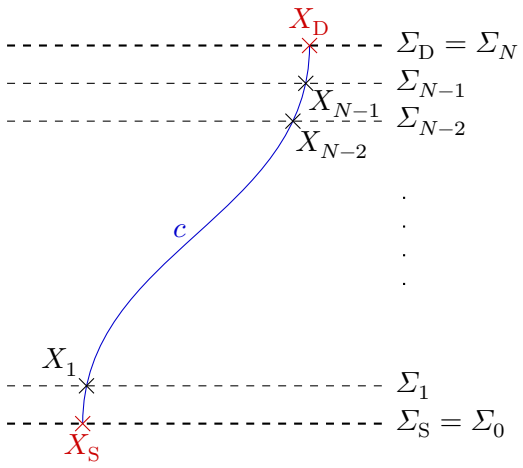

Figure 5.1: Sketch of the step-by-step neutrino propagation along the geodesic c originating from the source of the neutrinos S located on the source hypersurface Σ_{S} and ending in the detection point D located on the detection hypersurface Σ_{D}.

integrate to be the locally inertial coordinate system z_i centered at X_i. Afterwards, we make use of our assumption that all neutrino mass eigenstate WPs are sufficiently localised within the region $U_\nu \cap \Sigma_i$, containing the geodesic c that connects the production and detection events. This means that c is chosen such that it minimises the error introduced by approximating the mode functions $\xi^{X_{\mathrm{S}} \to X_i}$ by their flat spacetime form (2.66) on $U_\nu \cap \Sigma_i$. For n sufficiently big, X_i and X_{i+1} become arbitrarily close and we can approximate

$$\bar{\xi}^{X_{\mathrm{S}} \to X_{i+1}}_{\vec{p},s}(z_{i+1}(z_i))\Big|_{U_\nu \cap \Sigma_i} = u_s(p) \frac{e^{-ip_\mu z^\mu_{i+1}(z_i)}}{\sqrt{(2\pi)^3 2p^0}} + \mathcal{O}(R_i^{\max} \sigma^2_{x,i})\,, \tag{5.21}$$

where $\mathcal{O}(R_i^{\max}\sigma^2_{x,i})$ contains all terms arising from solving the Dirac equation expanded to second order in the normal coordinates z_{i+1}. These terms will naturally be accompanied by curvature terms induced by the spin connection and we take $R_i^{\max}$ to be the maximal entry of the Riemann tensor on the intersection of U_ν and the i-th hypersurface Σ_i. Furthermore, we define $\sigma_{x,i}$ to be the diameter[4], i.e. the maximal spatial extend, of the region U_ν within Σ_i. On the whole region of integration, the combination $R_i^{\max}\sigma^2_{x,i}$ constitutes a conservative estimate for the error introduced by using the approximation from Equation (5.21).

Now, the remaining task is to explicitly write the scalar product $p_\mu z^\mu_{i+1}(z_i)$ in terms of the coordinates z_i in order to obtain a relation between the mode functions $\xi^{X_{\mathrm{S}} \to X_{i+1}}$ and $\xi^{X_{\mathrm{S}} \to X_i}$. Note that the momentum components p^μ represent the values the observer O_{S} would measure in their rest frame, and hence, are defined with respect to the local inertial frame z_{S}. Hence, when parallel transporting the vector $p_{\mathrm{S}} := p^\mu E_\mu(X_{\mathrm{S}})$ along the geodesic, its components

[4]The diameter of a spacelike set S like $U_\nu \cap \Sigma_i$ is defined as $\mathrm{diam}(S) := \sup_{x,y \in S} d_g(x,y)$, where d is the positive definite spatial distance function induced by the metric tensor g on S.

remain constant in terms of the transported local inertial frames, i.e.

$$P^c_{\tau_S \to \tau_i} p_S = p^\mu P^c_{\tau_S \to \tau_i} E_\mu(\tau_S) = p^\mu E_\mu(\tau_i) = p^\mu \frac{\partial}{\partial z_i^\mu}(X_i)\,, \tag{5.22}$$

where $P^c_{a\to b}$ denotes the parallel transport map from a to b along c.

Next, we write the scalar product in coordinate invariant form and parallel transport it back to X_i, i.e.

$$\begin{aligned} p^\mu \eta_{\mu\nu} z^\nu_{i+1}(z_i) &= g_{X_{i+1}}(p^\mu E_\mu(\tau_{i+1}), z^\nu_{i+1}(z_i) E_\nu(\tau_{i+1})) && (5.23)\\ &= g_{X_i}(P^c_{\tau_{i+1}\to\tau_i} p^\mu E_\mu(\tau_{i+1}), P^c_{\tau_{i+1}\to\tau_i} z^\nu_{i+1}(z_i) E_\nu(\tau_{i+1}))\,. && (5.24)\end{aligned}$$

Here, we have used that the parallel transport is an isometric map. Again exploiting the parallel property of the basis vectors E_μ along the curve c in the left argument of the metric g, we get

$$P^c_{\tau_{i+1}\to\tau_i} p^\mu E_\mu(\tau_{i+1}) = p^\mu E_\mu(\tau_i)\,. \tag{5.25}$$

For the second argument of the metric, we first note that

$$z^\nu_{i+1}(z_i) E_\nu(\tau_{i+1}) = \exp^{-1}_{c(\tau_{i+1})}\left(\exp_{X_i}(z_i^\mu E_\mu(\tau_i))\right)\,, \tag{5.26}$$

where $\exp_p(v) : \mathcal{E}_p \subset T_p\mathcal{M} \to \mathcal{M}$ is the exponential map of the manifold defined by the unique geodesics $c_{x,v}$ emanating from x with initial velocity v, i.e.

$$\exp_x(v) = c_{x,v}(1)\,, \qquad c_{x,v}(0) = x\,, \qquad \dot c_{x,v}(0) = v\,, \qquad \frac{\nabla}{\mathrm{d}\tau}\dot c(\tau) \equiv 0\,, \tag{5.27}$$

and $\mathcal{E}_p$ is the set of tangent vectors for that $\exp_p$ is well-defined. Next for $\varepsilon > 0$, we define the map

$$\zeta : (-\varepsilon, \varepsilon) \to T_{X_i}\mathcal{M}\,, \qquad \zeta(\delta\tau) := P^c_{\tau_i+\delta\tau\to\tau_i} \exp^{-1}_{c(\tau_i+\delta\tau)}\left(\exp_{X_i}(z_i^\mu E_\mu(\tau_i))\right)\,, \tag{5.28}$$

which exactly coincides with the second argument of the metric in Equation (5.23) for $\delta\tau = \Delta\tau$. For this map to be well-defined, ε needs to be sufficiently small such that $\exp_{X_i}(z_i^\mu E_\mu(\tau_i))$ is in the domain of $\exp^{-1}_{c(\tau_i+\delta\tau)}$ for all $\delta\tau$ with $|\delta\tau| < \varepsilon$. At the same time, also $\Delta\tau$ needs to be in $(-\varepsilon, \varepsilon)$ which we can easily achieve by choosing n sufficiently large.

As we prove in full detail in Appendix D.1, Taylor expanding ζ around $\delta\tau = 0$ up to first order and evaluating it at $\delta\tau = \Delta\tau$ yields:

$$\zeta(\Delta\tau) = z_i^\nu E_\nu(\tau_i) - \dot c(\tau_i)\Delta\tau + \mathcal{O}(\Delta\tau^2, R_{\max}[\sigma^{\max}_{z_i,i}]^2)\,. \tag{5.29}$$

Substituting this result back into Equation (5.20) leads to the desired relation:

$$\phi^{\mathrm{S}\to i+1}(\vec{p},s) \approx e^{-ip_\mu \dot{c}^\mu \Delta\tau} \int\limits_{U_\nu \cap \Sigma_i} \mathrm{d}^3\sigma_\rho(z_i)\, \frac{e^{ip_\mu z_i^\mu}\, \bar{u}_s(\vec{p})}{\sqrt{(2\pi)^3 2p^0}} \gamma^\rho(z_i)\psi^{\mathrm{S}}(z_i) \tag{5.30}$$

$$\approx e^{-ip_\mu \dot{c}^\mu(\tau_i)\Delta\tau} \langle \xi_{\vec{p},s}^{X_{\mathrm{S}}\to X_i}, \psi^{\mathrm{S}} \rangle \tag{5.31}$$

$$= e^{-ip_\mu \dot{c}^\mu(\tau_i)\Delta\tau} \phi^{\mathrm{S}\to i}(\vec{p},s)\,. \tag{5.32}$$

Rewriting Equation (5.32) in coordinate-independent form and applying it recursively yields

$$\begin{aligned}\phi^{\mathrm{prop}}(\vec{p},s) = \phi^{\mathrm{S}}(\vec{p},s) \exp\left(-i \sum_{k=0}^{n} g_{c(\tau_k)}(P^c_{\tau_{\mathrm{S}}\to\tau_k} p, \dot{c}(\tau_k))\Delta\tau + \mathcal{O}(\Delta\tau^2) \right) \\ + \mathcal{O}\left(\sum_{k=1}^{n} R_k^{\max} \sigma_{x,k}^2 \right)\,,\end{aligned} \tag{5.33}$$

where we have used that $P^c_{\tau_{\mathrm{D}}\to\tau_k} E_\mu(\tau_{\mathrm{D}}) = P^c_{\tau_{\mathrm{S}}\to\tau_k} E_\mu(\tau_{\mathrm{S}})$ holds as can be inferred from Equation (5.22).

Finally, in the limit $n \to \infty$ we obtain

$$\phi^{\mathrm{prop}}(\vec{p},s) \approx \exp\left(-i \int\limits_{\tau_{\mathrm{S}}}^{\tau_{\mathrm{D}}} g_{c(\tau)}(p(\tau), \dot{c}(\tau))\, \mathrm{d}\tau \right) \phi^{\mathrm{S}}(\vec{p},s)\,, \tag{5.34}$$

within the adopted approximation scheme and with the definition

$$p(\tau) := P^c_{\tau_{\mathrm{D}}\to\tau}\left[p^\mu \frac{\partial}{\partial z^\mu_{\mathrm{D}}} \right] \equiv p^\mu E_\mu(\tau) \equiv P^c_{\tau_{\mathrm{S}}\to\tau}\left[p^\mu \frac{\partial}{\partial z^\mu_{\mathrm{S}}} \right]\,. \tag{5.35}$$

5.2.2 Matching the Different Frames in the Detector

The last step in our derivation is to perform the matching of the parallel transported local inertial frame z_{D} and the original local inertial frame in the detector $\tilde{z}_{\mathrm{D}}$, i.e. to compute

$$\phi^{\mathrm{match}}(\vec{p},s) = \int\limits_{\Sigma_{\mathrm{D}}} \mathrm{d}^3\sigma_\mu(\tilde{z}_{\mathrm{D}})\, \bar{\xi}^{X_{\mathrm{S}}\to X_{\mathrm{D}}}_{\vec{p}s}(\tilde{z}_{\mathrm{D}}) \gamma^\mu(\tilde{z}_{\mathrm{D}}) \psi^{\mathrm{D}}(\tilde{z}_{\mathrm{D}}) \tag{5.36}$$

$$\approx \int\limits_{U^{\mathrm{D}}_\nu \cap \Sigma_{\mathrm{D}}} \mathrm{d}^3\sigma_\rho(\tilde{z}_{\mathrm{D}})\, \frac{\overline{\Lambda_{1/2}(\tilde{z}_{\mathrm{D}}) u_s(p)}}{\sqrt{(2\pi)^3 2p^0}} e^{ip_\mu z^\mu_{\mathrm{D}}(\tilde{z}_{\mathrm{D}})} \gamma^\rho(\tilde{z}_{\mathrm{D}}) \psi^{\mathrm{D}}(\tilde{z}_{\mathrm{D}})\,, \tag{5.37}$$

where U^{D}_ν is a region containing the world tubes of all detected neutrino mass eigenstate WPs. We evaluate the integral on the detection hypersurface Σ_{D} in terms of the local inertial frame $\tilde{z}_{\mathrm{D}}$ associated with the local rest frame of the detection observer O_{D}. So far, the frame fields e_α are used implicitly to define a basis on the spin bundle of $\mathcal{M}$ enabling the coordinate

representation of all spinor valued functions. These frame fields e_α are in general different from the frame fields $\tilde{e}_\alpha$, that the detection observer naturally defines to match the coordinate axes of their local inertial frame $\tilde{z}_\mathrm{D}$ at X_D. Both frame fields are related by a local Lorentz transformation $\Lambda^\mu{}_\nu(\tilde{z}_\mathrm{D})$ via

$$\tilde{e}_\alpha(\tilde{z}_\mathrm{D}) = \Lambda_\alpha{}^\beta(\tilde{z}_\mathrm{D}) e_\beta(z_\mathrm{D}(\tilde{z}_\mathrm{D}))\,, \tag{5.38}$$

and therefore, also the different spinor representations are connected by the corresponding spin-1/2 representation $\Lambda_{1/2}$ of $\Lambda^\mu{}_\nu$. Moreover, since the frame fields e_α fulfil the requirement to coincide with the tangent basis $\partial/\partial z^\alpha_\mathrm{D}$ at X_D and the frame fields $\tilde{e}_\alpha$ coincide with the tangent basis $\partial/\partial \tilde{z}^\alpha_\mathrm{D}$ at the same point, we know that

$$\frac{\partial}{\partial \tilde{z}^\alpha_\mathrm{D}}(X_\mathrm{D}) = \Lambda_\alpha{}^\beta(\tilde{z}_\mathrm{D} = 0) \frac{\partial}{\partial z^\beta_\mathrm{D}}(X_\mathrm{D})\,, \tag{5.39}$$

holds. Note that we always apply the Lorentz transformation $\Lambda(0)$ to vectors that have been parallel transported from the production point X_S to the detection point X_D. As argued above, the coordinate representations of these vectors in terms of $\partial/\partial z^\alpha_\mathrm{S}$ and $\partial/\partial z^\alpha_\mathrm{D}$ are the same. Therefore, from Equation (5.39) we can derive that the Lorentz transformation of such vectors can be expressed as

$$\Lambda^\alpha{}_\beta(0) = \left.\frac{\partial \tilde{z}^\alpha_\mathrm{D}}{\partial x^\sigma}\right|_{X_\mathrm{D}} [P^c_{\tau_\mathrm{S}\to\tau_\mathrm{D}}]^\sigma{}_\rho \left.\frac{\partial x^\rho}{\partial z^\beta_\mathrm{S}}\right|_{X_\mathrm{S}}\,, \tag{5.40}$$

where x^μ represents an arbitrary coordinate system and $[P^c_{\tau_\mathrm{S}\to\tau_\mathrm{D}}]^\sigma{}_\rho$ is the representation matrix of the parallel transport in these coordinates. Next, neglecting all curvature terms by exploiting the strong localisation of the neutrino detection WP, we can write

$$\begin{aligned}
\phi^\mathrm{match}(\vec{p}, s) \approx{}& \sum_{s'} D^{1/2*}_{s's}(\Lambda(0), p) \sqrt{\frac{(\Lambda(0)p)^0}{p^0}} \\
&\times \int_{\Sigma_\mathrm{D}} \mathrm{d}^3\sigma_\rho(\tilde{z}_\mathrm{D})\, \frac{\bar{u}_{s'}(\Lambda(0)p)\gamma^\rho(\tilde{z}_\mathrm{D})\psi^\mathrm{D}(\tilde{z}_\mathrm{D})}{\sqrt{(2\pi)^3 2(\Lambda(0)p)^0}} e^{i\Lambda^\mu{}_\sigma(0)p^\sigma \eta_{\mu\nu}\tilde{z}^\nu_\mathrm{D}}
\end{aligned} \tag{5.41}$$

$$= \sum_{s'} D^{1/2*}_{s's}(\Lambda(0), p) \sqrt{\frac{(\Lambda(0)p)^0}{p^0}} \langle \xi^\mathrm{D}_{[\Lambda p]s'}, \psi^\mathrm{D}\rangle \tag{5.42}$$

$$= \sum_{s'} D^{1/2*}_{s's}(\Lambda(0), p) \sqrt{\frac{(\Lambda(0)p)^0}{p^0}} \phi^\mathrm{D}(\tilde{\vec{p}}, s)\,, \tag{5.43}$$

where we have defined $\tilde{p}^k = \Lambda^k{}_\nu(0)p^\nu$. Moreover, we have expressed the Lorentz transformed spinor $\Lambda_{1/2}u_s(p)$ in terms of the basis spinors with transformed momentum and the spin-1/2 Wigner rotation coefficients[5] $D^{1/2}_{s's}$ associated with the Lorentz transformation $\Lambda(0)$ and the neutrino momentum p. Here, s and s' assume values between $-1/2$ to $1/2$ as usual and from now on we only write $\Lambda \equiv \Lambda(0)$ for clarity.

[5] Here, we use the same convention for the Wigner D-matrix as in Reference [1].

5.2.3 The Master Formula for the Flavour Transition Amplitude

Restoring all mass eigenstate indices, the neutrino oscillation amplitude becomes

$$\mathcal{A}_{ab}(X_{\mathrm{S}}, X_{\mathrm{D}}) = \sum_j U^*_{aj} U_{bj} \sum_{s=\pm 1/2} \int \mathrm{d}^3\vec{p}\, \tilde{\phi}^{\mathrm{D}*}_j(\vec{p}, s) \phi^{\mathrm{S}}_j(\vec{p}, s) e^{-i\Phi_j(p_j, X_{\mathrm{S}}, X_{\mathrm{D}})}\,, \tag{5.44}$$

$$\tilde{\phi}^{\mathrm{D}}_j(\vec{p}, s) := \sqrt{\frac{(\Lambda p_j)^0}{p^0_j}} \sum_{s'=\pm 1/2} D^{1/2*}_{s's}(\Lambda, p_j) \phi^{\mathrm{D}}_j(\tilde{\vec{p}}_j, s')\,, \tag{5.45}$$

$$\Phi_j(p_j, X_{\mathrm{S}}, X_{\mathrm{D}}) := \int_0^{\Delta\tau} g_{c(\tau)}(p_j(\tau), \dot{c}(\tau))\, \mathrm{d}\tau\,, \tag{5.46}$$

which is the main result of this section. Here, we have redefined $\Delta\tau$ to denote the proper time elapsed for the curve c. Furthermore, we have used that we can set the initial proper time τ_{S} of the trajectory c to zero. The Lorentz transformation Λ implicitly encodes the information of the parallel transport of the neutrino momentum p_j from the source to the detector as well as the relative motion of the source and the detection device. By virtue of the unitary Wigner D-matrix, also the spin composition of the detected neutrino states are affected by the transport transformation Λ. Thereby, the Wigner D-matrix encodes a lowest order, net gravitational effect on the neutrino spin. Moreover, the modified oscillation phase Φ_j incorporates the integral of the scalar product between the neutrino momentum p_j and the mean four-velocity $\dot{c}$ along the geodesic c.

This phase is a generalisation of the so-called Stodolsky phase [191] employed in the plane wave approaches to neutrino oscillations (cf. e.g. References [192, 193, 200])

$$\Phi^{\mathrm{Stodolsky}}_j(X_{\mathrm{S}}, X_{\mathrm{D}}) := m_j \int_0^{\Delta\tau} g_{c_j(\tau)}(\dot{c}_j(\tau), \dot{c}(\tau))\, \mathrm{d}\tau \approx \Phi_j(m_j \dot{c}_j(0), X_{\mathrm{S}}, X_{\mathrm{D}})\,, \tag{5.47}$$

where we have used that the geodesic parallel transports its own tangent vector along itself and that $c \approx c_j$. Since for strongly peaked momentum space WPs the mean momentum of a WP is proportional to the velocity of its mean geodesic c_j, Equation (5.44) evidently reproduces the plane wave limit. This result supports the usual ad-hoc replacements of the neutrino oscillation phases by the Stodolsky phase. However, special care must be taken when considering neutrino WPs of non-negligible width. In these scenarios, it is more appropriate to use Equation (5.44).

Because usually the neutrino oscillation formula is expressed in terms of the quantities relevant to the neutrino detector, we can also shift the Lorentz transformation Λ to the source WP. Performing all steps of the derivation shown in Sections 5.2.1 and 5.2.2 by interchanging the

roles of the source and the detector yields

$$\mathcal{A}_{ab}(X_{\mathrm{S}}, X_{\mathrm{D}}) = \sum_j U^*_{aj} U_{bj} \sum_{s=\pm 1/2} \int \mathrm{d}^3\vec{q}\, \phi_j^{\mathrm{D}*}(\vec{q}, s) \widehat{\phi}_j^{\mathrm{S}}(\vec{q}, s) e^{-i\Phi'_j(q_j, X_{\mathrm{S}}, X_{\mathrm{D}})}\,, \tag{5.48}$$

$$\widehat{\phi}_j^{\mathrm{S}}(\vec{q}, s) := \sqrt{\frac{(\Lambda^{-1} q_j)^0}{q_j^0}} \sum_{s'=\pm 1/2} D^{1/2*}_{ss'}(\Lambda^{-1}, q_j) \phi_j^{\mathrm{D}}(\widehat{\vec{q}}_j, s')\,, \tag{5.49}$$

$$\Phi'_j(q_j, X_{\mathrm{S}}, X_{\mathrm{D}}) := \int_0^{\Delta\tau} g_{c(\tau)}(q_j(\tau), \dot{c}(\tau))\, \mathrm{d}\tau\,, \tag{5.50}$$

with the back-transported neutrino momentum $q_j(\tau) := P^c_{\Delta\tau\to\tau} q_j$ and the definition $\widehat{\vec{q}}_j := [\Lambda^{-1}]^k{}_\nu q_j^\nu \vec{e}_k$. The same result can, of course, also be obtained from equation (5.44) by performing the integral transform $q_j^k(p_j) = [\Lambda]^k{}_\nu p_j^\nu$. Thus, Equation (5.48) and Equation (5.44) are fully equivalent, but Equation (5.48) is more convenient for applications involving astrophysical neutrinos.

Assuming that the neutrino production and detection processes are strongly localised, such that they are well described by Lorentz covariant QFT in flat spacetime, implies that the produced and detected neutrino WPs are also Lorentz covariant quantities. In our adopted normalisation convention, this means that the full neutrino WPs $\phi_j^{\mathrm{S/D}}$ can be written in terms of Lorentz scalars $\varphi_j^{\mathrm{S/D}}$ as

$$\phi_j^{\mathrm{S/D}}(\vec{p}, s) = \frac{\varphi_j^{\mathrm{S/D}}(p_j, s)}{\sqrt{(2\pi)^3 2p_j^0}}\,. \tag{5.51}$$

The functions $\varphi_j^{\mathrm{S/D}}$, therefore, transform as

$$\tilde{\varphi}_j^{\mathrm{S/D}}(\Lambda^{-1} p_j, s) = \varphi_j^{\mathrm{S/D}}(p_j, s) \qquad \Leftrightarrow \qquad \tilde{\varphi}_j^{\mathrm{S/D}}(p_j, s) = \varphi_j^{\mathrm{S/D}}(\Lambda p_j, s)\,, \tag{5.52}$$

under a general Lorentz transformation Λ. Consequently, the transformation properties of the full WPs ϕ_j become much simpler. For example, the transformed detection WP in Equation (5.44) becomes

$$\tilde{\phi}_j^{\mathrm{D}}(\vec{p}, s) = \sum_{s'=\pm 1/2} D^{1/2*}_{s's}(\Lambda, p) \frac{\tilde{\varphi}_j^{\mathrm{D}}(p_j, s')}{\sqrt{(2\pi)^3 2p_j^0}}\,. \tag{5.53}$$

If the function $\varphi_j(p, s) \equiv \varphi_j(p, s; P_j, \Sigma_j)$ then is, for example, fully characterised by its mean momentum P_j and width-tensor

$$\Sigma_j^{\mu\nu} := \sum_{s=\pm 1/2} \int \frac{\mathrm{d}^3\vec{p}}{(2\pi)^3 2p_j^0} |\varphi_j(p, s)|^2 p^\mu p^\nu - P_j^\mu P_j^\nu\,, \tag{5.54}$$

we only need to replace these quantities by the properly Lorentz transformed ones. For the transformed detection WP from Equation (5.44) this yields

$$\varphi_j^{\mathrm{D}}(\Lambda p_j, s'; P_{\mathrm{D}j}, \Sigma_{\mathrm{D}j}) = \varphi_j^{\mathrm{D}}(p_j, s'; \Lambda^{-1} P_{\mathrm{D}j}, \Lambda^{-1T} \Sigma_{\mathrm{D}j} \Lambda^{-1}) \,. \tag{5.55}$$

This tremendously simplifies the task of computing the momentum space integrals present in Equation (5.44). Using this Lorentz covariant parametrisation, we can write the amplitude in Equation (5.44) as

$$\begin{aligned} \mathcal{A}_{ab} = \sum_j U_{aj}^* U_{bj} \sum_{ss'=\pm 1/2} \int \frac{\mathrm{d}^3\vec{p}}{(2\pi)^3 2p_j^0} D^{1/2}_{s's}(\Lambda, p_j) \\ \times \varphi_j^{\mathrm{D}*}(p_j, s'; \hat{P}_{\mathrm{D}j}, \hat{\Sigma}_{\mathrm{D}j}) \varphi_j^{\mathrm{S}}(p_j, s; P_{\mathrm{S}j}, \Sigma_{\mathrm{S}j}) e^{-i\Phi_j(p_j, X_{\mathrm{S}}, X_{\mathrm{D}})} \end{aligned} \tag{5.56}$$

$$\begin{aligned} = \sum_j U_{aj}^* U_{bj} \sum_{ss'=\pm 1/2} \int \frac{\mathrm{d}^3\vec{p}}{(2\pi)^3 2p_j^0} D^{1/2*}_{s's}(\Lambda^{-1}, p_j) \\ \times \varphi_j^{\mathrm{D}*}(p_j, s; P_{\mathrm{D}j}, \Sigma_{\mathrm{D}j}) \varphi_j^{\mathrm{S}}(p_j, s'; \tilde{P}_{\mathrm{S}j}, \tilde{\Sigma}_{\mathrm{S}j}) e^{-i\Phi'_j(p_j, X_{\mathrm{S}}, X_{\mathrm{D}})} \,. \end{aligned} \tag{5.57}$$

Here, $\hat{P}_{\mathrm{D}j} := \Lambda^{-1} P_{\mathrm{D}j}$, $\tilde{P}_{\mathrm{S}j} := \Lambda P_{\mathrm{S}j}$ and analogously for $\hat{\Sigma}_{\mathrm{D}j}$ and $\tilde{\Sigma}_{\mathrm{S}j}$.

For two inertial observers O_{S} and O_{D} at rest in the same inertial frame in flat spacetime, Equation (5.44) reduces to the well known result

$$\mathcal{A}_{ab}(X_{\mathrm{S}}, X_{\mathrm{D}}) = \sum_j U_{aj}^* U_{bj} \sum_{s=\pm 1/2} \int \mathrm{d}^3\vec{p}\, \phi_j^{\mathrm{D}*}(\vec{p}, s) \phi_j^{\mathrm{S}}(\vec{p}, s) e^{-i(X_{\mathrm{D}\mu} - X_{\mathrm{S}\mu}) p^\mu} \,, \tag{5.58}$$

where we use that the Lorentz transformations become trivial in this scenario, i.e. $[\Lambda]^\mu{}_\nu = \delta^\mu{}_\nu$.

Lastly, we comment on the spin transformation coefficients $D^{1/2}_{s's}$ that appear within the neutrino oscillation amplitude as soon as the Lorentz transformation Λ becomes non-trivial. Usually, spin is not measured in neutrino oscillation experiments. Thus, we should sum (average) over all possible final (initial) state spin compositions after taking the square of the oscillation amplitude. In addition to that, also the quantisation axes are usually defined such that the neutrino WPs are of well-defined spin $\bar{s}$, i.e.

$$\phi_j(\vec{p}, s) \propto \delta_{s\bar{s}} \,. \tag{5.59}$$

Summing over the final state spin then amounts to a summation over $\bar{s}$ for the detected WP. Also averaging over the initial state spin $\bar{s}'$, the flavour transition amplitude becomes

$$\begin{aligned} \overline{|\mathcal{A}_{ab}|^2} = \sum_{jk} U_{aj}^* U_{ak} U_{bj} U_{bk}^* \iint \mathrm{d}^6(\vec{p}, \vec{q})\, a_j(\vec{p}) a_k^*(\vec{q}) \\ \times \frac{1}{2} \sum_{\bar{s}\bar{s}'=\pm 1/2} D^{1/2}_{\bar{s}'\bar{s}}(\Lambda, p_j) D^{1/2*}_{\bar{s}'\bar{s}}(\Lambda, q_k) \,. \end{aligned} \tag{5.60}$$

The momentum integrand $a_j(\vec{p})$ contains all other momentum-dependent quantities such as the neutrino WPs or the oscillation phase. Evaluating the Wigner D-matrices at the mean momenta $\bar{p}_j$, where the integrands $a_j(\vec{p})$ usually exhibit a narrow peak, yields

$$\begin{aligned} |\mathcal{A}_{ab}|^2 \approx \sum_{jk} U^*_{aj} U_{ak} U_{bj} U^*_{bk} \frac{1}{2} \sum_{\bar{s}\bar{s}'=\pm 1/2} D^{1/2}_{\bar{s}'\bar{s}}(\Lambda, \bar{p}_j) D^{1/2*}_{\bar{s}'\bar{s}}(\Lambda, \bar{p}_k) \\ \times \iint \mathrm{d}^6(\vec{p}, \vec{q})\, a_j(\vec{p}) a^*_k(\vec{q})\,. \end{aligned} \tag{5.61}$$

Due to the spin transformation coefficients, one, hence, obtains small corrections to the oscillating terms, i.e. the off-diagonal elements $j \neq k$ of the sum. This is because of the mismatch of $\bar{p}_j \neq \bar{p}_k$. However, at lowest order in $\Delta\bar{p}_{jk} := \bar{p}_j - \bar{p}_k$, we get

$$\sum_{\bar{s}'=\pm 1/2} D^{1/2}_{\bar{s}'\bar{s}}(\Lambda, \bar{p}_j) D^{1/2*}_{\bar{s}'\bar{s}}(\Lambda, \bar{p}_k) = 1 + \mathcal{O}(\Delta\bar{p}_{jk})\,, \tag{5.62}$$

and one can usually neglect the higher order terms since they are not amplified by large factors like the propagation distance in contrast to the oscillation phase differences. Therefore, in most relevant scenarios the spin flip effects are irrelevant for oscillation experiments.

5.3 Applications: Neutrino Oscillations in Linearised Gravity

In order to see the consequences of weak gravitational fields on neutrino flavour transitions, we apply Equation (5.44) to the simple scenario of linear gravity where the metric can be written as

$$g_{\mu\nu} = \eta_{\mu\nu} + \varepsilon h_{\mu\nu} + \mathcal{O}(\varepsilon^2)\,, \tag{5.63}$$

with $0 < \varepsilon \ll 1$ in suitable coordinate systems x^μ. In particular, we consider two of the most prominent scenarios: Static, i.e. Newtonian, gravitational fields and GWs in vacuum. We consider the case of Gaussian neutrino WPs, as discussed in Section 2.3.2, and apply them to our master formula (5.48). To be precise, we use Gaussian shape functions to parametrise the neutrino WPs within the detection frame of reference. Hence, the respective peak momenta of the j-th neutrino mass eigenstate WP are $\tilde{\vec{P}}_{\mathrm{S}j}$ for the produced neutrino and $\vec{P}_{\mathrm{D}j}$ for the detected neutrino. Since the most part of the calculation can be done in a general manner for gravitational fields of the form (5.63), we proceed to do so and only restrict our considerations to the aforementioned special cases later on.

For Gaussian neutrino WPs, Equation (5.48) becomes

$$\begin{aligned} \mathcal{A}_{ab}(X^\mu_{\mathrm{S}}, X^\mu_{\mathrm{D}}) = \sum_j U^*_{aj} U_{bj} \sqrt{\frac{2\pi}{\sigma_{\mathrm{S}j}\sigma_{\mathrm{D}j}}} \\ \times \int \mathrm{d}^3\vec{p} \exp\left(-\frac{(\vec{p} - \tilde{\vec{P}}_{\mathrm{S}j})^2}{4\sigma^2_{\mathrm{S}j}} - \frac{(\vec{p} - \vec{P}_{\mathrm{D}j})^2}{4\sigma^2_{\mathrm{D}j}} - i\Phi'_j(p_j, X_{\mathrm{S}}, X_{\mathrm{D}}) \right)\,, \end{aligned} \tag{5.64}$$

with the WP widths $\sigma_{\mathrm{S}j}$ and $\sigma_{\mathrm{D}j}$. Similarly to the mean momentum, also the width tensor $\Sigma_{\mathrm{S}j}$ of the produced neutrino WP has to be translated to the detection frame. However, since the Lorentz transformation Λ corresponds to non-relativistic boost velocities $v \ll 1$, as shown below, we neglect the distortion of the produced neutrino WP, i.e. $\tilde{\Sigma}_{\mathrm{S}j} \approx \Sigma_{\mathrm{S}j} = \mathbb{1}\sigma_{\mathrm{S}j}$. Moreover, we assume the neutrino source and detector to be approximately at rest in the same frame of reference. We parametrise their world lines, $X^\mu_{\mathrm{S}}(T_{\mathrm{S}}) \approx (T_{\mathrm{S}}, \vec{X}_{\mathrm{S}})$ and $X^\mu_{\mathrm{D}}(T_{\mathrm{D}}) \approx (T_{\mathrm{D}}, \vec{X}_{\mathrm{D}})$, in terms of the coordinate time in this reference frame. Furthermore, we denote the livetime intervals of the neutrino source and detector by $[T_{\mathrm{S}1}, T_{\mathrm{S}2}]$ and $[T_{\mathrm{D}1}, T_{\mathrm{D}2}]$, respectively.

Using that the scalar product of two parallel transported vectors is a constant of motion, we can write the oscillation phase Φ'_j as

$$\Phi'_j(p_j, X_{\mathrm{S}}, X_{\mathrm{D}}) = \eta_{\mu\nu} L^\mu p^\nu_j \,, \tag{5.65}$$

with the effective spacetime distance four-vector

$$L^\mu := \dot{\tilde{c}}^\mu(\Delta\tau)\Delta\tau. \tag{5.66}$$

In the spirit of Equation (5.48), we evaluate the phase Φ'_j in the local inertial frame at the detector. Equation (5.65) is not only valid in the context of linear gravity, but applies to any scenario where curvature effects are negligible on the scale of the neutrino WPs at any given time. Moreover, it proves that the oscillation phase depends on the modified distance vector L^μ the same way it would depend on the simple coordinate distance $\Delta X^\mu := X^\mu_{\mathrm{D}} - X^\mu_{\mathrm{S}}$ in flat spacetime.

Using these relations, we are able to write the neutrino oscillation amplitude in an analogous way to the flat spacetime computation, discussed in Section 2.3.2, and we can solve the momentum space integral in the same way as shown there. We just need to replace the mean momentum at the neutrino source as well as the propagation four vector L^μ by the appropriate cursed spacetime quantities, as they do not depend on the integral momentum $\vec{p}$. Using the usual approximation $|\vec{L}|^2 \gg \sigma^2_{\perp j}$, and hence, $\vec{L} \parallel \vec{\bar{p}}_j$, we obtain

$$\begin{aligned} \mathcal{A}_{ab}(X^\mu_{\mathrm{S}}, X^\mu_{\mathrm{D}}) = \sum_j & \frac{U^*_{aj} U_{bj}}{\sqrt{\sigma^3_{\mathrm{S}j}\sigma^3_{\mathrm{D}j}\sigma^2_{\parallel j}\sigma^4_{\perp j}}} \\ & \times \exp\left(-\frac{(\tilde{\vec{P}}_{\mathrm{S}j} - \vec{P}_{\mathrm{D}j})^2}{4(\sigma^2_{\mathrm{S}j} + \sigma^2_{\mathrm{D}j})} - \frac{(\bar{v}_j L^0 - |\vec{L}|)^2}{2\sigma^2_{\parallel j}} - i L_\mu \bar{p}^\mu_j \right) , \end{aligned} \tag{5.67}$$

with

$$\bar{p}^\mu_j := (\bar{E}_j, \vec{\bar{p}}_j) \,, \qquad \bar{E}_j := \sqrt{|\vec{\bar{p}}_j|^2 + m_j^2} \,, \qquad \vec{\bar{p}}_j := \frac{\tilde{\vec{P}}_{\mathrm{S}j}\sigma^2_{\mathrm{D}j} + \vec{P}_{\mathrm{D}j}\sigma^2_{\mathrm{S}j}}{\sigma^2_{\mathrm{S}j} + \sigma^2_{\mathrm{D}j}} \,, \qquad \vec{\bar{v}}_j := \frac{\vec{\bar{p}}_j}{\bar{E}_j} \,, \tag{5.68}$$

and the modified effective position space widths

$$\sigma^2_{\parallel j} := \frac{1}{2}\left(\frac{1}{\sigma^2_{\mathrm{S}j}} + \frac{1}{\sigma^2_{\mathrm{D}j}}\right) + \frac{iL^0}{\bar{E}^2_j}(1 - |\vec{\bar{v}}_j|^2) \,, \qquad \sigma^2_{\perp j} := \frac{1}{2}\left(\frac{1}{\sigma^2_{\mathrm{S}j}} + \frac{1}{\sigma^2_{\mathrm{D}j}}\right) + \frac{iL^0}{\bar{E}^2_j} \,. \tag{5.69}$$

Note that all quantities depending on the mean momentum $\vec{\bar{p}}_j$ of mass eigenstate j also depend on the parallel transport along the geodesic c. It is, thus, now mandatory to specify the parallel transport as well as the geodesic to be able to compute the neutrino oscillation probability according to Equation (5.10). Furthermore, note that until now we have not used the explicit form of the metric shown in Equation (5.63), and hence, all results obtained so far apply to all scenarios of sufficiently localised Gaussian neutrino WPs.

Before we proceed, we can already gain some insights of the physical meaning of the neutrino oscillation amplitude shown in Equation (5.67). From the first exponential suppression term in Equation (5.67), we see that only those neutrinos emitted from the source contribute to the process if their parallel transported momentum approximately matches that of the detected neutrino WP, i.e. $\vec{P}_{\mathrm{D}j} \sim \tilde{\vec{P}}_{\mathrm{S}j}$. Thus, as expected, neutrino momentum is not necessarily conserved in general spacetimes and the momentum distributions of neutrinos in the source could, for example, appear redshifted for a distant observer. Furthermore, from the Gaussian position space shape factor we can infer that $\bar{v}_j L^0 \sim L \coloneqq |\vec{L}|$ must hold within the uncertainties of the neutrino WPs in order for the amplitude to yield a significant contribution. Therefore, the overall behaviour of the amplitude in weak gravitational fields remains the same as in the flat spacetime case justifying the usual approach to ignore gravitational effects especially at short propagation lengths, as we will see below. Nonetheless, the group velocities $\bar{v}_j$ as well as the propagation distance L^μ encode the spacetime geometry and may lead to a modified neutrino oscillation pattern. This could in principle be observable in experiments.

We continue the derivation of the oscillation probability by computing the solution to the geodesic Equation (2.29) given the boundary conditions

$$c^\mu(0) = X^\mu_{\mathrm{S}}\,, \qquad\qquad c^\mu(\Delta\tau) = X^\mu_{\mathrm{D}}\,, \tag{5.70}$$

and the metric (5.63) in the respective coordinate system x^μ. The corresponding Christoffel symbols are $\mathcal{O}(\varepsilon)$ quantities and read

$$\Gamma^\mu_{\sigma\rho}(x) = \frac{\varepsilon}{2}\eta^{\mu\nu}\left(\partial_\sigma h_{\nu\rho}(x) + \partial_\rho h_{\nu\sigma}(x) - \partial_\nu h_{\rho\sigma}(x)\right) + \mathcal{O}(\varepsilon^2)\,. \tag{5.71}$$

In general spacetimes, the boundary value problem for the geodesic equation is not well posed since there may exist more than one geodesic connecting the source and the detector coordinates, while maximising the neutrino proper time. In this case, the information about the neutrino momentum is mandatory in order to determine along which geodesic the neutrinos have travelled. However, since the spacetime under consideration is close to Minkowskian, we can safely assume that the boundary value problem is well posed. Solving the geodesic equation to linear order in ε, given the boundary conditions (5.70), we obtain

$$c^\mu(\tau) = c^\mu_0(\tau) + \varepsilon c^\mu_1(\tau)\,, \tag{5.72}$$

$$c^\mu_0(\tau) = u^\mu\tau + X^\mu_{\mathrm{S}}\,, \tag{5.73}$$

$$c^\mu_1(\tau) = \int_0^\tau \mathrm{d}\tau' \int_0^{\tau'} \mathrm{d}\tau''\, a^\mu(\tau'') - \frac{\tau}{\Delta\tau}\int_0^{\Delta\tau} \mathrm{d}\tau' \int_0^{\tau'} \mathrm{d}\tau''\, a^\mu(\tau'')\,, \tag{5.74}$$

with the zeroth order neutrino four-velocity $u^\mu = \Delta X^\mu / \Delta\tau$ and the geodesic acceleration

$$\varepsilon a^\mu(\tau) = -\Gamma^\mu_{\sigma\rho}(c_0(\tau)) u^\sigma u^\rho \,. \tag{5.75}$$

From these expressions, we can simply compute the derivative of the geodesic at the detection point and transform it to the local inertial frame of the detector to get

$$L^\mu = \left(\delta^\mu{}_\nu + \frac{\varepsilon}{2}\delta\ell^\mu{}_\nu\right)\Delta X^\nu \,, \tag{5.76}$$

$$\begin{aligned}\delta\ell^\mu{}_\nu = {} & \langle h^\mu{}_\nu \circ c_0\rangle - [h^\mu{}_\nu(X_\mathrm{D}) - \langle h^\mu{}_\nu \circ c_0\rangle] \\ & + \left[\langle \partial^\mu h_{\sigma\nu} \circ c_0\rangle - \left\langle \tau \mapsto \int_0^\tau \frac{\mathrm{d}\tau'}{\Delta\tau} \partial^\mu h_{\sigma\nu}(c_0(\tau'))\right\rangle\right]\Delta X^\sigma \,,\end{aligned} \tag{5.77}$$

where we have defined the component wise average along the geodesic by

$$\langle f\rangle := \langle \tau \mapsto f(\tau)\rangle := \int_0^{\Delta\tau} \frac{\mathrm{d}\tau}{\Delta\tau} f(\tau) \,. \tag{5.78}$$

The proper time interval is defined by $L^\mu L_\mu = \Delta\tau^2$ and the considerations above show how the geodesic as well as $\Delta\tau$ are determined by the production and detection events, respectively.

The next step is to compute the parallel transport transformation from Equation (5.40), translating between the local inertial frames of the source and the detector. To this end, we need the coordinate transformations

$$\left.\frac{\partial x^\mu}{\partial z^\nu_\mathrm{S}}\right|_{X_\mathrm{S}} = \delta^\mu{}_\nu - \frac{\varepsilon}{2} h^\mu{}_\nu(X_\mathrm{S}) \,, \qquad \left.\frac{\partial \tilde{z}^\mu_\mathrm{D}}{\partial x^\nu}\right|_{X_\mathrm{D}} = \delta^\mu{}_\nu + \frac{\varepsilon}{2} h^\mu{}_\nu(X_\mathrm{D}) \,, \tag{5.79}$$

and the parallel transport operator in x^μ coordinates

$$[P^c_{0\to\tau}]^\sigma{}_\rho = \delta^\sigma{}_\rho - \int_0^\tau \mathrm{d}\tau'\, u^\lambda \Gamma^\sigma_{\lambda\rho}(c_0(\tau')) \,. \tag{5.80}$$

Putting everything together yields

$$\Lambda^\mu{}_\nu = \delta^\mu{}_\nu - \frac{\varepsilon}{2}\left[\langle \partial_\nu h^\mu{}_\lambda \circ c_0\rangle - \langle \partial^\mu h_{\nu\lambda} \circ c_0\rangle\right]\Delta X^\lambda =: \delta^\mu{}_\nu - \frac{\varepsilon}{2}\lambda^\mu{}_\nu \,, \tag{5.81}$$

$$[\Lambda^{-1}]^\mu{}_\nu = \delta^\mu{}_\nu + \frac{\varepsilon}{2}\left[\langle \partial_\nu h^\mu{}_\lambda \circ c_0\rangle - \langle \partial^\mu h_{\nu\lambda} \circ c_0\rangle\right]\Delta X^\lambda =: \delta^\mu{}_\nu + \frac{\varepsilon}{2}\lambda^\mu{}_\nu \,. \tag{5.82}$$

As already conjectured above, we see that the gravitational corrections to L^μ and Λ are proportional to the coordinate distance ΔX^μ justifying the use of the flat spacetime formula in weak gravitational fields for non-astronomical distances. This includes Earth-bound as well as atmospheric neutrino oscillation experiments. Furthermore, the Lorentz transformation deviates from the identity only by terms of order $\varepsilon \ll 1$ implying that the effective boost velocity must be non-relativistic.

Now that we have successfully derived the explicit expressions needed for the gravitationally corrected neutrino oscillation formula, we proceed to compute the neutrino oscillation probability according to Equation (5.10). Here, we take the proper times of the source and detector trajectories to coincide with the coordinate time of our general reference frame x^μ. Moreover, we use the same-width-approximation for all neutrino mass eigenstates, i.e. $\sigma_{\mathrm{S}} \equiv \sigma_{\mathrm{S}j}$ and $\sigma_{\mathrm{D}} \equiv \sigma_{\mathrm{D}j}$, as well as the ultra-relativistic approximation. For the latter, we introduce the momentum $\vec{p} = p\vec{L}/L$ of a massless neutrino, compatible with the kinematics of the observed detection process, and we introduce the momentum splittings

$$\Delta\vec{P}_{\mathrm{D}j} := \vec{P}_{\mathrm{D}j} - \vec{p}\,, \qquad \Delta\tilde{\vec{P}}_{\mathrm{S}j} := \tilde{\vec{P}}_{\mathrm{S}j} - \vec{p}\,, \qquad \Delta\vec{p}_j := \vec{\bar{p}}_j - \vec{p} = \frac{\sigma_{\mathrm{D}}^2 \Delta\tilde{\vec{P}}_{\mathrm{S}j} + \sigma_{\mathrm{S}}^2 \Delta\vec{P}_{\mathrm{D}j}}{\sigma_{\mathrm{S}}^2 + \sigma_{\mathrm{D}}^2}\,. \tag{5.83}$$

Using this parametrisation, we already anticipate that we are going to set $\tilde{\vec{P}}_{\mathrm{S}j} \simeq \vec{P}_{\mathrm{D}j}$ for some fixed time in the end. In order to apply the ultra-relativistic and weak field approximations consistently, we take into account terms up to second order in the small quantities

$$\frac{\Delta\vec{\bar{p}}_j}{E}\,, \frac{m_j^2}{E^2} \sim \varepsilon_{\mathrm{UR}} \ll 1\,, \tag{5.84}$$

with $E := |\vec{p}|$, and also include terms of the order $\varepsilon_{\mathrm{UR}}\varepsilon$ but we still neglect ε^2 terms since we assume $\varepsilon \ll \varepsilon_{\mathrm{UR}}$. The inclusion of $\varepsilon_{\mathrm{UR}}\varepsilon$ terms is necessary if we want to consider gravitational corrections for the oscillation phase and coherence length. This automatically implies the need to also keep $\varepsilon_{\mathrm{UR}}^2$ terms to maintain consistency of the approximation scheme. Another important reason to keep $\varepsilon_{\mathrm{UR}}^2$ is that since we are mainly interested in large propagation distances, we have to take the effect of WP spreading into account that only occurs on the order of $\varepsilon_{\mathrm{UR}}^2$ due to the time-dependent imaginary part of $\sigma_{\parallel j}^2$.

Now, we can write the oscillation probability as

$$P_{ab}(\vec{X}_{\mathrm{S}}, \vec{X}_{\mathrm{D}}; E) \approx \frac{\sum_{jk} U_{aj}^* U_{ak} U_{bj} U_{bk}^* \mathcal{J}_{jk}(\vec{X}_{\mathrm{S}}, \vec{X}_{\mathrm{D}}; E)}{\sum_j |U_{aj}|^2 \mathcal{J}_{jj}(\vec{X}_{\mathrm{S}}, \vec{X}_{\mathrm{D}}; E)}\,, \tag{5.85}$$

with the integral

$$\begin{aligned}\mathcal{J}_{jk}(\vec{X}_{\mathrm{S}}, \vec{X}_{\mathrm{D}}; E) := \int_{T_{\mathrm{D}1}}^{T_{\mathrm{D}2}} \mathrm{d}T_{\mathrm{D}} \int_{T_{\mathrm{S}1}}^{T_{\mathrm{S}2}} \mathrm{d}T_{\mathrm{S}} \exp\left(-\frac{(\Delta\tilde{\vec{P}}_{\mathrm{S}j} - \Delta\vec{P}_{\mathrm{D}j})^2 + (\Delta\tilde{\vec{P}}_{\mathrm{S}k} - \Delta\vec{P}_{\mathrm{D}k})^2}{4(\sigma_{\mathrm{S}}^2 + \sigma_{\mathrm{D}}^2)}\right) \\ \times \exp\left(-\frac{(\bar{v}_j L^0 - L)^2}{2\sigma_{\parallel j}^2} - \frac{(\bar{v}_k L^0 - L)^2}{2(\sigma_{\parallel k}^*)^2}\right) \\ \times \exp\left(-i(L^0 \Delta\bar{E}_{jk} - L\Delta\bar{p}_{jk})\right)\,.\end{aligned} \tag{5.86}$$

Here, we define $\bar{p}_j := |\vec{\bar{p}}_j|$ and $\bar{v}_j := |\vec{\bar{v}}_j|$. Moreover, we only keep the $\mathcal{O}(1)$ contribution from the product of widths in front of the exponential in Equation (5.67). This way we are able to pull

it out of the integrals and cancel it against the same contribution from the normalisation. All higher order contributions are negligible compared to the $\mathcal{O}(1)$ term as they are not amplified by large factors like, for example, the propagation distance L.

It is now convenient to introduce an integral transformation from $(T_\mathrm{S}, T_\mathrm{D})$ to $(\Delta T \coloneqq T_\mathrm{D} - T_\mathrm{S}, T_\mathrm{D})$, similar to the treatment presented in Section 2.3.2. This is because at lowest order the amplitude only depends on ΔT and the time translation symmetry of the spacetime is only potentially broken by the $\mathcal{O}(\varepsilon)$ contributions. Hence, the integral over the detection time span induces an averaging due to time-dependent gravitational fields, at most. If on the contrary the spacetime is static, the remaining T_D integral trivialises as in the flat spacetime case. Even in the absence of time translation symmetry, we can solve for the maximum $\Delta T^\star_{jk}$ of the envelope of the integrand of $\mathcal{I}_{jk}$ at $\mathcal{O}(\varepsilon)$ and expand the exponent to quadratic order around the maximum $\Delta T^\star_{jk}$. This enables us to solve the ΔT integral analytically in the Gaussian approximation and we obtain an oscillation probability of the form

$$P_{ab}(\vec{X}_\mathrm{S}, \vec{X}_\mathrm{D}; E) = \int_{T_{\mathrm{D}1}}^{T_{\mathrm{D}2}} \frac{\mathrm{d}T_\mathrm{D}}{T_{\mathrm{D}2} - T_{\mathrm{D}1}} \tilde{P}_{ab}(\vec{X}_\mathrm{S}, \vec{X}_\mathrm{D}, T_\mathrm{D}; E)\,, \tag{5.87}$$

where $\tilde{P}_{ab}$ represents the flat spacetime oscillation probability at lowest order in ε.

At the maximum $\Delta T^\star_{jk}$ and for $\tilde{\vec{P}}_{\mathrm{S}j}(\Delta T_{jk}) \equiv \vec{P}_{\mathrm{D}j}$, we obtain

$$L^0(\Delta T^\star_{jk}) = \frac{L(\Delta T^\star_{jk})}{\bar{v}_{jk}}\,, \tag{5.88}$$

$$\begin{aligned}\frac{1}{\bar{v}_{jk}} \coloneqq 1 &+ \frac{m_j^2 + m_k^2}{4E^2} + \varepsilon\frac{\delta v_j + \delta v_k}{2} \\ &- \frac{\Delta p_j m_j^2 + \Delta p_k m_k^2}{2E^3} - \frac{(\Delta m^2_{jk})^2}{8E^4} - \frac{m_j^4 + m_k^4}{16E^4}\,,\end{aligned} \tag{5.89}$$

$$L(\Delta T^\star_{jk}) = \left(\Delta X + \frac{\varepsilon}{2}\left[\frac{\Delta\vec{X}}{\Delta X}\cdot\vec{e}_k\right]\delta\ell^k{}_\mu(\Delta T^\star_{jk}, \Delta\vec{X})\Delta X^\mu\right)\,, \tag{5.90}$$

with $\Delta X \coloneqq |\Delta\vec{X}|$, cf. Appendix D.2. This closely resembles the corresponding flat spacetime expression apart from the geometrical velocity deviations

$$\varepsilon\delta v_j \coloneqq -\frac{\varepsilon}{2}\frac{\sigma_\mathrm{D}^2}{\sigma_\mathrm{S}^2 + \sigma_\mathrm{D}^2}\frac{m_j^2}{E^2}\frac{(\vec{\ell}\cdot\vec{e}_k)\lambda^k{}_\beta p^\beta}{E}\,, \qquad \vec{\ell} \coloneqq \frac{\vec{L}}{L}\,, \tag{5.91}$$

caused by the deviations of the neutrino geodesics c_j from the average geodesic c.

Finally, expanding the full function in the exponent in Equation (5.86)

$$\begin{aligned}\Xi_{jk} :=& -\frac{(\Delta\tilde{\vec{P}}_{\mathrm{S}j} - \Delta\vec{P}_{\mathrm{D}j})^2 + (\Delta\tilde{\vec{P}}_{\mathrm{S}k} - \Delta\vec{P}_{\mathrm{D}k})^2}{4(\sigma_{\mathrm{S}}^2 + \sigma_{\mathrm{D}}^2)} - \frac{(\bar{v}_j L^0 - L)^2}{2\sigma_{\parallel j}^2} \\ & - \frac{(\bar{v}_k L^0 - L)^2}{2(\sigma_{\parallel k}^*)^2} - i(L^0 \Delta\bar{E}_{jk} - L\Delta\bar{p}_{jk})\,,\end{aligned} \tag{5.92}$$

to second order around the maximal overlap time $\Delta T_{jk}^\star$, and using that only a small neighbourhood around $\Delta T_{jk}^\star$ really contributes to the value of $\mathcal{I}_{jk}$, enables us to rewrite

$$\begin{aligned}\mathcal{I}_{jk}(\vec{X}_{\mathrm{S}}, \vec{X}_{\mathrm{D}}; E) \approx & \int_{T_{\mathrm{D}1}}^{T_{\mathrm{D}2}} \mathrm{d}T_{\mathrm{D}} \sqrt{\frac{2\pi}{-\Xi_{jk}''(\Delta T_{jk}^\star)}} \exp\left(\Xi_{jk}(\Delta T_{jk}^\star)\right) \\ & \times \exp\left(\frac{\mathrm{Im}(\Xi_{jk}')^2(\Delta T_{jk}^\star)}{2\Xi_{jk}''(\Delta T_{jk}^\star)}\right).\end{aligned} \tag{5.93}$$

The exponent function evaluated at the mean propagation time $\Delta T_{jk}^\star$ includes the modified oscillation phase as well as damping terms associated with the separation of neutrino WPs. Within the adopted scheme of approximation, we arrive at

$$\mathrm{Im}(\Xi_{jk}) \approx -\frac{\Delta m_{jk}^2}{2E}\left(1 - \frac{\Delta p_j + \Delta p_k}{2E}\right) L\,, \tag{5.94}$$

$$\mathrm{Re}(\Xi_{jk}) = -\left(\frac{L}{L_{jk}^{\mathrm{coh}}}\right)^2, \tag{5.95}$$

where we have dropped an additional sub-leading phase correction in the imaginary part further discussed in Appendix D.2. Thus, we obtain the usual oscillation phase including $\varepsilon_{\mathrm{UR}}^2$ corrections as well as the coherence length

$$L_{jk}^{\mathrm{coh}} := 2\sigma_X \left[\left(\frac{\Delta v_{jk}^+}{1 + \chi_j^2 (L^0)^2}\right)^2 + \left(\frac{\Delta v_{jk}^-}{1 + \chi_k^2 (L^0)^2}\right)^2\right]^{-\frac{1}{2}}, \tag{5.96}$$

$$\Delta v_{jk}^\pm := \mp\frac{\Delta m_{jk}^2}{4E^2} + \varepsilon\left(\frac{\delta v_j + \delta v_k}{2}\right) \pm \frac{\Delta p_j m_j^2 - \Delta p_k m_k^2}{2E^3} \pm \frac{\Delta m_{jk}^4}{8E^4} \mp \left(\frac{\Delta m_{jk}^2}{4E^2}\right)^2. \tag{5.97}$$

At lowest non-vanishing order in $\varepsilon_{\mathrm{UR}}$ and by setting $\varepsilon = 0$, the coherence length reduces to the usual expression $L_{jk}^{\mathrm{coh}} = 4\sqrt{2}\sigma_X E^2/\Delta m_{jk}^2$. To the next higher orders in $\varepsilon_{\mathrm{UR}}$ and ε the coherence length receives geometrical corrections due to the deviations of mass eigenstate geodesics c_j from the mean geodesic c as well as from the effect of WP spreading. The former is encoded within the geometrical velocity corrections δv_j, while the latter is parametrised by the WP spreading factors $\chi_j := (1 - \bar{v}_j^2)/(2\bar{E}_j \sigma_X^2)$. As in Section 2.3.2, we also have introduced the effective position space width

$$\sigma_X^2 := \frac{1}{4}\left(\frac{1}{\sigma_{\mathrm{S}}^2} + \frac{1}{\sigma_{\mathrm{D}}^2}\right). \tag{5.98}$$

For a more detailed derivation of these expressions see Appendix D.2.

Finally, for the last exponential in Equation (5.93), we get

$$\frac{\mathrm{Im}(\Xi'_{jk})^2(\Delta T^\star_{jk})}{2\Xi''_{jk}(\Delta T^\star_{jk})} \approx -\frac{1}{2}\left(\frac{\Delta E_{jk}}{\sigma_E}\right)^2 , \tag{5.99}$$

where $\sigma_E^2 \approx 1/\sigma_X^2$. This so-called production and detection coherence term induces oscillation suppression as soon as the mass or momentum splittings can be resolved at the source or detector. Since this term is already of order $\mathcal{O}(\varepsilon^2_{\mathrm{UR}})$ in flat spacetime, any higher order correction would need to be of $\mathcal{O}(\varepsilon^2_{\mathrm{UR}}\varepsilon)$, and hence, the flat spacetime expression is recovered.

Finally, assuming that the mass eigenstate energy differences cannot be resolved at the experiment under consideration, we arrive at the final expression

$$\begin{aligned}\tilde{P}_{ab}(\vec{X}_{\mathrm{S}}, \vec{X}_{\mathrm{D}}, T_{\mathrm{D}}; E) = \sum_{j,k} U^*_{aj}U_{ak}U_{bj}U^*_{bk} \exp\left(-\left(\frac{L(T_{\mathrm{D}})}{L^{\mathrm{coh}}_{jk}(T_{\mathrm{D}})}\right)^2\right) \\ \times \exp\left(-i\frac{\Delta m^2_{jk}}{2E}\left(1 - \frac{\Delta p_j + \Delta p_k}{2E}\right)L(T_{\mathrm{D}})\right) .\end{aligned} \tag{5.100}$$

This proves that at $\mathcal{O}(\varepsilon_{\mathrm{UR}}\varepsilon, \varepsilon^2_{\mathrm{UR}})$ the neutrino oscillation pattern still depends on the physical distance L in the same way as in flat spacetime. Nevertheless, for time-dependent gravitational fields, this distance may change during the detector livetime, inducing a time average of $\tilde{P}_{ab}$ due to the integral in Equation (5.87). Furthermore, the coherence length is modified by the spacetime geometry and the produced neutrino energy distribution is affected by the parallel transport transformation, potentially resulting in a redshift of the distribution. These findings confirm the validity of heuristic approaches to neutrino oscillations in weak gravitational fields, as have been undertaken e.g. in References [189, 207]. In these approaches, the flat spacetime expression for the oscillation probability is modified by replacing ΔX by the physical distance L, computed for the respective spacetime, and by taking into account potential redshift effects on the energy of the neutrino system.

Neutrino Oscillations in Static, Newtonian Gravitational Fields Applying Equation (5.100) to the scenario of static spacetimes, we immediately notice that the detection time integral can be solved trivially. Performing this integration results in the standard oscillation behaviour in terms of the physical distance L. Therefore, for a fixed propagation distance L no difference to the flat spacetime oscillation pattern can be observed, as long as $L \ll L^{\mathrm{coh}}_{jk}$ for all energies under consideration. At $L \sim L^{\mathrm{coh}}_{jk}$, the impact of WP separation becomes relevant, and thus, also the influence of the spacetime geometry on L^{coh}_{jk} becomes experimentally accessible. In addition to that, another noticeable effect in the current scenario is the parallel transport of neutrino energy distributions from the source to the detector. Given a fixed initial neutrino energy E, this leads to a distortion of the length-dependent oscillation pattern. However, especially for neutrinos produced and detected in the vicinity of Earth, all these effect are too

small to be observable. Consequently, in terrestrial neutrino experiments corrections of the standard neutrino oscillation formula due to Earth's gravitational field can be neglected, as one would expect.

Neutrino Oscillations in the Presence of Gravitational Waves The situation, however, is different in time-dependent gravitational fields, such as in the presence of GWs. Here, the physical distance between source and detector changes with the frequency of the GW passing through the setup. Consequently, the reference distance $L_0 := L(T_{\mathrm{D0}})$ does not remain the same over the detection period $T_{\mathrm{D2}} - T_{\mathrm{D1}}$, and hence, the oscillation pattern is influenced by the changing metric perturbation $h_{\mu\nu}$. Conceivable consequences are a shifting oscillation pattern during different detection periods or gravitationally induced decoherence. The latter effect occurs if the detection period is large compared to the period of the passing GW and the time integral leads to an averaging of the oscillation pattern. In order to observe the former effect, the GW must be sufficiently slowly oscillating compared to the time of data taking such that an undisturbed oscillation pattern arises in the data. To accumulate a sufficient amount of neutrino statistics, this implies that the GW frequency must be of the order $\mathcal{O}(\mathrm{nHz})$ or even less corresponding to a time of data taking of at least one year. This is because one needs to consider astrophysical neutrino sources[6] for a noticeable effect in the oscillation pattern since the gravitationally induced shift in the oscillation pattern is proportional to the travel distance. And since $\varepsilon \ll 1$ the propagation distance must be sufficiently large in order to result in $L(T_{\mathrm{D}}) - L_0 = \mathcal{O}(L_{jk}^{\mathrm{osc}})$.

The same requirement for the propagation distance also applies to the search for gravitationally induced decoherence. However, for the observation of this effect one does not need to time the crests and troughs of the GW. Instead, the impact of gravitationally induced decoherence increases for longer periods of data taking. Comparing the observed oscillation pattern versus the standard expectation can then tell if a GW has passed through the setup during the livetime of the detector. However, because of the large propagation distances, decoherence due to WP separation and the averaging of the oscillation pattern due to the finite width energy binning could hide this new source of decoherence. In the next section, we explore this idea in more detail and also discuss the effect of the stochastic gravitational wave background (SGWB) on neutrino oscillations.

5.4 Decoherence in Neutrino Oscillations induced by Gravitational Waves

The first detections of GWs by the laser interferometry experiments Laser Interferometer Gravitational-Wave Observatory (LIGO) and VIRGO [208, 209] have shown that this phenomenon predicted by GR can be used to study the Universe complementing EM and neutrino based astronomy. Thus, GWs represent an exciting new addition to the field of multi messenger

[6] In this work, also solar neutrinos are considered to be astrophysical.

astronomy opening a new window of observation of astrophysical events like black hole and neutron star mergers [210] providing possibly new insights into the behaviour of quantum matter in extreme gravitational environments [211]. Moreover, GWs can be used to search for signatures of primordial black holes [212–215], cosmic strings [216, 217] and also provide the possibility to distinguish between different inflationary models [218]. Thereby, GWs represent an important new tool to search for new physics beyond the SM and the ΛCDM model. Furthermore, recently, pulsar timing array (PTA) collaborations like the North American Nanohertz Observatory for Gravitational Waves (NANOGrav) have observed the first evidence for the existence of a SGWB [219].

Also, lately, interest has grown in the question which role neutrinos could play for the observation of GWs in the future [220–228]. As shown in the last section the neutrino oscillation phase is sensitive to the alteration of the structure of spacetime due to time-dependent gravitational phenomena like GWs. The influence of a GW hence might lead to an additional source of oscillation damping that in principle could be observable in neutrino experiments. While in References [220, 222–227] especially the influence of the SGWB on neutrino oscillations is studied, we also investigate the impact of coherent signals on neutrino oscillations. These coherent signals are defined as being emitted by a single GW source, i.e. are of the type studied by current and future laser interferometry experiments. This would then provide a complementary way of observing those signals.

The main challenge in observing effects of GWs on the neutrino oscillation pattern lies in the distinction from other, well known sources of decoherence or oscillation damping—we use both phrases interchangeably from now on—discussed earlier in Section 2.3. In the setting of vacuum neutrino oscillations these damping effects amount to the effect of WP separation or incoherent averaging procedures that need to be employed due to the fact that in any experiment oscillation probabilities are studied by accumulating multiple neutrino events over a certain detection time interval.

In the following, we first develop a general set of criteria that must be fulfilled in order to be able to observe any new decoherence effect resulting in the standard decoherence limit. This especially applies to the GW induced effect studied in this work. Given these criteria, we briefly discuss which neutrino sources are potentially interesting for a hypothetical future neutrino oscillation experiment designed for the search for GW signatures. Afterwards, we discuss under which circumstances coherent and stochastic GWs can be observed at a neutrino based experiment.

5.4.1 Criteria for the Observability of Gravitational Wave Induced Decoherence

In addition to the already extensively discussed effect of WP separation, oscillation averaging occurs since neutrino events are usually accumulated in finite width energy bins in order to yield sufficient statistics to be able to reconstruct the corresponding bin averaged oscillation

probability distributions. Moreover, if neutrinos originate from a natural source of non-negligible spatial extent like, for example, the sun, an averaging of the neutrino baseline is mandatory in order to account for the distribution of propagation distances the different neutrinos have travelled from their origin to the detector. In the fully decohered limit all these effects lead to the same asymptotic probability distribution, i.e.

$$P_{ab}^{\text{deco}} \sim \sum_j |U_{aj}|^2 |U_{bj}|^2 \,, \tag{5.101}$$

since the oscillating terms are averaged to zero such that only the incoherent sum of mixing matrix elements remains.

In order to observe any non-standard decoherence effect resulting in the same limit as shown in Equation (5.101), the following conditions must be fulfilled:

(i) Decoherence due to WP separation occurs later, i.e. at larger baselines L or smaller energies E, than the new decoherence effect.

(ii) The energy resolution and the chosen energy binning of the neutrino experiment are sufficiently fine grained such that oscillations in the desired energy range can be observed. Therefore, neutrino oscillations must be sufficiently slow such that one energy bin does not contain multiple oscillation cycles.

(iii) The spatial extent of the neutrino production region must be small compared to the oscillation length such that the source can be considered to be approximately point-like.

(iv) The expected baseline change due to relative motion of source and detector during the measurement period needs to be much smaller than the oscillation length.

For the observation of decoherence induced by GWs one may add another, fifth, criterion to the list, namely that source and detector should not be strongly bound by EM forces such that the GW can indeed alter the neutrino propagation distance. Of course one can in principle alleviate this criterion and take additional forces into account, but this will naturally further weaken the effect of the GW on the neutrino system.

In order to be able to use this set of criteria in the current analysis, we further quantify the loose formulation in the following.

Criterion (i): WP Decoherence The requirement that WP decoherence shall be negligible compared to the new decoherence effect amounts to the simple requirement

$$L \ll L_{jk}^{\text{coh}} \,, \tag{5.102}$$

for the desired oscillation channel in which the new effect is supposed to be observed. In the lowest order of the ultra-relativistic approximation, this can also be simply translated into a condition for the neutrino energy, i.e.

$$E \gg \sqrt{\frac{|\Delta m_{jk}^2|}{4\sqrt{2}} \frac{L}{\sigma_X}} =: E_{jk}^{\text{coh}} \,. \tag{5.103}$$

At higher orders, the coherence length L_{jk}^{coh} is slightly increased and the coherence energy E_{jk}^{coh} is slightly reduced by the effect of WP spreading.

Criterion (ii): Energy Bin Averaging The second condition states that the energy bin widths ΔE must be sufficiently narrow in order to resolve the oscillation pattern. For a simple sinusoidal oscillation, this means that the associated frequency must at least be similar to the binning width. Since the neutrino oscillation pattern is not simply sinusoidal in terms of the neutrino energy E but rather in terms of the ratio L/E, we obtain

$$\left|\Delta\left(\frac{L}{E}\right)\right| \lesssim \frac{1}{\omega_{jk}} = \frac{2}{|\Delta m_{jk}^2|} \qquad \Leftrightarrow \qquad \frac{\Delta E}{E} \lesssim \frac{2E}{|\Delta m_{jk}^2| L}\,, \tag{5.104}$$

assuming a fixed baseline L. Defining the relative energy resolution $\delta E := \Delta E/E$, we can rewrite this condition as

$$\delta E \lesssim \frac{L_{jk}^{\mathrm{osc}}}{2\pi L} =: \delta E_{\mathrm{thr}}\,, \tag{5.105}$$

where we have also introduced the relative threshold binning or resolution δE_{thr}. For an increasing propagation distance, it becomes more difficult to fulfil this criterion which is one of the main reasons why it is troublesome to observe oscillating astrophysical neutrinos. Currently planned neutrino experiments have a relative energy resolution at the percent level [229] at most and the chosen energy binning for any oscillation analysis would be even coarser in order to ensure sufficient statistics per bin.

Criterion (iii) and (iv): Baseline Averaging A similar effect as described in the last paragraph arises if neutrinos are produced in a large region of characteristic size Σ_{S}—where the index S stands for neutrino source. It is then mandatory that the oscillation length L_{jk}^{osc} is large compared to Σ_{S} such that the averaging integral over the neutrino production region does not lead to substantial oscillation averaging, i.e.

$$\Sigma_{\mathrm{S}} \ll L_{jk}^{\mathrm{osc}} = 4\pi \frac{E}{|\Delta m_{jk}^2|}\,. \tag{5.106}$$

With the same reasoning one can argue that in case source and detector are moving relatively to each other that the maximal difference in propagation distances over the period of data taking must fulfil the same criterion as Σ_{S} does, i.e.

$$L_{jk}^{\mathrm{osc}} \gg \max_{t\in[T_{\mathrm{D1}},T_{\mathrm{D2}}]} L(t) - \min_{t\in[T_{\mathrm{D1}},T_{\mathrm{D2}}]} L(t)\,, \tag{5.107}$$

where $[T_{\mathrm{D1}}, T_{\mathrm{D2}}]$ is the detector livetime interval.

Judging from criteria (i) to (iv) together, it seems to be most promising to consider high energy neutrinos from relatively small baselines. This is because the oscillation length as well as the coherence length increase with growing energy, and therefore, high energies relax the

restrictiveness of any condition formulated above. The smallness of the neutrino baseline further weakens the constraints imposed by the WP decoherence and energy resolution criteria (i) and (ii). In the context of detecting GWs however, it, is most promising to consider neutrinos of astrophysical origin for two reasons:

1. The GW effect grows with increasing distance, as we will see in Section 5.4.3.
2. It is difficult to ensure the weak binding criterion if source and detector are placed on Earth.

The first point on this list is the main reason why none of the current or past terrestrial neutrino oscillation experiments have seen GW signatures yet. Typical strains, i.e. relative baseline deviations $h \sim \Delta L/L$ induced by a GW, are of the order of $h \sim 10^{-20}$ (see e.g. the comprehensive review presented in Reference [230]). This is by far too minuscule to induce significant oscillation averaging at baselines of several hundreds or thousands of kilometres, as the necessary criterion $\Delta L = hL \sim L_{jk}^{\mathrm{osc}}$ is never fulfilled. Moreover, if source and detector are placed on or within Earth's ground, their physical distance is approximately held fixed by strong binding forces, and hence, the GW influence is further reduced.

5.4.2 Potentially Interesting Neutrino Sources

Based on the considerations presented in the last section, we are now interested in identifying potentially interesting astrophysical neutrino sources. The most obvious candidate source for neutrinos that comes to mind is the sun as it provides sufficient neutrino fluxes and the distance between Earth and sun is well known. The sun produces neutrinos in the energy range from a few hundred keV to MeV and the corresponding oscillation length can be expressed as

$$L_{jk}^{\mathrm{osc}} \approx 249.87 \left(\frac{E}{\mathrm{MeV}}\right) \left(\frac{10^{-5}\,\mathrm{eV}^2}{|\Delta m_{jk}^2|}\right) \mathrm{km}\,. \tag{5.108}$$

For the solar neutrino energies, we therefore obtain oscillation lengths on the order of several up to a few hundred kilometres. Since the region in which neutrinos are produced within the sun is already significantly larger than that, we can infer by criterion (iii) that the average over all contributing neutrinos from the sun already erases all oscillations. Moreover, since $L_{jk}^{\mathrm{osc}} \ll L$, also the energy resolution condition (ii) suggests that all oscillations will be averaged out. It is, therefore, impractical to use solar neutrinos for the search for GW induced decoherence effects.

This also implies that for the search for more suitable candidate neutrino sources, we need to consider sources from outside our solar system. Here, Supernovae are extensively studied neutrino sources producing neutrinos in the MeV energy range [168, 231–239], and therefore, represent a possible candidate. Unfortunately, utilising Supernovae for the detection of GW induced decoherence faces the same and even worse problems as using solar neutrinos since

the propagation distance is several orders of magnitude larger making also WP decoherence a relevant effect [168].

Consequently, we can also exclude Supernovae from our list of possibly interesting sources. This commands us to consider ultra high energy neutrinos starting at a few TeV up to EeV energies as they can occur for example in neutrinos emitted from pulsars [240–246] or blazars [247–254]. Blazars—or active galactic nuclei—have the immediate disadvantage that they are located outside of our own Galaxy, and hence, are too far away to allow for the observation of neutrino oscillations. For example considering the blazar TXS 0506+056 at an approximate distance of $L \approx 1.75\,\mathrm{Gpc}$ [255] that has been identified as the source of an ultra high energy neutrino event by IceCube [256], we would need a relative energy binning of $\delta E \sim 10^{-8}\,\%$ at $E = 1\,\mathrm{EeV}$. Moreover, due to the large distance to the source, neutrino fluxes are presumably too small for an actual analysis of the oscillation pattern.

Candidate sources that still remain interesting in the light of conditions (i) to (iv) are pulsars from our Galaxy, like for example the Cas A ($L = 3.5 \pm 0.2\,\mathrm{kpc}$ [257]), Crab ($L = 1.90^{+0.22}_{-0.18}\,\mathrm{kpc}$ [258]) or Vela pulsars ($L = 294^{+76}_{-50}\,\mathrm{pc}$ [259]). Neutrinos produced in the vicinity of these stellar objects can reach very high energies on the order of $\mathcal{O}(\mathrm{PeV})$ [244] or higher depending on the properties of the pulsar. Considering the Vela pulsar as an example, this would imply a relative energy resolution of $\delta E \sim 10^{-5}\,\%$ at $E \sim 1\,\mathrm{TeV}$ for Δm^2_{21}, which is still out of reach for current and near-future neutrino telescopes, but might be achievable in the far future. Furthermore, pulsars are very compact objects and neutrinos are produced within its magnetosphere [260] or the surrounding pulsar wind nebula by strongly accelerated protons scattering off of other protons or X-rays from the pulsar's surface. Depending on the physical properties of the given pulsar the neutrino production region can be considered sufficiently small such that oscillations are not completely averaged out and all conditions (i) to (iv) are fulfilled assuming sufficiently narrow energy binning. Moreover, due to the relatively high estimated neutrino fluxes of $\Phi_\nu \sim 30\mathrm{km}^{-2}\mathrm{yr}^{-1}$ [244] sufficiently high event counts at future $100\,\mathrm{km}^2$ neutrino telescopes can be expected. A potential problem when considering pulsars as neutrino sources are the rather large uncertainties of the distance between the Earth and the corresponding pulsar. In any analysis, the neutrino baseline would introduce an additional nuisance parameter that needs to be fitted simultaneously with the other model parameters reducing the potential sensitivity of the corresponding effect.

In summary, the prospects to observe oscillating astrophysical neutrinos are rather bleak, but we have identified galactic pulsars as the most promising candidate sources as soon as the relative energy resolution and binning can be chosen smaller than $\delta E \sim 10^{-5}\,\%$. Thus, utilising astrophysical neutrinos for the observation of any non-standard decoherence effect resulting in the same standard decoherence limit shown in Equation (5.101) are rather unrealistic in the near future. This is mainly due to the energy binning and production region criteria (ii) and (iii) formulated in the last section. If, however, a neutrino source at smaller distances ($L = \mathcal{O}(10\,\mathrm{lyr})$) emitting very high energy neutrinos ($E = \mathcal{O}(100\,\mathrm{PeV})$) are found the situation might change drastically as the respective relative threshold energy resolution would be $\delta E_{\mathrm{thr}} = \mathcal{O}(1\,\%)$ which seems already much more promising.

5.4.3 Neutrino Oscillations Influenced by Coherent Gravitational Waves

Let's assume for now that we can indeed find an astrophysical neutrino source providing a sufficient flux of ultra high energy neutrinos at Earth and being able to choose our relative energy binning δE such that we would expect to observe neutrino oscillations according to the standard flat spacetime prediction. In this case, our neutrino experiment would be sensitive to new decoherence effects resulting in the standard decoherence limit like for example decoherence induced by GWs. As already briefly introduced in Section 5.3, this effect is caused by the time-dependent neutrino baseline variation due to the GW passing through the neutrino path. Since we usually accumulate neutrino data over the course of several years all detected neutrinos will have travelled different spacetime distances from the source to the detector, and hence, the oscillation pattern is averaged depending on the magnitude of the relative baseline deviation.

The baseline variation induced by the GW is described by

$$\Delta L(T_\mathrm{D}) \coloneqq L(T_\mathrm{D}) - \Delta X \approx -\frac{1}{2}\int_0^{\Delta\tau(T_\mathrm{D})} \mathrm{d}\tau h_\parallel(c_0(\tau;T_\mathrm{D})) + \Delta L^0(T_\mathrm{D})\,, \tag{5.109}$$

with the parallel projection of the GW tensor and the propagation time correction

$$h_\parallel(x) = \frac{\Delta X^k \Delta X^l}{\Delta X^2} h_{kl}(x)\,, \tag{5.110}$$

$$\Delta L^0 = \frac{1}{2}\left[\langle \partial^0 h_\parallel \circ c_0\rangle - \left\langle \tau \mapsto \int_0^\tau \frac{\mathrm{d}\tau'}{\Delta\tau}\partial^0 h_\parallel(c_0(\tau'))\right\rangle\right]\Delta X^2\,, \tag{5.111}$$

respectively. Note that we have absorbed the expansion parameter ε into the GW tensor to simplify our notation. This expression is still given in terms of the unphysical coordinate distance ΔX that cannot be observed directly in any experiment measuring the distance between the source and the detector. Instead, such a distance measurement yields a physical reference length $L^\star$ evaluated at the reference time $T_\mathrm{D}^\star$. It is therefore much more meaningful for our setup to formulate the neutrino baseline with respect to this reference length, i.e.

$$L(T_\mathrm{D}) = L^\star + \Delta L(T_\mathrm{D}) - \Delta L(T_\mathrm{D}^\star)\,. \tag{5.112}$$

This becomes especially important when considering GWs that do not vary significantly during the detection time interval. In this case, the length stays approximately constant and the gravitationally modified oscillation probability should reduce to the flat spacetime prediction evaluated at $L^\star$.

From Equation (5.112), we can infer that a neutrino-based GW detector would be sensitive to the amplitude of the relative baseline deviation

$$h \coloneqq \frac{\Delta L^\star}{L^\star}\,, \qquad\qquad \Delta L^\star \coloneqq \max_{T_\mathrm{D}\in[T_{\mathrm{D}1},T_{\mathrm{D}2}]} |L(T_\mathrm{D}) - L^\star|\,, \tag{5.113}$$

typically called the strain of the GW. In order for the time averaging procedure, applied to the flavour transition probability, to yield a significant impact, it is crucial that the maximal baseline deviation is comparable to the oscillation length, i.e.

$$\Delta L^{\star} \gtrsim L_{jk}^{\mathrm{osc}} \qquad \Leftrightarrow \qquad h \gtrsim \frac{L_{jk}^{\mathrm{osc}}}{L^{\star}} \,. \tag{5.114}$$

The minimal strain an experiment can be sensitive to is, therefore, given by $h_{\mathrm{min}} := L_{jk}^{\mathrm{osc}}/L$ and can be directly related to the relative threshold energy width $h_{\mathrm{min}} = 2\pi\delta E_{\mathrm{thr}}$ by Equation (5.105).

Thus, in order for neutrino oscillation experiments to compete with currently used laser interferometry experiments that are sensitive to strains on the order of $h \sim 10^{-20}$ and lower, we would at least need a relative energy resolution of the same order of magnitude, i.e. $\delta E \sim 10^{-18}\,\%$ which is at best unrealistic. We can hence conclude that using neutrino oscillation experiments to detect coherent GW signals from a single source is highly impractical at present as well as future neutrino telescopes.

5.4.4 Neutrino Oscillations Influenced by a Stochastic Gravitational Wave Background

Besides coherent GW signals from single sources, the SGWB produced by a multitude of different sources throughout the history of the Universe is an interesting phenomenon that has also been studied already in the context of neutrino oscillations [220, 222–227]. In the light of the results of the previous sections, it is, however, questionable if the transition from coherent to a stochastic superposition of GW signals will indeed improve the sensitivity of neutrino experiments to GW influences. To investigate this in more detail, we adopt the same framework discussed in Reference [227] and perform a quantitative, statistical analysis including the effects of WP separation as well as the impact of finite energy binning in order to estimate the sensitivity of neutrino experiments on the SGWB. Apart from these adversary effects, we assume ideal conditions for our neutrino toy experiment in order to provide an estimate of the maximally achievable sensitivity in any conceivable experiment. We thus neglect any systematic effects, effects of energy and directional reconstruction, the uncertainty of the neutrino baseline and assume abundant neutrino event counts also in the ultra high energy bins, as described in more detail below.

Within the framework of Reference [227], the impact of the SGWB on neutrino oscillations is parametrised by the decoherence function[7]

$$\mathcal{D}_{jk}^{\mathrm{SGWB}}(E,L) := -\left(\frac{2H_0}{8\pi L_{jk}^{\mathrm{osc}}}\right)^2 \int_{f_{\mathrm{min}}}^{f_{\mathrm{max}}} \frac{\mathrm{d}f}{f^5} \Omega^{\mathrm{SGWB}}(f) \sin^2(\pi f L) \,, \tag{5.115}$$

[7] Here, we adopt the same notation and conventions as described in Section 2.3.3.

where H_0 is the Hubble rate today and $\Omega^{\mathrm{SGWB}}(f)$ is the differential fractional energy density of the SGWB with respect to the GW frequency f. Equation (5.115) is derived in a semiclassical approach to neutrino oscillations in the presence of a stochastically perturbed spacetime [224]. This approach is based on the Hamilton–Jacobi equation for neutrinos in a curved background that is also tightly connected to the derivation of the Stodolsky phase [191]. Since we have already shown before that our master Equation (5.48) reproduces this semiclassical limit for sufficiently narrow WPs, we consider this approach to be sufficiently congruent with our approach[8] without further proof.

In accordance with Reference [227], we parametrise the SGWB spectrum as

$$\Omega^{\mathrm{sgwb}}(f) = |A_*|^2 \frac{2\pi^2}{3H_0^2} f_{\mathrm{yr}}^2 \left(\frac{f}{f_{\mathrm{yr}}}\right)^{1-\gamma} , \tag{5.116}$$

where we choose $f_{\mathrm{yr}} = 1\,\mathrm{yr}^{-1} \approx 31.7\,\mathrm{nHz}$ as the reference frequency, γ denotes the spectral index and A_* the strain amplitude. Since the integrand in $\mathcal{D}_{jk}^{\mathrm{SGWB}}$ is strongly suppressed in the ultraviolet, we can safely consider the limit $f_{\mathrm{max}} \to \infty$ as has been done in Reference [227]. Therefore, the remaining free model parameters are A_*, γ as well as the infrared (IR) cutoff frequency f_{min} of the SGWB. To estimate the most stringent exclusion limits that can potentially be achieved using neutrino experiments, we assume an idealised toy setup in the following. In this setup, neutrinos are detected from an astrophysical point-source at distance L and accumulated in energy bins of equal width ΔE. Moreover, we consider the ultra high energy scenario implicitly defined in Reference [227] corresponding to neutrinos from a hypothetical source at a distance $L = 50\,\mathrm{lyr}$ with energies $E \in [1, 100]\,\mathrm{PeV}$ and a relative energy bin width $\delta E = 0.1\,\%$ at $E = 100\,\mathrm{PeV}$.

The likelihood of our simple counting experiment is given by the product of Poisson distributions

$$\mathcal{L}(A_*, \gamma, f_{\mathrm{min}}|\vec{X}) = \prod_{b=1}^{3} \prod_{l=1}^{n_{\mathrm{bins}}} \frac{N_{bl}(A_*, \gamma, f_{\mathrm{min}})^{X_{bl}}}{X_{bl}!} \exp\left(-N_{bl}(A_*, \gamma, f_{\mathrm{min}})\right) , \tag{5.117}$$

where n_{bins} is the total number of energy bins, b denotes the detected neutrino flavour, $N_{bl}(A_*, \gamma, f_{\mathrm{min}})$ is the theory prediction of ν_b events in bin l given the input parameter set $(A_*, \gamma, f_{\mathrm{min}})$ and X_{bl} is the experimentally measured ν_b event count in bin l. Since we are conducting a toy experiment, the pseudo-data vector $\vec{X}$ is generated according to the standard prediction, i.e. for $A_* = 0$, without the influence of the SGWB. This way we are able to estimate potential exclusion limits on the SGWB parameter space by performing a log likelihood ratio test.

[8] To properly account for the SGWB in our formalism, we would need to average the neutrino oscillation probability over all possible GW configurations according to some probability density, like e.g. a Gaussian noise distribution, in order to accurately represent the fact that each neutrino detected over a certain time period has been immersed in a different GW background.

For the theory prediction, we assume a fixed total number of events of $N_{\text{tot}} = 2 \times 10^4$ across all bins and compute the bin wise event counts using the probability density

$$\rho_{bl} = \sum_a \int_{E_l}^{E_{l+1}} \mathrm{d}E \, \varphi_a(E) P_{ab}(E, L) \,, \tag{5.118}$$

for neutrino flavour b to be detected in energy bin l. Here, we use a simple flat, ν_e-only, power-law spectrum $\varphi_a \propto \delta_{ae} E^{-2}$ for the initial neutrino distribution. We employ this kind of flat spectrum in order to avoid strong suppression in the high energy bins that are most sensitive to the effect such that we prepare a close to ideal setup for the detection of the effect. A more realistic spectral index for the neutrino energy distribution would for example be $\varphi \sim E^{-3.2}$ as found by the IceCube collaboration for the blazar NGC-1068 [261]. The assumption of an initially pure electron neutrino beam is again inherited from Reference [227].

In the following, we carry out two different likelihood ratio tests by either fixing the minimal frequency f_{min} to values in $f_{\text{min}} \in \{10^{-18}, 10^{-17}, 10^{-16}, 10^{-15}\}\,\text{Hz}$ or by assuming a flat SGWB spectrum, i.e. $\gamma = 3$. For both cases, we define the negative log likelihood ratio by

$$\Lambda := -2 \ln \left(\frac{\sup_{(A_*, \gamma, f_{\text{min}}) \in \Xi_0} \mathcal{L}(A_*, \gamma, f_{\text{min}})}{\sup_{(A_*, \gamma, f_{\text{min}}) \in \Xi} \mathcal{L}(A_*, \gamma, f_{\text{min}})} \right) \,, \tag{5.119}$$

where Ξ_0 and Ξ are the null hypothesis and full parameter spaces, respectively. In case we fix the minimal frequency of the spectrum to $f^\star_{\text{min}}$, we have $\Xi \equiv \mathbb{R}^2 \times \{f^\star_{\text{min}}\}$. Assuming a flat SGWB spectrum, on the other hand, implies $\Xi \equiv \mathbb{R} \times \{3\} \times (0, \infty)$. The null hypothesis space always contains only one point corresponding to the tested parameter configuration. Hence, in the limit of large event counts, Wilk's theorem states that Λ is χ^2 distributed with two DOFs for both scenarios.

The results for the likelihood ratio test in the (γ, A_*) plane are presented in Figure 5.2. The green ellipses represent the 68 % (dark green) and 95 % (light green) credible regions obtained by the NANOGrav collaboration [219] using their 15 year data set. The other blueish and black lines indicate the 68 % CL contours we obtain for our test statistics, cf. Equation (5.119), for different fixed minimal frequencies $f_{\text{min}} \in \{10^{-18}, 10^{-17}, 10^{-16}, 10^{-15}\}\,\text{Hz}$ within the toy neutrino setup outlined above. The parameter region to the upper right, corresponding to higher strains and larger spectral indices, are excluded. For these parameter configurations, oscillation averaging due to the SGWB leads to a significant deviation of the expected event counts from the standard expectation. Since in Reference [227] the same scenario and parameter configurations are considered, we can directly compare our results to those obtained in Reference [227]. While the qualitative behaviour of the exclusion limits approximately matches that seen in Reference [227], we obtain much weaker bounds on the SGWB parameters in our approach. In Reference [227], the exclusion contours are derived by setting $\mathcal{D}^{\text{SGWB}}_{jk}(E_{\text{thr}}, L) \equiv 1$ for a chosen threshold energy $E_{\text{thr}} = 100\,\text{PeV}$. The reason for the discrepancy between their and our results is the limit $L \gg 1/f_{\text{min}}$ assumed in Reference [227] that does not apply for $L = 50\,\text{lyr}$ used here. In the first part of their analysis they do not specify a value for the baseline L,

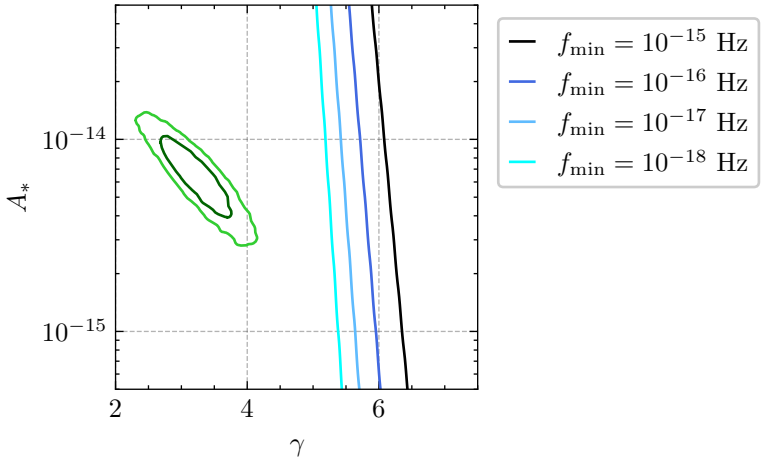

Figure 5.2: Shown in light blue to black are the 68 % CL exclusion contours for the spectral index γ and strain amplitude A_* assuming various minimal frequencies $f_{\min} \in \{10^{-18}, 10^{-17}, 10^{-16}, 10^{-15}\}$. If no SGWB induced decoherence is observed in an experiment with $L = 50\,\text{lyr}$, $E \in [1, 100]\,\text{PeV}$ and bin widths $\Delta E \sim 0.1\,\text{PeV}$ all parameter configurations to the right of these contours are excluded. Moreover, we report the 68 % and 95 % credible regions obtained by the NANOGrav collaboration [219] in dark and light green, respectively.

but later on they discuss threshold energy resolutions of $\delta E(E_{\text{thr}} = 100\,\text{PeV}) \sim 0.1\,\%$. The implied baseline $L = 50\,\text{lyr}$ is much smaller than any of the inverse frequencies leading to a significant cancellation in the exact expression for $\mathcal{D}_{jk}^{\text{SGWB}}$, drastically reducing the significance of the corresponding neutrino experiment. Note that the results shown in Figure 5.2 are obtained in an extremely idealised scenario of a very high energy neutrino source very close to Earth providing abundant event counts similar to those obtained in atmospheric neutrino experiments. Moreover, we assume an optimistic relative energy binning of $\delta E \sim 0.1\,\%$ which is at least one order of magnitude below what current experiments can achieve. In the light of these ideal conditions, it becomes clear that neither current nor near-future neutrino telescopes will be sensitive to SGWB effects in the neutrino oscillation pattern. These poor prospects are further substantiated by the fact that the obtained constraints correspond to a statistical significance of at most $1.5\,\sigma$ which is far below the level needed for the discovery of a new effect. This significance can only be improved by increasing the neutrino event counts. Indeed, bounds derived from the CMB, see e.g. Reference [262], even already exclude the parameter region that would be allowed in our approach. Assuming SGWB parameters on the exclusion contours, the respective energy fractions Ω^{SGWB} become exceedingly large, surpassing those allowed by cosmological observations by several orders of magnitude.

Considering much smaller IR cutoff frequencies $f_{\min} \in [10^{-12}, 10^{-9}]\,\text{Hz}$, neutrinos in the MeV energy range would be needed to yield any observable effect. On astrophysical scales, the most prominent candidate sources of neutrinos in the said energy range are supernovae implying WP widths of $\sigma_X \sim 0.1\,\text{pm}$ [263]. As already discussed in Section 5.4.2, decoherence due to WP

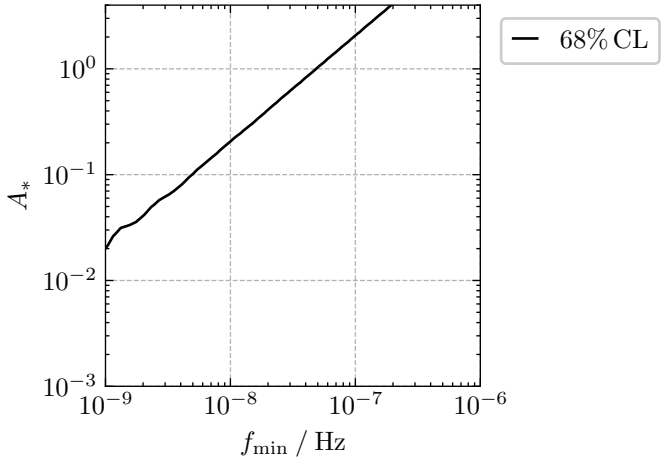

Figure 5.3: The black line indicates the 68 % CL exclusion contour for the same hypothetical experimental setup as in Figure 5.2 in the minimal frequency $f_{\min}$ and strain amplitude A_* plane for a flat SGWB frequency spectrum, i.e. $\gamma = 3$. All parameter configurations to the upper left of the contour are excluded if no effect due to the SGWB is observed.

separation has already occurred at these energies and baselines. Coherence can in principle be restored in the so-called catch-up effect [168] as the neutrino system crosses the boundary between the vacuum and Earth matter as well as the boundaries of the different density layers within the Earth. However, this will only lead to oscillations within the different layers of Earth matter starting from a fully decohered initial state even in the standard scenario. Since the propagation through Earth proceeds over very small distances, the SGWB can be neglected for the description of in-matter oscillations and therefore, the detected neutrino event counts will always coincide with the standard prediction. Moreover, if non-adiabatic matter effects can be neglected the energy averaging due to finite bin widths implies a relative threshold resolution of

$$\delta E_{\text{thr}} \sim 4.17 \times 10^{-10} \left(\frac{E}{\text{MeV}}\right) \left(\frac{10^{-5}\,\text{eV}^2}{\Delta m^2_{jk}}\right) \left(\frac{\text{lyr}}{L}\right) \%\,, \tag{5.120}$$

in order to resolve the neutrino oscillations. In addition to that, also baseline uncertainties would further reduce the sensitivity of neutrino experiments to the SGWB.

Lastly, in Figure 5.3 we also show the 68 % exclusion contour in the $f_{\min}$–A_* plane for cutoff frequencies NANOGrav is sensitive to. Here, we fix $\gamma = 3$, i.e. we assume a flat SGWB spectrum that is compatible with the NANOGrav best fit. We obtain that the neutrino toy experiment under consideration would be sensitive to strain amplitudes $A_* \sim 0.1$ and poses no competition for PTA based SGWB detectors.

5.5 Prospects of Observing Gravitational Effects in Neutrino Experiments

Now that we have shown that neither GWs nor weak static gravitational fields can have an observable effect in current or near-future neutrino experiments, we take a more systematic approach and discuss why this statement can be extended to: *The influence of gravitational fields on the neutrino flavour transition probability can be neglected for all neutrino experiments as long as oscillations of astrophysical neutrinos cannot be observed.* The simple reasoning behind this is that all present and near-future neutrino detectors will be located on or near Earth, i.e. are immersed in very weak, approximately static gravitational fields. The only way how neutrinos, detected in such an experiment, would experience any kind of strong gravitational field is if they originate from an astrophysical source that either causes the strong field itself or if neutrinos pass through such a field on their way to Earth.

In case neutrinos are produced near Earth, the flavour transition probability is very well approximated by the flat spacetime formula, as discussed in Section 5.3. In the opposite scenario, where neutrinos experience strong gravitational fields, and hence, are produced far away from Earth, it is currently and also in the foreseeable future impossible to resolve their flavour oscillations because of the criteria formulated in Section 5.4.1. These criteria are based on the flat spacetime formula, but they remain valid even in the context of gravitational fields for which the master Equation (5.48) for the flavour transition amplitude applies. This is because we can write the oscillation phase in a way analogous to the respective flat spacetime expression, as demonstrated explicitly in Equation (5.67) for Gaussian neutrino WPs. For general Lorentz-invariant WPs $\varphi(p, P)$ centered around the mean momentum P, we equivalently obtain

$$\mathcal{A}_{ab} = \sum_j U^*_{aj} U_{bj} \underbrace{\int \frac{\mathrm{d}^3\vec{p}}{(2\pi)^3 2p^0} \varphi_j^{\mathrm{D}*}(p, P_{\mathrm{D}j}) \varphi_j^{\mathrm{S}}(p, \Lambda P_{\mathrm{S}j}) e^{-iL_\mu p_j^\mu}}_{=\langle \psi_j^{\mathrm{D}}, \psi_j^{\mathrm{S}} \rangle} , \tag{5.121}$$

where the only difference to the Minkowski spacetime formula is that the mean momenta at the source are red- or blue-shifted according to the Lorentz transformation Λ, and the spacetime distance vector L^μ contains information about the geometry. The dependence of the oscillation phase on the physical distance, however, remains the same as in flat spacetime. It could now, for example, be that the oscillation pattern with respect to the neutrino energy E is influenced by the curvature of spacetime in that lower energy neutrinos travel along different geodesics than higher energy neutrinos. This would manifest itself as an additional energy dependence in the relation between the mean propagation time L^0 and the propagation distance L. In this case, one can use the smallest baseline, a neutrino from the given energy spectrum has travelled, in order to estimate the energy binning threshold. In astrophysical applications, this minimal propagation distance is usually still much larger than all oscillation lengths, and therefore, oscillations are averaged due to finite energy resolution and binning and also due to the effect of WP separation.

Therefore, the only observable influence of gravity would be a change of the decoherence limit of the flavour transition probability. As we have seen in Chapter 4, QG could indeed cause such a modification of the decoherence limit. In the majority of cases, this, however, is not true for classical gravity since in the large baseline limit, we can omit all oscillating terms in the oscillation probability and get

$$P_{ab} \to \sum_j \frac{|U_{aj}|^2 |U_{bj}|^2}{N} \iint \mathrm{d}^2(\mathcal{T}_\mathrm{S}, \mathcal{T}_\mathrm{D}) \, |\langle \psi_j^\mathrm{D}, \psi_j^\mathrm{S} \rangle|^2 \,, \tag{5.122}$$

in close analogy to the flat spacetime scenario. The last overlap integral enforces the usual momentum conservation relation $P_{\mathrm{D}j} \sim \Lambda P_{\mathrm{S}j}$ as well as the condition $\vec{v}_j L^0 \sim \vec{L}$, where $\vec{v}_j$ is the mean velocity of the j-th neutrino mass eigenstate. The integral, therefore, only contributes a real valued suppression factor for each term of the sum. If all mass eigenstates have quasi degenerate masses, they also have very similar WPs and all terms of the sum approximately contain the same suppression factor $|\langle \psi_j^\mathrm{D}, \psi_j^\mathrm{S} \rangle|^2 \approx |\langle \psi_k^\mathrm{D}, \psi_k^\mathrm{S} \rangle|^2$. Consequently, these suppression factors can be pulled out of the sum over j and cancel against the same contributions appearing in the normalisation N. Thus, what remains of P_{ab} is the flat spacetime decoherence limit shown in Equation (5.101).

By the same argument, it is also reasonable to assume the same behaviour for the more general oscillation formula shown in Equation (5.8), in terms of the Bogoliubov coefficients, as long as neutrino WPs are sufficiently localised such that we can employ the use of the equivalence principle. The only way this can be modified by gravity is if the mass eigenstates follow very different geodesics or the mass eigenstate WPs are spread out over a region larger than the local curvature radius. Both scenarios require areas of strong curvature in the vicinity of the path between source and detector. If the mass eigenstates were produced with the same four-velocities, the equivalence principle demands that all mass eigenstate geodesics exactly coincide with each other. The kinematics of the production process, however, imply that neutrinos of different masses are produced with *different* four-velocities. In the quasi degeneracy limit, $\Delta m_{jk}^2 \ll E^2$,—that we assume to apply—these four-velocity differences are very small, but arbitrarily strong gravitational fields can, in principle, lead to arbitrarily diverging mass eigenstate geodesics. In addition to that, as soon as the curvature is strong enough to amplify the small deviations between the different mass eigenstate WPs, the different terms in Equation (5.101) are multiplied by different suppression factors $|\langle \psi_j^\mathrm{D}, \psi_j^\mathrm{S} \rangle|^2 \neq |\langle \psi_k^\mathrm{D}, \psi_k^\mathrm{S} \rangle|^2$ and the decoherence limit is modified.

A conceivable example would be a neutrino source in the vicinity of a very small black hole where some mass eigenstates trajectories are bend towards the horizon while others are not. This, however, represents an extreme special case and does not apply to the majority of astrophysical neutrino sources, i.e. the accretion discs around super massive black holes (see e.g. Reference [264] for a recent overview of astrophysical neutrino sources). Furthermore, also the presence of small black holes near the neutrino path would give rise to strong curvature effects. Due to the inherent smallness of these objects and the low black hole densities compared to stellar densities (see e.g. Reference [265]), a neutrino–black hole encounter is rather improbable for a given point-source.

5.6 Summary and Conclusion

We have considered neutrino flavour transitions in globally hyperbolic spacetimes and have discussed why the independent neutrino oscillation probability can only be well-defined if gravitational particle production is negligible for the energy modes measured in an experiment. The main reason for this is that in the presence of significant gravitational particle production, the interaction topologies can become more complicated than the simple one-neutrino-exchange diagram. This invalidates the underlying single particle picture and prevents the necessary factorisation of the production, propagation and detection processes, since these sub-processes cannot be considered to be independent anymore. We have then focused on scenarios where gravitational particle production is indeed negligible and have derived a general formula for the neutrino flavour transition process.

Since this master formula is difficult to be further simplified without restricting to a specific spacetime, we have then considered a narrower but still quite general class of scenarios. In particular, we have required that, at any given time during propagation, curvature effects can be safely neglected on a region containing all neutrino WPs. This also implies that all neutrino mass eigenstate geodesics need to stay sufficiently close to each other. The latter assumption is justified by the equivalence principle and can only be violated if spacetime curvature is strong enough to significantly amplify the very small initial mass eigenstate velocity differences due to the production process. We find that the qualitative behaviour of neutrino oscillations remains very similar to the flat spacetime case. The only difference is that now parallel transport effects, such as redshift, are included within the oscillation probability and the physical distance appearing in the oscillation phase depends on possibly more complicated geodesic mean trajectories than in Minkowski spacetime. This dependence can in principle induce observable effects by altering the neutrino oscillation pattern.

We have then applied this approximated formula for the flavour transition amplitude to the case of linearised gravity and have specifically discussed the consequences for the explicit examples of static—i.e. Newtonian—gravitational fields, and GW spacetimes. For Newtonian gravity, we find that the coherence length receives gravitational corrections and the initial neutrino energy distribution is redshifted. Apart from that, the oscillation pattern remains the same as in flat spacetime. In the case of time-dependent fields, like for example in the presence of GWs, the physical distance also becomes time-dependent, representing a potential new source of decoherence. For current or near-future Earth-bound or atmospheric neutrino oscillation experiments, however, these effects are too minuscule to be observable.

In a detailed analysis, we show that it is currently impossible to observe effects on neutrino flavour transitions, induced by either coherent GWs or the SGWB, despite contrary claims in the Literature [224, 227]. To show this, we have developed a set of criteria that need to be met in order to be able to observe any new decoherence effect that does not alter the standard decoherence limit $P_{ab} \to \sum_j |U_{aj}|^2 |U_{bj}|^2$. Furthermore, in order to investigate the claims of Reference [227] that SGWB effects could indeed be observable in near-future neutrino experiments, we have applied an idealised statistical analysis to the framework presented

in References [224, 227]. In doing so, we incorporate the effects of the previously discussed observability conditions but neglect systematic effects as well as the large uncertainties of measured cosmological distances.

Even for ultra high energy neutrinos, the most constraining effect in this regard is the rapid oscillating behaviour of P_{ab} within the finite width energy bins. This is caused by the exceedingly large astrophysical baselines L and is equivalent to the oscillation length L_{jk}^{osc} being much smaller than the propagation distance L, leading to a complete averaging of oscillations. To overcome this effect, we find that the relative energy bin width needs to be reduced to at least $\delta E \sim 10^{-5}\,\%$ when observing neutrinos in the PeV range from Galactic pulsars. Moreover, we find the latter to be the most promising candidate sources for decoherence searches in astrophysical neutrinos.

Finally, inspired by these results, we apply our approximated formula for the flavour transition amplitude in order to show that any gravitationally induced effect can be safely neglected at current and near-future neutrino experiments. This is again mainly due to the reason that currently no oscillations can be observed in astrophysical neutrinos and because ultra-relativistic or quasi degenerate non-relativistic mass eigenstates follow geodesics that are too similar to each other in order to yield a different decoherence limit than the standard one. Observing a different decoherence limit in astrophysical neutrinos either implies the presence of regions of strong curvature near the neutrino path or new physics, like e.g. a violation of the equivalence principle.

6 Conclusion and Outlook

In this thesis, we have demonstrated that neutrino flavour transitions are a powerful and versatile tool in fundamental physics. From cosmology to multimessenger astronomy to collider experiments, neutrino flavour dynamics offer key insights into a wide range of new physics scenarios. As each chapter already includes detailed summaries, we now briefly highlight the main results and place them in a broader context.

In Chapter 3, we have examined the cosmological impact of a light sterile neutrino with altered dispersion relations (ADRs) and a feeble Yukawa coupling to axion-like particle (ALP) dark matter (DM). Our focus has been on how this additional light degree of freedom (DOF) influences early Universe observables such as the cosmic microwave background (CMB) and the helium abundance from big bang nucleosynthesis (BBN), as well as its effects on structure formation at later stages of the cosmic evolution.

Using the density matrix formalism to consistently account for neutrino oscillations and interactions with the thermal plasma, we have shown that the ALP-induced, time-dependent sterile neutrino mass can suppress its early-time population while still permitting active–sterile oscillations today. This demonstrates that a light sterile neutrino with ADRs still remains a viable explanation of the short baseline (SBL) anomalies without necessarily coming in conflict with cosmological observations or the results of long baseline (LBL) and atmospheric neutrino oscillation experiments.

The deep connection between neutrino physics and cosmology is further pronounced by the latest Dark Energy Spectroscopic Instrument (DESI) data release [266, 267]. When combining CMB observations with late-time expansion data, fitting the standard cosmological-constant-cold-dark-matter (ΛCDM) model with three light neutrinos results in a neutrino mass sum that conflicts with laboratory constraints by up to 3σ [268]. In contrast, fitting the data with evolving dark energy (DE) models—such as the $\omega_0\omega_a$CDM model—significantly reduces this tension, highlighting the crucial role of neutrino physics in shaping a consistent cosmological standard model.

If future data confirm this discrepancy with ΛCDM, it would be compelling to explore how bounds on sterile neutrino mass and mixing parameters change, assuming different evolving DE models. First analyses on this subject have been conducted for example in References [269, 270]. Like active neutrinos, light sterile neutrinos act as radiation before last scattering but become non-relativistic earlier than their lighter counterparts, potentially affecting structure formation more strongly. This makes them a DM component, that can be constrained by DESI's late-time expansion and baryon acoustic oscillation measurements.

In parallel with these model-dependent cosmological probes, upcoming results from the Karlsruhe Tritium Neutrino (KATRIN) [271, 272] and Princeton Tritium Observatory for Light, Early Universe, Massive Neutrino Yield (PTOLEMY) [273, 274] experiments could reveal crucial, model-independent insights about the absolute neutrino mass scale, the existence of mostly sterile mass eigenstates and the properties of the cosmic neutrino background (CνB). Integrating these experimental findings into the analyses of cosmological data may not only enhance our understanding of neutrino physics, but also offer new perspectives on the nature of DE—potentially redefining the cosmological standard model.

Beyond early Universe physics, neutrinos may also offer a window into the fundamental nature of spacetime, as discussed in Chapter 4. There, we have explored phenomenological quantum gravity (QG) models predicting a flavour-independent decoherence signature in ultra-high-energy neutrinos that have travelled over astrophysical distances. These models are motivated by the idea that QG interactions may violate global charges [154, 155]. Extending this concept, we have proposed that QG effects could induce transitions between neutrinos and hypothetical dark fermions, leading to a uniform transition probability $P_{ab} \to 1/n_f$, where n_f is the total number of participating fermion species. Candidates for such dark fermions include light sterile neutrinos—as the one discussed in Chapter 3—or potentially heavier species, depending on the extent of Poincaré symmetry violation in QG.

With state-of-the-art neutrino telescopes, like IceCube at the south pole, the Cubic Kilometre Neutrino Telescope (KM3NeT) detector in the Mediterranean as well as the proposed Pacific Ocean Neutrino Experiment (P-ONE) in the pacific ocean, we are at the dawn of ultra-high-energy neutrino astronomy. Over the coming decades, these observatories will collect atmospheric and astrophysical neutrino events—like the recent $E_\nu \sim 220\,\mathrm{PeV}$ neutrino event reported by the KM3NeT collaboration [275]—to study neutrino properties and the mechanisms behind cosmic particle acceleration. This effort is supported by collider-based neutrino experiments such as the Forward Search Experiment (FASER) [276, 277] and Scattering and Neutrino Detector at the Large Hadron Collider (SND@LHC) [277, 278] that refine our understanding of hadronic neutrino production. Together, these developments open new possibilities for detecting exotic decoherence effects, like those discussed in Chapter 4, offering novel insights into the quantum nature of spacetime and a hypothetical fermionic dark sector.

Promising targets include neutrino point sources like the active galactic nucleus NGC 1068 [261]. Identifying multiple *standard-candle* sources with similar neutrino production mechanisms would enable flux dip searches, as proposed in Section 4.2, reducing uncertainties rooted in neutrino flux modelling. These analyses will also benefit from atmospheric neutrino studies, where the additional distance information helps to distinguish between competing new physics scenarios, as shown in Section 4.3.

Neutrino flavour dynamics may be influenced not only by QG effects but also by classical gravity. This is due to the fact that the interference between mass eigenstate wave packets (WPs) strongly depends on their individual trajectories, which are, in turn, determined by the global spacetime geometry. However, as discussed in Chapter 5, such effects are only significant for astrophysical neutrinos, since Earth's gravitational field is too weak to cause observable

consequences. For astrophysical neutrinos, flavour oscillations are nearly impossible to resolve, leaving a gravitationally altered decoherence limit as the only detectable signature. This requires the presence of regions with extreme curvature, leading to a significant distortion of the shape or average geodesics of neutrino mass eigenstate WPs. If electromagnetic (EM) or gravitational wave (GW) data can rule out classical curvature as the cause of such effects, any observation of an altered decoherence limit would point to new physics, as considered in Chapter 4.

For the opposite scenario where neutrinos originate from or traverse extreme gravitational environments, such that the assumptions underlying the weak-field approximation—cf. Section 5.2—are violated, it is worthwhile exploring if the more general expression for the flavour transition amplitude from Section 5.1 can be further evaluated by employing path integral techniques. Moreover, in order to extend the framework developed in Chapter 5 to account for even more extreme scenarios, we propose treating the entire production–propagation–detection process within the formalism of interacting quantum field theory (QFT) in curved spacetime. This is, for example, necessary as soon as gravitational particle production becomes non-negligible, or if the production, propagation, and detection processes cannot be treated independently from each other anymore.

A Appendix - Theoretical Foundations

In this appendix chapter, we provide supplemental material for the discussion of the theoretical foundations of this thesis, outlined in Chapter 2. In Section A.1, we start with a detailed discussion of the semiclassical Boltzmann equation, introduced in Section 2.2.

A.1 Full Collision Term for the Boltzmann Equation

The collision terms introduced in Equation (2.44) are given by [31]

$$\begin{aligned}\mathcal{C}_i[t,p,\{f_j\}_j] = \sum_{\mathcal{P}} \frac{1}{E_i} \left[\prod_{l\neq i} \int \frac{g_l}{(2\pi)^3} \frac{\mathrm{d}^3\vec{k}_l}{2E_l}\right] (2\pi)^4 \delta^{(4)} \left(\sum_{j\in I_{\mathcal{P}}} k_j^\mu - \sum_{f\in F_{\mathcal{P}}} k_f^\mu\right) \\ \times \left\{ \overline{|\mathcal{M}(I_{\mathcal{P}} \to F_{\mathcal{P}})|}^2 \prod_{j\in I_{\mathcal{P}}} f_j(t,k_j) \prod_{f\in F_{\mathcal{P}}} (1 \pm f_f(t,k_f)) \right. \\ \left. - \overline{|\mathcal{M}(F_{\mathcal{P}} \to I_{\mathcal{P}})|}^2 \prod_{f\in F_{\mathcal{P}}} f_f(t,k_f) \prod_{j\in I_{\mathcal{P}}} (1 \pm f_j(t,k_j)) \right\}.\end{aligned} \tag{A.1}$$

Here, we sum over all processes $\mathcal{P}$ involving the particle i with momentum p in the corresponding final state $F_{\mathcal{P}}$. We account for the corresponding back reaction, where the particle i with momentum p is in the initial state I, by subtracting the rate for the inverse process in the second term in curly braces. The forward directed process $I \to F$ hence produces the particle i with momentum p while the inverse process $F \to I$ annihilates the particle i with momentum p from the particle ensemble. This may happen either due to scattering of the same particle to a different momentum state p' or by decay or scattering processes resulting in entirely different particle species. Moreover, for each accompanying particle state l in the initial and final states we integrate over the respective phase space and multiply by the corresponding internal number of DOFs g_l. The probabilities of the respective processes are determined by the spin averaged squared matrix elements $\overline{|\mathcal{M}|^2}$, the momentum conserving delta function as well as by the phase space distribution functions for all participating particles. For each particle in the initial state of a process we simply need to include a factor of the appropriate phase space density f_j parametrising the availability of the corresponding particle. In contrast to that, for final state particles, we include the so-called bose enhancement factors $(1 + f_f)$ or Pauli blocking factors $(1 - f_f)$ depending on whether the corresponding particle is of bosonic or fermionic type, respectively. In the former case an already occupied final state attracts new particles while in the latter case an occupied final state suppresses the production of the same state.

Particles fulfilling the Boltzmann limit $E_i \gg T$, where T is the temperature of photons[1], are sufficiently suppressed such that the blocking and enhancement factors can be approximated by $1 \pm f \approx 1$. This is for example the case if $m_i \gg T$.

Moreover, if a process is CP or T symmetric the corresponding matrix elements for the forward and backward reactions are equal to each other simplifying the respective collision term. . Then, in Sections A.2 to A.4, we present extended computations and discussions on the quantum field theoretical approach to neutrino oscillations, also called the external WP formalism. Afterwards in Section A.5, we perform detailed computations of the neutrino flavour transition amplitude and probability for the example of Gaussian neutrino WPs considered within the quantum mechanical internal WP approach to neutrino oscillations. This topic is introduced in Section 2.3.2. Finally, we list the full expressions for matter attenuation terms in the effective flavour space approach to neutrino oscillations in Section A.6.

A.2 Lehmann–Symanzik–Zimmerman Reduction of the Macroscopic Amplitude

Applying the Lehmann–Symanzik–Zimmerman (LSZ) reduction formula to the process shown in Figure 2.1 yields the following expression for the associated amplitude at lowest order in

[1]Photons are chosen as the reference particle species as they are massless, and hence, represent exact radiation. Moreover, from the CMB we know that photons almost exactly follow their equilibrium distribution due to the very fast EM interactions.

the skeleton expansion

$$
\begin{aligned}
\mathcal{A}_{ab} = & \iint \mathrm{d}^4 z_1 \, \mathrm{d}^4 z_2 \iint \mathrm{d}^4 y_1 \, \mathrm{d}^4 y_2 \\
& \times \int \frac{\mathrm{d}^3 \vec{q}_1'}{(2\pi)^3 2 q_1^{0\prime}} \varphi_n^{\mathrm{D}}(\vec{q}_1', \vec{Q}_1') \\
& \times \iint \mathrm{d}^3 \vec{k}_1' (2\pi)^3 2 k_1^{0\prime} \frac{\mathrm{d}^3 \vec{k}_2'}{(2\pi)^3 2 k_2^{0\prime}} \varphi_p^{\mathrm{D}*}(\vec{k}_1', \vec{K}_1') \varphi_b^{\mathrm{D}*}(\vec{k}_2', \vec{K}_2') \\
& \times \left[\bar{u}_{r_1'}^p(k_1') e^{ik_1' \left(z_1 - X_1^{\mathrm{D}_F} \right)} \frac{g}{\sqrt{2}} \gamma^\mu P_L u_{s_1'}^n(q_1') e^{-iq_1' \left(z_1 - X_1^{\mathrm{D}_I} \right)} \right] \\
& \times D_{\mu\nu}^W(z_1 - z_2) \\
& \times \left[\bar{u}_{r_2'}^b(k_2') e^{ik_2' (z_2 - X_2^{\mathrm{D}_F})} \frac{g}{\sqrt{2}} \gamma^\nu P_L \right] \\
& \times \sum_j U_{bj} S_j(z_2 - y_2) U_{aj}^* \\
& \times \iint \frac{\mathrm{d}^3 \vec{q}_1}{(2\pi)^3 2 q_1^0} \frac{\mathrm{d}^3 \vec{q}_2}{(2\pi)^3 2 q_2^0} \varphi_p^{\mathrm{S}}(\vec{q}_1, \vec{Q}_1) \varphi_a^{\mathrm{S}}(\vec{q}_2, \vec{Q}_2) \\
& \times \int \frac{\mathrm{d}^3 \vec{k}_1}{(2\pi)^3 2 k_1^0} \varphi_n^{\mathrm{S}*}(\vec{k}_1, \vec{K}_1) \\
& \times \left[\frac{g}{\sqrt{2}} \gamma^\sigma P_L u_{s_2}^a(q_2) e^{iq_2 (y_2 - X_2^{\mathrm{S}_I})} \right] \\
& \times D_{\sigma\rho}^W(y_2 - y_1) \\
& \times \left[\bar{u}_{r_1}^n(k_1) e^{-ik_1 \left(y_1 - X_1^{\mathrm{S}_F} \right)} \frac{g}{\sqrt{2}} \gamma^\rho P_L u_{s_1}^p(q_1) e^{iq_1 \left(y_1 - X_1^{\mathrm{S}_I} \right)} \right] .
\end{aligned}
\tag{A.2}
$$

In fact, the simple left-handed currents describing the weak interactions of hadrons in the formula for the amplitude need to be replaced by the appropriate, more complicated hadronic currents as described in Reference [54]. As this is of no further significance for the following discussion, we stick to this simple picture in order to simplify the calculations.

As one can easily see, the amplitude above separates into one neutrino detection and one neutrino production complex solely connected by the neutrino propagator. By substituting in the momentum space representation of the boson propagators and rearranging the integrals

and phase factors, we arrive at the expression

$$\begin{aligned}
\mathcal{A}_{ab} = &\int \mathrm{d}^3\tilde{q}_1'\, \varphi_n^{\mathrm{D}}(\vec{q}_1', \vec{Q}_1') \iint \mathrm{d}^3\tilde{k}_1'\, \mathrm{d}^3\tilde{k}_2'\, \varphi_p^{\mathrm{D}*}(\vec{k}_1', \vec{K}_1')\varphi_b^{\mathrm{D}*}(\vec{k}_2', \vec{K}_2') \\
&\times e^{iq_1' X_1^{\mathrm{D}\,I} - ik_1' X_1^{\mathrm{D}\,F} - ik_2' X_2^{\mathrm{D}\,F}} \\
&\int \frac{\mathrm{d}^4\pi_{\mathrm{D}}}{(2\pi)^4} \int \mathrm{d}^4 z_1\, e^{-i(q_1'+\pi_{\mathrm{D}}-k_1')z_1} \int \mathrm{d}^4 z_2\, e^{i(k_2'+\pi_{\mathrm{D}})z_2} \\
&\times \left[\bar{u}^p_{r_1'}(k_1') \frac{g}{\sqrt{2}} \gamma^\mu P_L u^n_{s_1'}(q_1')\right] \tilde{D}^W_{\mu\nu}(\pi_{\mathrm{D}}) \left[\bar{u}^b_{r_2'}(k_2') \frac{g}{\sqrt{2}} \gamma^\nu P_L\right] \\
&\times \int \mathrm{d}^4 y_2 \sum_j U_{bj} S_j(z_2 - y_2) U^*_{aj} \\
&\times \iint \mathrm{d}^3\tilde{q}_1\, \mathrm{d}^3\tilde{q}_2\, \varphi_p^{\mathrm{S}}(\vec{q}_1, \vec{Q}_1)\varphi_a^{\mathrm{S}}(\vec{q}_2, \vec{Q}_2) \int \mathrm{d}^3\tilde{k}_1\, \varphi_n^{\mathrm{S}*}(\vec{k}_1, \vec{K}_1) \\
&\times e^{-iq_2 X_2^{\mathrm{S}\,I} + ik_1 X_1^{\mathrm{S}\,F} - iq_1 X_1^{\mathrm{S}\,I}} \\
&\times \int \frac{\mathrm{d}^4\pi_{\mathrm{S}}}{(2\pi)^4} \int \mathrm{d}^4 y_1\, e^{-i(k_1 - q_1 - \pi_{\mathrm{S}})y_1} e^{-i(\pi_{\mathrm{S}} - q_2)y_2} \\
&\times \left[\frac{g}{\sqrt{2}} \gamma^\sigma P_L u^a_{s_2}(q_2)\right] \tilde{D}^W_{\sigma\rho}(\pi_{\mathrm{S}}) \left[\bar{u}^n_{r_1}(k_1) \frac{g}{\sqrt{2}} \gamma^\rho P_L u^p_{s_1}(q_1)\right] ,
\end{aligned} \tag{A.3}$$

where we introduce the short form for the Lorentz-invariant phase space measures

$$\mathrm{d}^3\tilde{q} := \frac{\mathrm{d}^3\vec{q}}{(2\pi)^3 2q^0} \,. \tag{A.4}$$

Next, we can execute all spacetime coordinate integrals of all vertices apart from those to which the neutrino propagator is attached. Of course we could also decompose the neutrino propagator in the same fashion as we have decomposed the boson propagators, but for the further calculation it will be useful to apply a different procedure to S_j.

From the remaining vertex integrals we get momentum conservation delta functions as usual

allowing us to also execute all explicit internal propagator integrals to get

$$\begin{aligned}\mathcal{A}_{ab} = &\int \mathrm{d}^3\tilde{q}_1'\, \varphi_n^{\mathrm{D}}(\vec{q}_1', \vec{Q}_1') \iint \mathrm{d}^3\tilde{k}_1'\, \mathrm{d}^3\tilde{k}_2'\, \varphi_p^{\mathrm{D}*}(\vec{k}_1', \vec{K}_1')\varphi_b^{\mathrm{D}*}(\vec{k}_2', \vec{K}_2') \\ &\times e^{iq_1' X_1^{\mathrm{D}_I} - ik_1' X_1^{\mathrm{D}_F} - ik_2' X_2^{\mathrm{D}_F}} \int \mathrm{d}^4 z_2\, e^{i(k_2'+k_1'-q_1')z_2} \\ &\times \iint \mathrm{d}^3\tilde{q}_1\, \mathrm{d}^3\tilde{q}_2\, \varphi_p^{\mathrm{S}}(\vec{q}_1, \vec{Q}_1)\varphi_a^{\mathrm{S}}(\vec{q}_2, \vec{Q}_2) \int \mathrm{d}^3\tilde{k}_1\, \varphi_n^{\mathrm{S}*}(\vec{k}_1, \vec{K}_1) \\ &\times e^{-iq_2 X_2^{\mathrm{S}_I} + ik_1 X_1^{S_F} - iq_1 X_1^{\mathrm{S}_I}} \int \mathrm{d}^4 y_2\, e^{-i(k_1-q_1-q_2)y_2} \\ &\times \left[\bar{u}_{r_1'}^p(k_1')\frac{g}{\sqrt{2}}\gamma^\mu P_L u_{s_1'}^n(q_1')\right] \tilde{D}_{\mu\nu}^W(k_1'-q_1') \left[\bar{u}_{r_2'}^b(k_2')\frac{g}{\sqrt{2}}\gamma^\nu P_L\right] \\ &\times \sum_j U_{bj} S_j(z_2-y_2) U_{aj}^* \\ &\times \left[\frac{g}{\sqrt{2}}\gamma^\sigma P_L u_{s_2}^a(q_2)\right] \tilde{D}_{\sigma\rho}^W(k_1-q_1) \left[\bar{u}_{r_1}^n(k_1)\frac{g}{\sqrt{2}}\gamma^\rho P_L u_{s_1}^p(q_1)\right] .\end{aligned} \tag{A.5}$$

Even though the momentum space WPs of the external particles are not given by delta functions, we assume they are still strongly peaked in momentum space. Therefore, we can evaluate the weakly momentum-dependent, incomplete matrix elements,

$$\tilde{M}_{\mathrm{S}}(q_1, q_2, k_1) := \frac{g^2}{2}\left[\gamma^\sigma P_L u_{s_2}^a(q_2)\right] \tilde{D}_{\sigma\rho}^W(k_1-q_1)\left[\bar{u}_{r_1}^n(k_1)\gamma^\rho P_L u_{s_1}^p(q_1)\right] , \tag{A.6}$$

$$\tilde{M}_{\mathrm{D}}(q_1', k_1', k_2') := \frac{g^2}{2}\left[\bar{u}_{r_1'}^p(k_1')\gamma^\mu P_L u_{s_1'}^n(q_1')\right] \tilde{D}_{\mu\nu}^W(k_1'-q_1')\left[\bar{u}_{r_2'}^b(k_2')\gamma^\nu P_L\right] , \tag{A.7}$$

at the mean momenta of the WPs and pull them out of the momentum integrals. Note that these partial matrix elements are fully independent of the properties of the neutrino. Furthermore, we define the source and detector overlap functions,

$$\begin{aligned}\mathbb{V}_{\mathrm{S}}(y_2) := &\iiint \mathrm{d}^3\tilde{q}_1\, \mathrm{d}^3\tilde{q}_2\, \mathrm{d}^3\tilde{k}_1\, \varphi_p^{\mathrm{S}}(\vec{q}_1, \vec{Q}_1)\varphi_a^{\mathrm{S}}(\vec{q}_2, \vec{Q}_2)\varphi_n^{\mathrm{S}*}(\vec{k}_1, \vec{K}_1) \\ &\times e^{-iq_2 X_2^{\mathrm{S}_I} + ik_1 X_1^{\mathrm{S}_F} - iq_1 X_1^{\mathrm{S}_I}} e^{-i(k_1-q_1-q_2)y_2} ,\end{aligned} \tag{A.8}$$

$$\begin{aligned}\mathbb{V}_{\mathrm{D}}(z_2) := &\iiint \mathrm{d}^3\tilde{q}_1'\, \mathrm{d}^3\tilde{k}_1'\, \mathrm{d}^3\tilde{k}_2'\, \varphi_n^{\mathrm{D}}(\vec{q}_1', \vec{Q}_1')\varphi_p^{\mathrm{D}*}(\vec{k}_1', \vec{K}_1')\varphi_b^{\mathrm{D}*}(\vec{k}_2', \vec{K}_2') \\ &\times e^{iq_1' X_1^{\mathrm{D}_I} - ik_1' X_1^{\mathrm{D}_F} - ik_2' X_2^{\mathrm{D}_F}} e^{i(k_2'+k_1'-q_1')z_2} ,\end{aligned} \tag{A.9}$$

representing the product of the Fourier transforms of the momentum space WPs, i.e. the position space WPs,

$$\chi_\psi(x; \vec{P}) := \int \mathrm{d}^3\tilde{p}\, \varphi_\psi(\vec{p}, \vec{P}) e^{-ipx} . \tag{A.10}$$

Therefore, we can also write them as

$$\mathbb{V}_{\mathrm{S}}(y_2) = \chi_p^{\mathrm{S}}\left(z_2 - X_1^{\mathrm{S}_I}; \vec{Q}_1\right)\chi_a^{\mathrm{S}}\left(z_2 - X_2^{\mathrm{S}_I}; \vec{Q}_2\right)\chi_n^{\mathrm{S}*}\left(z_2 - X_1^{\mathrm{S}_F}; \vec{K}_1\right) , \tag{A.11}$$

$$\mathbb{V}_{\mathrm{D}}(z_2) = \chi_n^{\mathrm{D}}\left(y_2 - X_1^{\mathrm{D}_I}; \vec{Q}_1'\right)\chi_p^{\mathrm{D}*}\left(y_2 - X_1^{\mathrm{D}_F}; \vec{K}_1'\right)\chi_b^{\mathrm{D}*}\left(y_2 - X_2^{\mathrm{D}_F}; \vec{K}_2'\right) . \tag{A.12}$$

The full amplitude can then be expressed as

$$\begin{aligned}\mathcal{A}_{ab} = \sum_j U^*_{aj} U_{bj} \iint \mathrm{d}^4 z\, \mathrm{d}^4 y\, \mathbb{V}_{\mathrm{D}}(z) \mathbb{V}_{\mathrm{S}}(y) \\ \times \tilde{M}_{\mathrm{D}}(Q_1', K_1', K_2') S_j(z-y) \tilde{M}_{\mathrm{S}}(Q_1, Q_2, K_1)\,.\end{aligned} \tag{A.13}$$

Here, the overlap functions indicate the regions in spacetime where the external particles meet each other, and therefore, contain the information about the relative position of the neutrino source and detector. As we assume them to be macroscopically separated from each other the spacetime regions $U_{\mathrm{S/D}}$ where $\mathbb{V}_{\mathrm{S/D}}$ are significantly different from zero are disjoint.

The reasoning above indeed works for any neutrino production–propagation–detection process with an arbitrary number of external particles, as in we have not used the individual properties of the specific process under consideration in any step: For every external particle we get one momentum space integral, WP and spacetime shift phase. The correlation function of the neutrino production–propagation–detection process always separates into one production and detection complex connected by a single neutrino propagator attached to one vertex of each complex. Applying the LSZ reduction procedure to this correlator then leads to the incomplete production and detection matrix elements and accompanying phase factors for the external particles. Executing all vertex integrals, except those to which the neutrino propagator is attached, enforces momentum conservation and allows the definition of the overlap functions containing the products of (scalar) position space wave functions of all external particles.

A.3 From the External to the Internal Wave Packet Approach

We show that the flavour transition amplitude given in Equation (2.90) can be rewritten as an amplitude describing the propagation of a superposition of free single-particle state. To this end, we mainly use the fact that by construction the spacetime regions, U_{S} and U_{D}, where the overlap volumes, $\mathbb{V}_{\mathrm{S}}$ and $\mathbb{V}_{\mathrm{D}}$, are significantly different from zero, are spatially macroscopically separated. Note that, however, these regions need not necessarily also be separated macroscopically in the time direction. This will be enforced by the causal structure of the amplitude itself, i.e. the amplitude vanishes if the average world line of the exchanged neutrino cannot connect the regions, U_{S} and U_{D}.

To see this, we use that the vacuum neutrino propagator can be expressed in two different ways

$$S_j(z,y) = \sum_s \int \mathrm{d}^3\vec{p} \left[\Theta(z^0-y^0)\xi^j_{s\vec{p}}(z)\bar{\xi}^j_{s\vec{p}}(y) - \Theta(y^0-z^0)\epsilon^j_{s\vec{p}}(y)\bar{\epsilon}^j_{s\vec{p}}(z)\right] \tag{A.14}$$

$$= \lim_{\varepsilon\to 0} \int \frac{\mathrm{d}^4\vec{p}}{(2\pi)^4} i \frac{\not{p}+m}{p^2-m^2+i\varepsilon} e^{-ip(z-y)}\,. \tag{A.15}$$

In the following, we call the first form the *on-shell* form, that is formulated in terms of the neutrino and antineutrino mode functions, ξ and ϵ, respectively, whereas we call the second

form the *off-shell* form. First by using the off-shell form of the propagator, we can use the findings from References [53, 54] that the antiparticle contribution essentially vanishes for spatially macroscopically separated source and detection vertices. We can see this as follows: First, shifting the origins of the coordinate systems within the vertex integrals around the respective production and detection mean vertices yields

$$\begin{aligned}\mathcal{A}_{ab} = \lim_{\varepsilon\to 0}\sum_j U_{aj}^* U_{bj} \int \frac{\mathrm{d}^4 p}{(2\pi)^4} \iint \mathrm{d}^4 z'\, \mathrm{d}^4 y'\, \mathbb{V}'_{\mathrm{D}}(z') e^{-ipz'} \mathbb{V}'_{\mathrm{S}}(y') e^{ipy'} \\ \times \tilde{M}_{\mathrm{D}}(\{Q'_B\},\{K'_D\}) \frac{\not{p} + m_j}{p^2 - m_j^2 + i\varepsilon} e^{-ip(X_{\mathrm{D}} - X_{\mathrm{S}})} \tilde{M}_{\mathrm{S}}(\{Q_A\},\{K_C\})\,.\end{aligned} \tag{A.16}$$

Here, $\mathbb{V}'_{\mathrm{S/D}}$ are the shifted overlap volumes centered around the origin of the primed coordinate systems. Integrating them together with the phase factors yields [54]

$$\tilde{\delta}^{(4)}_{\mathrm{S}}(p - P_{\mathrm{S}}) := \int \mathrm{d}^4 y'\, \mathbb{V}'_{\mathrm{S}}(y') e^{ipy'}\,, \tag{A.17}$$

$$\tilde{\delta}^{(4)}_{\mathrm{D}}(p + P_{\mathrm{D}}) := \int \mathrm{d}^4 z'\, \mathbb{V}'_{\mathrm{D}}(z') e^{-ipz'}\,. \tag{A.18}$$

The functions $\tilde{\delta}^{(4)}_{\mathrm{S/D}}$ play the role of smeared delta functions enforcing approximate four-momentum conservation at the production and detection vertices. In total the amplitude then becomes

$$\begin{aligned}\mathcal{A}_{ab} = \lim_{\varepsilon\to 0}\sum_j U_{aj}^* U_{bj} \int \frac{\mathrm{d}^4 p}{(2\pi)^4} \frac{\tilde{\delta}^{(4)}(p - P_{\mathrm{S}}) \tilde{\delta}^{(4)}(p + P_{\mathrm{D}}) e^{i\vec{p}\vec{L}}}{p^2 - m_j^2 + i\varepsilon} e^{-ip^0(X^0_{\mathrm{D}} - X^0_{\mathrm{S}})} \\ \times \tilde{M}_{\mathrm{D}}(\{Q'_B\},\{K'_D\}) \left(\not{p} + m_j\right) \tilde{M}_{\mathrm{S}}(\{Q_A\},\{K_C\})\,,\end{aligned} \tag{A.19}$$

where we have defined the spatial distance vector $\vec{L} := \vec{X}_{\mathrm{D}} - \vec{X}_{\mathrm{S}}$. Since $\vec{L}$ is large per construction, the associated phase factor oscillates rapidly erasing all off-shell contributions of the neutrino propagator under the integral. Only the particle and antiparticle pole contribute at leading order in the $1/|\vec{L}|$ expansion as can be shown using the Grimus–Stockinger theorem [51]. Depending on the exact structure of the process, the energy conservation part of the smeared delta functions then selects whether the particle or the antiparticle pole contributes to the overall amplitude. In the currently considered scenario, of course, the particle pole is picked up.

Using the on-shell representation of the propagator this immediately translates to

$$\begin{aligned}\mathcal{A}_{ab} = \sum_j U^*_{aj}U_{bj} \iint \mathrm{d}^4z\,\mathrm{d}^4y\,\mathbb{V}_{\mathrm{D}}(z)\mathbb{V}_{\mathrm{S}}(y) \\ \times \Big\{\Theta(z^0-y^0)\sum_s \int \mathrm{d}^3\vec{p}\,\tilde{M}_{\mathrm{D}}(\{Q'_B\},\{K'_D\})\xi_{j;s\vec{p}}(z)\bar{\xi}_{j;s\vec{p}}(y)\tilde{M}_{\mathrm{S}}(\{Q_A\},\{K_C\}) \\ - \Theta(y^0-z^0)\sum_s \int \mathrm{d}^3\vec{p}\,\tilde{M}_{\mathrm{D}}(\{Q'_B\},\{K'_D\})\epsilon_{j;s\vec{p}}(z)\bar{\epsilon}_{j;s\vec{p}}(y)\tilde{M}_{\mathrm{S}}(\{Q_A\},\{K_C\})\Big\}\end{aligned} \tag{A.20}$$

$$\begin{aligned}\approx \sum_j U^*_{aj}U_{bj}\sum_s \int \mathrm{d}^3\vec{p} \iint \mathrm{d}^4z\,\mathrm{d}^4y\,\mathbb{V}_{\mathrm{D}}(z)\mathbb{V}_{\mathrm{S}}(y)\Theta(z^0-y^0) \\ \times \tilde{M}_{\mathrm{D}}(\{Q'_B\},\{K'_D\})\xi_{j;s\vec{p}}(z)\bar{\xi}_{j;s\vec{p}}(y)\tilde{M}_{\mathrm{S}}(\{Q_A\},\{K_C\})\,.\end{aligned} \tag{A.21}$$

In order to be able to define effective neutrino WPs, we next evaluate the Heaviside function at the mean production and detection times and pull it out of the integrals, i.e.

$$\begin{aligned}\mathcal{A}_{ab} \approx \Theta(X^0_{\mathrm{D}}-X^0_{\mathrm{S}})\sum_j U^*_{aj}U_{bj}\sum_s \int \mathrm{d}^3\vec{p} \iint \mathrm{d}^4z\,\mathrm{d}^4y\,\mathbb{V}_{\mathrm{D}}(z)\mathbb{V}_{\mathrm{S}}(y) \\ \times \tilde{M}_{\mathrm{D}}(\{Q'_B\},\{K'_D\})\xi_{j;s\vec{p}}(z)\bar{\xi}_{j;s\vec{p}}(y)\tilde{M}_{\mathrm{S}}(\{Q_A\},\{K_C\})\,.\end{aligned} \tag{A.22}$$

Here, we use that the amplitude approximately vanishes for all U_{S} and U_{D} that are spatially macroscopically separated, but close to each other in time, i.e. in all cases where the Heaviside function could not be simply pulled out of the integral. This is indeed the case as the integral

$$D_j(z-y) := \sum_s \int \mathrm{d}^3\vec{p}\,\xi_{j;s\vec{p}}(z)\bar{\xi}_{j;s\vec{p}}(y)\,, \tag{A.23}$$

is exponentially suppressed at space-like distances, and therefore, approximately vanishes for large $\vec{L}$ but small $X^0_{\mathrm{D}}-X^0_{\mathrm{S}} \ll |\vec{L}|$.

The final step in the transition from the external to the internal WP approach now is to expand the generic mode functions ξ in terms of the mode functions accustom to the observers, O_{S} and O_{D}, at the source and detector, respectively. As in the main text, we call them ξ^{S} and ξ^{D} and we assume them to give rise to equivalent notions of particles as the one defined by ξ. This requirement implies

$$\langle \xi^{\mathrm{S}}_{j;s\vec{p}}, \epsilon^{\mathrm{D}}_{j;s'\vec{p}'}\rangle \equiv \langle \xi^{\mathrm{S}}_{j;s\vec{p}}, \epsilon_{j;s'\vec{p}'}\rangle \equiv \langle \xi^{\mathrm{D}}_{j;s\vec{p}}, \epsilon_{j;s'\vec{p}'}\rangle \equiv 0\,, \tag{A.24}$$

and analogously for the scalar products with $\xi \leftrightarrow \epsilon$. From this we furthermore infer that the identity on the one-particle sub-spaces of all mode constructions can be expressed as

$$\mathbb{1}|_{\text{1-particle}}[\cdot] = \sum_s \int \mathrm{d}^3\vec{p}\,\langle \xi^{\mathrm{S}}_{j;s\vec{p}}, \cdot\rangle \xi^{\mathrm{S}}_{j;s\vec{p}} \tag{A.25}$$

$$= \sum_s \int \mathrm{d}^3\vec{p}\,\langle \xi^{\mathrm{D}}_{j;s\vec{p}}, \cdot\rangle \xi^{\mathrm{D}}_{j;s\vec{p}} \tag{A.26}$$

$$= \sum_s \int \mathrm{d}^3\vec{p}\,\langle \xi_{j;s\vec{p}}, \cdot\rangle \xi_{j;s\vec{p}}\,, \tag{A.27}$$

being equivalent to the statement that the different particle modes fulfil a completeness relation on all spaces spanned by the different mode functions. Using this property, we can insert two identities within Equation (A.22) and get

$$\begin{aligned}\mathcal{A}_{ab} \approx\ & \Theta(X_{\mathrm{D}}^0 - X_{\mathrm{S}}^0) \sum_j U_{aj}^* U_{bj} \sum_s \int \mathrm{d}^3\vec{p} \iint \mathrm{d}^4 z\, \mathrm{d}^4 y\, \mathbb{V}_{\mathrm{D}}(z) \mathbb{V}_{\mathrm{S}}(y) \\ & \times \tilde{M}_{\mathrm{D}}(\{Q'_B\}, \{K'_D\}) \left(\sum_r \int \mathrm{d}^3\vec{q}\, \langle \xi^{\mathrm{D}}_{j;r\vec{q}}, \xi_{j;s\vec{p}} \rangle \xi^{\mathrm{D}}_{j;r\vec{q}}(z) \right) \\ & \times \left(\sum_{r'} \int \mathrm{d}^3\vec{q}'\, \langle \xi_{j;s\vec{p}}, \xi^{\mathrm{S}}_{j;r'\vec{q}'} \rangle \bar{\xi}^{\mathrm{S}}_{j;r'\vec{q}'}(y) \right) \tilde{M}_{\mathrm{S}}(\{Q_A\}, \{K_C\}) \end{aligned} \tag{A.28}$$

$$\begin{aligned} =\ & \Theta(X_{\mathrm{D}}^0 - X_{\mathrm{S}}^0) \sum_j U_{aj}^* U_{bj} \sum_{rr'} \iint \mathrm{d}^3\vec{q}\, \mathrm{d}^3\vec{q}' \iint \mathrm{d}^4 z\, \mathrm{d}^4 y\, \mathbb{V}_{\mathrm{D}}(z) \mathbb{V}_{\mathrm{S}}(y) \\ & \times \left(\tilde{M}_{\mathrm{D}}(\{Q'_B\}, \{K'_D\}) \xi^{\mathrm{D}}_{j;r\vec{q}}(z) \right) \left(\bar{\xi}^{\mathrm{S}}_{j;r'\vec{q}'}(y) \tilde{M}_{\mathrm{S}}(\{Q_A\}, \{K_C\}) \right) \\ & \times \left(\sum_s \int \mathrm{d}^3\vec{p}\, \langle \xi^{\mathrm{D}}_{j;r\vec{q}}, \xi_{j;s\vec{p}} \rangle \langle \xi_{j;s\vec{p}}, \xi^{\mathrm{S}}_{j;r'\vec{q}'} \rangle \right) \end{aligned} \tag{A.29}$$

$$\begin{aligned} =\ & \Theta(X_{\mathrm{D}}^0 - X_{\mathrm{S}}^0) \sum_j U_{aj}^* U_{bj} \sum_{rr'} \iint \mathrm{d}^3\vec{q}\, \mathrm{d}^3\vec{q}' \iint \mathrm{d}^4 z\, \mathrm{d}^4 y\, \mathbb{V}_{\mathrm{D}}(z) \mathbb{V}_{\mathrm{S}}(y) \\ & \times \left(\tilde{M}_{\mathrm{D}}(\{Q'_B\}, \{K'_D\}) \xi^{\mathrm{D}}_{j;r\vec{q}}(z) \right) \left(\bar{\xi}^{\mathrm{S}}_{j;r'\vec{q}'}(y) \tilde{M}_{\mathrm{S}}(\{Q_A\}, \{K_C\}) \right) \langle \xi^{\mathrm{D}}_{j;r\vec{q}}, \xi^{\mathrm{S}}_{j;r'\vec{q}'} \rangle \,. \end{aligned} \tag{A.30}$$

Now defining the effective internal neutrino WPs as

$$\Phi^{\mathrm{S}}_{j;r'}(\vec{q}') := \int \mathrm{d}^4 x\, \mathbb{V}_{\mathrm{S}}(x) \bar{\xi}^{\mathrm{S}}_{j;r'\vec{q}'}(x) \tilde{M}_{\mathrm{S}}(\{Q_A\}, \{K_C\}) \,, \tag{A.31}$$

$$\Phi^{\mathrm{D}}_{j;r}(\vec{q}) := \int \mathrm{d}^4 x\, \mathbb{V}_{\mathrm{D}}(x) \tilde{M}_{\mathrm{D}}(\{Q'_B\}, \{K'_D\}) \xi^{\mathrm{D}}_{j;r\vec{q}}(z) \,, \tag{A.32}$$

yields the simple expression

$$\mathcal{A}_{ab} \approx \Theta(X_{\mathrm{D}}^0 - X_{\mathrm{S}}^0) \sum_j U_{aj}^* U_{bj} \sum_{rr'} \iint \mathrm{d}^3\vec{q}\, \mathrm{d}^3\vec{q}'\, \Phi^{\mathrm{D}}_{j;r}(\vec{q}) \Phi^{\mathrm{S}}_{j;r'}(\vec{q}') \langle \xi^{\mathrm{D}}_{j;r\vec{q}}, \xi^{\mathrm{S}}_{j;r'\vec{q}'} \rangle \,. \tag{A.33}$$

A.4 Neutrino Oscillation Probability in the External Wave Packet Approach

It can be shown that the squared amplitude of the production–propagation–detection process assumes the form [54]

$$\begin{aligned} |\mathcal{A}_{ab}|^2 = \int \mathrm{d}E & \frac{(2\pi)^4 \delta_{\mathrm{S}}(q - P_{\mathrm{S}}) |M_{\mathrm{S}}|^2 \mathcal{V}_{\mathrm{S}}}{\prod_{A=1}^{n_I} 2Q_A^0 \prod_{C=1}^{n_F} 2K_C^0} \frac{(2\pi)^4 \delta_{\mathrm{D}}(q + P_{\mathrm{D}}) |M_{\mathrm{D}}|^2 \mathcal{V}_{\mathrm{D}}}{\prod_{B=1}^{m_I} 2Q_B^{0\prime} \prod_{D=1}^{m_F} 2K_D^{0\prime}} \\ & \times \frac{\tilde{\mathcal{P}}_{ab}(E; X_{\mathrm{S}}, X_{\mathrm{D}})}{|\vec{X}_{\mathrm{D}} - \vec{X}_{\mathrm{S}}|^2} \,, \end{aligned} \tag{A.34}$$

where E is the neutrino energy, q the neutrino four-momentum and $\delta_{\mathrm{S/D}}$ are the smeared momentum conserving delta functions in the source and detector with the mean four-momenta of the produced and detected effective neutrino WPs,

$$P^{\mu}_{\mathrm{S}} = \sum_{A} Q^{\mu}_{A} - \sum_{C} K^{\mu}_{C}\,, \qquad\qquad P^{\mu}_{\mathrm{D}} = \sum_{B} Q^{\mu\prime}_{B} - \sum_{D} K^{\mu\prime}_{D}\,. \tag{A.35}$$

Furthermore, $\mathcal{V}_{\mathrm{S/D}}$ represents the overlap factor of the external WPs in the source / detector depending on the mean spacetime coordinates $X_A^{\mathrm{S/D}_{I/F}}$ and mean momenta of the external particles. Moreover, $|M_{\mathrm{S/D}}|^2$ are the full production / detection matrix elements and $\widetilde{\mathcal{P}}_{ab}$ is the progenitor of what will result in the oscillation probability.

Now, in order to obtain the experimentally measurable event count we average $|\mathcal{A}_{ab}|^2$ over the mean momenta, mean positions and spin configurations of all initial state particles using the phase space densities $f_{\psi}(s, \vec{P}, X)$, defined such that when integrated over phase space the particle number of species ψ at time X^0 is obtained, i.e.

$$N_{\psi}(X^0) = \sum_{s} \iint \mathrm{d}^3\vec{X}\, \frac{\mathrm{d}^3\vec{P}}{(2\pi)^3} f_{\psi}(s, \vec{P}, X)\,. \tag{A.36}$$

The mean positions $\vec{X}$ are identical with the spacetime shifts that we have embedded into the definition of the external WPs as starting / ending points before and after the collisions. For the final state particles we integrate and sum over all spins, momenta and positions except the mean particle momenta in the detector which we assume to be registered by the experiment. The differential count rate is then given by

$$\begin{aligned}
\mathrm{d}N_{ab} = \sum_{\text{spins}} \prod_{A=1}^{n_I} \int \mathrm{d}^3\vec{X}_A^{\mathrm{S}_I} \int \frac{\mathrm{d}^3\vec{Q}_A}{(2\pi)^3} f_A^{\mathrm{S}}(s_A, \vec{Q}_A, X_A^{\mathrm{S}_I}) \\
\times \prod_{B=1}^{m_I} \int \mathrm{d}^3\vec{X}_B^{\mathrm{D}_I} \int \frac{\mathrm{d}^3\vec{Q}'_B}{(2\pi)^3} f_B^{\mathrm{D}}(s_B, \vec{Q}'_B, X_B^{\mathrm{D}_I}) \\
\times \prod_{C=1}^{n_F} \int \mathrm{d}^3\vec{X}_C^{\mathrm{S}_F} \int \frac{\mathrm{d}^3\vec{K}_C}{(2\pi)^3} \prod_{D=1}^{m_F} \int \mathrm{d}^3\vec{X}_D^{\mathrm{D}_F} \frac{\mathrm{d}^3\vec{K}'_D}{(2\pi)^3} |\mathcal{A}_{ab}|^2\,.
\end{aligned} \tag{A.37}$$

Note that (in our idealised model) we do not have to include a time integral for each particle coordinate as we assume the only processes happening is the neutrino production–propagation–detection process, and hence, knowing the average positions and momenta of any particle species at a fixed time X^0_A is sufficient, as all the particle dynamics is encoded within $\mathcal{A}_{ab}$.

Next, we disassemble the overlap factors [54],

$$\mathcal{V}_{\mathrm{S}} = N_{\mathrm{S}} \int \mathrm{d}^4 y \prod_{A} |\chi_A(y - X_A^{\mathrm{S}_I}; Q_A)|^2 \prod_{C} |\chi_C(y - X_C^{\mathrm{S}_F}; K_C)|^2\,, \tag{A.38}$$

$$\mathcal{V}_{\mathrm{D}} = N_{\mathrm{D}} \int \mathrm{d}^4 z \prod_{B} |\chi_B(z - X_B^{\mathrm{D}_I}; Q'_B)|^2 \prod_{D} |\chi_D(z - X_D^{\mathrm{D}_F}; K'_D)|^2\,, \tag{A.39}$$

in order to further evaluate Equation (A.37) and to extract the oscillation probability. As discussed already for the similar overlap functions $\mathbb{V}_{\mathrm{S/D}}$, the integrands of $\mathcal{V}_{\mathrm{S/D}}$ are different from zero only in the small overlap region around the mean impact points $X_{\mathrm{S/D}}$ defined by the external spacetime points,

$$\{X_{\mathrm{ext}}\} := \underbrace{\{X_A^{\mathrm{S}_I}\} \cup \{X_C^{\mathrm{S}_F}\}}_{\{X_{\mathrm{ext}}^{\mathrm{S}}\}} \cup \underbrace{\{X_B^{\mathrm{D}_I}\} \cup \{X_D^{\mathrm{D}_F}\}}_{\{X_{\mathrm{ext}}^{\mathrm{D}}\}} . \tag{A.40}$$

By pulling out the spacetime integrals, d^4y and d^4z, from $\mathcal{V}_{\mathrm{S}}$ and $\mathcal{V}_{\mathrm{D}}$, respectively, we can execute all newly introduced spatial integrals over the $\vec{X}_{\mathrm{ext}}$ using only a few approximations. To this end, note that for fixed production and detection coordinates y, z and a given mean momentum configuration only those positions $\vec{X}_{\mathrm{ext}}$ contribute that lead to world lines of the external particles going through the close neighbourhood of y and z, respectively. Indeed, by using the shift symmetry [54] of the integrands of equations (A.38) and (A.39) in the X_{ext} along the world lines of the WPs, we can approximate $X_{\mathrm{ext}}^{\mathrm{S}} \equiv y$ and $X_{\mathrm{ext}}^{\mathrm{D}} \equiv z$ in all other functions in $\mathrm{d}N_{ab}$. In doing so, we assume that the phase space densities and $\tilde{\mathcal{P}}_{ab}(\{X_{\mathrm{ext}}\})/|\vec{X}_{\mathrm{D}} - \vec{X}_{\mathrm{S}}|^2$ only change significantly for variations in all external spacetime points on the order of the source or detector volumes. After these approximations only the squared position space WPs of the external particles depend on the external spacetime points and executing them leads to a factor of $N_{\mathrm{S/D}}^{-1}$ cancelling the corresponding normalisation factors [54] appearing in $\mathcal{V}_{\mathrm{S/D}}$. In total we arrive at

$$\mathrm{d}N_{ab} = \sum_{\text{spins}} \int \mathrm{d}^4y \int \mathrm{d}^4z \int \mathrm{d}E \int \mathrm{d}\mathcal{P}_{\mathrm{S}}(y)\, \mathrm{d}\mathcal{P}_{\mathrm{D}_F} \int \mathrm{d}\mathcal{P}_{\mathrm{D}_I}(z) \frac{\tilde{\mathcal{P}}_{ab}(E; y, z)}{|\vec{z} - \vec{y}|^2} , \tag{A.41}$$

where the Lorentz-invariant production and detection forms,

$$\begin{aligned} \mathrm{d}\mathcal{P}_{\mathrm{S}}(y) &:= \prod_{A=1}^{n_I} \frac{\mathrm{d}^3\vec{Q}_A}{(2\pi)^3 2Q_A^0} f_A^{\mathrm{S}}(s_A, \vec{Q}_A, y) \prod_{C=1}^{n_F} \frac{\mathrm{d}^3\vec{K}_C}{(2\pi)^3 2K_C^0} \\ &\quad \times (2\pi)^4 \delta_{\mathrm{S}}(q - P_{\mathrm{S}}) |M_{\mathrm{S}}|^2 , \end{aligned} \tag{A.42}$$

$$\mathrm{d}\mathcal{P}_{\mathrm{D}_I}(z) := \prod_{B=1}^{m_I} \frac{\mathrm{d}^3\vec{Q}'_B}{(2\pi)^3 2Q_B^{0\prime}} f_B^{\mathrm{D}}(s_B, \vec{Q}'_B, z) (2\pi)^4 \delta_{\mathrm{D}}(q + P_{\mathrm{D}}) |M_{\mathrm{D}}|^2 , \tag{A.43}$$

$$\mathrm{d}\mathcal{P}_{\mathrm{D}_F} := \prod_{D=1}^{m_F} \frac{\mathrm{d}^3\vec{K}'_D}{(2\pi)^3 2K_D^{0\prime}} , \tag{A.44}$$

contain the information about the production and detection kinematics and dynamics.

A further simplification commonly assumed is that the phase space functions of the external in-state particles only depend weakly on time corresponding to a steady influx of particles. In the following, we hence approximate them as step functions of the form [54]

$$f_\psi^{\mathrm{S}}(s, \vec{P}, y) = \Theta(y_2^0 - y^0)\Theta(y^0 - y_1^0) \tilde{f}_\psi^{\mathrm{S}}(s, \vec{P}, \vec{y}) , \tag{A.45}$$

$$f_\psi^{\mathrm{D}}(s, \vec{P}, z) = \Theta(z_2^0 - z^0)\Theta(z^0 - z_1^0) \tilde{f}_\psi^{\mathrm{D}}(s, \vec{P}, \vec{z}) , \tag{A.46}$$

that are only different from zero during the livetime interval of the source and the detector, i.e. $T_{\mathrm{S}} := y_2^0 - y_1^0$ and $T_{\mathrm{D}} := z_2^0 - z_1^0$, respectively. Using this assumption the time integrals over detector and source livetimes only affect the probability progenitor and we finally get [54]

$$\begin{aligned} \mathrm{d}N_{ab} = T_{\mathrm{D}} \sum_{\text{spins}} \int \mathrm{d}E \int \mathrm{d}^3\vec{y} \int \mathrm{d}^3\vec{z} \int \frac{\mathrm{d}\mathcal{P}_{\mathrm{S}}\left(\vec{y}\right)}{2(2\pi)^3 |\vec{z}-\vec{y}|^2} \frac{\mathrm{d}\mathcal{P}_{\mathrm{D}_F}}{2} \int \mathrm{d}\mathcal{P}_{\mathrm{D}_I}\left(\vec{z}\right) \\ \times \iint\limits_{y_1^0 z_1^0}^{y_2^0 z_2^0} \frac{\mathrm{d}y^0\, \mathrm{d}z^0}{T_{\mathrm{D}}} \tilde{\mathcal{P}}_{ab}(E; y, z)\,. \end{aligned} \tag{A.47}$$

The last factor containing the double time integral of $\tilde{\mathcal{P}}_{ab}$ yields the final oscillation "probability" [54] $\mathcal{P}_{ab}(E; \vec{y}, \vec{z})$, whereas the production and detection integrals can be interpreted as a differential incident flux of neutrinos and a differential detection cross section, respectively. Moreover, we can divide $\mathrm{d}N_{ab}$ by the detection time interval in order to obtain the total differential event rate

$$\mathrm{d}\Gamma_{ab} := \frac{\mathrm{d}N_{ab}}{T_{\mathrm{D}}} = \int \mathrm{d}E \int \mathrm{d}^3\vec{y} \int \mathrm{d}^3\vec{z}\, \frac{\Phi^{\mathrm{S}}(E, \vec{y})}{4\pi |\vec{z}-\vec{y}|^2} \mathcal{P}_{ab}(E; \vec{y}, \vec{z})\, \mathrm{d}\sigma^{\mathrm{D}}\left(E, \vec{z}, \{\vec{K}'_D\}\right), \tag{A.48}$$

with the incident neutrino flux and differential detection cross section,

$$\Phi^{\mathrm{S}}(E, \vec{y}) = \int \frac{\mathrm{d}\mathcal{P}_{\mathrm{S}}\left(E, \vec{y}\right)}{(2\pi)^2}\,, \tag{A.49}$$

$$\mathrm{d}\sigma^{\mathrm{D}}\left(E, \vec{z}, \{\vec{K}'_D\}\right) = \frac{\mathrm{d}\mathcal{P}_{\mathrm{D}_F}}{2} \int \mathrm{d}\mathcal{P}_{\mathrm{D}_I}\left(E, \vec{z}, \{\vec{K}'_D\}\right). \tag{A.50}$$

With this we have arrived at the last result of this section and it implies many critical insights that we discuss in the following.

The total rate (A.48) factorises only if all neutrino mass eigenstates are quasi degenerate in mass with almost identical effective WPs. In this case the incident neutrino flux as well as the detection cross section become approximately independent of the produced neutrino mass eigenstate. Otherwise the detection and production dynamics could not be disentangled from the propagation part that leads to the oscillation probability. Moreover, one needs to integrate over the source and detector volumes in order to obtain the measured event counts as experimentalists usually do not explicitly resolve or use the position and time data of the neutrino production / detection vertices for oscillation analyses. Only if the source and detector are much smaller compared to the scale on which $\mathcal{P}_{ab}$ varies significantly, one can extract $\mathcal{P}_{ab}$ from $\mathrm{d}\Gamma_{ab}$ by dividing by the initial flux and the detection cross section. This is because, only in this case it is well justified to evaluate $\mathcal{P}_{ab}$ at some reference point within source and detector and pull it out of the respective integrals. This smallness condition is usually fulfilled for the detector (unless very low energy neutrinos are considered), but it may be violated for very large neutrino sources like, for example, the sun.

Furthermore, if the detector moves significantly relative to the source during the propagation time of the neutrino the time integral must be rewritten as an integral along the world lines of

detector and source respectively. Also the initial flux $\propto |\vec{X}_{\mathrm{D}}(\tau_{\mathrm{D}}) - \vec{X}_{\mathrm{S}}(\tau_{\mathrm{S}})|^{-2}$ then depends on time and cannot be disentangled from the probability anymore. However, if the baseline changes significantly only with respect to the neutrino oscillation length but is negligible compared to the average baseline one can approximately evaluate the in-flux at this average baseline and only integrate the oscillation probability progenitor $\widetilde{\mathcal{P}}_{ab}$ again.

If one can extract $\mathcal{P}_{ab}$ it is still not guaranteed that it fulfils the unitarity condition

$$\sum_b \mathcal{P}_{ab} = 1\,, \tag{A.51}$$

as has been shown in Reference [54]. This is only the case if the detector exposure time is offset from the source livetime interval by roughly the propagation distance $L := |\vec{X}_{\mathrm{D}} - \vec{X}_{\mathrm{S}}|$ and if T_{D} is shorter than T_{S}. In case both are equal, they need to be much larger than the inverse energy uncertainty of the effective neutrino WP. The simple reasoning behind these criteria is that the detector needs to be exposed to a stream of neutrinos as otherwise the counting rate will always be smaller than expected.

Redefining the oscillation probability by factoring out the responsible suppression function [54] S_0 from $\mathcal{P}_{ab} = S_0 P_{ab}$ and absorbing it into the source flux Φ^{S} results in the usual (approximately) normalised oscillation probability P_{ab} and in the expression (2.103) for the interaction rate. This probability then includes coherence damping effects due to WP separation, possible resolution of which mass eigenstate has propagated as well as mismatch of the produced and detected effective neutrino momenta. The latter effect may be neglected as this kind of process only contributes significantly to the count rate in case of very broad momentum space WPs of the external particles contradicting assumptions we made previously. This is because only then the widths of the smeared delta functions at production or detection are sufficiently large such that a miss-match between P_{S} and P_{D} is not strongly suppressed.

A.5 Internal Wave Packet Approach for Gaussian Wave Packets

The flavour transition amplitude in the internal WP approach to neutrino oscillations in flat spacetime and in vacuum is given by

$$\mathcal{A}_{ab} = \sum_j U^*_{aj} U_{bj} \int \mathrm{d}^3\vec{p}\, \Phi^{\mathrm{D}*}_j(\vec{p}) \Phi^{\mathrm{S}}_j(\vec{p}\,') e^{-i(E_p T - \vec{p}\vec{L})}\,, \tag{A.52}$$

where we use the simple Gaussian momentum space WPs,

$$\phi^{\mathrm{S}}_j(\vec{p}, \vec{P}_j) = \left(2\pi\sigma^2_{\mathrm{S}j}\right)^{-\frac{3}{4}} \exp\left(-\frac{1}{4}\frac{(\vec{p} - \vec{P}_j)^2}{\sigma^2_{\mathrm{S}j}}\right)\,, \tag{A.53}$$

$$\phi^{\mathrm{D}}_j(\vec{p}, \vec{Q}_j) = \left(2\pi\sigma^2_{\mathrm{D}j}\right)^{-\frac{3}{4}} \exp\left(-\frac{1}{4}\frac{(\vec{p} - \vec{Q}_j)^2}{\sigma^2_{\mathrm{D}j}}\right)\,, \tag{A.54}$$

centered around $\vec{P}_j$ ($\vec{Q}_j$) with width $\sigma_{\mathrm{S}j}$ ($\sigma_{\mathrm{D}j}$) at the neutrino source (detector).

In the following, we explicitly perform all steps of the calculation necessary to obtain the flavour transition probability. The main steps of this procedure are to perform the momentum space integral appearing within $\mathcal{A}_{ab}$ followed by a double time integral over the production and detection time coordinates, i.e. T_{S} and T_{D}, respectively. Due to the time translation symmetry of the physical system, the amplitude only depends on the time difference $\Delta T := T_{\mathrm{D}} - T_{\mathrm{S}}$ and one can show that the double integral over the neutrino production and detection intervals,

$$I(T_{\mathrm{S1}}, T_{\mathrm{S2}}; T_{\mathrm{D1}}, T_{\mathrm{D2}}) := \int_{T_{\mathrm{S1}}}^{T_{\mathrm{S2}}} \mathrm{d}T_{\mathrm{S}} \int_{T_{\mathrm{D1}}}^{T_{\mathrm{D2}}} \mathrm{d}T_{\mathrm{D}} \, |\mathcal{A}_{ab}(T_{\mathrm{D}} - T_{\mathrm{S}})|^2 \,, \tag{A.55}$$

reduces to a simple integral over the relative time coordinate $\Delta T := T_{\mathrm{D}} - T_{\mathrm{S}}$. We start by proving this claim in the next section using only the assumption of time translation invariance such that the proof remains valid in arbitrary stationary spacetimes.

A.5.1 Reduction of the Double Time Integral

In order to approximate the double integral (A.55) by a simpler, one-dimensional integral, consider the time coordinate transformation

$$\lambda : \mathbb{R}^2 \to \mathbb{R}^2 \,, \qquad \lambda(T_{\mathrm{S}}, T_{\mathrm{D}}) := \begin{pmatrix} T_{\mathrm{D}} - T_{\mathrm{S}} \\ T_{\mathrm{D}} + T_{\mathrm{S}} \end{pmatrix} \,, \tag{A.56}$$

$$\lambda^{-1} : \mathbb{R}^2 \to \mathbb{R}^2 \,, \qquad \lambda^{-1}(\Delta T, \bar{T}) := \frac{1}{2} \begin{pmatrix} \bar{T} - \Delta T \\ \bar{T} + \Delta T \end{pmatrix} \,, \tag{A.57}$$

to an absolute and a relative time coordinate, i.e. $\bar{T}$ and ΔT, respectively. The Jacobian of this transformation is given by

$$\mathrm{d}\lambda \, (T_{\mathrm{S}}, T_{\mathrm{D}}) = \begin{pmatrix} -1 & 1 \\ 1 & 1 \end{pmatrix} \qquad \Leftrightarrow \qquad \det(\mathrm{d}\lambda) \equiv -2 \,. \tag{A.58}$$

Using the standard rules for integration by substitution

$$\int_V \mathrm{d}^n \vec{v} \, f(\lambda(\vec{v})) = \int_{\lambda(V)} \mathrm{d}^n \vec{u} \, f(\vec{u}) |\det(\mathrm{d}\lambda^{-1}(u))| \,, \tag{A.59}$$

and that $\lambda(\mathbb{R}^2) = \mathbb{R}^2$, we get

$$I(T_{\mathrm{S1}}, T_{\mathrm{S2}}; T_{\mathrm{D1}}, T_{\mathrm{D2}}) = \int_{T_{\mathrm{S1}}}^{T_{\mathrm{S2}}} \mathrm{d}T_{\mathrm{S}} \int_{T_{\mathrm{D1}}}^{T_{\mathrm{D2}}} \mathrm{d}T_{\mathrm{D}} \, |\mathcal{A}_{ab}(T_{\mathrm{D}} - T_{\mathrm{S}})|^2 \tag{A.60}$$

$$= \iint_{\mathbb{R}^2} \mathrm{d}^2(T_{\mathrm{S}}, T_{\mathrm{D}}) \, |\mathcal{A}_{ab}(T_{\mathrm{D}} - T_{\mathrm{S}})|^2 \chi(T_{\mathrm{S}}, T_{\mathrm{D}}) \tag{A.61}$$

$$= \iint_{\mathbb{R}^2} \frac{\mathrm{d}^2(\Delta T, \bar{T})}{2} |\mathcal{A}_{ab}(\Delta T)|^2 \chi\left(\frac{\bar{T} - \Delta T}{2}, \frac{\bar{T} + \Delta T}{2}\right), \tag{A.62}$$

for the integral (A.55). The indicator function χ of the integration region is simply given by

$$\chi(T_{\mathrm{S}}, T_{\mathrm{D}}) = \Theta(T_{\mathrm{D2}} - T_{\mathrm{D}})\Theta(T_{\mathrm{S2}} - T_{\mathrm{S}})\Theta(T_{\mathrm{D}} - T_{\mathrm{D1}})\Theta(T_{\mathrm{S}} - T_{\mathrm{S1}}) \,. \tag{A.63}$$

Next, we use the function χ in order to determine the new region of integration. In our case, it will be beneficial to choose the $\bar{T}$ integration as the inner integration since it can be trivially executed. Its bounds then explicitly depend on ΔT and the old bounds of integration. The indicator function defines the following constraints for the integration variables:

$$\left\{\begin{matrix} T_{\mathrm{D2}} - T_{\mathrm{D}} \geq 0 \\ T_{\mathrm{S2}} - T_{\mathrm{S}} \geq 0 \\ T_{\mathrm{D}} - T_{\mathrm{D1}} \geq 0 \\ T_{\mathrm{S}} - T_{\mathrm{S1}} \geq 0 \end{matrix}\right\} \quad \Leftrightarrow \quad \left\{\begin{matrix} 2T_{\mathrm{D2}} - (\bar{T} + \Delta T) \geq 0 \\ 2T_{\mathrm{S2}} - (\bar{T} - \Delta T) \geq 0 \\ \bar{T} + \Delta T - 2T_{\mathrm{D1}} \geq 0 \\ \bar{T} - \Delta T - 2T_{\mathrm{S1}} \geq 0 \end{matrix}\right\} . \tag{A.64}$$

Adding the first and last and the second and third constraints yields the new bounds of integration for ΔT, i.e.

$$T_{\mathrm{D1}} - T_{\mathrm{S2}} \leq \Delta T \leq T_{\mathrm{D2}} - T_{\mathrm{S1}} \,. \tag{A.65}$$

For the absolute time coordinate, we then get the constraints

$$\bar{T} - (2T_{\mathrm{D1}} - \Delta T) \geq 0 \qquad \wedge \qquad \bar{T} - (2T_{\mathrm{S1}} + \Delta T) \geq 0 \,, \tag{A.66}$$

$$(2T_{\mathrm{D2}} - \Delta T) - \bar{T} \geq 0 \qquad \wedge \qquad (2T_{\mathrm{S2}} + \Delta T) - \bar{T} \geq 0 \,, \tag{A.67}$$

translating to:

$$\bar{T}_{\min}(\Delta T) \leq \bar{T} \leq \bar{T}_{\max}(\Delta T) \,, \tag{A.68}$$

$$\bar{T}_{\min}(\Delta T) = \max\left(2T_{\mathrm{D1}} - \Delta T, 2T_{\mathrm{S1}} + \Delta T\right), \tag{A.69}$$

$$\bar{T}_{\max}(\Delta T) = \min\left(2T_{\mathrm{D2}} - \Delta T, 2T_{\mathrm{S2}} + \Delta T\right). \tag{A.70}$$

Using these designations, the integral becomes

$$I(T_{\mathrm{S1}}, T_{\mathrm{S2}}; T_{\mathrm{D1}}, T_{\mathrm{D2}}) = \int_{T_{\mathrm{D1}} - T_{\mathrm{S2}}}^{T_{\mathrm{D2}} - T_{\mathrm{S1}}} \mathrm{d}\Delta T |\mathcal{A}_{ab}(\Delta T)|^2 \int_{\bar{T}_{\min}(\Delta T)}^{\bar{T}_{\max}(\Delta T)} \frac{\mathrm{d}\bar{T}}{2} \tag{A.71}$$

$$= \int_{T_{\mathrm{D1}} - T_{\mathrm{S2}}}^{T_{\mathrm{D2}} - T_{\mathrm{S1}}} \mathrm{d}\Delta T |\mathcal{A}_{ab}(\Delta T)|^2 \frac{\bar{T}_{\max}(\Delta T) - \bar{T}_{\min}(\Delta T)}{2} \,. \tag{A.72}$$

In order to simplify the following discussion while still maintaining generality of our results, we assume synchronised time windows of neutrino production and detection. This means that for a given time span τ of neutrino production, the detector is assumed to operate for precisely that amount of time such that the slowest and fastest, significantly contributing neutrino modes are able to travel from the source to the detector. Any excess production or detection time for that either the produced neutrino arrives at a switched off detector or where no new neutrinos arrive at the still running detector will not contribute to the result and we can simply omit them.

This consideration is justified by the analytical structure of the squared transition amplitude: In general it can be decomposed into the form,

$$|\mathcal{A}_{ab}(\Delta T)|^2 = \sum_{j,k} a_{jk}(\Delta T)\,, \tag{A.73}$$

where for each index combination (j,k) the function a_{jk} has exactly one sharply peaked global maximum at a certain time $\Delta T_{jk} = L/\bar{v}_{jk}$ corresponding to the weighted average between the times the j-th and k-th mass eigenstate WPs need to enter the detector. The associated average velocity $\bar{v}_{jk} \sim 1$ and width of the maximum are determined by the inherent properties of the WPs, as we will see in following sections for the explicit example of Gaussian WPs. For now, we leave them implicit and only impose rather general assumptions on their properties. The key insight, however, is that the different terms contributing to the squared amplitude are only significantly different from zero in a small window around ΔT_{jk}, and hence, the condition $\Delta T \sim L$ is enforced within the uncertainties of the WPs. This enables us to define a minimal and maximal propagation time $\Delta T_a < \Delta T_b$, the fastest and slowest momentum modes need in order to reach the detector, respectively. More precisely, these times are defined such that the significant support of all a_{jk} falls into this window, i.e.

$$\Delta T_a := \min_{jk} \left\{ \min \overline{\{\Delta T : |a_{jk}(\Delta T)| \geq \delta\}} \right\}\,, \tag{A.74}$$

$$\Delta T_b := \max_{jk} \left\{ \max \overline{\{\Delta T : |a_{jk}(\Delta T)| \geq \delta\}} \right\}\,, \tag{A.75}$$

where $\delta \ll 1$ is some chosen precision parameter defining the degree of approximation. An illustration of the minimal and maximal propagation times is shown in Figure A.1. Now, we use this discussion to redefine our time coordinate system such that

$$T_{\mathrm{S1}} = 0\,, \qquad T_{\mathrm{S2}} = \tau, \qquad T_{\mathrm{D1}} = \Delta T_a\,, \qquad T_{\mathrm{D2}} = \tau + \Delta T_b \approx \tau + \Delta T_a\,, \tag{A.76}$$

where τ is the approximate time span of neutrino production. Since we consider ultra-relativistic neutrinos the times ΔT_a and ΔT_b are very close to each other, and hence, fulfil $\Delta T_b - \Delta T_a \ll \tau$ if δ is not chosen too small.

Next, exploiting the aforementioned properties of the squared amplitude and substituting

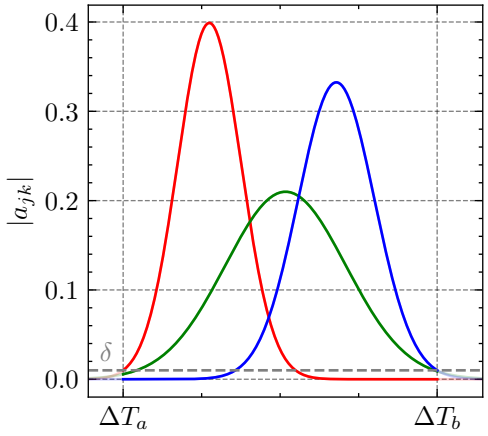

Figure A.1: Illustration of the definition of the time window $[\Delta T_a, \Delta T_b]$ between the arrival of the fastest and slowest neutrino momentum modes in terms of the envelope $|a_{jk}|$ of the different terms contributing to the amplitude $|\mathcal{A}_{ab}|^2$.

everything into our expression for the integral, we get

$$
\begin{aligned}
I(0,\tau;\Delta T_a,\tau+\Delta T_b) = &\int_{\Delta T_a-\tau}^{\Delta T_a} \mathrm{d}\Delta T |\mathcal{A}_{ab}(\Delta T)|^2(\tau+\Delta T-\Delta T_a) \\
&+\tau\int_{\Delta T_a}^{\Delta T_b} \mathrm{d}\Delta T |\mathcal{A}_{ab}|^2(\Delta T) \qquad \text{(A.77)} \\
&+\int_{\Delta T_b}^{\Delta T_b+\tau} \mathrm{d}\Delta T |\mathcal{A}_{ab}|^2(\Delta T)(\tau-(\Delta T-\Delta T_b)) \\
\approx\ &\tau\int_{\Delta T_a}^{\Delta T_b} \mathrm{d}\Delta T |\mathcal{A}_{ab}|^2(\Delta T) \qquad \text{(A.78)} \\
\approx\ &\tau\int_{-\infty}^{\infty} \mathrm{d}\Delta T |\mathcal{A}_{ab}|^2(\Delta T)\,, \qquad \text{(A.79)}
\end{aligned}
$$

since we have agreed to approximate $|\mathcal{A}_{ab}(\Delta T)|^2 \approx 0$ for $\Delta T \leq \Delta T_a$ or $\Delta T \geq \Delta T_b$. This leaves us with the main result of this section, i.e.

$$
P_{ab}(L) \approx \frac{\int_{-\infty}^{\infty} |\mathcal{A}_{ab}(\Delta T, L)|^2 \,\mathrm{d}\Delta T}{\int_{-\infty}^{\infty} \sum_b |\mathcal{A}_{ab}(\Delta T, L)|^2 \,\mathrm{d}\Delta T}. \qquad \text{(A.80)}
$$

A.5.2 Computing the Momentum Integral

Now, we return to our specific example of Gaussian shaped neutrino WPs. In this setup the flavour transition amplitude reads

$$\begin{aligned}\mathcal{A}_{ab} = \sum_j U_{aj}^* U_{bj} \int \mathrm{d}^3\vec{p} \left(2\pi\sigma_{\mathrm{D}j}\sigma_{\mathrm{S}j}\right)^{-\frac{3}{2}} \\ \times \exp\left(-\frac{1}{4}\frac{(\vec{p}-\vec{Q}_j)^2}{\sigma_{\mathrm{D}j}^2} - \frac{1}{4}\frac{(\vec{p}-\vec{P}_j)^2}{\sigma_{\mathrm{S}j}^2} - i(E_p T - \vec{p}\vec{L})\right) .\end{aligned} \tag{A.81}$$

In order to be able to solve the momentum space integral, we expand the exponent,

$$\varepsilon_j(\vec{p}) := -\frac{1}{4}\frac{(\vec{p}-\vec{Q}_j)^2}{\sigma_{\mathrm{D}j}^2} - \frac{1}{4}\frac{(\vec{p}-\vec{P}_j)^2}{\sigma_{\mathrm{S}j}^2} - i(E_p T - \vec{p}\vec{L}) , \tag{A.82}$$

to quadratic order around the maximum $\bar{\vec{p}}_j$ of the envelope of the integrand. Due to the monotonicity of the real exponential function, this maximum can also be obtained from setting the derivative of the real part of the exponent to zero, i.e.

$$0 = \nabla_{\vec{p}}\mathrm{Re}(\varepsilon_j)(\vec{p})\big|_{\vec{p}=\bar{\vec{p}}_j} . \tag{A.83}$$

This yields

$$\nabla_{\vec{p}}\mathrm{Re}(\varepsilon_j)(\vec{p}) = -\frac{1}{2}\frac{\vec{p}-\vec{Q}_j}{\sigma_{\mathrm{D}j}^2} - \frac{1}{2}\frac{\vec{p}-\vec{P}_j}{\sigma_{\mathrm{S}j}^2} \qquad \Rightarrow \qquad \bar{\vec{p}}_j = \frac{\vec{P}_j\sigma_{\mathrm{D}j}^2 + \vec{Q}_j\sigma_{\mathrm{S}j}^2}{\sigma_{\mathrm{S}j}^2 + \sigma_{\mathrm{D}j}^2} . \tag{A.84}$$

Then, the second order Taylor polynomial of the full exponent function reads

$$\varepsilon_j(\vec{p}) \approx \bar{\varepsilon}_j - i(\bar{\vec{v}}_j T - \vec{L})^T(\vec{p}-\bar{\vec{p}}_j) - \frac{1}{2}(\vec{p}-\bar{\vec{p}}_j)^T\Sigma_j(\vec{p}-\bar{\vec{p}}_j) , \tag{A.85}$$

$$\bar{\varepsilon}_j = -\frac{1}{4}\frac{\vec{\Delta}_j^2}{\sigma_{\mathrm{S}j}^2 + \sigma_{\mathrm{D}j}^2} - i(\bar{E}_j T - \bar{\vec{p}}_j\vec{L}) , \tag{A.86}$$

where we have defined the following quantities:

$$\vec{\Delta}_j := \vec{Q}_j - \vec{P}_j , \tag{A.87}$$

$$\bar{E}_j := \sqrt{\bar{\vec{p}}_j^2 + m_j^2} , \tag{A.88}$$

$$\bar{\vec{v}}_j := \frac{\bar{\vec{p}}_j}{\bar{E}_j} , \tag{A.89}$$

$$\Sigma_j := \frac{\mathbb{1}}{2}\left(\frac{1}{\sigma_{\mathrm{S}j}^2} + \frac{1}{\sigma_{\mathrm{D}j}^2}\right) + \frac{iT}{\bar{E}_j}\left(\mathbb{1} - \bar{\vec{v}}_j \otimes \bar{\vec{v}}_j\right) , \tag{A.90}$$

representing the deviation of the mean momenta at the source and in the detector, the mean energy, the mean group velocity and the position space overlap covariance matrix of the produced and detected j-th mass eigenstate WP, respectively. That the latter quantity indeed serves this purpose becomes obvious after completing the square in the exponent and after executing the resulting Gaussian integration. Before, we proceed to do exactly this we first need to examine the properties of Σ_j. First, note that Σ_j is symmetric since it emerges from the Hessian of ε_j. Furthermore, its real part,

$$\mathrm{Re}(\Sigma_j) = \frac{\mathbb{1}}{2}\left(\frac{1}{\sigma_{\mathrm{S}j}^2} + \frac{1}{\sigma_{\mathrm{D}j}^2}\right), \tag{A.91}$$

is positive definite simultaneously proving that we indeed have found a maximum of $\mathrm{Re}(\varepsilon_j)$. One eigenvector of Σ_j can be expressed as

$$\vec{s}_{\parallel}^{\,j} = \frac{\bar{\vec{p}}_j}{|\bar{\vec{p}}_j|} \propto \bar{\vec{p}}_j, \bar{\vec{v}}_j\,, \tag{A.92}$$

whereas the remaining two eigenvectors are just given by any set of mutually orthonormal, non-zero vectors, $(\vec{s}_{\perp,1}^{\,j}, \vec{s}_{\perp,2}^{\,j})$, fulfilling $\vec{s}_{\perp,a}^{\,j} \cdot \vec{s}_{\parallel}^{\,j} = 0$. Since we consider ultra-relativistic neutrinos, we always have $\vec{s}_{\parallel}^{\,j} \neq 0$.

Moreover, the eigenvalues associated with these eigenvectors read

$$\sigma_{\parallel j}^2 = \frac{1}{2}\left(\frac{1}{\sigma_{\mathrm{S}j}^2} + \frac{1}{\sigma_{\mathrm{D}j}^2}\right) + i\frac{T}{\bar{E}_j}(1-\bar{v}_j^2)\,, \tag{A.93}$$

$$\sigma_{\perp j}^2 = \frac{1}{2}\left(\frac{1}{\sigma_{\mathrm{S}j}^2} + \frac{1}{\sigma_{\mathrm{D}j}^2}\right) + i\frac{T}{\bar{E}_j}\,, \tag{A.94}$$

where the latter eigenvalue is degenerate and corresponds to both, $\vec{s}_{\perp,1}^{\,j}$ and $\vec{s}_{\perp,2}^{\,j}$. Since all of the above eigenvalues are non-zero, Σ_j is invertible with (symmetric) inverse,

$$\Sigma_j^{-1} = \frac{1}{\sigma_{\parallel j}^2}\vec{s}_{\parallel}^{\,j} \otimes \vec{s}_{\parallel}^{\,j} + \frac{1}{\sigma_{\perp j}^2}\sum_{a=1}^{2}\vec{s}_{\perp,a}^{\,j} \otimes \vec{s}_{\perp,a}^{\,j}\,. \tag{A.95}$$

With these technical details at hand, we are now ready to complete the square in ε_j:

$$\varepsilon_j(\vec{p}) \approx \bar{\varepsilon}_j - \frac{1}{2}\left(i(\bar{\vec{v}}_j T - \vec{L})^T(\vec{p} - \bar{\vec{p}}_j) + (\vec{p} - \bar{\vec{p}}_j)^T\Sigma_j(\vec{p} - \bar{\vec{p}}_j)\right) \tag{A.96}$$

$$\begin{aligned} &= \bar{\varepsilon}_j - \frac{1}{2}\Big\{2i(\bar{\vec{v}}_j T - \vec{L})^T\Sigma_j^{-1}\Sigma_j(\vec{p} - \bar{\vec{p}}_j) + (\vec{p} - \bar{\vec{p}}_j)^T\Sigma_j(\vec{p} - \bar{\vec{p}}_j) \\ &\quad - (\bar{\vec{v}}_j T - \vec{L})^T\Sigma_j^{-1}(\bar{\vec{v}}_j T - \vec{L}) + (\bar{\vec{v}}_j T - \vec{L})^T\Sigma_j^{-1}(\bar{\vec{v}}_j T - \vec{L})\Big\} \end{aligned} \tag{A.97}$$

$$\begin{aligned} &= \bar{\varepsilon}_j - \frac{1}{2}(\bar{\vec{v}}_j T - \vec{L})^T\Sigma_j^{-1}(\bar{\vec{v}}_j T - \vec{L}) \\ &\quad - \frac{1}{2}\left[p - \bar{\vec{p}}_j + i\Sigma_j^{-1}(\bar{\vec{v}}_j T - \vec{L})\right]^T\Sigma_j\left[p - \bar{\vec{p}}_j + i\Sigma_j^{-1}(\bar{\vec{v}}_j T - \vec{L})\right]\,. \end{aligned} \tag{A.98}$$

Substituting this back into the amplitude results in

$$\begin{aligned}\mathcal{A}_{ab} = &\sum_j U_{aj}^* U_{bj} \left(2\pi\sigma_{\mathrm{D}j}\sigma_{\mathrm{S}j}\right)^{-\frac{3}{2}} \exp\left(\bar{\varepsilon}_j - \frac{1}{2}(\bar{\vec{v}}_j T - \vec{L})^T \Sigma_j^{-1} (\bar{\vec{v}}_j T - \vec{L})\right) \\ &\times \int \mathrm{d}^3\vec{p} \exp\left(-\frac{1}{2}\left[\vec{p} - \vec{b}^j\right]^T \Sigma_j \left[\vec{p} - \vec{b}^j\right]\right) ,\end{aligned} \tag{A.99}$$

$$\vec{b}^j := \bar{\vec{p}}_j - i\Sigma_j^{-1}(\bar{\vec{v}}_j T - \vec{L}) . \tag{A.100}$$

Next, we perform an orthogonal integral transformation

$$\vec{q} := O_j^T \vec{p} , \qquad\qquad O_j := \vec{s}_\parallel^j \otimes \vec{s}_\parallel^j + \sum_{a=1}^{2} \vec{s}_{\perp,a}^j \otimes \vec{s}_{\perp,a}^j , \tag{A.101}$$

that diagonalises Σ_j, reducing the remaining integral to the form

$$\begin{aligned}&\int \mathrm{d}^3\vec{p} \exp\left(-\frac{1}{2}\left[p - \vec{b}^j\right]^T \Sigma_j \left[p - \vec{b}^j\right]\right) \\ &= \int \mathrm{d}^3\tilde{\vec{q}} \exp\left(-\frac{1}{2}\left[\vec{q} - O_j^T\vec{b}^j\right]^T O_j^T \Sigma_j O_j \left[\vec{q} - O_j^T\vec{b}^j\right]\right)\end{aligned} \tag{A.102}$$

$$= \int \mathrm{d}q_\parallel \exp\left(-\frac{1}{2}\frac{\left[q_\parallel - b_\parallel^j\right]^2}{\sigma_{\parallel j}^2}\right) \prod_{a=1}^{2} \int \mathrm{d}q_{\perp,a} \exp\left(-\frac{1}{2}\frac{\left[q_{\perp,a} - b_{\perp,a}^j\right]^2}{\sigma_{\perp j}^2}\right) \tag{A.103}$$

$$= \sqrt{\frac{(2\pi)^3}{\det\Sigma_j}} , \tag{A.104}$$

with

$$b_\parallel^j := \vec{s}_\parallel^j \cdot \vec{b}^j , \qquad\qquad b_{\perp,a}^j := \vec{s}_{\perp,a}^j \cdot \vec{b}^j . \tag{A.105}$$

Thus, we finally arrive at

$$\begin{aligned}\mathcal{A}_{ab} = &\sum_j U_{aj}^* U_{bj} \left(\sigma_{\mathrm{D}j}^3 \sigma_{\mathrm{S}j}^3 \det(\Sigma_j)\right)^{-\frac{1}{2}} \exp\left(-i(\bar{E}_j T - \bar{\vec{p}}_j \vec{L})\right) \\ &\times \exp\left(-\frac{1}{4}\frac{\vec{\Delta}_j^2}{\sigma_{\mathrm{S}j}^2 + \sigma_{\mathrm{D}j}^2} - \frac{1}{2}(\bar{\vec{v}}_j T - \vec{L})^T \Sigma_j^{-1} (\bar{\vec{v}}_j T - \vec{L})\right) .\end{aligned} \tag{A.106}$$

In terms of the eigenvalue decomposition of the covariance matrix Σ_j, this result can be written as

$$\begin{aligned}\mathcal{A}_{ab} = &\sum_j U_{aj}^* U_{bj} \left(\sigma_{\mathrm{D}j}^3 \sigma_{\mathrm{S}j}^3 \sigma_{\parallel j}^2 \sigma_{\perp j}^4\right)^{-\frac{1}{2}} \exp\left(-i(\bar{E}_j \Delta T - \bar{p}_j L_{\parallel j})\right) \\ &\times \exp\left(-\frac{1}{4}\frac{\vec{\Delta}_j^2}{\sigma_{\mathrm{S}j}^2 + \sigma_{\mathrm{D}j}^2} - \frac{1}{2}\frac{(\bar{v}_j \Delta T - L_{\parallel j})^2}{\sigma_{\parallel j}^2} - \frac{1}{2}\frac{L_{\perp j}^2}{\sigma_{\perp j}^2}\right) ,\end{aligned} \tag{A.107}$$

where $L_{\parallel j} = |\vec{s}_\parallel^j \cdot \vec{L}|$ and $L_{\perp j} = \sqrt{(\vec{s}_{\perp,1}^j \cdot \vec{L})^2 + (\vec{s}_{\perp,2}^j \cdot \vec{L})^2}$.

A.5.3 Computing the Time Integral

Using the approximation $\vec{L} \approx \vec{L}_{\parallel j}$, the squared flavour transition amplitude reads

$$\begin{aligned} |\mathcal{A}_{ab}(\vec{L}, \Delta T)|^2 = \sum_{j,k} & U^*_{aj} U_{bj} U_{ak} U^*_{bk} \left(\sigma^3_{\mathrm{S}j} \sigma^3_{\mathrm{D}j} \sigma^3_{\mathrm{S}k} \sigma^3_{\mathrm{D}k}\right)^{-\frac{1}{2}} \\ & \times \exp\left(-\frac{\vec{\Delta}_j^2}{4(\sigma^2_{\mathrm{S}j} + \sigma^2_{\mathrm{D}j})} - \frac{\vec{\Delta}_k^2}{4(\sigma^2_{\mathrm{S}k} + \sigma^2_{\mathrm{D}k})} + i\Delta p_{jk} L \right) \\ & \times \exp\left(-\frac{1}{2}\mathrm{Tr}(\ln \Sigma_j) - \frac{1}{2}\mathrm{Tr}(\ln \Sigma_k)^* - i\Delta E_{jk} \Delta T \right. \\ & \qquad \left. - \frac{(L - \bar{v}_j \Delta T)^2}{2\sigma^2_{\parallel j}} - \frac{(L - \bar{v}_k \Delta T)^2}{2\sigma^{2*}_{\parallel k}} \right). \end{aligned} \tag{A.108}$$

Here, we have already gathered all time-dependent parts in the last exponential factor. Now, in order to solve the ΔT integral, present in Equation (A.80), needed to obtain the oscillation probability, we expand the exponent function,

$$\begin{aligned} \Xi_{jk}(\Delta T) := & -\frac{1}{2}\mathrm{Tr}(\ln \Sigma_j) - \frac{1}{2}\mathrm{Tr}(\ln \Sigma_k)^* - i\Delta E_{jk} \Delta T \\ & - \frac{(L - \bar{v}_j \Delta T)^2}{2\sigma^2_{\parallel j}} - \frac{(L - \bar{v}_k \Delta T)^2}{2\sigma^{2*}_{\parallel k}}, \end{aligned} \tag{A.109}$$

up to second order around the time ΔT_{jk} that maximises the envelope of the time integrand. Thus, this time is defined by

$$0 \stackrel{!}{=} \left. \frac{\mathrm{dRe}(\Xi_{jk})}{\mathrm{d}\Delta T} \right|_{\Delta T = \Delta T_{jk}}. \tag{A.110}$$

To simplify our notation, we introduce the leading order position uncertainty,

$$\Theta_j^2 := \mathrm{Re}(\sigma^2_{\parallel j}) = \frac{1}{2}\left(\frac{1}{\sigma^2_{\mathrm{S}j}} + \frac{1}{\sigma^2_{\mathrm{D}j}} \right), \tag{A.111}$$

as well as the WP spreading coefficients,

$$\chi_{\parallel j}(\Delta T) := \frac{\Delta T}{\bar{E}_j \Theta_j^2}(1 - \bar{v}_j^2), \qquad \chi_{\perp j}(\Delta T) := \frac{\Delta T}{\bar{E}_j \Theta_j^2}. \tag{A.112}$$

In terms of these quantities, the effective position space widths simply read

$$\sigma^2_{\parallel j}(\Delta T) = \Theta_j^2 (1 + i\chi_{\parallel j}(\Delta T)), \tag{A.113}$$

$$\sigma^2_{\perp j}(\Delta T) = \Theta_j^2 (1 + i\chi_{\perp j}(\Delta T)), \tag{A.114}$$

and the time-dependent exponent becomes

$$\begin{aligned}\Xi_{jk}(\Delta T) = &-\frac{3}{2}\ln\Theta_j^2 - \frac{3}{2}\ln\Theta_k^2 - i\Delta E_{jk}\Delta T \\ &- \frac{1}{2}\left[\ln\big(1+i\chi_{\parallel j}\big) + \ln\big(1-i\chi_{\parallel k}\big)\right] - \left[\ln(1+i\chi_{\perp j}) + \ln(1-i\chi_{\perp k})\right] \\ &- \frac{(L-\bar{v}_j\Delta T)^2}{2\Theta_j^2(1+\chi_{\parallel j}^2)}(1-i\chi_{\parallel j}) - \frac{(L-\bar{v}_k\Delta T)^2}{2\Theta_k^2(1+\chi_{\parallel k}^2)}(1+i\chi_{\parallel k}) \\ = &-\frac{3}{2}\ln\Theta_j^2 - \frac{3}{2}\ln\Theta_k^2 - i\Delta E_{jk}\Delta T \\ &- \frac{1}{2}\left[\ln\Big(\sqrt{1+\chi_{\parallel j}^2}\Big) + \ln\Big(\sqrt{1+\chi_{\parallel k}^2}\Big) + i\arctan\big(\chi_{\parallel j}\big) - i\arctan\big(\chi_{\parallel k}\big)\right] \\ &- \left[\ln\Big(\sqrt{1+\chi_{\perp j}^2}\Big) + \ln\Big(\sqrt{1+\chi_{\perp k}^2}\Big) + i\arctan(\chi_{\perp j}) - i\arctan(\chi_{\perp k})\right] \\ &- \frac{(L-\bar{v}_j\Delta T)^2}{2\Theta_j^2(1+\chi_{\parallel j}^2)}(1-i\chi_{\parallel j}) - \frac{(L-\bar{v}_k\Delta T)^2}{2\Theta_k^2(1+\chi_{\parallel k}^2)}(1+i\chi_{\parallel k})\,.\end{aligned} \tag{A.115, A.116}$$

The real part of Ξ_{jk} is, therefore, given by

$$\begin{aligned}\mathrm{Re}(\Xi_{jk})(\Delta T) = &-\frac{3}{2}\ln\Theta_j^2 - \frac{3}{2}\ln\Theta_k^2 - \frac{1}{2}\left[\ln\Big(\sqrt{1+\chi_{\parallel j}^2}\Big) + \ln\Big(\sqrt{1+\chi_{\parallel k}^2}\Big)\right] \\ &- \left[\ln\Big(\sqrt{1+\chi_{\perp j}^2}\Big) + \ln\Big(\sqrt{1+\chi_{\perp k}^2}\Big)\right] \\ &- \frac{(L-\bar{v}_j\Delta T)^2}{2\Theta_j^2(1+\chi_{\parallel j}^2)} - \frac{(L-\bar{v}_k\Delta T)^2}{2\Theta_k^2(1+\chi_{\parallel k}^2)}\,.\end{aligned} \tag{A.117}$$

The next steps are tedious but straight forward:

1. Determine the maximum ΔT_{jk} of $\mathrm{Re}(\Xi_{jk})$.
2. Expand Ξ_{jk} up to quadratic order around ΔT_{jk}.
3. Complete the square and perform the Gaussian time integral.

For simplicity, we perform them in the stationary WP approximation, i.e. with $\chi_{\perp/\parallel j} \approx 0$. In this case, we simply get

$$\mathrm{Re}(\Xi_{jk})(\Delta T) = -\frac{3}{2}\ln\Theta_j^2 - \frac{3}{2}\ln\Theta_k^2 - \frac{(L-\bar{v}_j\Delta T)^2}{2\Theta_j^2} - \frac{(L-\bar{v}_k\Delta T)^2}{2\Theta_k^2}\,, \tag{A.118}$$

and its maximum is located at

$$\Delta T_{jk} = \frac{L}{\bar{v}_{jk}}\,, \qquad\qquad \bar{v}_{jk} := \frac{\Theta_j^2\bar{v}_k^2 + \Theta_k^2\bar{v}_j^2}{\Theta_j^2\bar{v}_k + \Theta_k^2\bar{v}_j}\,. \tag{A.119}$$

Since in this approximation Ξ_{jk} is indeed exactly quadratic in ΔT, Taylor expanding it up to second order in $(\Delta T - \Delta T_{jk})$ does not introduce any more truncation error and we get

$$\begin{aligned}\Xi_{jk}(\Delta T) = &-\frac{3}{2}\ln\Theta_j^2 - \frac{3}{2}\ln\Theta_k^2 - i\frac{\Delta E_{jk}}{\bar{v}_{jk}}L - \frac{(\bar{v}_j-\bar{v}_k)^2}{\Theta_j^2\bar{v}_k^2+\Theta_k^2\bar{v}_j^2}\frac{L^2}{2}\\ &- i\Delta E_{jk}(\Delta T - \Delta T_{jk}) - \frac{1}{2}\left(\frac{\bar{v}_j^2}{\Theta_j^2}+\frac{\bar{v}_k^2}{\Theta_k^2}\right)(\Delta T-\Delta T_{jk})^2\,.\end{aligned} \tag{A.120}$$

Moreover, completing the square yields

$$\begin{aligned}\Xi_{jk}(T) = &-\frac{3}{2}\ln\Theta_j^2 - \frac{3}{2}\ln\Theta_k^2 - i\frac{\Delta E_{jk}}{\bar{v}_{jk}}L - \frac{(\bar{v}_j-\bar{v}_k)^2}{\Theta_j^2\bar{v}_k^2+\Theta_k^2\bar{v}_j^2}\frac{L^2}{2}\\ &- \frac{(\Delta E_{jk})^2}{2}\left(\frac{\bar{v}_j^2}{\Theta_j^2}+\frac{\bar{v}_k^2}{\Theta_k^2}\right)^{-1} + \Delta\tau^2\,,\end{aligned} \tag{A.121}$$

where

$$\Delta\tau^2 := \Delta T - \Delta T_{jk} + i\Delta E_{jk}\left(\frac{\bar{v}_j^2}{\Theta_j^2}+\frac{\bar{v}_k^2}{\Theta_k^2}\right)^{-\frac{1}{2}}\,. \tag{A.122}$$

The final Gaussian time integral then results in

$$I := \int_{-\infty}^{\infty}\mathrm{d}\Delta T|\mathcal{A}_{ab}(\Delta T)|^2 \tag{A.123}$$

$$\begin{aligned}=&\sum_{j,k}U_{aj}^*U_{bj}U_{ak}U_{bk}^*\left(\Theta_j^2\sigma_{\mathrm{S}j}\sigma_{\mathrm{D}j}\Theta_k^2\sigma_{\mathrm{S}k}\sigma_{\mathrm{D}k}\right)^{-\frac{3}{2}}\\ &\times\exp\left(-\frac{\vec{\Delta}_j^2}{4(\sigma_{\mathrm{S}j}^2+\sigma_{\mathrm{D}j}^2)}-\frac{\vec{\Delta}_k^2}{4(\sigma_{\mathrm{S}k}^2+\sigma_{\mathrm{D}k}^2)}+i\Delta p_{jk}L-i\frac{\Delta E_{jk}}{\bar{v}_{jk}}L\right)\\ &\times\exp\left(-\frac{(\bar{v}_j-\bar{v}_k)^2}{\Theta_j^2\bar{v}_k^2+\Theta_k^2\bar{v}_j^2}\frac{L^2}{2}-\frac{(\Delta E_{jk})^2}{2}\left(\frac{\bar{v}_j^2}{\Theta_j^2}+\frac{\bar{v}_k^2}{\Theta_k^2}\right)^{-1}\right)\\ &\times\int_{-\infty}^{\infty}\mathrm{d}\Delta\tau\exp\left(-\frac{1}{2}\left(\frac{\bar{v}_j^2}{\Theta_j^2}+\frac{\bar{v}_k^2}{\Theta_k^2}\right)\Delta\tau^2\right)\end{aligned} \tag{A.124}$$

$$\begin{aligned}=&\sum_{j,k}U_{aj}^*U_{bj}U_{ak}U_{bk}^*\left(\Theta_j^2\sigma_{\mathrm{S}j}\sigma_{\mathrm{D}j}\Theta_k^2\sigma_{\mathrm{S}k}\sigma_{\mathrm{D}k}\right)^{-\frac{3}{2}}\left(\frac{2\pi}{\frac{\bar{v}_j^2}{\Theta_j^2}+\frac{\bar{v}_k^2}{\Theta_k^2}}\right)^{\frac{1}{2}}\\ &\times\exp\left(-\frac{\vec{\Delta}_j^2}{4(\sigma_{\mathrm{S}j}^2+\sigma_{\mathrm{D}j}^2)}-\frac{\vec{\Delta}_k^2}{4(\sigma_{\mathrm{S}k}^2+\sigma_{\mathrm{D}k}^2)}+i\Delta p_{jk}L-i\frac{\Delta E_{jk}}{\bar{v}_{jk}}L\right)\\ &\times\exp\left(-\frac{(\bar{v}_j-\bar{v}_k)^2}{\Theta_j^2\bar{v}_k^2+\Theta_k^2\bar{v}_j^2}\frac{L^2}{2}-\frac{(\Delta E_{jk})^2}{2}\left(\frac{\bar{v}_j^2}{\Theta_j^2}+\frac{\bar{v}_k^2}{\Theta_k^2}\right)^{-1}\right)\,.\end{aligned} \tag{A.125}$$

Next, we define the coherence length of the jk-oscillation,

$$L_{jk}^{\mathrm{coh}} := \sqrt{2}\frac{\sqrt{\Theta_j^2\bar{v}_k^2 + \Theta_k^2\bar{v}_j^2}}{|\bar{v}_j - \bar{v}_k|}\,, \tag{A.126}$$

the critical energy resolution,

$$\sigma_{Ejk}^2 := \left(\frac{\bar{v}_j^2}{\Theta_j^2} + \frac{\bar{v}_k^2}{\Theta_k^2}\right)\,, \tag{A.127}$$

as well as the effective momentum uncertainties,

$$\sigma_{Pj}^2 = 2(\sigma_{\mathrm{S}j}^2 + \sigma_{\mathrm{D}j}^2)\,, \tag{A.128}$$

leading to a much cleaner expression for the time integrated amplitude

$$\begin{aligned} I = &\sum_{j,k} U_{aj}^* U_{bj} U_{ak} U_{bk}^* \left(\Theta_j^2\sigma_{\mathrm{S}j}\sigma_{\mathrm{D}j}\Theta_k^2\sigma_{\mathrm{S}k}\sigma_{\mathrm{D}k}\right)^{-\frac{3}{2}} \left(\frac{2\pi}{\frac{\bar{v}_j^2}{\Theta_j^2} + \frac{\bar{v}_k^2}{\Theta_k^2}}\right)^{\frac{1}{2}} \\ &\times \exp\left(i\Delta p_{jk}L - i\frac{\Delta E_{jk}}{\bar{v}_{jk}}L\right) \\ &\times \exp\left(-\frac{\vec{\Delta}_j^2}{2\sigma_{Pj}^2} - \frac{\vec{\Delta}_k^2}{2\sigma_{Pk}^2} - \left(\frac{L}{L_{jk}^{\mathrm{coh}}}\right)^2 - \frac{1}{2}\left(\frac{\Delta E_{jk}}{\sigma_{Ejk}}\right)^2\right)\,. \end{aligned} \tag{A.129}$$

Now, in order to exploit the assumption of quasi-degenerate neutrino mass eigenstates, we define the reference neutrino mass scale $\bar{m}^2$ fulfilling $|m_j^2 - \bar{m}^2| \ll p^2$. Here, p is the reference momentum associated with the mass $\bar{m}$ and that is compatible with the kinematics of the neutrino production and detection processes. Moreover, we define the respective energy $E := \sqrt{p^2 + \bar{m}^2}$ and assume equal WP widths for all mass eigenstate WPs, i.e.

$$\sigma_{\mathrm{S}}^2 \equiv \sigma_{\mathrm{S}j}^2\,, \qquad\qquad \sigma_{\mathrm{D}}^2 \equiv \sigma_{\mathrm{D}j}^2\,, \tag{A.130}$$

for all j. The quasi-degeneracy condition also implies that the deviations of the mean momenta $\bar{p}_j$ from p are also small. This allows us to expand all quantities to first order in

$$\frac{|\bar{p}_j - p|}{p} \ll 1\,, \qquad\qquad \frac{|m_j^2 - \bar{m}^2|}{p^2} \ll 1\,. \tag{A.131}$$

In this approximation, the energy differences, for example, read

$$\Delta E_{jk} \approx \frac{\Delta m_{jk}^2}{2E} + \Delta p_{jk} v\,, \qquad\qquad v := \frac{p}{E}\,. \tag{A.132}$$

Moreover, for the oscillation phase and coherence length, we get

$$\Phi_{jk} := \frac{\Delta E_{jk}}{\bar{v}_{jk}} - \Delta p_{jk} \approx \frac{\Delta m_{jk}^2}{2p}\,, \qquad L_{jk}^{\mathrm{coh}} \approx \Theta\left|\frac{\Delta m_{jk}^2}{4E^2} - \frac{\bar{m}^2}{2E^2}\frac{\Delta p_{jk}}{p}\right|^{-1}\,, \tag{A.133}$$

respectively. Finally, the production and detection coherence exponent reads

$$\frac{1}{2}\left(\frac{\Delta E_{jk}}{\sigma_{Ejk}}\right)^2 \approx \frac{1}{2}\left(\frac{\Delta E_{jk}}{\sigma_E}\right)^2 , \tag{A.134}$$

with $\sigma_E^2 := 2v^2/\Theta^2$.

A.6 Matter Attenuation Terms in the Effective Flavour Space Approach to Neutrino Oscillations

The exact expressions for the attenuation terms, $\Gamma(x,E)$ and $\bar{\Gamma}(x,E)$, in equations (2.144) and (2.145) read [66, 72]

$$\Gamma(x,E) = \frac{1}{2}\sum_a \frac{\mathrm{Pr}_{\nu_a}(E)}{\lambda_a^{\mathrm{NC}}(x,E) + \lambda_a^{\mathrm{CC}}(x,E)} , \tag{A.135}$$

$$\bar{\Gamma}(x,E) = \frac{1}{2}\sum_a \frac{\mathrm{Pr}_{\bar{\nu}_a}(E)}{\bar{\lambda}_a^{\mathrm{NC}}(x,E) + \bar{\lambda}_a^{\mathrm{CC}}(x,E) + \delta_{ae}\bar{\lambda}_e^{\mathrm{GR}}(x,E)} , \tag{A.136}$$

where Pr_{ν_a} is the projector onto the a-th flavour eigenstate and $\lambda_a^{\mathrm{NC}}(x,E)$ and $\lambda_a^{\mathrm{CC}}(x,E)$ denote the neutral and charged current (CC) interaction lengths of the a-th neutrino flavour computed in References [279–283]. For electron antineutrinos in common matter, i.e. electrons and nucleons, also the mean free path $\bar{\lambda}_e^{\mathrm{GR}}$ for the Glashow resonance, i.e. for the process $\bar{\nu}_e + e^- \to W^-$, becomes important at very high energies [280] $E = \mathcal{O}(\mathrm{PeV})$.

Moreover, the neutrino collision terms can be written as

$$\mathcal{C}[x,E,\rho,\bar{\rho}] = \sum_{a=e,\mu,\tau} \mathcal{C}_a^{\mathrm{NC}}[x,E,\rho,\bar{\rho}] + \sum_{a=e,\mu,\tau} \mathcal{C}_{\tau a}^{\mathrm{CC}}[x,E,\rho,\bar{\rho}] , \tag{A.137}$$

$$\mathcal{C}_a^{\mathrm{NC}}[x,E,\rho,\bar{\rho}] = \mathrm{Pr}_{\nu_a}(E)\int_E^\infty \mathrm{d}E' \, \frac{1}{\lambda_a^{\mathrm{NC}}\sigma_a^{\mathrm{NC}}(E')}\frac{\partial\sigma_a^{\mathrm{NC}}(E',E)}{\partial E}\mathrm{Tr}[\mathrm{Pr}_{\nu_a}(E')\rho(E')] , \tag{A.138}$$

$$\begin{aligned}\mathcal{C}_{\tau a}^{\mathrm{CC}}[x,E,\rho,\bar{\rho}] = {}& \mathrm{Pr}_{\nu_a}(E)\mathrm{Br}_{\tau a}\int_E^\infty \mathrm{d}E_\tau \int_{E_\tau}^\infty \mathrm{d}E' \, \frac{1}{\bar{\lambda}_\tau^{\mathrm{CC}}(x,E')\bar{\sigma}_\tau^{\mathrm{CC}}(E')}\frac{\partial\bar{\sigma}_\tau^{\mathrm{CC}}(E',E_\tau)}{\partial E_\tau} \\ & \times \frac{1}{\bar{\Gamma}_\tau^{\mathrm{lep}}(E_\tau)}\frac{\partial\bar{\Gamma}_\tau^{\mathrm{lep}}(E_\tau,E)}{\partial E}\mathrm{Tr}[\bar{\mathrm{Pr}}_{\nu_\tau}(E')\bar{\rho}(E')] , \quad (a=e,\mu)\end{aligned} \tag{A.139}$$

$$\begin{aligned}\mathcal{C}_{\tau\tau}^{\mathrm{CC}}[x,E,\rho,\bar{\rho}] = {}& \mathrm{Pr}_{\nu_\tau}(E)\int_E^\infty \mathrm{d}E_\tau \int_{E_\tau}^\infty \mathrm{d}E' \, \frac{1}{\lambda_\tau^{\mathrm{CC}}(x,E')\sigma_\tau^{\mathrm{CC}}(E')}\frac{\partial\sigma_\tau^{\mathrm{CC}}(E',E_\tau)}{\partial E_\tau} \\ & \times \frac{1}{\bar{\Gamma}_\tau^{\mathrm{all}}(E_\tau)}\frac{\partial\bar{\Gamma}_\tau^{\mathrm{all}}(E_\tau,E)}{\partial E}\mathrm{Tr}[\mathrm{Pr}_{\nu_\tau}(E')\rho(E')] .\end{aligned} \tag{A.140}$$

The term $\mathcal{C}_a^{\mathrm{NC}}$ describes neutral current scatterings $\nu_a(E') \to \nu_a(E)$ with the associated differential cross section $\mathrm{d}\sigma_a^{\mathrm{NC}}$. The other terms correspond to the CC production and subsequent decay of τ leptons that fuels off of ν_τ and $\bar{\nu}_\tau$ in the beam and leads to the regeneration of all active flavour components with different probabilities. Here, $\mathrm{d}\sigma_\tau^{\mathrm{CC}}$ is the differential cross section for the CC production of τ due to ν_τ scattering off of ambient matter, $\mathrm{d}\Gamma_\tau^{\mathrm{lep}}$ is the differential decay width of the decay of τ into any leptonic mode in the lab-frame and $\mathrm{Br}_{\tau a}$ is the branching ratio for a leptonically decaying τ to produce ν_a. Furthermore, $\mathrm{d}\Gamma_\tau^{\mathrm{all}}$ is the differential τ decay width into any final state. A detailed study of the τ decay widths and distributions is presented in Reference [284].

Lastly, the antineutrino collision terms are given by

$$\bar{\mathcal{C}}[x, E, \rho, \bar{\rho}] = \sum_{a=e,\mu,\tau} \bar{\mathcal{C}}_a^{\mathrm{NC}}[x, E, \rho, \bar{\rho}] + \sum_{a=e,\mu,\tau} \bar{\mathcal{C}}_{\tau a}^{\mathrm{CC}}[x, E, \rho, \bar{\rho}] + \sum_{a=e,\mu,\tau} \bar{\mathcal{C}}_{ea}^{\mathrm{GR}}[x, E, \rho, \bar{\rho}]\,, \tag{A.141}$$

$$\bar{\mathcal{C}}_{ea}^{\mathrm{GR}}[x, E, \rho, \bar{\rho}] = \bar{\mathrm{Pr}}_{\nu_a}(E) \int_E^\infty \mathrm{d}E' \, \frac{1}{\lambda_e^{\mathrm{GR}} \sigma_e^{\mathrm{GR}}(E')} \frac{\partial \sigma_e^{\mathrm{GR}}(E', E)}{\partial E} \mathrm{Tr}[\mathrm{Pr}_{\nu_a}(E') \rho(E')]\,, \tag{A.142}$$

and all other terms with a neutrino analogue are easily obtained from the corresponding terms by exchanging all barred with unbarred quantities and vice versa. The last term $\bar{\mathcal{C}}_{ea}^{\mathrm{GR}}$ that only applies to antineutrinos originates from the Glashow resonance and quantifies the resonant production of antineutrinos of any flavour. Here, $\mathrm{d}\sigma_e^{\mathrm{GR}}$ is the differential cross section for the process $\bar{\nu}_e + e^- \to W^- \to \nu_a + \ell_a^-$.

B Appendix - Altered Dispersion Relations

This appendix chapter provides the full list of all differential equations solved for the analysis presented in Chapter 3. In addition to that, we also discuss our numerical methods in Section B.4, as well as the choice of initial conditions for the solution of the quantum kinetic equations (QKEs) in Section B.3.

B.1 Neutrino Collision Terms

In the integration of the QKEs, the dominant scattering processes are:

1. $\nu_e e^- \longleftrightarrow \nu_e e^-$
2. $\nu_e e^+ \longleftrightarrow \nu_e e^+$
3. $\nu_e \bar{\nu}_e \longleftrightarrow e^- e^+$

We only include the collision terms corresponding to these processes in the solution of the QKEs. The collision terms for the neutrino–electron scattering reads [100]

$$\begin{aligned}\mathcal{C}_1[t,p,\varrho] = \frac{32G_F^2}{p}\int \frac{\mathrm{d}^3\vec{p}_1}{(2\pi)^3 2E_1}\frac{\mathrm{d}^3\vec{p}_2}{(2\pi)^3 2|\vec{p}_2|}\frac{\mathrm{d}^3\vec{p}_3}{(2\pi)^3 2E_3}(2\pi)^4\delta^4(p^\mu + p_1^\mu - p_2^\mu - p_3^\mu) \\ \times \left\{g_R^2(p_\alpha p_3^\alpha)(p_{1\beta}p_2^\beta) + g_L^2(p_\alpha p_1^\alpha)(p_{2\beta}p_3^\beta) - g_L g_R(p_\alpha p_2^\alpha)m_e^2\right\} \\ \times \Phi_1(t,p^\mu,p_1^\mu,p_2^\mu,p_3^\mu)\,,\end{aligned} \tag{B.1}$$

the collision term for neutrino–positron scattering reads [100]

$$\begin{aligned}\mathcal{C}_2[t,p,\varrho] = \frac{32G_F^2}{p}\int \frac{\mathrm{d}^3\vec{p}_1}{(2\pi)^3 2E_1}\frac{\mathrm{d}^3\vec{p}_2}{(2\pi)^3 2|\vec{p}_2|}\frac{\mathrm{d}^3\vec{p}_3}{(2\pi)^3 2E_3}(2\pi)^4\delta^4(p^\mu + p_1^\mu - p_2^\mu - p_3^\mu) \\ \times \left\{g_L^2(p_\alpha p_3^\alpha)(p_{1\beta}p_2^\beta) + g_R^2(p_\alpha p_1^\alpha)(p_{2\beta}p_3^\beta) - g_L g_R(p_\alpha p_2^\alpha)m_e^2\right\} \\ \times \Phi_2(t,p^\mu,p_1^\mu,p_2^\mu,p_3^\mu)\,,\end{aligned} \tag{B.2}$$

and the collision term for neutrino–neutrino annihilation reads [100]

$$\begin{aligned}\mathcal{C}_3[t,p,\varrho] = \frac{32G_F^2}{p}\int \frac{\mathrm{d}^3\vec{p}_1}{(2\pi)^3 2|\vec{p}_1|}\frac{\mathrm{d}^3\vec{p}_2}{(2\pi)^3 2E_2}\frac{\mathrm{d}^3\vec{p}_3}{(2\pi)^3 2E_3}(2\pi)^4\delta^4(p^\mu + p_1^\mu - p_2^\mu - p_3^\mu) \\ \times \left\{g_L^2(p_\alpha p_3^\alpha)(p_{1\beta}p_2^\beta) + g_R^2(p_\alpha p_2^\alpha)(p_{1\beta}p_3^\beta) + g_L g_R(p_\alpha p_1^\alpha)m_e^2\right\} \\ \times \Phi_3(t,p^\mu,p_1^\mu,p_2^\mu,p_3^\mu)\,.\end{aligned} \tag{B.3}$$

The statistical functions are defined by

$$\Phi_i(t,p^\mu,p_1^\mu,p_2^\mu,p_3^\mu) \coloneqq \Phi_i^+(t,p^\mu,p_1^\mu,p_2^\mu,p_3^\mu) - \Phi_i^-(t,p^\mu,p_1^\mu,p_2^\mu,p_3^\mu)\,, \quad \forall i \in \{1,2,3\}\,, \tag{B.4}$$

$$\Phi_1^+(t,p^\mu,p_1^\mu,p_2^\mu,p_3^\mu) \coloneqq f_{e^-}(t,p_3)(1-f_{e^-}(t,p_1))\{\mathbb{P}_e\varrho(t,p_3)\mathbb{P}_e, \mathbb{1}-\varrho(t,p)\}\,, \tag{B.5}$$

$$\Phi_1^-(t,p^\mu,p_1^\mu,p_2^\mu,p_3^\mu) \coloneqq (1-f_{e^-}(t,p_3))f_{e^-}(t,p_1)\{\mathbb{P}_e(\mathbb{1}-\varrho(t,p_3))\mathbb{P}_e, \varrho(t,p)\}\,, \tag{B.6}$$

$$\Phi_3^+(t,p^\mu,p_1^\mu,p_2^\mu,p_3^\mu) \coloneqq f_{e^-}(t,p_2)f_{e^+}(t,p_3)\{\mathbb{P}_e(\mathbb{1}-\varrho(t,p_1))\mathbb{P}_e, \mathbb{1}-\varrho(t,p)\}\,, \tag{B.7}$$

$$\Phi_3^-(t,p^\mu,p_1^\mu,p_2^\mu,p_3^\mu) \coloneqq (1-f_{e^-}(t,p_2))(1-f_{e^+}(t,p_3))\{\mathbb{P}_e\varrho(t,p_1)\mathbb{P}_e, \varrho(t,p)\}\,, \tag{B.8}$$

where $f_{e^\pm}$ are the phase space distributions of electrons and positrons, respectively. The functions $\Phi_2^\pm$ can be easily obtained from $\Phi_1^\pm$ by replacing all f_{e^-} by the corresponding f_{e^+}. Lastly, the effective left- and right-handed couplings are $g_L = 1/2 + g_R$ and $g_r = \sin^2\theta_\mathrm{w}$, and $E_i = \sqrt{p_i^2 + m_e^2}$ denotes the electron and positron energy.

B.2 Evolution of the Photon Temperature

From the cosmic continuity Equation (2.38), i.e.

$$\dot\rho_\mathrm{tot}(t) = -3H(\rho_\mathrm{tot}(t) + P_\mathrm{tot}(t))\,, \tag{B.9}$$

we can derive an evolution equation for the photon temperature by explicitly executing the time derivative of those energy densities depending on T_γ and solving after the inner derivative $\dot T_\gamma$. Before we apply this procedure to the energy density discussed in Section 3.3, we first consider the case where all particle species contributing to ρ_tot are ultra-relativistic and in thermal equilibrium with each other, and hence, all depend on t only through T_γ. In this case, the total energy density can be written as

$$\rho_\mathrm{tot}(t) = CT_\gamma^4(t)\,, \tag{B.10}$$

and the time derivative yields

$$\dot\rho_\mathrm{tot}(t) = \frac{\mathrm{d}\rho_\mathrm{tot}}{\mathrm{d}T_\gamma}\frac{\mathrm{d}T_\gamma}{\mathrm{d}t} = 4CT_\gamma^3(t)\dot T_\gamma = 4\rho_\mathrm{tot}(t)\frac{\dot T_\gamma}{T_\gamma}\,. \tag{B.11}$$

Furthermore, we have $P_\mathrm{tot} = \rho_\mathrm{tot}/3$ and the cosmic continuity equation becomes

$$4\rho_\mathrm{tot}(t)\frac{\dot T_\gamma}{T_\gamma} = -3H(t)\left(1+\frac{1}{3}\right)\rho_\mathrm{tot}(t) = -4H(t)\rho_\mathrm{tot}(t) \qquad \Leftrightarrow \qquad \frac{\dot T_\gamma}{T_\gamma} = -H(t)\,. \tag{B.12}$$

Since the time derivative transforms to

$$\frac{\mathrm{d}}{\mathrm{d}t} = \frac{\mathrm{d}x}{\mathrm{d}t}\frac{\mathrm{d}}{\mathrm{d}x} = a(t)\frac{\dot a(t)}{a(t)}\frac{\mathrm{d}}{\mathrm{d}x} = xH\frac{\mathrm{d}}{\mathrm{d}x}\,, \tag{B.13}$$

using the new time variable $x = a(t)$, the temperature evolution can ultimately be written as

$$xHT'_\gamma = -HT_\gamma \qquad \Leftrightarrow \qquad T'_\gamma = -\frac{T_\gamma}{x}\,, \tag{B.14}$$

which has the solution $T_\gamma(x) = T_\gamma(x_0)x_0/x$.

Now that we have shown that in the ultra-relativistic, equilibrium case the photon temperature decreases with growing scale factor as expected, we can proceed to the more general case, where the total neutrino energy density has a more complicated x-dependence and the charged leptons do follow their equilibrium distribution, but may not be ultra-relativistic, i.e.

$$\rho_{\mathrm{tot}}(x) = \rho_\gamma(T_\gamma(x)) + \rho_{\nu,\mathrm{tot}}(x) + \sum_\alpha \rho_\alpha(T_\gamma(x))\,, \tag{B.15}$$

with

$$\rho_\gamma(T_\gamma(x)) = g_\gamma \frac{\pi^2}{30} T_\gamma^4(x)\,, \tag{B.16}$$

$$\rho_\alpha(T_\gamma(x)) = \frac{g_\alpha}{2\pi^2}\int_0^\infty \mathrm{d}p\, \frac{p^2 E_\alpha}{e^{\frac{E_\alpha}{T_\gamma(x)}}+1}\,, \tag{B.17}$$

$$P_\alpha(T_\gamma(x)) = \frac{g_\alpha}{6\pi^2}\int_0^\infty \mathrm{d}p\, \frac{p^4}{E_\alpha\left(e^{\frac{E_\alpha}{T_\gamma(x)}}+1\right)}\,. \tag{B.18}$$

Taking the derivative of each partial energy density depending on x only through T_γ yields

$$\rho'_\alpha = \frac{\mathrm{d}\rho_\alpha}{\mathrm{d}T_\gamma} T'_\gamma\,, \tag{B.19}$$

$$\frac{\mathrm{d}\rho_\alpha}{\mathrm{d}T_\gamma} = \frac{g_\alpha}{2\pi^2 T_\gamma^2}\int_0^\infty \mathrm{d}p\, p^2 E_\alpha^2 \frac{e^{\frac{E_\alpha}{T_\gamma}}}{\left(e^{\frac{E_\alpha}{T_\gamma}}+1\right)^2}\,. \tag{B.20}$$

In total we, thus, have

$$xH\rho'_{\mathrm{tot}} = -3H(\rho_{\mathrm{tot}} + P_{\mathrm{tot}}) \tag{B.21}$$

$$\Leftrightarrow x\left[\frac{\mathrm{d}\rho_\gamma}{\mathrm{d}T_\gamma}T_\gamma + \sum_\alpha \frac{\mathrm{d}\rho_\alpha}{\mathrm{d}T_\gamma}T_\gamma\right]\frac{T'_\gamma}{T_\gamma} + x\rho'_{\nu,\mathrm{tot}} = -3(\rho_{\mathrm{tot}} + P_{\mathrm{tot}})\,, \tag{B.22}$$

and finally get

$$T'_\gamma = -\frac{T_\gamma}{x}\frac{3(\rho_{\mathrm{tot}} + P_{\mathrm{tot}}) + x\rho'_{\nu,\mathrm{tot}}}{\Xi(x)}\,, \tag{B.23}$$

$$\Xi(x) = 4\rho_\gamma + \sum_\alpha \frac{g_\alpha}{2\pi^2 T_\gamma}\int_0^\infty \mathrm{d}p\, p^2 E_\alpha^2 \frac{e^{\frac{E_\alpha}{T_\gamma}}}{\left(e^{\frac{E_\alpha}{T_\gamma}}+1\right)^2}\,. \tag{B.24}$$

B.3 Choice of Initial Conditions

In the following, we discuss and justify the choice of initial conditions for the integration of the QKEs that can be summarised as:

$$x_0 = 0.01\,, \qquad \varrho(x_0, y) \equiv (\exp(y) + 1)^{-1} \cdot \mathbb{P}_{e}\,, \qquad T_\gamma(x_0) = \bar{T}(x_0)\,, \tag{B.25}$$

where the initial comoving temperature simply evaluates to $\bar{T}(x_0) = 1\,\mathrm{MeV}/x_0 = 100\,\mathrm{MeV}$. The primary reason behind the choice of these initial conditions for any given x_0 is the assumption that no initial population of sterile neutrinos ($\varrho_{ss}(x_0) \equiv 0$), and hence, also no active–sterile correlations ($\varrho_{es}(x_0) \equiv 0$) exist as they can only be produced indirectly by active–sterile oscillations in the underlying model. Moreover, active neutrinos are in thermal equilibrium with the Standard Model (SM) plasma due to rapid weak interactions at least until $T_\gamma \geq 1\,\mathrm{GeV}$. This justifies that the phase space distributions of active neutrinos are essentially given by the Fermi–Dirac distribution. Furthermore, as we prove in this section, the structure of the QKEs also implies that rapid weak interactions between active neutrinos and other SM particles suppress active–sterile oscillations, meaning that $\varrho \propto \mathbb{P}_{e}$ is maintained as long as this condition is fulfilled. Therefore, the desired choice for the initial time x_0 is the latest value at which the initial conditions (B.25) still represent a good approximation in order to reduce numerical efforts.

Suppression of Active–Sterile Oscillations We start by rewriting the QKEs (3.31) in the form

$$xH(x)\frac{\partial \varrho}{\partial x} = -i[\hat{H}(x,y), \varrho(x,y)] + \{\Gamma^+(x,y), \mathbb{1} - \varrho(x,y)\} - \{\Gamma^-(x,y), \varrho(x,y)\}\,, \tag{B.26}$$

where the gain and loss terms Γ^+ and Γ^- encode the production and annihilation rates of neutrinos in the primordial plasma, respectively. We suppress the explicit dependence of the gain and loss terms on the phase space density matrix (PSDM) for notational convenience. In order to analyse the structure of these equations in more detail, it is convenient to expand all matrix valued quantities in the basis of SU(2) generators

$$\tau^\mu = \frac{1}{2}\sigma^\mu\,, \tag{B.27}$$

where σ^k are the Pauli matrices for $k = 1, 2, 3$ and $\sigma^0 = \mathbb{1}$. This is possible since all appearing matrices $\varrho, \hat{H}$ and $\Gamma^\pm$ are hermitian and can be represented as real vectors, i.e.

$$A =: a_\mu \tau^\mu = \frac{1}{2}\begin{pmatrix} a_0 + a_3 & a_1 - ia_2 \\ a_1 + ia_2 & a_0 - a_3 \end{pmatrix}\,, \qquad a_\mu = 2\mathrm{Tr}(A \cdot \tau^\mu)\,, \qquad A \in \mathbb{H}(2)\,. \tag{B.28}$$

Using this basis, the QKEs can be cast into the form

$$xH\frac{\partial \rho_0}{\partial x} = 2\gamma^+ - (\gamma^+ + \gamma^-)(\rho_0 + \rho_3)\,, \tag{B.29}$$

$$xH\frac{\partial \vec{\rho}}{\partial x} = \vec{h} \times \vec{\rho} - (\gamma^+ + \gamma^-)\vec{\rho} + (2\gamma^+ - (\gamma^+ + \gamma^-)\rho_0)\vec{e}_3\,, \tag{B.30}$$

with the following vector representations of the PSDM, Hamiltonian and gain and loss terms:

$$\varrho =: \rho_\mu \tau^\mu \,, \qquad \hat{H} =: h_\mu \tau^\mu \,, \qquad \Gamma^\pm =: \underbrace{\gamma^\pm}_{>0}(\tau^0 + \tau^3) \,, \tag{B.31}$$

where we define $\vec{a} := (a_1, a_2, a_3)$ and use $\Gamma^\pm \propto \mathbb{P}_e = \tau^0 + \tau^3$. In this representation, it is obvious that the flavour oscillations originate from the commutator term. To further discuss the impact of the collisions, we first consider the evolution equations for the correlation elements of the PSDM, i.e.

$$xH\frac{\partial \rho_j}{\partial x} = (\vec{h} \times \vec{\rho})_j - (\gamma^+ + \gamma^-)\rho_j \,, \qquad j = 1, 2 \,. \tag{B.32}$$

In the rapid interaction regime $\gamma^+ + \gamma^- \gg |\vec{h}|$, these equations result in an exponential damping of the active–sterile correlations, and hence, also impede the associated oscillations since the evolution of $\varrho_{ss} \equiv (\rho_0 - \rho_3)/2$ is governed solely by the oscillations and the damped off-diagonal elements:

$$xH\frac{\partial \varrho_{ss}}{\partial x} = -\frac{1}{2}(\vec{h} \times \vec{\rho})_3 = -\frac{(h_1\rho_2 - h_2\rho_1)}{2} \,. \tag{B.33}$$

Therefore, rapid weak interactions suppress active–sterile oscillations, and thereby, also the population of sterile neutrinos. Lastly, the electron neutrino density $\varrho_{ee} \equiv (\rho_0 + \rho_3)/2$ evolves as

$$xH\frac{\partial \varrho_{ee}}{\partial x} = \frac{1}{2}(\vec{h} \times \vec{\rho})_3 + 2\gamma^+(1 - \varrho_{ee}) - 2\gamma^- \varrho_{ee} \,. \tag{B.34}$$

Neglecting contributions from oscillations at very rapid interaction rates $\gamma^\pm \gg xH$, the structure of these terms coincides with that of the usual classical Boltzmann equation, and therefore, also has the same equilibrium limit. In total this proves all statements made above leading to the choice of initial conditions for a given, suitable initial time x_0.

Choice of the Initial Time In order to assess the validity of the initial conditions in Equation (B.29) at a starting point x_0, corresponding to temperatures $T_\gamma < 1\,\mathrm{GeV}$, we need to solve the QKEs from a save starting point, like $T_\gamma(\tilde{x}_0) = 10\,\mathrm{GeV}$, down to x_0. At this new starting point, we know that our assumption of rapid neutrino interactions is true. In the following, we do this for $x_0 = 0.01$ for a representative set of model configurations considered in this work. In this high temperature range $T_\gamma \in [100\,\mathrm{MeV}, 10\,\mathrm{GeV}]$ many more ultra-relativistic SM particles—like quarks and heavy leptons—participate in the weak interactions with neutrinos, and hence, only considering the subset of processes described in Section 3.3.1 would underestimate the true values of the interaction rates. This, however, always results in a conservative estimate of x_0 that is smaller or equal to the true value one would obtain using the full set of collision terms. Hence, we proceed our estimation of x_0 using the partial set of rates, as it is also done e.g. in Reference [101]. This is actually a good approximation as electron–neutrino processes are already rapid enough to maintain full thermal equilibrium of ν_e with the plasma and to suppress neutrino oscillations.

Table B.1: Representative benchmark points used for the validity check of the adopted initial conditions summarised in Equation (B.25).

Model	m_ϕ / eV	m_{s0} / eV	b
ADR-only	-	-	10^{-17}
ADR-only	-	-	10^{-6}
ADR-only	-	-	10^{-4}
ADR+ALP ($\widehat{p}_1$)	10^{-20}	50	10^{-17}
ADR+ALP ($\widehat{p}_2$)	10^{-12}	250	10^{-17}

Moreover, since we are mainly interested in those models leading to a strongly suppressed sterile neutrino production even long after x_0, i.e. that produce SM-compatible values of ΔN_{eff} and $Y_{^4\text{He}}$, we establish the following rule for when to accept the validity of the initial conditions (B.25): *If a model, assuming the initial conditions from Equation* (B.25)*, leads to SM-compatible values for* ΔN_{eff} *and* $Y_{^4\text{He}}$ *at the end of the full integration, it needs to fulfil the initial conditions precisely at* x_0 *when starting the integration from the much smaller value of* $\widetilde{x}_0 = 10^{-4}$. In contrast to that, if the considered model already fails to produce SM-compatible values for our main quantities given the initial conditions in Equation (B.25), it would especially fail to do so if $\varrho_{ss} \neq 0$ at x_0. This is because a preexisting population of ν_s at x_0 always increases the disagreement of the central cosmological parameters and their SM values at the end of the full integration.

We present our results for all components of the PSDM for a representative set of models, listed in Table B.1, in Figure B.1. Inspecting the behaviour of the electron neutrino density $\varrho_{ee}(x_0, y)$, shown in the upper left hand panel of Figure B.1, proves that the electron neutrino density indeed follows its equilibrium value at x_0 for all models. In contrast to that, we find that there exist models (ADR-only with $b = 10^{-17}$) for that ϱ_{ss}, as well as the real and imaginary part of ϱ_{es} are not sufficiently negligible, but still small compared to the equilibrium distribution f_ν^{eq}. Fortunately, the affected models are those that also fail to provide proper mixing suppression after x_0, and hence, do not result in SM-compatible values of our central quantities ΔN_{eff}, m_s^{eff} and $Y_{^4\text{He}}$. In all other cases, i.e. where either the shortcut parameter or the additional sterile mass contribution from the scalar field are sufficiently large to suppress ν_s population, the initial conditions (B.25) represent a good approximation. For the purposes of our analysis it is, thus, sufficient to use (B.25) for all models, but we stress that for a precision estimate of ΔN_{eff}—or any other observable depending on ϱ—it is mandatory to start the QKE evolution earlier than $x_0 = 0.01$.

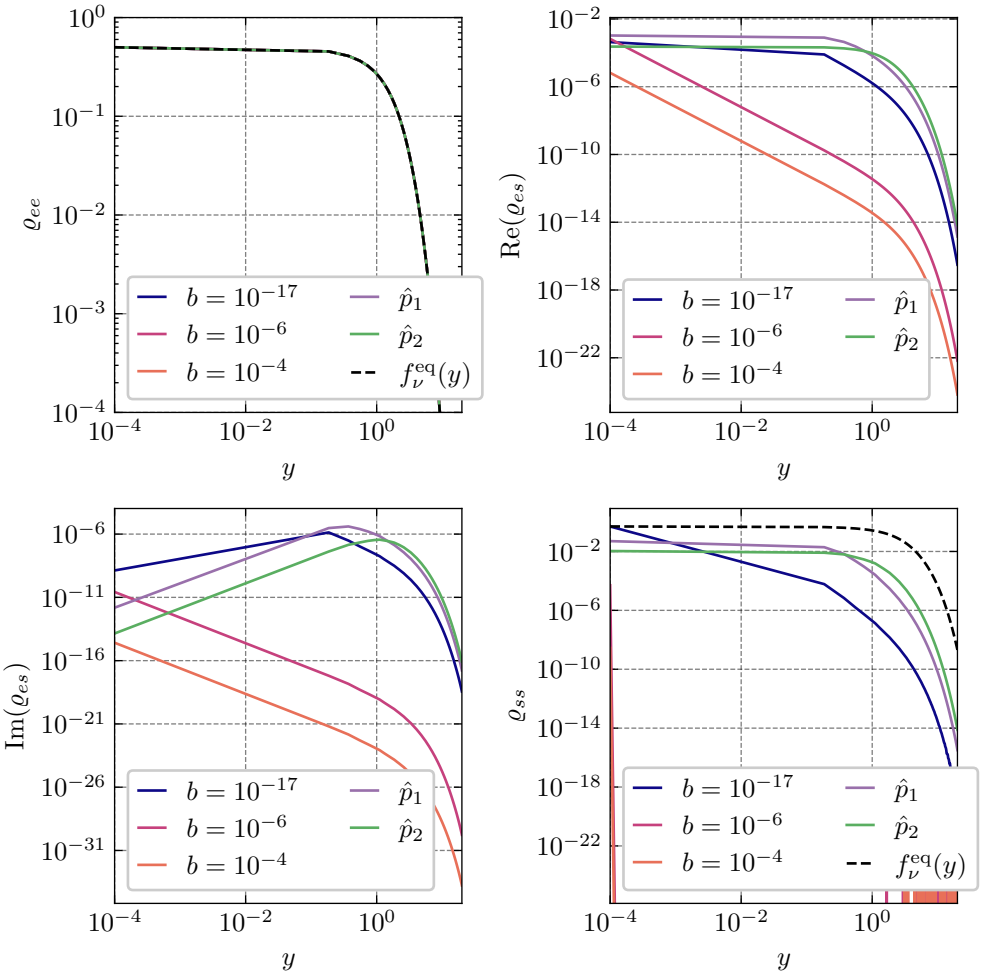

Figure B.1: All components of the PSDM evaluated at $x_0 = 0.01$ after integrating the QKEs from $\tilde{x}_0 = 10^{-4}$, plotted against the dimensionless momentum y for the representative set of models shown in Table B.1.

B.4 Numerical Solution of the QKEs

The QKEs, as well as the differential equation for the evolution of the photon temperature, are solved using the GNU Scientific Library [285] in combination with `C++`. We use a fixed step size `Burlisch-Stoer` algorithm with $N \sim 10^4$ time steps between $x_0 = 0.01$ and $x_{\text{fin}} = 50$.

The computation of the interaction terms involve (multiple) integrations for which we employ the closed Newton–Cotes formula of order 6, suggesting a number of $N_y = 109$ equally spaced points for the momentum space grid. If the neutrino density matrices need to be evaluated at momenta between the grid points, we use a cubic Steffen spline [286] to ensure a monotonically in- or decreasing interpolation between the reference points.

B.5 Boltzmann Equation for the Neutron Fraction

According to Reference [21], the Boltzmann equation for the neutron fraction X_n reads

$$xH(x)\frac{\mathrm{d}X_n}{\mathrm{d}x}(x) = \lambda_{pn}(x)\,(1 - X_n(x)) - \lambda_{np}(x)X_n(x)\,, \tag{B.35}$$

where the thermal reaction rates, λ_{pn} and λ_{np}, can be further subdivided into partial rates, i.e.

$$\lambda_{np}(x) = \lambda_{n+e^+\to p+\bar{\nu}_e} + \lambda_{n+\nu_e\to p+e^-} + \lambda_{n\to p+\bar{\nu}_e+e^-}\,, \tag{B.36}$$

$$\lambda_{pn}(x) = \lambda_{n+e^+\leftarrow p+\bar{\nu}_e} + \lambda_{n+\nu_e\leftarrow p+e^-} + \lambda_{n\leftarrow p+\bar{\nu}_e+e^-}\,. \tag{B.37}$$

Moreover, the corresponding partial rates are given by

$$\lambda_{n+\nu_e\to p+e^-}(x) = A\int_0^\infty p_\nu^2 p_e E_e[1 - f_e(E_e, T_\gamma(x))]\varrho_{ee}\left(x, \frac{p_\nu}{\Lambda}a(x)\right)\,\mathrm{d}p_\nu\,, \tag{B.38}$$

$$\lambda_{n+e^+\to p+\bar{\nu}_e}(x) = A\int_0^\infty p_e^2 p_\nu E_\nu\left[1 - \varrho_{ee}\left(x, \frac{p_\nu}{\Lambda}a(x)\right)\right] f_e(E_e, T_\gamma(x))\,\mathrm{d}p_e\,, \tag{B.39}$$

$$\lambda_{n\to p+e^-+\bar{\nu}_e}(x) = A\int_0^{p_0} p_e^2 p_\nu E_\nu\left[1 - \varrho_{ee}\left(x, \frac{p_\nu}{\Lambda}a(x)\right)\right][1 - f_e(E_e, T_\gamma(x))]\,\mathrm{d}p_e\,. \tag{B.40}$$

Here, $f_e(E, T_\gamma)$ and $\varrho_{ee}(x, y)$ represent the electron and electron neutrino phase space distributions, respectively, and p_e and p_ν denote the e^- and ν_e momenta. Moreover, E_e is the electron energy, $\Delta m = m_n - m_p$ is the neutron–proton mass splitting, and in order to enforce four-momentum conservation the following relations must hold:

1. Equation (B.38): $E_e = E_\nu + \Delta m$
2. Equation (B.39): $E_\nu = E_e + \Delta m$

3. Equation (B.40): $E_\nu = \Delta m - E_e$

The constant A is computed from the lifetime of the neutron in its rest frame τ_n and amounts to

$$A \approx \left\{0.0157(\Delta m)^5 \tau_n\right\}^{-1} . \tag{B.41}$$

The proton-to-neutron reaction rates λ_{pn} are obtained from Equations (B.38) to (B.40) by replacing $f \to 1 - f$ for all phase space distribution functions. Lastly, the upper bound of integration in Equation (B.40) is given by $p_0 = \sqrt{\Delta m^2 - m_e^2}$.

B.6 Full Set of Differential Equations

For completeness, we list the full set of differential equations in the form in which they are integrated simultaneously in our code. The central variables are defined in Section 3.2, i.e.

$$x(t,p) = a(t)\,, \qquad\qquad y(t,p) = a(t)\frac{p}{\Lambda}\,, \tag{B.42}$$

with $\Lambda = 1\,\mathrm{MeV}$ and the scale factor normalised such that $a(t_0) = \Lambda/T_\gamma(t_0)$ at the initial time t_0. The target quantities for that we solve in our implementation are the PSDM $\varrho(x,y)$, the neutron fraction $X_n(x)$ as well as the dimensionless photon temperature

$$z := x\frac{T_\gamma}{\Lambda}\,. \tag{B.43}$$

To be precise, we solve the differential equations for the PSDM and the dimensionless photon temperature simultaneously between $x_0 = 0.01$ and $x_{\mathrm{fin}} = 50$, whereas we solve the differential equations for the neutron fraction X_n between $\hat{x}_0$ and $\hat{x}_{\mathrm{fin}}$ such that $T_\gamma(\hat{x}_0) = 5\,\mathrm{MeV}$ and $t(\hat{x}_{\mathrm{fin}}) = 300\,\mathrm{s}$. The full expressions of the differential equations in terms of the dimensionless variables read

$$\frac{\mathrm{d}z}{\mathrm{d}x}(x) = \frac{z(x)}{x}\left(1 - \frac{3[\tilde{\rho}_{\mathrm{tot}}(x) + \tilde{P}_{\mathrm{tot}}(x)] + x\frac{\mathrm{d}\tilde{\rho}_{\nu,\mathrm{tot}}}{\mathrm{d}x}(x)}{\tilde{\Xi}(x)}\right)\,, \tag{B.44}$$

$$\frac{\partial\varrho}{\partial x}(x,y) = \frac{m_{\mathrm{Pl}}}{\Lambda}\sqrt{\frac{3}{8\pi\tilde{\rho}_{\mathrm{tot}}(x)}}\left\{-ix^2[\hat{\tilde{H}}(x,y),\varrho(x,y)] + \frac{1}{x^4}\tilde{C}[x,y,\varrho(x,y)]\right\}\,, \tag{B.45}$$

$$\frac{\mathrm{d}X_n}{\mathrm{d}x}(x) = \frac{m_{\mathrm{Pl}}}{\Lambda}\sqrt{\frac{3}{8\pi\tilde{\rho}_{\mathrm{tot}}(x)}}\frac{1}{x^4}\left\{\tilde{\lambda}_{pn}(x)\,(1 - X_n(x)) - \tilde{\lambda}_{np}(x)X_n(x)\right\}\,. \tag{B.46}$$

Equation (B.44) is the evolution equation for the photon temperature, Equation (B.45) specifies the QKEs and Equation (B.46) is the differential equation for the neutron fraction. In the following, we list the precise definitions of all quantities and functions appearing in Equations (B.44) to (B.46).

Quantities for the Photon Temperature Evolution The dimensionless energy densities $\tilde{\rho}$ appearing in Equations (B.44) to (B.46) are defined as

$$\tilde{\rho}_{\mathrm{tot}} := \sum_{i\in\mathcal{R}} \tilde{\rho}_i \,, \qquad \tilde{\rho}_{\nu,\mathrm{tot}} := \sum_{i\in\mathcal{V}} \tilde{\rho}_i \,, \qquad \tilde{\rho}_i := \frac{g_i}{2\pi^2} \int_0^\infty \mathrm{d}y\, y^2 \tilde{E}_i(x,y) \tilde{f}(x,y) \,, \tag{B.47}$$

with the set of contributing radiation species $\mathcal{R} := \{\gamma, e, \nu_1, \nu_2, \nu_3, \nu_4\}$ and the set of neutrino species $\mathcal{V} := \{\nu_1, \nu_2, \nu_3, \nu_4\}$. Moreover, the pressure is defined as

$$\tilde{P} = \sum_{i\in\mathcal{R}} \tilde{P}_i \,, \qquad \tilde{P}_i = \frac{g_i}{2\pi^2} \int_0^\infty \mathrm{d}y\, y^2 \left(\frac{y^2}{3\tilde{E}_i(x,y)} \right) \tilde{f}(x,y) \,, \tag{B.48}$$

and the respective phase space distribution functions read

$$\tilde{f}_{\nu_i}(x,y) \approx \varrho^{\mathrm{m}}_{11}(x,y) \,, \quad i \in \{1,2,3\} \,, \qquad \tilde{f}_{\nu_4}(x,y) \approx \varrho^{\mathrm{m}}_{22}(x,y) \,, \tag{B.49}$$

$$\tilde{f}_e(x,y) := \left(1 + \exp\left(\frac{\tilde{E}(x,y)}{z(x)} \right) \right)^{-1} , \qquad \tilde{f}_\gamma(x,y) := \left(1 - \exp\left(\frac{y}{z(x)} \right) \right)^{-1} , \tag{B.50}$$

where $\varrho^{\mathrm{m}}_{ij}$ denote the components of the PSDM in the mass eigenstate basis. Furthermore, the dimensionless one-particle energy for a particle of mass m reads

$$\tilde{E}(x,y) := \sqrt{y^2 + \left(x \frac{m}{\Lambda} \right)^2} \,. \tag{B.51}$$

Finally, the function $\tilde{\Xi}$ reads

$$\tilde{\Xi}(x) = 4\tilde{\rho}_\gamma(x) + \frac{g_e}{2\pi^2} \int_0^\infty \mathrm{d}y\, y^2 \frac{\tilde{E}^2(x,y)}{z(x)} \frac{\exp\left(\frac{\tilde{E}(x,y)}{z(x)} \right)}{\left(1 + \exp\left(\frac{\tilde{E}(x,y)}{z(x)} \right) \right)^2} \,. \tag{B.52}$$

In the limit where all particle masses are negligible and all species are in thermal equilibrium with the plasma or do not contribute at all to the energy density, we get $\mathrm{d}z \,/\, \mathrm{d}x \equiv 0$.

Quantities for the Quantum Kinetic Equations In addition to the Planck mass m_{Pl} and the total dimensionless energy density $\tilde{\rho}_{\mathrm{tot}}$, the QKEs contain the dimensionless Hamiltonian

$$\hat{\tilde{H}}(x,y) := \frac{1}{2y} \frac{\hat{M}^2}{\Lambda^2} - \frac{8\sqrt{2}(G_{\mathrm{F}}\Lambda^2)y}{3x^6} \left(\frac{\Lambda^2}{m_W^2} \tilde{\rho}_e + \frac{\Lambda^2}{m_Z^2} \tilde{\rho}_{\nu_e} \right) \mathbb{P}_e - b \frac{y}{2x^2} \mathbb{P}_s \,, \tag{B.53}$$

as well as the dimensionless collision term

$$\tilde{C}[x,y,\varrho] = \frac{4(G_{\mathrm{F}}\Lambda^2)^2}{(2\pi)^2 y^2} \sum_{i=1}^{3} \tilde{c}_i[x,y,\varrho] \,. \tag{B.54}$$

The partial collision terms are given by

$$\begin{aligned}\tilde{c}_1[x,y,\varrho] = &\iint \mathrm{d}^2(y_1,y_3)\,\frac{y_1}{\tilde{E}_1}\frac{y_3}{\tilde{E}_3}\tilde{\Phi}_1(x,y,y_1,y_2,y_3)\\ &\times\Bigg\{g_R^2\kappa_1(y,y_1,y_2,y_3)+g_L^2\kappa_2(y,y_1,y_2,y_3)\\ &\quad -g_Lg_Rx^2\frac{m_e^2}{\Lambda^2}\kappa_3(y,y_1,y_2,y_3)\Bigg\}\Bigg|_{y_2=y+\tilde{E}_1-\tilde{E}_3},\end{aligned}\tag{B.55}$$

$$\begin{aligned}\tilde{c}_2[x,y,\varrho] = &\iint \mathrm{d}^2(y_1,y_3)\,\frac{y_1}{\tilde{E}_1}\frac{y_3}{\tilde{E}_3}\tilde{\Phi}_2(x,y,y_1,y_2,y_3)\\ &\times\Bigg\{g_L^2\kappa_1(y,y_1,y_2,y_3)+g_R^2\kappa_2(y,y_1,y_2,y_3)\\ &\quad -g_Lg_Rx^2\frac{m_e^2}{\Lambda^2}\kappa_3(y,y_1,y_2,y_3)\Bigg\}\Bigg|_{y_2=y+\tilde{E}_1-\tilde{E}_3},\end{aligned}\tag{B.56}$$

$$\begin{aligned}\tilde{c}_3[x,y,\varrho] = &\iint \mathrm{d}^2(y_2,y_3)\,\frac{y_2}{\tilde{E}_2}\frac{y_3}{\tilde{E}_3}\tilde{\Phi}_3(x,y,y_1,y_2,y_3)\\ &\times\Bigg\{g_L^2\kappa_1(y,y_1,y_2,y_3)+g_R^2\kappa_4(y,y_1,y_2,y_3)\\ &\quad +g_Lg_Rx^2\frac{m_e^2}{\Lambda^2}\kappa_5(y,y_1,y_2,y_3)\Bigg\}\Bigg|_{y_2=\tilde{E}_2+\tilde{E}_3-y},\end{aligned}\tag{B.57}$$

with the kinematics functions

$$\begin{aligned}\kappa_1(y,y_1,y_2,y_3) = 2\Big(&y\tilde{E}_1\tilde{E}_2\tilde{E}_3D_1(y,y_1,y_2,y_3)-\tilde{E}_1\tilde{E}_2D_2(y_1,y_2;y,y_3)\\ &-y\tilde{E}_3D_2(y,y_3;y_1,y_2)+D_3(y,y_1,y_2,y_3)\Big),\end{aligned}\tag{B.58}$$

$$\begin{aligned}\kappa_2(y,y_1,y_2,y_3) = 2\Big(&y\tilde{E}_1\tilde{E}_2\tilde{E}_3D_1(y,y_1,y_2,y_3)+y\tilde{E}_1D_2(y,y_1;y_2,y_3)\\ &+\tilde{E}_2\tilde{E}_3D_2(y_2,y_3;y,y_1)+D_3(y,y_1,y_2,y_3)\Big),\end{aligned}\tag{B.59}$$

$$\kappa_3(y,y_1,y_2,y_3) = y\tilde{E}_2D_1(y,y_1,y_2,y_3)-D_2(y_1,y_3;y,y_2)\,,\tag{B.60}$$

$$\begin{aligned}\kappa_4(y,y_1,y_2,y_3) = 2\Big(&y\tilde{E}_1\tilde{E}_2\tilde{E}_3D_1(y,y_1,y_2,y_3)-y\tilde{E}_2D_2(y,y_2;y_1,y_3)\\ &-\tilde{E}_1\tilde{E}_3D_2(y_1,y_3;y,y_2)+D_3(y,y_1,y_2,y_3)\Big),\end{aligned}\tag{B.61}$$

$$\kappa_5(y,y_1,y_2,y_3) = y\tilde{E}_1D_1(y,y_1,y_2,y_3)+D_2(y_2,y_3;y,y_1)\,,\tag{B.62}$$

and the statistical functions as defined in Appendix B.1 with the replacements $f \to \tilde{f}$. Moreover, the so-called Dolgov–Hansen–Semikoz (DHS)-integrals [287] are given by

$$D_1(y_1, y_2, y_3, y_4) := \frac{4}{\pi} \int_0^\infty \frac{\mathrm{d}\lambda}{\lambda^2} \prod_{l=1}^{4} \sin(\lambda y_l)\,, \tag{B.63}$$

$$D_2(y_1, y_2; y_3, y_4) := \frac{4}{\pi} \int_0^\infty \frac{\mathrm{d}\lambda}{\lambda^4} \prod_{k=1}^{2} \sin(\lambda y_k) \prod_{l=3}^{4} [\lambda y_l \cos(\lambda y_l) - \sin(\lambda y_l)]\,, \tag{B.64}$$

$$D_3(y_1, y_2, y_3, y_4) := \frac{4}{\pi} \int_0^\infty \frac{\mathrm{d}\lambda}{\lambda^6} \prod_{l=1}^{4} [\lambda y_l \cos(\lambda y_l) - \sin(\lambda y_l)]\,, \tag{B.65}$$

and can be computed analytically as shown in Reference [126]. Note that our conventions for the DHS-integrals match those in References [126, 287], and hence, differ from the ones employed in Reference [100]. The DHS-integrals from Reference [100] can be obtained by multiplying ours by 4, changing sign of D_2 and swapping $(y_1, y_2) \leftrightarrow (y_3, y_4)$ in the argument of D_2. Moreover, the dimensionless energy $\tilde{E}_i$ for a neutrino coincides with its dimensionless momentum y_i, i.e. $\tilde{E}_i = y_i$.

Quantities for the Evolution Equation of the Neutron Fraction Finally, we present the dimensionless interaction rates appearing within the evolution equation of the neutron fraction:

$$\tilde{\lambda}_{np}(x) = \tilde{\lambda}_{n+e^+ \to p+\bar{\nu}_e} + \tilde{\lambda}_{n+\nu_e \to p+e^-} + \tilde{\lambda}_{n \to p+\bar{\nu}_e+e^-}\,, \tag{B.66}$$

$$\tilde{\lambda}_{pn}(x) = \tilde{\lambda}_{n+e^+ \leftarrow p+\bar{\nu}_e} + \tilde{\lambda}_{n+\nu_e \leftarrow p+e^-} + \tilde{\lambda}_{n \leftarrow p+\bar{\nu}_e+e^-}\,, \tag{B.67}$$

with

$$\tilde{\lambda}_{n+\nu_e \to p+e^-}(x) = \tilde{A} \int_0^\infty y_\nu^2 y_e \tilde{E}_e [1 - \tilde{f}_e(x, y_e)] \varrho_{ee}\,(x, y_\nu)\; \mathrm{d}y_\nu\,, \tag{B.68}$$

$$\tilde{\lambda}_{n+e^+ \to p+\bar{\nu}_e}(x) = \tilde{A} \int_0^\infty y_e^2 y_\nu^2\, [1 - \varrho_{ee}\,(x, y_\nu)]\, f_e(x, y_e)\, \mathrm{d}y_e\,, \tag{B.69}$$

$$\tilde{\lambda}_{n \to p+e^-+\bar{\nu}_e}(x) = \tilde{A} \int_0^{y_0} y_e^2 y_\nu^2\, [1 - \varrho_{ee}\,(x, y_\nu)]\, [1 - f_e(x, y_e)]\, \mathrm{d}y_e\,, \tag{B.70}$$

and the inverse reaction rates can be obtained by replacing $f \leftrightarrow 1 - f$. Furthermore, using the definitions

$$\Delta\tilde{m} := \frac{\Delta m}{\Lambda}\,, \qquad \tilde{A} := \Lambda^4 A\,, \qquad y_0 := x \frac{p_0}{\Lambda}\,, \tag{B.71}$$

energy conservation implies

1. In $\tilde{\lambda}_{n+\nu_e \to p+e^-}$: $\tilde{E}_e = y_\nu + x\Delta\tilde{m}$
2. In $\tilde{\lambda}_{n+e^+ \to p+\bar{\nu}_e}$: $y_\nu = \tilde{E}_e + x\Delta\tilde{m}$
3. In $\tilde{\lambda}_{n \to p+e^- +\bar{\nu}_e}$: $y_\nu = x\Delta\tilde{m} - \tilde{E}_e$

The original quantities are defined in Appendix B.5.

C Appendix - Quantum Gravitational Decoherence

This appendix chapter contains important supplemental material for the considerations in Chapter 4. The contents of Sections C.1 and C.2 are important for the derivation of the neutrino oscillation probability in vacuum, assuming the phenomenological QG model described in Section 4.1. Then, in Section C.3 we derive and discuss the neutrino flux at Earth produced by a source that emits unstable primary particles that decay into neutrinos. Finally, in Section C.4, we compute the differential energy distribution for neutrinos emerging from beta decay. This is important for our considerations of cosmic neutron sources in Section 4.2.

C.1 Basis Matrix Decomposition

The set of hermitian $N \times N$ matrices,

$$\mathbb{H}(N) := \left\{ A \in \mathbb{C}^{N\times N} : A^\dagger = A \right\} , \tag{C.1}$$

forms a vector space over $\mathbb{R}$ and can be equipped with an inner product

$$\langle A, B \rangle := 2\mathrm{Tr}\left[A \cdot B\right] , \qquad \forall A, B \in \mathbb{H}(N) . \tag{C.2}$$

The dimension of this vector space is $\dim(\mathbb{H}(N)) = N^2$. For the considerations of this work it is convenient to decompose all hermitian matrices in terms of a certain set of basis matrices,

$$\{\lambda_A : A = 0, \dots, N^2 - 1\} , \tag{C.3}$$

$$\lambda_0 = \frac{1}{\sqrt{2N}} \mathbb{1} , \tag{C.4}$$

$$\lambda_A = \frac{\alpha_A}{2} \left[\vec{e}_{J(A)} \otimes \vec{e}_{K(A)}\right] + \frac{\alpha_A^*}{2} \left[\vec{e}_{K(A)} \otimes \vec{e}_{J(A)}\right] , \quad A = 1, \dots, N(N-1) , \tag{C.5}$$

$$\lambda_{N(N-1)+m} = \frac{1}{\sqrt{2m(m+1)}} \left\{ \sum_{j=1}^{m} \left[\vec{e}_j \otimes \vec{e}_j\right] - m \left[\vec{e}_{m+1} \otimes \vec{e}_{m+1}\right] \right\} , \tag{C.6}$$

where $m = 1, \dots, N-1$ and the index functions α_A, $J(A)$ and $K(A)$ read

$$\alpha_A = \begin{cases} 1 , & A \text{ odd} \\ -i , & A \text{ even} \end{cases} , \tag{C.7}$$

$$J(A) = \sum_{a=1}^{N-1} \Theta \left(\left\lfloor \frac{A+1}{2} \right\rfloor - 1 - \sum_{b=1}^{a-1} (N-b) \right) , \tag{C.8}$$

$$K(A) = J(A) + \left\lfloor \frac{A+1}{2} \right\rfloor - \sum_{a=1}^{J(A)-1} (N-a) . \tag{C.9}$$

Here, Θ is the Heaviside step function with the convention $\Theta(0) = 1$. The zeroth matrix of this set just represents the scaled identity matrix while the next $N(N-1)$ matrices each correspond to the real and imaginary parts of the off-diagonal entries of a hermitian matrix in an alternating fashion. For $N = 3$, for example, they are simply given by the off-diagonal SU(3) generators

$$\lambda_1 = \frac{1}{2}\begin{pmatrix} 0 & 1 & 0 \\ 1 & 0 & 0 \\ 0 & 0 & 0 \end{pmatrix}, \qquad \lambda_2 = \frac{1}{2}\begin{pmatrix} 0 & -i & 0 \\ i & 0 & 0 \\ 0 & 0 & 0 \end{pmatrix}, \tag{C.10}$$

$$\lambda_3 = \frac{1}{2}\begin{pmatrix} 0 & 0 & 1 \\ 0 & 0 & 0 \\ 1 & 0 & 0 \end{pmatrix}, \qquad \lambda_4 = \frac{1}{2}\begin{pmatrix} 0 & 0 & -i \\ 0 & 0 & 0 \\ i & 0 & 0 \end{pmatrix}, \tag{C.11}$$

$$\lambda_5 = \frac{1}{2}\begin{pmatrix} 0 & 0 & 0 \\ 0 & 0 & 1 \\ 0 & 1 & 0 \end{pmatrix}, \qquad \lambda_6 = \frac{1}{2}\begin{pmatrix} 0 & 0 & 0 \\ 0 & 0 & -i \\ 0 & i & 0 \end{pmatrix}. \tag{C.12}$$

The index functions, $J(A)$ and $K(A)$, always ensure that $J(A) < K(A)$ and that the non-zero element in the upper triangle of the off-diagonal λ_A traces the upper triangle row-wise. Finally, the remaining diagonal basis matrices λ_A with $A > N(N-1)$ are traceless and for $N = 3$ they are given by

$$\lambda_7 = \frac{1}{2}\begin{pmatrix} 1 & 0 & 0 \\ 0 & -1 & 0 \\ 0 & 0 & 0 \end{pmatrix}, \qquad \lambda_8 = \frac{1}{2\sqrt{3}}\begin{pmatrix} 1 & 0 & 0 \\ 0 & 1 & 0 \\ 0 & 0 & -2 \end{pmatrix}. \tag{C.13}$$

It is now straight forward to show that the λ_A form an orthonormal basis (ONB) by computing all mutual scalar products. Since all λ_A with $A \geq 1$ are traceless, it is obvious that they are orthogonal to λ_0, i.e.

$$\langle \lambda_0, \lambda_A \rangle = 2\mathrm{Tr}\left[\lambda_0 \lambda_A\right] = \sqrt{\frac{1}{2N}}\mathrm{Tr}\left[\lambda_A\right] = 0\,. \tag{C.14}$$

Moreover, the zeroth basis element is properly normalised,

$$\langle \lambda_0, \lambda_0 \rangle = 2\mathrm{Tr}\left[\lambda_0^2\right] = \frac{2}{2N}\mathrm{Tr}\left[\mathbb{1}\right] = 1\,. \tag{C.15}$$

The scalar products of two off-diagonal basis matrices with $1 \leq A, B \leq N(N-1)$ yield

$$\begin{aligned}\langle \lambda_A, \lambda_B \rangle = 2\mathrm{Tr}\Bigg(&\left\{ \frac{\alpha_A}{2} \left[\vec{e}_{J(A)} \otimes \vec{e}_{K(A)} \right] + \frac{\alpha_A^*}{2} \left[\vec{e}_{K(A)} \otimes \vec{e}_{J(A)} \right] \right\} \\ &\times \left\{ \frac{\alpha_B}{2} \left[\vec{e}_{J(B)} \otimes \vec{e}_{K(B)} \right] + \frac{\alpha_B^*}{2} \left[\vec{e}_{K(B)} \otimes \vec{e}_{J(B)} \right] \right\} \Bigg) \end{aligned} \tag{C.16}$$

$$\begin{aligned} = \frac{1}{2} \Big[&\alpha_A \alpha_B \delta_{K(A)J(B)} \mathrm{Tr}\left(\vec{e}_{J(A)} \otimes \vec{e}_{K(B)} \right) \\ &+ \alpha_A \alpha_B^* \delta_{K(A)K(B)} \mathrm{Tr}\left(\vec{e}_{J(A)} \otimes \vec{e}_{J(B)} \right) \\ &+ \alpha_A^* \alpha_B \delta_{J(A)J(B)} \mathrm{Tr}\left(\vec{e}_{K(A)} \otimes \vec{e}_{K(B)} \right) \\ &+ \alpha_A^* \alpha_B^* \delta_{J(A)K(B)} \mathrm{Tr}\left(\vec{e}_{K(A)} \otimes \vec{e}_{K(B)} \right) \Big] \end{aligned} \tag{C.17}$$

$$\begin{aligned} = \frac{1}{2} \Big[&(\alpha_A \alpha_B + \alpha_A^* \alpha_B^*) \delta_{K(A)J(B)} \delta_{J(A)K(B)} \\ &+ (\alpha_A \alpha_B^* + \alpha_A^* \alpha_B) \delta_{J(A)J(B)} \delta_{K(A)K(B)} \Big] . \end{aligned} \tag{C.18}$$

Since $J(A) < K(A)$ the first term can never contribute since otherwise $K(A) = J(B) < K(B) = J(A)$ contradicting the construction. Moreover, in the second term $J(A) = J(B)$ and $K(A) = K(B)$ can only happen for either the same off-diagonal matrix, i.e. $A = B$, or for two neighboring matrices with $\lfloor (A+1)/2 \rfloor = \lfloor (B+1)/2 \rfloor$. In the first case, we simply get

$$\langle \lambda_A, \lambda_A \rangle = \frac{2|\alpha_A|^2}{2} = 1 , \tag{C.19}$$

and

$$\langle \lambda_A, \lambda_B \rangle = \pm \frac{i - i}{2} = 0 , \qquad \left\lfloor \frac{A-1}{2} \right\rfloor = \left\lfloor \frac{B-1}{2} \right\rfloor \wedge A \neq B , \tag{C.20}$$

in the latter case. In all other cases, the inner product also vanishes proving the mutual orthonormality of the off-diagonal matrices.

For pairings of off-diagonal and diagonal matrices, we find

$$\begin{aligned}\langle \lambda_A, \lambda_{N(N-1)+m} \rangle = \frac{2}{\sqrt{2m(m+1)}} \mathrm{Tr} \Bigg(& \left\{ \frac{\alpha_A}{2} \left[\vec{e}_{J(A)} \otimes \vec{e}_{K(A)} \right] + \frac{\alpha_A^*}{2} \left[\vec{e}_{K(A)} \otimes \vec{e}_{J(A)} \right] \right\} \\ & \times \left\{ \sum_{j=1}^{m} \left[\vec{e}_j \otimes \vec{e}_j \right] - m \left[\vec{e}_{m+1} \otimes \vec{e}_{m+1} \right] \right\} \Bigg) \end{aligned} \tag{C.21}$$

$$\begin{aligned} = \frac{1}{\sqrt{2m(m+1)}} \Bigg(& \sum_{j=1}^{m} \alpha_A \delta_{K(A)j} \mathrm{Tr} \left(\vec{e}_{J(A)} \otimes \vec{e}_j \right) \\ & + \sum_{j=1}^{m} \alpha_A^* \delta_{J(A)j} \mathrm{Tr} \left(\vec{e}_{K(A)} \otimes \vec{e}_j \right) \\ & - m \alpha_A \delta_{K(A)(m+1)} \mathrm{Tr} \left(\vec{e}_{J(A)} \otimes \vec{e}_{m+1} \right) \\ & - m \alpha_A^* \delta_{J(A)(m+1)} \mathrm{Tr} \left(\vec{e}_{K(A)} \otimes \vec{e}_{m+1} \right) \Bigg) \end{aligned} \tag{C.22}$$

$$= \frac{[\alpha_A + \alpha_A^*]}{\sqrt{2m(m+1)}} \left(\sum_{j=1}^{m} \delta_{K(A)j} \delta_{J(A)j} - m \delta_{K(A)(m+1)} \delta_{J(A)(m+1)} \right). \tag{C.23}$$

This expression can only be non-zero iff $J(A) = K(A)$ which is not possible by construction. Hence, off-diagonal and diagonal λ_A are orthogonal.

Finally, we prove the mutual orthonormality of the traceless diagonal λ_A, i.e.

$$\begin{aligned} \langle \lambda_{N(N-1)+k}, \lambda_{N(N-1)+m} \rangle = & \frac{2}{\sqrt{2k(k+1)}\sqrt{2m(m+1)}} \mathrm{Tr} \left(\left\{ \sum_{l=1}^{k} \left[\vec{e}_l \otimes \vec{e}_l \right] - k \left[\vec{e}_{k+1} \otimes \vec{e}_{k+1} \right] \right\} \right. \\ & \left. \times \left\{ \sum_{j=1}^{m} \left[\vec{e}_j \otimes \vec{e}_j \right] - m \left[\vec{e}_{m+1} \otimes \vec{e}_{m+1} \right] \right\} \right) \\ = & \frac{1}{\sqrt{km(k+1)(m+1)}} \left(\sum_{l=1}^{k} \sum_{j=1}^{m} \delta_{lj} \mathrm{Tr} \left(\vec{e}_l \otimes \vec{e}_j \right) - m \sum_{l=1}^{k} \delta_{l(m+1)} \mathrm{Tr} \left(\vec{e}_l \otimes \vec{e}_{m+1} \right) \right. \\ & \left. - k \sum_{j=1}^{m} \delta_{j(k+1)} \mathrm{Tr} \left(\vec{e}_{k+1} \otimes \vec{e}_j \right) + km \delta_{(m+1)(k+1)} \mathrm{Tr} \left(\vec{e}_{k+1} \otimes \vec{e}_{m+1} \right) \right) \\ = & \frac{1}{\sqrt{km(k+1)(m+1)}} \left(\sum_{j=1}^{\min(m,k)} 1 - m\Theta(k-(m+1)) - k\Theta(m-(k+1)) + m^2 \delta_{mk} \right). \end{aligned}$$

Without loss of generality, let $m \leq k$ in the following. Then, we get

$$\langle \lambda_{N(N-1)+k}, \lambda_{N(N-1)+m} \rangle = \frac{(m - m\Theta(k-(m+1)) + m^2\delta_{mk})}{\sqrt{km(k+1)(m+1)}} = \begin{cases} 1\,, & m = k \\ 0\,, & m < k \end{cases}. \tag{C.24}$$

This also proves that the λ_A form a linearly independent set of vectors. That they indeed form a complete basis is easy to see by taking an arbitrary hermitian matrix $A \in \mathbb{H}(N)$ with entries a_{jk}. Obviously, the a_{jk} fulfil $a_{jk} = a_{kj}^*$ and A can be decomposed into a diagonal and an off-diagonal part by using the canonical basis on $\mathbb{C}^{N\times N}$, i.e.

$$A = \sum_{j,k=1}^{N} a_{jk} \left[\vec{e}_j \otimes \vec{e}_k\right] \tag{C.25}$$

$$= \underbrace{\sum_{j} a_{jj} \left[\vec{e}_j \otimes \vec{e}_j\right]}_{A_{\text{diag}}} + \underbrace{\sum_{j<k} (a_{jk} \left[\vec{e}_j \times \vec{e}_k\right] + a_{kj}^* \left[\vec{e}_k \times \vec{e}_j\right])}_{A_{\text{off}}} . \tag{C.26}$$

We can yet introduce another set of N^2 matrices,

$$\beta_{jj} := \left[\vec{e}_j \otimes \vec{e}_j\right] , \qquad j = 1, \ldots, N, \tag{C.27}$$

$$\gamma_{jk} := \left[\vec{e}_j \otimes \vec{e}_k\right] + \left[\vec{e}_k \otimes \vec{e}_j\right] , \qquad 1 \le j < k \le N, \tag{C.28}$$

$$\tilde{\gamma}_{jk} := i \left[\vec{e}_j \otimes \vec{e}_k\right] - i \left[\vec{e}_k \otimes \vec{e}_j\right] , \qquad 1 \le j < k \le N. \tag{C.29}$$

These matrices are linearly independent and we can use them to write the arbitrary matrix A as

$$A = \sum_{j=1}^{N} a_{jj}\beta_{jj} + \sum_{j<k} \mathrm{Re}(a_{jk})\gamma_{jk} + \sum_{j<k} \mathrm{Im}(a_{jk})\tilde{\gamma}_{jk} . \tag{C.30}$$

Therefore, the dimension of $\mathbb{H}(N)$ is indeed N^2 and since $|\{\lambda_A : 0 \le A \le N^2 - 1\}| = N^2$ and all λ_A are linearly independent we have successfully constructed a basis of $\mathbb{H}(N)$.

The last property, we prove in this section is the total antisymmetry of the structure constants f_{ABC} defined by

$$[\lambda_A, \lambda_B] =: i \sum_C f_{ABC}\lambda_C . \tag{C.31}$$

We can use the orthonormality of the λ_A to write the structure constants as

$$f_{ABC} = -i\langle [\lambda_A, \lambda_B], \lambda_C \rangle . \tag{C.32}$$

The antisymmetry in the first two indices, $f_{ABC} = -f_{BAC}$, is inherited from the antisymmetry of the commutator and for the total antisymmetry we therefore only have to prove the antisymmetry property in the last two indices, $f_{ABC} = -f_{ACB}$, since then we automatically get

$$f_{ABC} = -f_{ACB} = f_{CAB} = -f_{CBA} . \tag{C.33}$$

The antisymmetry in the last two indices can be shown as follows:

$$\begin{aligned} f_{ABC} &= -i\langle[\lambda_A, \lambda_B], \lambda_C\rangle \\ &= -2i\mathrm{Tr}((\lambda_A\lambda_B - \lambda_B\lambda_A)\lambda_C) \\ &= -2i\mathrm{Tr}(\lambda_C\lambda_A\lambda_B - \lambda_C\lambda_B\lambda_A) \\ &= -2i\mathrm{Tr}(\lambda_C\lambda_A\lambda_B - \lambda_A\lambda_C\lambda_B) \\ &= -2i\mathrm{Tr}((\lambda_C\lambda_A - \lambda_A\lambda_C)\lambda_B) \\ &= 2i\mathrm{Tr}([\lambda_A, \lambda_C]\lambda_B) \\ &= i\langle[\lambda_A, \lambda_C], \lambda_B\rangle = -f_{ACB}\,. \end{aligned}$$

C.2 Neutrino Oscillation Probability in Vacuum in the Presence of Maximally Flavour Violating Quantum Gravity

The neutrino oscillation probability in the density matrix formalism is computed by taking the trace of the product of the evolved, initial density matrix and the density matrix of the detected state. Thus, the probability for an initial neutrino of flavour ν_a to be detected as a neutrino of flavour ν_b is given by

$$P_{ab}(L) = \mathrm{Tr}\left[\mathbb{P}_b\rho_a(L)\right]\,, \tag{C.34}$$

where $\mathbb{P}_b$ is the projector onto flavour ν_b and $\rho_a(L)$ solves the evolution Equation (4.1) with initial condition $\rho_a(0) = \mathbb{P}_a$. The dissipator under consideration is explicitly parametrised as

$$D[\rho(x)] = D_{\mathrm{WP}}[\rho(x)] + D_{\mathrm{QG}}[\rho(x)]\,, \tag{C.35}$$

$$D_{\mathrm{WP}}[\rho(x)] = -\sum_{j\neq k}\frac{\mathrm{d}\Gamma^{\mathrm{WP}}_{jk}(x)}{\mathrm{d}x}\Pi_j\rho(x)\Pi_k\,, \tag{C.36}$$

$$D_{\mathrm{QG}}[\rho(x)] = -\sum_{A,B=1}^{n_f^2-1}\gamma^A{}_B\left(\frac{E}{E_0}\right)^n\langle\lambda_B, \rho(x)\rangle\lambda_A\,, \tag{C.37}$$

and therefore contains the effect of WP separation as well as the impact of QG DOFs on the neutrino system. The QG dissipator is already conveniently parametrised in terms of the basis matrices λ_A introduced in Section C.1. Next, we also translate all other components of Equation (4.1) into this representation ultimately allowing us to write it as a vector valued ordinary differential equation.

In the following, we work in the mass basis. The WP dissipator in the λ_A basis becomes

$$[\mathcal{D}_{\mathrm{WP}}]^A{}_B = \langle \lambda_A, D_{\mathrm{WP}}[\lambda_B]\rangle \tag{C.38}$$

$$= -\sum_{j\neq k} \frac{\mathrm{d}\Gamma^{\mathrm{WP}}_{jk}(x)}{\mathrm{d}x}\langle \lambda_A, \Pi_j\lambda_B\Pi_k\rangle \tag{C.39}$$

$$= -\sum_{k>j} \frac{\mathrm{d}\Gamma^{\mathrm{WP}}_{jk}(x)}{\mathrm{d}x}\langle \lambda_A, \Pi_j\lambda_B\Pi_k + \Pi_k\lambda_B\Pi_j\rangle\,. \tag{C.40}$$

As we have $j \neq k$ none of the diagonal λ_B contribute to this sum and only the off-diagonal ones yield a non-zero dissipator matrix element. Moreover, for any off-diagonal dissipator matrix, we get

$$\Pi_j\lambda_B\Pi_k + \Pi_k\lambda_B\Pi_j = [\lambda_B]_{jk}\vec{e}_j\otimes\vec{e}_k + [\lambda_B]_{kj}\vec{e}_k\otimes\vec{e}_j\,, \tag{C.41}$$

which is non-zero iff $J(B) = j$ and $K(B) = k$ and then this procedure yields

$$\Pi_j\lambda_B\Pi_k + \Pi_k\lambda_B\Pi_j = \lambda_B\delta_{J(B)j}\delta_{K(B)k}\,. \tag{C.42}$$

In total, we therefore get

$$[\mathcal{D}_{\mathrm{WP}}]^A{}_B = -\sum_{k>j}\frac{\mathrm{d}\Gamma^{\mathrm{WP}}_{jk}(x)}{\mathrm{d}x}\delta_{J(B)j}\delta_{K(B)k}\delta_{AB} = -\frac{\mathrm{d}\Gamma^{\mathrm{WP}}_{J(B)K(B)}(x)}{\mathrm{d}x}\delta_{AB}\,. \tag{C.43}$$

Furthermore, the initial and final density matrices, i.e. the flavour projectors, in the mass basis read

$$[\mathbb{P}_a]^m = U^\dagger[\mathbb{P}_a]^f U \tag{C.44}$$

$$= \sum_{jk}\sum_{bc} U^*_{bj}\delta_{ab}\delta_{ac}U_{ck}\vec{e}_j\otimes\vec{e}_k \tag{C.45}$$

$$= \sum_{jk} U^*_{aj}U_{ak}\vec{e}_j\otimes\vec{e}_k\,. \tag{C.46}$$

In terms of the $\mathrm{SU}(n_f)$ basis, this corresponds to the following vector components:

$$\pi^0_a = \sqrt{\frac{2}{n_f}}\,, \qquad \pi^1_a = \mathrm{Re}(U^*_{a2}U_{a1})\,, \tag{C.47}$$

$$\pi^2_a = \mathrm{Im}(U^*_{a2}U_{a1})\,, \qquad \pi^3_a = \mathrm{Re}(U^*_{a3}U_{a1})\,, \tag{C.48}$$

$$\pi^4_a = \mathrm{Im}(U^*_{a3}U_{a1})\,, \qquad \pi^{2n_f-1}_a = \mathrm{Re}(U^*_{a3}U_{a2})\,, \tag{C.49}$$

$$\pi^{2n_f}_a = \mathrm{Im}(U^*_{a3}U_{a2})\,, \qquad \pi^{n_f(n_f-1)+1}_a = |U_{a1}|^2 - |U_{a2}|^2\,, \tag{C.50}$$

$$\pi^{n_f(n_f-1)+2}_a = \frac{|U_{a1}|^2 + |U_{a2}|^2 - 2|U_{a3}|^2}{\sqrt{3}}\,, \qquad \pi^{n_f(n_f-1)+k}_a = \sqrt{\frac{2}{k(k+1)}}\,, \quad \forall k\geq 3\,. \tag{C.51}$$

All other components vanish.

Next, the full evolution equation in the mass basis and $\mathrm{SU}(n_f)$ vector representation becomes

$$\frac{\mathrm{d}\varrho^A(x)}{\mathrm{d}x} = \sum_B \left(\mathcal{C}^A{}_B + \mathcal{D}^A{}_B(x)\right)\varrho^B(x)\,, \tag{C.52}$$

$$\mathcal{C}^A{}_B := -i\langle\lambda_A, [\hat{H}, \lambda_B]\rangle = -\sum_C h^C f_{CAB}\,, \tag{C.53}$$

$$\mathcal{D}^A{}_B(x) := [\mathcal{D}_{\mathrm{WP}}]^A{}_B(x) + [\mathcal{D}_{\mathrm{QG}}]^A{}_B(x)\,, \tag{C.54}$$

where f_{ABC} are the totally antisymmetric structure constants of the basis λ_A and $h^A := \langle\lambda_A, \hat{H}\rangle$. Since we work in the mass basis, it is, however, simpler and much more instructive to consider the action of the commutator matrix in terms of the entries of the Hamiltonian, i.e.

$$[C[\rho]]^{\mathrm{mass}}_{jk} := [-i[\hat{H}, \rho]]^{\mathrm{mass}}_{jk} \tag{C.55}$$

$$= -i\sum_l \left([\hat{H}]^{\mathrm{mass}}_{jl}[\rho]^{\mathrm{mass}}_{lk} - [\rho]^{\mathrm{mass}}_{jl}[\hat{H}]^{\mathrm{mass}}_{lk}\right) \tag{C.56}$$

$$= -i\sum_l \left(E_j\delta_{jl}[\rho]^{\mathrm{mass}}_{lk} - [\rho]^{\mathrm{mass}}_{jl}E_l\delta_{lk}\right) \tag{C.57}$$

$$= -i\Delta E_{jk}[\rho]^{\mathrm{mass}}_{jk} \tag{C.58}$$

$$= \Delta E_{jk}(-i\mathrm{Re}\rho_{jk} + \mathrm{Im}\rho_{jk})\,. \tag{C.59}$$

This expression is only non-zero for $j \neq k$, i.e. only the off-diagonal elements of ρ contribute to the result. Consequently, $\mathcal{C}^A{}_B \equiv 0$ for $B = 0, n_f(n_f-1)+1, \ldots, n_f^2-1$. Moreover, all diagonal elements of $[C[\rho]]^{\mathrm{mass}}$ vanish implying $\mathcal{C}^A{}_B \equiv 0$ for $A = 0, n_f(n_f-1)+1, \ldots, n_f^2-1$. This is also obvious from the antisymmetry of the matrix $\mathcal{C}^A{}_B$. The next crucial observation is that only $[\rho_{jk}]^{\mathrm{mass}}$ contributes to $[C[\rho]]^{\mathrm{mass}}_{jk}$. Let L be the index of the real, off-diagonal matrix λ_L with non-zero components at the j,k entry with $k > j$ without loss of generality. Then on the one hand, we can write

$$[C[\rho]]^{\mathrm{mass}}_{jk} = \mathrm{Re}[C[\rho]]^{\mathrm{mass}}_{jk} + i\mathrm{Im}[C[\rho]]^{\mathrm{mass}}_{jk} \tag{C.60}$$

$$= [\mathcal{C}\vec{\varrho}]_L[\lambda_L]_{jk} + [\mathcal{C}\vec{\varrho}]_{L+1}[\lambda_{L+1}]_{jk} \tag{C.61}$$

$$= [\mathcal{C}\vec{\varrho}]_L - i[\mathcal{C}\vec{\varrho}]_{L+1}\,, \tag{C.62}$$

where we make use of the fact that $[\lambda_L]_{jk} = 1$ and $[\lambda_{L+1}]_{jk} = -i$, and on the other hand we have

$$[C[\rho]]^{\mathrm{mass}}_{jk} = \Delta E_{jk}(\mathrm{Im}\rho_{jk} - i\mathrm{Re}\rho_{jk}) \tag{C.63}$$

$$= -\Delta E_{jk}\rho_{L+1} - i\Delta E_{jk}\rho_L\,. \tag{C.64}$$

Comparing coefficients yields

$$\begin{pmatrix}[\mathcal{C}\vec{\varrho}]_L \\ [\mathcal{C}\vec{\varrho}]_{L+1}\end{pmatrix} = \begin{pmatrix}0 & -\Delta E_{jk} \\ \Delta E_{jk} & 0\end{pmatrix}\begin{pmatrix}\varrho_L \\ \varrho_{L+1}\end{pmatrix}\,. \tag{C.65}$$

Hence, the commutator matrix $\mathcal{C}$ can be decomposed into a block-diagonal matrix of the form

$$\mathcal{C} = 0_{1\times 1} \oplus \left[\bigoplus_{L=1}^{\frac{n_f(n_f-1)}{2}} -\Delta E_{J(2L)K(2L)}\epsilon \right] \oplus 0_{(n_f-1)\times(n_f-1)}\,, \tag{C.66}$$

$$\epsilon = \begin{pmatrix} 0 & 1 \\ -1 & 0 \end{pmatrix}. \tag{C.67}$$

Here, one value of L corresponds to the pair of real and imaginary off-diagonal basis matrices and has to be scaled by two when plugged into the index functions, J and K, introduced in Section C.1, in order to yield the correct indices.

From now on we only consider diagonal QG dissipators and define the full matrix operator of the right hand side of the Lindblad equation as

$$\mathcal{E}(x) := \mathcal{C} + \mathcal{D}_{\mathrm{WP}}(x) + \mathcal{D}_{\mathrm{QG}}\,. \tag{C.68}$$

In this scenario, $\mathcal{E}(x)$ commutes with itself for different distances x, since in all non-trivial (2×2) blocks induced by $\mathcal{C}$ $\mathcal{D}_{\mathrm{WP}}(x)$ is proportional to the identity and $\mathcal{D}_{\mathrm{QG}}$ is constant and diagonal. Thus, the full solution to the Lindblad equation is given by

$$\vec{\varrho}(x, x_0) = \exp\left(\int_{x_0}^{x} \mathrm{d}x'\, \mathcal{E}(x')\right) \vec{\varrho}_0\,, \tag{C.69}$$

for initial state $\vec{\varrho}(x_0, x_0) = \vec{\varrho}_0$.

The oscillation probability can then be computed from

$$P_{ab}(L) = \mathrm{Tr}[\mathbb{P}_b \rho_a(L)] = \frac{\langle \mathbb{P}_b, \rho_a(L)\rangle}{2} = \frac{\vec{\pi}_b^T \exp\left(\int_0^L \mathrm{d}x\, \mathcal{E}(x)\right) \vec{\pi}_a}{2}\,. \tag{C.70}$$

Since $\mathcal{E}$ is block diagonal with non-trivial blocks that are at most (2×2), we can solve this system of equations analytically. Let S_L be the matrix that diagonalises the matrix

$$\mathcal{E}_L := \begin{pmatrix} -\frac{\mathrm{d}\Gamma_{J(2L)K(2L)}}{\mathrm{d}x} - \Gamma_{2L-1} & -\Delta E_{J(2L)K(2L)} \\ \Delta E_{J(2L)K(2L)} & -\frac{\mathrm{d}\Gamma_{J(2L)K(2L)}}{\mathrm{d}x} - \Gamma_{2L} \end{pmatrix}, \tag{C.71}$$

i.e. $\tilde{\mathcal{E}}_L = S_L^{-1}\mathcal{E}_L S_L$, for $L = 1, \ldots, n_f(n_f-1)/2$. The probability then decomposes into the following sum:

$$\begin{aligned} P_{ab}(L) = \frac{\pi_b^0 \pi_a^0}{2} &+ \frac{1}{2} \sum_{A\in\{1,2,n_f\}} [\vec{\pi}_b]_A^T S_A e^{\int_0^L \mathrm{d}x \tilde{\mathcal{E}}_A(x)} S_A^{-1} [\vec{\pi}_a]_A \\ &+ \sum_{k=1}^{n_f-1} \frac{\pi_b^{n_f(n_f-1)+k} \pi_a^{n_f(n_f-1)+k}}{2} e^{-\Gamma_{n_f(n_f-1)+k} L}\,. \end{aligned} \tag{C.72}$$

Using the explicit form of the vector representations for the flavour projectors given by (C.47) and

$$S_L := \begin{pmatrix} -i\omega_{J(2L)K(2L)} + \frac{\Delta\Gamma_{2L}}{\Delta E_{J(2L)K(2L)}} & i\omega_{J(2L)K(2L)} + \frac{\Delta\Gamma_{2L}}{\Delta E_{J(2L)K(2L)}} \\ 1 & 1 \end{pmatrix}, \tag{C.73}$$

$$\tilde{\mathcal{E}}_A(x) = \begin{pmatrix} -i\omega_{J(2L)K(2L)} - \bar{\Gamma}_{2L} & 0 \\ 0 & i\omega_{J(2L)K(2L)} - \bar{\Gamma}_{2L} \end{pmatrix}, \tag{C.74}$$

$$\bar{\Gamma}_{2L} := \frac{\Gamma_{2L} + \Gamma_{2L-1}}{2}, \tag{C.75}$$

$$\Delta\Gamma_{2L} := \frac{\Gamma_{2L} - \Gamma_{2L-1}}{2}, \tag{C.76}$$

$$\omega_{J(2L)K(2L)} := \sqrt{(\Delta E_{J(2L)K(2L)})^2 - (\Delta\Gamma_{2L})^2}, \tag{C.77}$$

$$[\vec{\pi}_a]^T_A := \begin{pmatrix} \pi_a^{2A-1} & \pi_a^{2A} \end{pmatrix}, \tag{C.78}$$

results in the oscillation probability (4.14).

C.3 Derivation of the General Neutrino Flux Formula

We derive the general formula for the flux $\phi_b(E, L, \Omega)$ of neutrinos of flavour ν_b and energy E at a given distance L from a source S under a solid angle Ω in a coordinate system with origin at S. We assume the source to emit unstable, primary particles η featuring decay modes with one neutrino in the final state. The term *flux* here refers to the number of particles N per unit area A, time t, solid angle Ω and energy E, i.e.

$$\phi \equiv \frac{1}{A}\frac{\partial^4 N}{\partial t \partial E \partial^2 \Omega}. \tag{C.79}$$

In order to prepare the derivation of the neutrino flux formula in terms of the flux of primary particles at the surface of the source with radius R_S, we first consider the relation between the flux of stable particles at a distance ℓ from the surface of the source and at the surface of S.

Distance Behaviour of Fluxes of Stable Particles The total flux of stable particles in a solid angle region $U \subset S^2$, where S^2 is the unit sphere is constant on the surface of any two balls with radii R_1 and R_2, i.e.

$$\Phi_{\text{tot}}(R_1, U) := R_1^2 \int_U \phi(R_1, \Omega)\, \mathrm{d}^2\Omega = R_2^2 \int_U \phi(R_2, \Omega)\, \mathrm{d}^2\Omega = \Phi_{\text{tot}}(R_2, U). \tag{C.80}$$

Here, we use that the surface measure on the sphere with radius R is $R^2\, \mathrm{d}^2\Omega$. Since this relation holds for arbitrary U and $\phi(R, \Omega) \geq 0$, we can identify the integrands and get

$$\phi(R_2, \Omega) = \frac{R_1^2}{R_2^2}\phi(R_1, \Omega). \tag{C.81}$$

For the case of fluxes of the type

$$\phi(R,\Omega) \equiv \begin{cases} \phi_0(R)\,, & \Omega \in U_0 \\ 0\,, & \Omega \in S^2 \setminus U_0 \end{cases}\,, \tag{C.82}$$

we can furthermore derive

$$\phi(R_2,\Omega) = \frac{R_1^2}{R_2^2}\phi(R_1,\Omega) = \frac{1}{|U_0|}\frac{R_1^2}{R_2^2}\int\limits_{U_0}\phi(R_1,\Omega)\,\mathrm{d}^2\Omega = \frac{\Phi_{\mathrm{tot}}(R_1)}{|U_0|R_2^2}\,. \tag{C.83}$$

This especially also holds for isotropic fluxes corresponding to the case $U_0 = S^2$ and $|U_0| = 4\pi$.

Furthermore, we can define a probability density for the emission of a particle η with energy E_η on the surface of the source by

$$p^{\mathrm{em.}}(E_\eta, R_\mathrm{S}, \Omega_\eta) = \frac{R_\mathrm{S}^2}{\Phi_\eta^{\mathrm{tot}}}\phi_\eta(E_\eta, R_\mathrm{S}, \Omega_\eta)\,. \tag{C.84}$$

We normalise this density suh that it is a proper probability density with respect to the surface measure of the unit sphere. The normalisation condition then reads

$$1 = \int\limits_{E_\eta^{\min}}^{E_\eta^{\max}}\int\limits_{S^2} p^{\mathrm{em.}}(E_\eta, R_\mathrm{S}, \Omega_\eta)\,\mathrm{d}^2\Omega\,\mathrm{d}E_\eta\,, \tag{C.85}$$

with

$$\Phi_\eta^{\mathrm{tot}} = \int\limits_{E_\eta^{\min}}^{E_\eta^{\max}}\int\limits_{S^2} \phi_\eta(E_\eta, R_\mathrm{S}, \Omega_\eta) R_\mathrm{S}^2\,\mathrm{d}^2\Omega\,\mathrm{d}E_\eta\,. \tag{C.86}$$

In the following, we employ the law of total probability in order to derive a reliable formula relating the final neutrino flux $\phi_b(E, L, \Omega)$ to the flux of primary particles at the surface of the source. The main requirement we impose is that at $L \to \infty$ the summed, final neutrino flux is given by the sum of all total fluxes of the primary particles times their individual branching ratio to decay into any neutrino, i.e.

$$\lim_{L\to\infty}\Phi_\nu^{\mathrm{tot}}(L) = \lim_{L\to\infty}\sum_b\int\limits_0^\infty L^2\int_{S^2}\phi_b(E,L,\Omega)\,\mathrm{d}^2\Omega\,\mathrm{d}E \tag{C.87}$$

$$= \sum_{\eta\in\mathrm{S}}\Phi_\eta^{\mathrm{tot}}\sum_a\sum_X \mathcal{B}r(\eta\to\nu_a + X)\,. \tag{C.88}$$

Here, we sum over all possible additional final states X accompanying the neutrino production. This means we expect the neutrino flux to be equal to the flux of primary particles that have decayed into neutrinos after emission.

Law of Total Probability For discrete probability spaces Ω, the law of total probability states that we may express the probability for an event A by

$$P(A) = \sum_{n\in I} P(A|B_n)P(B_n)\,, \tag{C.89}$$

where $\{B_n\}_{n\in I}$ is a countable family of events that partition the probability space of all events while mutually excluding each other. Furthermore, $P(A|B_n)$ is the conditional probability that A happens given B_n has happened. In other words, we can reduce the task of evaluating $P(A)$ into several steps if it happens that computing $P(B_n)$ as well as $P(A|B_n)$ is much simpler. For continuous probability spaces this generalises to

$$P(A) = \int\limits_{\mathbb{R}^2} P(A|X=x)p_X(x)\,\mathrm{d}^n x\ , \tag{C.90}$$

where X is a random variable taking on values in $\mathbb{R}^n$ with corresponding probability density function p_X.

In order to find the flux $\phi_b(E, L, \Omega)$, we sum over all contributions of primary particles η emerging from the source and multiply by the probability for any of the primary particles from this set to cause the desired $\nu_b(E)$ at $\vec{L}(L, \Omega)$, i.e.

$$\phi_b(E, L, \Omega)\,\mathrm{d}E\,L^2\,\mathrm{d}^2\Omega = \sum_{\eta\in\mathrm{S}} \Phi_\eta^{\mathrm{tot}}(R_\mathrm{S})\mathbb{P}(\eta\to\nu_b(E, L, \Omega))\,\mathrm{d}E\,\mathrm{d}^2\Omega\ . \tag{C.91}$$

The non-trivial task is now to find the probability density $\mathbb{P}$. At this point the law of total probability comes into play and we use it to break the total process of η emission, decay, neutrino emission and neutrino propagation down into its constituents.

First, we divide the full probability into that for the emission of η and the conditional probability of detection of ν_b if η was indeed emitted, i.e.

$$\begin{aligned}\mathbb{P}(\eta\to\nu_b(E, L, \Omega)) = \int\limits_{E_\eta^{\min}}^{E_\eta^{\max}} \int\limits_{S^2} & p^{\mathrm{em.}}(E_\eta, R_\mathrm{S}, \Omega_\eta) \\ & \times \mathbb{P}(\eta\to\nu_b(E, L, \Omega)|\eta(E_\eta, R_\mathrm{S}, \Omega_\eta))\,\mathrm{d}^2\Omega_\eta\,\mathrm{d}E_\eta\ .\end{aligned} \tag{C.92}$$

As instructed by the law of total probability, we sum over all possible configurations of primary particles.

Next, we take the newly appearing conditional probability and break it further down into smaller pieces, i.e. the probability for η to decay and the probability for the definitely decayed η to produce $\nu_b(E, L, \Omega)$

$$\begin{aligned}&\mathbb{P}(\eta\to\nu_b(E, L, \Omega)|\eta(E_\eta, R_\mathrm{S}, \Omega_\eta)) \\ &= \int\limits_0^\infty p_\eta^{\mathrm{dec.}}(\ell)\mathbb{P}(\eta\to\nu_b(E, L, \Omega)|\eta(E_\eta, R_\mathrm{S}, \Omega_\eta)\text{ dec. at }R_\mathrm{S}+\ell)\,\mathrm{d}\ell\ .\end{aligned} \tag{C.93}$$

The decay probability density is simply given by the usual exponential decay law, i.e.

$$p_\eta^{\text{dec.}}(\ell) = \frac{e^{-\frac{\ell}{\lambda_\eta}}}{\lambda_\eta}\,, \tag{C.94}$$

with the mean free path $\lambda_\eta = p_\eta \tau_\eta / m_\eta$ of η in the reference frame under consideration.

The remaining conditional probability can then finally be expressed in terms of the probability for the decaying η to produce a neutrino of flavour ν_a with energy E, emitted such that it would arrive at $\vec{L}(L,\Omega)$ times the probability for it to oscillate into the final flavour summed over all initial flavours. This yields

$$\begin{aligned}&\mathbb{P}(\eta \to \nu_b(E,L,\Omega) | \eta(E_\eta, R_\text{S}, \Omega_\eta) \text{ dec. at } R_\text{S}+\ell) \\ &= \sum_{a=e,\mu,\tau} p_{\eta a}^{\text{spec.}}(E_\eta, R_\text{S}+\ell, \Omega_\eta; E, L, \Omega) P_{ab}(E, |\vec{L}(L,\Omega) - \vec{l}(R_\text{S}+\ell, \Omega_\eta)|)\,.\end{aligned} \tag{C.95}$$

Here, $p_{\eta a}^{\text{spec.}}$ encodes the spectral and angular distributions of the emitted neutrino in the decay $\eta \to \nu_a$ and is explicitly given by

$$p_{\eta a}^{\text{spec.}}(E_\eta, R_\text{S}+\ell, \Omega_\eta; E, L, \Omega) = \tilde{p}_{\eta a}^{\text{spec.}}(E_\eta, \Omega_\eta; E, \tilde{\omega}(\Omega))\, |\mathrm{d}_\Omega \tilde{\omega}(\Omega)| \tag{C.96}$$

$$\begin{aligned}\tilde{p}_{\eta a}^{\text{spec.}}(E_\eta, \Omega_\eta; E, \tilde{\Omega}) = \sum_X \int_0^\infty \int_{S^2} \frac{1}{\Gamma'_\eta} \frac{\partial^3 \Gamma'_{\eta\to\nu_a+X}}{\partial E' \partial^2 \Omega'}(E', \Omega') \\ \times E^2 \delta^{(3)}(\vec{p}(E,\tilde{\Omega}) - \vec{\lambda}(\vec{p}', \Lambda_\eta))\, \mathrm{d}^2\Omega'\, \mathrm{d}E'\,.\end{aligned} \tag{C.97}$$

This quantity, thus, corresponds to the differential decay width $\mathrm{d}\Gamma'_{\eta\to\nu_a+X}$ of the process $\eta \to \nu_a + X$ normalised to the total decay width of η Γ'_η evaluated in its rest frame, summed over all unobserved, additional final states X and then properly transformed into the lab frame. The transformation to the lab frame is carried out by integrating over all possible energy and solid angle configurations in the rest frame of the decaying particle and enforcing that the momentum in the lab frame matches the Lorentz transformed momentum

$$\vec{\lambda}(\vec{p}', \Lambda_\eta) := (\Lambda_\eta)^k{}_\mu p'^\mu\,, \qquad\qquad p'^0 := |\vec{p}'|\,, \tag{C.98}$$

where Λ_η is the Lorentz transform from the rest frame of the primary particle to the lab frame. Moreover, the direction $\vec{e}_r(\tilde{\Omega})$ of the neutrino in the lab frame is defined with respect to the point of decay at $(R_\text{S}+\ell)\vec{e}_r(\Omega_\eta)$. This has to be translated to Ω, i.e. the source centered solid angle, we are using in the remaining expression. The bijection $\tilde{\omega}$ that achieves this translation is defined by the requirement

$$\vec{e}_r(\tilde{\omega}(\Omega)) \stackrel{!}{=} \frac{L\vec{e}_r(\Omega) - (R_\text{S}+\ell)\vec{e}_r(\Omega_\eta)}{|L\vec{e}_r(\Omega) - (R_\text{S}+\ell)\vec{e}_r(\Omega_\eta)|}\,, \tag{C.99}$$

and therefore depends on the information about the distance vector connecting the point of ν_a emission and ν_b detection. Here, we also the define the unit vectors depending on the solid

angle Ω via

$$\vec{e}_r(\Omega) := \begin{pmatrix} \cos(\varphi)\sin(\theta) \\ \sin(\varphi)\sin(\theta) \\ \cos(\theta) \end{pmatrix}, \qquad \Omega = (\varphi, \cos(\theta))\,. \tag{C.100}$$

The Jacobian of $\tilde{\omega}$, i.e. $\mathrm{d}_\Omega\tilde{\omega}$, is then used to ensure that $p^{\text{spec.}}$ is properly normalised, i.e.

$$\begin{aligned}
&\int_0^\infty \int_{S^2} p_{\eta a}^{\text{spec.}}(E_\eta, R_\text{S} + \ell, \Omega_\eta; E, L, \Omega)\,\mathrm{d}^2\Omega\,\mathrm{d}E \\
&= \sum_X \int_0^\infty \int_{S^2} \frac{1}{\Gamma'_\eta} \frac{\partial^3 \Gamma'_{\eta\to\nu_a+X}}{\partial E' \partial^2 \Omega'}(E', \Omega') \qquad \text{(C.101)} \\
&\quad \times \int_0^\infty \int_{S^2} E^2 \delta^{(3)}(\vec{p}(E, \tilde{\omega}(\Omega)) - \vec{\lambda}(\vec{p}', \Lambda_\eta))\,|\mathrm{d}_\Omega\tilde{\omega}(\Omega)|\,\mathrm{d}^2\Omega\,\mathrm{d}E\,\mathrm{d}^2\Omega'\,\mathrm{d}E' \\
&= \sum_X \int_0^\infty \int_{S^2} \frac{1}{\Gamma'_\eta} \frac{\partial^3 \Gamma'_{\eta\to\nu_a+X}}{\partial E' \partial^2 \Omega'}(E', \Omega') \\
&\quad \times \int_0^\infty \int_{S^2} E^2 \delta^{(3)}(\vec{p}(E, \tilde{\Omega}) - \vec{\lambda}(\vec{p}', \Lambda_\eta))\,\mathrm{d}^2\tilde{\Omega}\,\mathrm{d}E\,\mathrm{d}^2\Omega'\,\mathrm{d}E' \qquad \text{(C.102)} \\
&= \sum_X \int_0^\infty \int_{S^2} \frac{1}{\Gamma'_\eta} \frac{\partial^3 \Gamma'_{\eta\to\nu_a+X}}{\partial E' \partial^2 \Omega'}(E', \Omega') \\
&\quad \times \int_{\mathbb{R}^3} \delta^{(3)}(\vec{p}(E, \tilde{\Omega}) - \vec{\lambda}(\vec{p}', \Lambda_\eta))\,\mathrm{d}^3\vec{p}\,\mathrm{d}^2\Omega'\,\mathrm{d}E' \qquad \text{(C.103)} \\
&= \sum_X \int_0^\infty \int_{S^2} \frac{1}{\Gamma'_\eta} \frac{\partial^3 \Gamma'_{\eta\to\nu_a+X}}{\partial E' \partial^2 \Omega'}(E', \Omega')\,\mathrm{d}^2\Omega'\,\mathrm{d}E' \qquad \text{(C.104)} \\
&= \sum_X \mathcal{BR}(\eta \to \nu_a + X)\,, \qquad \text{(C.105)}
\end{aligned}$$

which does not depend on the primary particle energy and solid angle since branching ratios are Lorentz-invariant and can be simply computed in the rest frame of the decaying primary. Here, also the reason for the E^2 factor becomes obvious: It is used to yield the proper integration measure to cancel the delta function when integrating over observed neutrino energies and solid angles.

This concludes our derivation and the full formula for the neutrino flux reads

$$\begin{aligned}\phi_b(E, L, \Omega) = \frac{R_\mathrm{S}^2}{L^2} \sum_{\eta \in \mathrm{S}} \sum_{a=e,\mu,\tau} \int_{E_\eta^\mathrm{min}}^{E_\eta^\mathrm{max}} \int_{S^2} \int_0^\infty \phi_\eta(E_\eta, R_\mathrm{S}, \Omega_\eta) \frac{e^{-\frac{\ell}{\lambda_\eta}}}{\lambda_\eta} \\ \times p_{\eta a}^\mathrm{spec.}(E_\eta, R_\mathrm{S} + \ell, \Omega_\eta; E, L, \Omega) P_{ab}(E, |\vec{L} - \vec{\ell}|) \, \mathrm{d}\ell \, \mathrm{d}^2\Omega_\eta \, \mathrm{d}E_\eta \, .\end{aligned} \tag{C.106}$$

Next, we show that the main contribution of the Ω_η integral stems from the region $\Omega_\eta \approx \Omega$ for highly boosted primaries, i.e. $E_\eta^\mathrm{min} \gg m_\eta$. To this end we consider the spectral energy and angular distribution in more detail.

C.3.1 Properties of the Spectral and Angular Primary Decay Distribution

Before we consider the case of strongly boosted, unpolarised primary particles, i.e. $E_\eta^\mathrm{min} \gg m_\eta$, representing the most common case when considering astrophysical neutrinos, we study the behaviour of $p^\mathrm{spec.}$ under Lorentz transformations. In particular, we claim that probabilities computed from $p^\mathrm{spec.}$ are invariant under changes of the frame of reference in the sense that the probability to find the emitted neutrino in a certain energy range $\mathcal{E} \subset (0, \infty)$ and angular region $U \subset S^2$ in one frame of reference is the same as to find it in the properly transformed regions in any other frame of reference. To show this, consider an arbitrary Lorentz transform ${\Lambda^\mu}_\nu$ and let

$$\hat{\lambda} : (0, \infty) \times S^2 \to (0, \infty) \times S^2 \, , \tag{C.107}$$

be the associated transformation on the energy and solid angle space. We then find

$$\begin{aligned}&\mathbb{P}_\eta^{\mathrm{spec.}\star}\left[(E^\star, \Omega^\star) \in \hat{\lambda}(\mathcal{E} \times U)\right] \\ &:= \int_{\hat{\lambda}(\mathcal{E}\times U)} \tilde{p}_{\eta a}^\mathrm{spec.}(E_\eta^\star, \Omega_\eta^\star; E^\star, \tilde{\omega}^\star(\Omega^\star)) \, |\mathrm{d}_{\Omega^\star}\tilde{\omega}^\star(\Omega^\star)| \, \mathrm{d}^3(E^\star, \Omega^\star) && \text{(C.108)} \\ &= \int_{\omega^\star(\hat{\lambda}(\mathcal{E}\times U))} \tilde{p}_{\eta a}^\mathrm{spec.}(E_\eta^\star, \Omega_\eta^\star; E^\star, \tilde{\Omega}^\star) \, \mathrm{d}^3\left(E^\star, \tilde{\Omega}^\star\right) && \text{(C.109)} \\ &= \int_{\hat{\lambda}^{-1}(\omega^\star(\hat{\lambda}(\mathcal{E}\times U)))} \tilde{p}_{\eta a}^\mathrm{spec.}(E_\eta, \Omega_\eta; E, \tilde{\Omega}) \, \mathrm{d}^3\left(E, \tilde{\Omega}\right) && \text{(C.110)} \\ &= \int_{\omega^{-1}(\hat{\lambda}^{-1}(\omega^\star(\hat{\lambda}(\mathcal{E}\times U))))} \tilde{p}_{\eta a}^\mathrm{spec.}(E_\eta, \Omega_\eta; E, \tilde{\omega}(\Omega)) \, |\mathrm{d}_\Omega\tilde{\omega}(\Omega)| \, \mathrm{d}^3(E, \Omega) && \text{(C.111)} \\ &= \mathbb{P}_\eta^\mathrm{spec.}\left[(E, \Omega) \in \omega^{-1} \circ \hat{\lambda}^{-1} \circ \omega^\star \circ \hat{\lambda}(\mathcal{E} \times U)\right] \, . && \text{(C.112)}\end{aligned}$$

The newly introduced function $\omega^{(\star)}$ is defined to extend the action of $\tilde{\omega}$ to the three dimensional energy–solid angle space. Thus, it performs the transformation between the source centered

and decay point centered solid angles, $\Omega^{(\star)}$ and $\tilde{\Omega}^{(\star)}$, respectively, while leaving the energy invariant. It is evident that these transformations need to fulfil

$$\omega^\star \circ \hat{\lambda} \equiv \hat{\lambda} \circ \omega \,, \tag{C.113}$$

since first performing a Lorentz transformation and then translating between the different solid angle prescriptions must yield the same outcome as first translating between the different solid angle prescriptions in the original frame of reference and then applying the Lorentz transform. Consequently, also $\omega = \hat{\lambda}^{-1} \circ \omega^\star \circ \hat{\lambda}$ holds and we have

$$\mathbb{P}_\eta^{\text{spec.}\star}\left[(E^\star, \Omega^\star) \in \hat{\lambda}(\mathcal{E} \times U)\right] = \mathbb{P}_\eta^{\text{spec.}}\left[(E, \Omega) \in (\mathcal{E} \times U)\right] . \tag{C.114}$$

Furthermore, we have used that

$$\begin{aligned}
&\tilde{p}_{\eta a}^{\text{spec.}}(E_\eta^\star, \Omega_\eta^\star; E^\star, \tilde{\Omega}^\star)\, \mathrm{d}^3\left(E^\star, \tilde{\Omega}^\star\right) \\
&= \sum_X \int_0^\infty \int_{S^2} \frac{1}{\Gamma'_\eta} \frac{\partial^3 \Gamma'_{\eta \to \nu_a + X}}{\partial E' \partial^2 \Omega'}(E', \Omega') \\
&\quad \times \delta^{(3)}\Big(\vec{p}(E^\star, \tilde{\Omega}^\star) - \vec{\lambda}(\vec{p}\,', \underbrace{\Lambda_\eta^\star}_{\Lambda\Lambda_\eta})\Big) E^{\star 2}\, \mathrm{d}^3\left(E^\star, \tilde{\Omega}^\star\right) \mathrm{d}^2\Omega'\, \mathrm{d}E' \,.
\end{aligned} \tag{C.115}$$

$$\begin{aligned}
&= \sum_X \int_0^\infty \int_{S^2} \frac{1}{\Gamma'_\eta} \frac{\partial^3 \Gamma'_{\eta \to \nu_a + X}}{\partial E' \partial^2 \Omega'}(E', \Omega') \\
&\quad \times \delta^{(3)}\left(\vec{\lambda}(\vec{p}(E, \tilde{\Omega}), \Lambda) - \vec{\lambda}(\vec{p}\,', \Lambda\Lambda_\eta)\right) \mathrm{d}^3\vec{p}^{\,\star}\, \mathrm{d}^2\Omega'\, \mathrm{d}E' \,.
\end{aligned} \tag{C.116}$$

$$\begin{aligned}
&= \sum_X \int_0^\infty \int_{S^2} \frac{1}{\Gamma'_\eta} \frac{\partial^3 \Gamma'_{\eta \to \nu_a + X}}{\partial E' \partial^2 \Omega'}(E', \Omega') \\
&\quad \times \delta^{(3)}\left(\vec{p} - \vec{\lambda}^{-1}(\vec{\lambda}(\vec{p}\,', \Lambda\Lambda_\eta), \Lambda)\right) \mathrm{d}^3\vec{p}\, \mathrm{d}^2\Omega'\, \mathrm{d}E' \,.
\end{aligned} \tag{C.117}$$

$$\begin{aligned}
&= \sum_X \int_0^\infty \int_{S^2} \frac{1}{\Gamma'_\eta} \frac{\partial^3 \Gamma'_{\eta \to \nu_a + X}}{\partial E' \partial^2 \Omega'}(E', \Omega') \\
&\quad \times \delta^{(3)}\left(\vec{p}(E, \tilde{\Omega}) - \vec{\lambda}(\vec{p}\,', \Lambda^{-1}\Lambda\Lambda_\eta)\right) E^2\, \mathrm{d}^3\left(E, \tilde{\Omega}\right) \mathrm{d}^2\Omega'\, \mathrm{d}E' \,.
\end{aligned} \tag{C.118}$$

$$= \tilde{p}_{\eta a}^{\text{spec.}}(E_\eta, \Omega_\eta; E, \tilde{\Omega})\, \mathrm{d}^3\left(E, \tilde{\Omega}\right) , \tag{C.119}$$

holds. Here, we have made use of the connection between the representations of the Lorentz transform Λ on the energy–solid angle space and the three momentum space, i.e.

$$\vec{p}^{\,\star} := \vec{p}(E^\star, \Omega^\star) = \vec{p}(\hat{\lambda}(E, \Omega)) = \vec{\lambda}(\vec{p}(E, \Omega), \Lambda) \,. \tag{C.120}$$

Moreover, the Lorentz transform on three vectors is a group homomorphism in the following sense:

$$\vec{\lambda}(\vec{\lambda}(\vec{p}, \Lambda_1), \Lambda_2) = \vec{\lambda}(\vec{p}, \Lambda_2\Lambda_1) \,, \tag{C.121}$$

which can be easily shown using its definition, i.e.

$$\lambda^k(\vec{\lambda}(\vec{p},\Lambda_1),\Lambda_2) = (\Lambda_2)^k{}_\mu(\Lambda_1)^\mu{}_\nu p^\nu = (\Lambda_2\Lambda_1 p)^k = \lambda^k(\vec{p},\Lambda_2\Lambda_1)\,, \tag{C.122}$$

since

$$(\Lambda_1)^0{}_\nu p^\nu = |\vec{\lambda}(\vec{p},\Lambda_1)|\,, \tag{C.123}$$

holds for light-like vectors p. Lastly, we have utilised the fact that the neutrinos are assumed to be massless in the computation of the decay width, and hence, the appearing integration measures fulfil

$$E^2\,\mathrm{d}^3(E,\Omega) = \mathrm{d}^3\vec{p}\ , \tag{C.124}$$

and

$$\delta^{(3)}(\vec{p}^\star-\vec{q}^\star)\,\mathrm{d}^3\vec{p}^\star = 2E^\star\delta^{(3)}(\vec{p}^\star-\vec{q}^\star)\frac{\mathrm{d}^3\vec{p}^\star}{2E^\star} \tag{C.125}$$

$$= 2E\delta^{(3)}(\vec{p}-\lambda^{-1}(\vec{q}^\star,\Lambda))\frac{\mathrm{d}^3\vec{p}}{2E} \tag{C.126}$$

$$= \delta^{(3)}(\vec{p}-\lambda^{-1}(\vec{q}^\star,\Lambda))\,\mathrm{d}^3\vec{p}\ . \tag{C.127}$$

C.3.2 Neutrino Fluxes from Ultra-Relativistic, Unpolarised Primary Particles

Now that we know that the spectral probability distribution defines a proper probability measure yielding the same probabilities for equivalent neutrino energy and directional configurations, we consider the most common application: Neutrinos from the decay of ultra-relativistic, unpolarised primary particles. In this case we can show that the spectral probability is only significantly different from zero in a small region around $\Omega_\eta \approx \Omega$ or $\tilde{\omega}(\Omega_\eta) \approx \tilde{\omega}(\Omega)$ when considering the situation in the decay centered coordinate system. We first consider the solid angles in the latter coordinate system in the following since the direction of neutrino momentum is naturally defined in this system.

The crucial observation needed to proof our claim is that the differential decay width in the rest frame of the decaying particle has a definite cutoff at $E' = m_\eta$. Indeed $E' < m_\eta$ is enforced in general. The rest frame Σ' and the arbitrary frame where η moves with $\vec{p}_\eta = |\vec{p}_\eta|\vec{e}_r(\tilde{\Omega}_\eta)$ are related by the Lorentz transformation $\Lambda := \Lambda_\eta^{-1}$, i.e.

$$\Lambda^\mu{}_\nu(E_\eta,\tilde{\Omega}_\eta) = \begin{pmatrix} \frac{E_\eta}{m_\eta} & -\frac{|\vec{p}_\eta|}{m_\eta}\vec{e}_r^{\,T}(\tilde{\Omega}_\eta) \\ -\frac{|\vec{p}_\eta|}{m_\eta}\vec{e}_r(\tilde{\Omega}_\eta) & \mathbb{1} + \left(\frac{E_\eta}{m_\eta}-1\right)\vec{e}_r(\tilde{\Omega}_\eta)\vec{e}_r^{\,T}(\tilde{\Omega}_\eta) \end{pmatrix}\,, \tag{C.128}$$

$$p'^\mu = \Lambda^\mu{}_\nu(E_\eta,\tilde{\Omega}_\eta)p^\nu\,. \tag{C.129}$$

The condition $m_\nu \leq E' < m_\eta$ can therefore be expressed as

$$m_\nu \leq \frac{E_\eta}{m_\eta} E - \frac{|\vec{p}_\eta|}{m_\eta} |\vec{p}| \vec{e}_r^{\,T}(\tilde{\Omega}_\eta)\vec{e}_r(\tilde{\Omega}) < m_\eta \tag{C.130}$$

$$\Leftrightarrow \frac{1 - \frac{m_\eta^2}{E_\eta^2}\frac{E_\eta}{E}}{\sqrt{1-\frac{m_\nu^2}{E^2}}\sqrt{1-\frac{m_\eta^2}{E_\eta^2}}} < \vec{e}_r^{\,T}(\tilde{\Omega}_\eta)\vec{e}_r(\tilde{\Omega}) \leq \frac{1 - \frac{m_\eta m_\nu}{E_\eta E}}{\sqrt{1-\frac{m_\nu^2}{E^2}}\sqrt{1-\frac{m_\eta^2}{E_\eta^2}}}\,. \tag{C.131}$$

Both boundaries are close to one in the limit $m_\eta/E_\eta, m_\nu/E \ll 1$, which we easily see by Taylor expanding them to second order in these quantities, leading to

$$\frac{1 - \frac{m_\eta^2}{E_\eta^2}\frac{E_\eta}{E}}{\sqrt{1-\frac{m_\nu^2}{E^2}}\sqrt{1-\frac{m_\eta^2}{E_\eta^2}}} \approx 1 + \frac{m_\nu^2}{2E^2} - \left(\frac{E_\eta}{E} - \frac{1}{2}\right)\frac{m_\eta^2}{E_\eta^2}\,, \tag{C.132}$$

$$\frac{1 - \frac{m_\eta m_\nu}{E_\eta E}}{\sqrt{1-\frac{m_\nu^2}{E^2}}\sqrt{1-\frac{m_\eta^2}{E_\eta^2}}} \approx 1 - \frac{1}{2}\left(\frac{m_\eta}{E_\eta} + \frac{m_\nu}{E}\right)^2\,. \tag{C.133}$$

Furthermore, neglecting the neutrino mass entirely, we get

$$1 - \frac{m_\eta^2}{2E_\eta^2} - \left(\frac{E_\eta}{E} - 1\right)\frac{m_\eta^2}{2E_\eta^2} < \vec{e}_r^{\,T}(\tilde{\Omega}_\eta)\vec{e}_r(\tilde{\Omega}) \leq 1 - \frac{m_\eta^2}{2E_\eta^2}\,, \tag{C.134}$$

enforcing $\tilde{\Omega}_\eta \approx \tilde{\Omega}$, since $E_\eta/E \gtrsim 1$.

According to the relation between solid angles centered about the decay point of η, i.e. $\tilde{\Omega}$, and those computed with respect to the source centered frame Ω, defined by Equation (C.99), we can easily translate $\tilde{\Omega}_\eta := \tilde{\omega}(\Omega_\eta)$ to Ω_η:

$$\vec{e}_r(\tilde{\omega}(\Omega_\eta)) := \frac{L\vec{e}_r(\Omega_\eta) - (R_\mathrm{S}+\ell)\vec{e}_r(\Omega_\eta)}{|L\vec{e}_r(\Omega_\eta) - (R_\mathrm{S}+\ell)\vec{e}_r(\Omega_\eta)|} = \vec{e}_r(\Omega_\eta) \qquad \Leftrightarrow \qquad \Omega_\eta \equiv \tilde{\Omega}_\eta\,. \tag{C.135}$$

Thereby, we get $\tilde{\Omega} \approx \tilde{\Omega}_\eta = \Omega_\eta$ and consequently

$$\vec{e}_r(\tilde{\Omega}) = \frac{L\vec{e}_r(\Omega) - (R_\mathrm{S}+\ell)\vec{e}_r(\Omega_\eta)}{|L\vec{e}_r(\Omega) - (R_\mathrm{S}+\ell)\vec{e}_r(\Omega_\eta)|} \overset{!}{=} \vec{e}_r(\Omega_\eta)\,, \tag{C.136}$$

which can only be fulfilled for $\Omega \equiv \Omega_\eta \equiv \tilde{\Omega}$ and $R_\mathrm{S} + \ell < L$.

Using these findings, we can rewrite the spectral probability density as

$$
\begin{aligned}
&p_{\eta a}^{\text{spec.}}(E_\eta, R_\text{S} + \ell, \Omega_\eta; E, L, \Omega) \\
&= \sum_X \int_0^\infty \int_{S^2} \frac{1}{\Gamma'_\eta} \frac{\partial^3 \Gamma'_{\eta \to \nu_a + X}}{\partial E' \partial^2 \Omega'}(E', \Omega') && \text{(C.137)} \\
&\quad \times E^2 \delta^{(3)}(\vec{p}(E, \tilde{\omega}(\Omega)) - \vec{\lambda}(\vec{p}', \Lambda_\eta)) \left| \mathrm{d}_\Omega \tilde{\omega}(\Omega) \right| \mathrm{d}^2\Omega' \, \mathrm{d}E' \\
&\approx \sum_X \int_0^\infty \int_{S^2} \frac{1}{\Gamma'_\eta} \frac{\partial^3 \Gamma'_{\eta \to \nu_a + X}}{\partial E' \partial^2 \Omega'}(E', \Omega') && \text{(C.138)} \\
&\quad \times \delta(E - E^*(E', \Omega'; E_\eta, \Omega_\eta)) \delta^{(2)}_{\tilde{\Omega}}(\tilde{\omega}(\Omega) - \tilde{\Omega}_\eta) \left| \mathrm{d}_\Omega \tilde{\omega}(\Omega) \right| \mathrm{d}^2\Omega' \, \mathrm{d}E' \\
&= \sum_X \int_0^\infty \int_{S^2} \frac{1}{\Gamma'_\eta} \frac{\partial^3 \Gamma'_{\eta \to \nu_a + X}}{\partial E' \partial^2 \Omega'}(E', \Omega') && \text{(C.139)} \\
&\quad \times \delta(E - E^*(E', \Omega'; E_\eta, \Omega_\eta)) \delta^{(2)}_{\Omega}(\Omega - \tilde{\omega}^{-1}(\tilde{\Omega}_\eta)) \, \mathrm{d}^2\Omega' \, \mathrm{d}E' \\
&= \sum_X \int_0^\infty \int_{S^2} \frac{1}{\Gamma'_\eta} \frac{\partial^3 \Gamma'_{\eta \to \nu_a + X}}{\partial E' \partial^2 \Omega'}(E', \Omega') && \text{(C.140)} \\
&\quad \times \delta(E - E^*(E', \Omega'; E_\eta, \Omega_\eta)) \delta^{(2)}_{\Omega}(\Omega - \Omega_\eta) \, \mathrm{d}^2\Omega' \, \mathrm{d}E' \ ,
\end{aligned}
$$

where we have used that the three dimensional delta distribution can be translated to spherical coordinates by

$$
\delta^{(3)}(\vec{p}(E, \tilde{\omega}(\Omega)) - \vec{\lambda}(\vec{p}', \Lambda_\eta)) = \delta(E - E^*) \delta^{(2)}_{\tilde{\Omega}}(\tilde{\Omega} - \tilde{\Omega}^*) \, , \tag{C.141}
$$

$$
\delta^{(2)}_{\tilde{\Omega}}(\tilde{\Omega} - \tilde{\Omega}^*) \ = \delta\left(\tilde{\varphi} - \tilde{\varphi}^*\right) \delta\left(\cos\left(\tilde{\theta}\right) - \cos\left(\tilde{\theta}^*\right)\right) \, , \tag{C.142}
$$

and where $(E^*, \tilde{\Omega}^*) = \hat{\lambda}(E', \Omega')$ are the Lorentz transformed energy and solid angle in the coordinate system centered around the decay point. Moreover, we have used that $\tilde{\Omega}^* \approx \tilde{\Omega}_\eta$ for ultra-relativistic primary particles as discussed above.

With this, we can finally simplify the general formula for ϕ_b to

$$\begin{aligned}\phi_b(E,L,\Omega) \approx &\sum_{\eta\in\mathrm{S}}\sum_{a=e,\mu,\tau}\int_{E_\eta^{\min}}^{E_\eta^{\max}}\int_0^{L-R_\mathrm{S}}\int_{S^2}\frac{\phi_\eta(E_\eta,R_\mathrm{S},\Omega_\eta)R_\mathrm{S}^2}{L^2}\frac{e^{-\frac{\ell}{\lambda_\eta}}}{\lambda_\eta}P_{ab}(E,L-\ell)\\ &\times\sum_X\int_0^\infty\int_{S^2}\frac{1}{\Gamma'_\eta}\frac{\partial^3\Gamma'_{\eta\to\nu_a+X}}{\partial E'\partial^2\Omega'}(E',\Omega')\\ &\times\delta(E-E^*(E',\Omega';E_\eta,\Omega_\eta))\delta^{(2)}_\Omega(\Omega-\Omega_\eta)\,\mathrm{d}^2\Omega'\,\mathrm{d}E'\,\mathrm{d}^2\Omega_\eta\,\mathrm{d}\ell\,\mathrm{d}E_\eta\end{aligned} \tag{C.143}$$

$$\begin{aligned}\approx &\sum_{\eta\in\mathrm{S}}\sum_{a=e,\mu,\tau}\int_{E_\eta^{\min}}^{E_\eta^{\max}}\int_0^{L}\frac{\phi_\eta(E_\eta,R_\mathrm{S},\Omega)R_\mathrm{S}^2}{L^2}\frac{e^{-\frac{\ell}{\lambda_\eta}}}{\lambda_\eta}P_{ab}(E,L-\ell)\\ &\times\sum_X\int_0^\infty\int_{S^2}\frac{1}{\Gamma'_\eta}\frac{\partial^3\Gamma'_{\eta\to\nu_a+X}}{\partial E'\partial^2\Omega'}(E',\Omega')\\ &\times\delta(E-E^*(E',\Omega';E_\eta,\Omega_\eta))\,\mathrm{d}^2\Omega'\,\mathrm{d}E'\,\mathrm{d}\ell\,\mathrm{d}E_\eta\end{aligned} \tag{C.144}$$

$$\begin{aligned}=:&\sum_{\eta\in\mathrm{S}}\sum_{a=e,\mu,\tau}\int_{E_\eta^{\min}}^{E_\eta^{\max}}\int_0^{L}\frac{\phi_\eta(E_\eta,R_\mathrm{S},\Omega)R_\mathrm{S}^2}{L^2}\frac{e^{-\frac{\ell}{\lambda_\eta}}}{\lambda_\eta}\\ &\times P_{ab}(E,L-\ell)\pi_{\eta a}(E_\eta,E)\,\mathrm{d}\ell\,\mathrm{d}E_\eta\ ,\end{aligned} \tag{C.145}$$

where we have used $L-R_\mathrm{S}\approx L$ to simplify the upper integration boundary of the ℓ integral and we define the purely spectral emission probability

$$\begin{aligned}\pi_{\eta a}(E_\eta,E) := &\sum_X\int_0^\infty\int_{S^2}\frac{1}{\Gamma'_\eta}\frac{\partial^3\Gamma'_{\eta\to\nu_a+X}}{\partial E'\partial^2\Omega'}(E',\Omega')\\ &\times\delta(E-E^*(E',\Omega';E_\eta,\Omega_\eta))\,\mathrm{d}^2\Omega'\,\mathrm{d}E'\ .\end{aligned} \tag{C.146}$$

Next, we exploit the fact that the primary particles are unpolarised and that, consequently, the spin averaged decay width in the rest frame of the decaying particle is independent of the neutrino emission angle. In in the rest frame of the particle η the differential decay width then simplifies to

$$\frac{\partial^3\Gamma'_{\eta\to\nu_a+X}}{\partial E'\partial^2\Omega'}(E',\tilde{\Omega}') = \frac{1}{4\pi}\frac{\partial\Gamma'_{\eta\to\nu_a+X}}{\partial E'}(E')\,. \tag{C.147}$$

This further reduces the expression for the purely spectral emission probability to

$$\pi_{\eta a}(E_\eta, E) := \sum_X \int_0^\infty \int_{S^2} \frac{1}{\Gamma'_\eta} \frac{1}{4\pi} \frac{\partial \Gamma'_{\eta\to\nu_a+X}}{\partial E'}(E') \delta(E - E^*(E', \Omega'; E_\eta, \Omega_\eta)) \,\mathrm{d}^2\Omega' \,\mathrm{d}E' \tag{C.148}$$

$$= \sum_X \int_0^\infty \frac{1}{\Gamma'_\eta} \frac{1}{4\pi} \frac{\partial \Gamma'_{\eta\to\nu_a+X}}{\partial E'}(E') \int_{S^2} \delta(E - E^*(E', \Omega'; E_\eta, \Omega_\eta)) \,\mathrm{d}^2\Omega' \,\mathrm{d}E' \tag{C.149}$$

$$= \sum_X \int_0^\infty \frac{1}{\Gamma'_\eta} \frac{\partial \Gamma'_{\eta\to\nu_a+X}}{\partial E'}(E') \int_{-1}^{1} \delta(E - E^*(E', E_\eta, \cos\theta'_{\eta\nu})) \frac{\mathrm{d}\cos\theta'_{\eta\nu}}{2} \,\mathrm{d}E' \,, \tag{C.150}$$

since the Lorentz transformed rest frame energy only depends on the relative angle $\theta'_{\eta\nu}$ between the rest frame neutrino momentum and the boost direction. This way the $\varphi'_{\eta\nu}$ integral can be transformed trivially.

Finally, with the definition

$$\mathrm{d}\Gamma_{\eta a} := \sum_X \mathrm{d}\Gamma_{\eta\to\nu_a+X} \,, \tag{C.151}$$

and for isotropic emission of primary particles, i.e

$$\frac{\phi_\eta(E_\eta, R_\mathrm{S}, \Omega) R_\mathrm{S}^2}{L^2} \equiv \frac{4\pi\phi_\eta(E_\eta, R_\mathrm{S}) R_\mathrm{S}^2}{4\pi L^2} = \frac{\Phi_\eta^\mathrm{S}}{4\pi L^2} \,, \tag{C.152}$$

from the source, we arrive at the expression shown in Equation (4.26).

C.4 Neutrino Energy Distributions from Beta Decay

We compute the differential decay width for beta decay with respect to the neutrino energy and emission angle in the neutron rest frame Σ' i.e.

$$\begin{aligned}\frac{\partial^3 \Gamma'_{ne}}{\partial E' \partial^2 \Omega'}(E', \Omega') = \frac{1}{2m_n} \frac{|\vec{p}'_\nu|}{2(2\pi)^3} \int \frac{\mathrm{d}^3\vec{p}'_p}{(2\pi)^3 2E'_p} \int \frac{\mathrm{d}^3\vec{p}'_e}{(2\pi)^3 2E'_e} \\ \times \overline{|\mathcal{M}|^2}(p'_n \to p'_p, p'_e, p'_\nu)(2\pi)^4 \delta^{(4)}(p'_n - p'_p - p'_e - p'_\nu) \,.\end{aligned} \tag{C.153}$$

In writing Equation (C.153) we have used that the Lorentz-invariant phase space measure for the neutrino momentum can be written as

$$\frac{\mathrm{d}^3\vec{p}'_\nu}{(2\pi)^3 2E'} = \mathrm{d}^2\Omega \,\mathrm{d}|\vec{p}'_\nu| \, \frac{|\vec{p}'_\nu|^2}{(2\pi)^3 2E'} = \mathrm{d}^2\Omega \,\mathrm{d}\vec{E}'_\nu \, \frac{|\vec{p}'_\nu|}{2(2\pi)^3} \,. \tag{C.154}$$

To explicitly evaluate the differential width, we first compute the squared, spin averaged, Lorentz-invariant matrix element in an arbitrary frame of reference and then use the kinematics in the neutron rest frame to perform the phase space integrals.

C.4.1 Beta Decay Matrix Element

We compute the beta decay matrix element within Fermi theory with spectator quarks. To effectively account for the internal structure of the nucleons, we simply modify their vector and axial couplings to the weak gauge bosons

$$\mathcal{L}_{CC}^{N} = \frac{g}{2\sqrt{2}} V_{ud} \bar{p}(x) \gamma^{\mu} (g_V - g_A \gamma_5) n(x) W_{\mu}^{+}(x) + \text{h.c.}\,. \tag{C.155}$$

In Fermi theory, we approximate the gauge boson propagators by

$$D_{\mu\nu}(x-y) \approx \frac{i}{m_W^2} \eta_{\mu\nu}\,. \tag{C.156}$$

In this approximation, the matrix element becomes

$$\begin{aligned} i\mathcal{M} &= \frac{(-ig)}{2\sqrt{2}} V_{ud} \left[\bar{u}^p_{s_p}(p_p)(g_V - g_A\gamma_5)\gamma^{\mu} u^p_{s_n}(p_n)\right] \frac{i}{m_W^2}\eta_{\mu\nu} \frac{(-ig)}{2\sqrt{2}} \\ &\quad \times \left[\bar{u}^p_{s_e}(p_e)(1-\gamma_5)\gamma^{\nu} v^p_{s_\nu}(p_\nu)\right] \qquad \text{(C.157)} \\ &= \frac{-ig^2}{8m_W^2} V_{ud} \left[\bar{u}^p_{s_p}(p_p)(g_V - g_A\gamma_5)\gamma^{\mu} u^p_{s_n}(p_n)\right] \left[\bar{u}^p_{s_e}(p_e)(1-\gamma_5)\gamma_{\mu} v^p_{s_\nu}(p_\nu)\right] \qquad \text{(C.158)} \\ &= \frac{-iG_F}{\sqrt{2}} V_{ud} \left[\bar{u}^p_{s_p}(p_p)(g_V - g_A\gamma_5)\gamma^{\mu} u^p_{s_n}(p_n)\right] \left[\bar{u}^p_{s_e}(p_e)(1-\gamma_5)\gamma_{\mu} v^p_{s_\nu}(p_\nu)\right]\,. \qquad \text{(C.159)} \end{aligned}$$

Next, we square the absolute value of $i\mathcal{M}$ and perform the spin average to get

$$\begin{aligned} \overline{|\mathcal{M}|^2} = 16 G_F^2 |V_{ud}|^2 \big\{ &(g_V + g_A)^2 (p_n \cdot p_\nu)(p_p \cdot p_e) + (g_V - g_A)^2 (p_n \cdot p_e)(p_p \cdot p_\nu) \\ &- (g_V^2 - g_A^2) m_n m_p (p_e \cdot p_\nu) \big\}\,. \end{aligned} \tag{C.160}$$

C.4.2 Phase Space Integrals for Three Body Decays

Next, we perform the phase space integrals for three body decay processes in the rest frame of the decaying particle. In this section, we drop the conventional prime on all rest frame quantities for notational convenience. We start with Equation (C.153) collect all constant factors and trivially perform the proton momentum integral by making use of the momentum conserving delta function and get

$$\frac{\partial^3 \Gamma_{ne}}{\partial E \partial^2 \Omega}(E, \Omega) = \frac{2}{(4\pi)^5 m_n} \int \mathrm{d}^3\vec{p}_e \, \frac{|\vec{p}_\nu|}{E_e E_p} \overline{|\mathcal{M}|^2} \delta(E_n - E_p - E_e - E)\Big|_{\vec{p}_p = -(\vec{p}_e + \vec{p}_\nu)}\,. \tag{C.161}$$

Next, we perform a rotation in the electron neutrino momentum integral such that its z-axis aligns with the neutrino momentum. Afterwards, we write the electron momentum integral

in spherical coordinates and reformulate the energy conserving delta as a constraint for the electron angle

$$\begin{aligned}
&\delta(E_n - E_p - E_e - E) \\
&= \delta\left(E_n - \sqrt{m_p^2 + \vec{p}_e^{\,2} + \vec{p}_\nu^{\,2} + 2|\vec{p}_e||\vec{p}_\nu|\cos\theta} - E_e - E\right) && \text{(C.162)} \\
&= \delta\left(E_n - \sqrt{m_p^2 - m_e^2 + E_e^2 + E^2 + 2|\vec{p}_e||\vec{p}_\nu|\cos\theta} - E_e - E\right) && \text{(C.163)} \\
&= \frac{E_p}{|\vec{p}_e||\vec{p}_\nu|}\delta(\cos\theta - \cos\theta^\star)\,, && \text{(C.164)} \\
&\cos\theta^\star(E, E_e) = \frac{m_n^2 - m_p^2 + m_e^2 + 2(m_n(E_e + E) - E_e E)}{2|\vec{p}_e|E}\,. && \text{(C.165)}
\end{aligned}$$

In total, we get

$$\begin{aligned}
\frac{\partial^3\Gamma_{ne}}{\partial E\partial^2\Omega}(E,\Omega) &= \frac{2}{(4\pi)^5 m_n}\int \mathrm{d}|\vec{p}_e| \int \mathrm{d}^2\Omega\, \frac{|\vec{p}_e|}{E_e}\overline{|\mathcal{M}|^2}\delta(\cos\theta - \cos\theta^\star) && \text{(C.166)} \\
&= \frac{1}{(4\pi)^4 m_n}\int_{m_e}^{\infty}\mathrm{d}E_e \int_{-1}^{1}\mathrm{d}\cos\theta\,\overline{|\mathcal{M}|^2}\delta(\cos\theta - \cos\theta^\star) && \text{(C.167)} \\
&= \frac{1}{(4\pi)^4 m_n}\int_{m_e}^{\infty}\mathrm{d}E_e \int_{-\infty}^{\infty}\mathrm{d}\cos\theta\,\overline{|\mathcal{M}|^2}\delta(\cos\theta - \cos\theta^\star) \\
&\quad \times \Theta(1 - \cos\theta)\Theta(1 + \cos\theta) && \text{(C.168)} \\
&= \frac{1}{(4\pi)^4 m_n}\int_{m_e}^{\infty}\mathrm{d}E_e\,\overline{|\mathcal{M}|^2}\Theta(1 - \cos\theta^\star)\Theta(1 + \cos\theta^\star)\,. && \text{(C.169)}
\end{aligned}$$

From the Heaviside functions we can infer the new boundaries of integration for the electron energy, i.e.

$$\begin{aligned}
E_e^{\pm} &= \frac{m_n - E}{2m_n}\frac{2Em_n - [m_n^2 - m_p^2 + m_e^2]}{2E - m_n} \pm \delta E_e\,, && \text{(C.170)} \\
\delta E_e &= \frac{E}{2m_n(2E - m_n)} \\
&\quad \times \sqrt{(2Em_n - m_n^2 + (m_p - m_e)^2)(2Em_n - m_n^2 + (m_p + m_e)^2)}\,. && \text{(C.171)}
\end{aligned}$$

Furthermore, using the conservation of energy and the constraint $E_e \geq m_e$, we can infer the end point of the neutrino energy spectrum

$$E_\nu^{\max} := \frac{(m_n - m_e)^2 - m_p^2}{2(m_n - m_e)} \approx 0.8\,\mathrm{MeV}\,. \qquad \text{(C.172)}$$

In total, the differential decay width becomes

$$\frac{\partial^3 \Gamma_{ne}}{\partial E \partial^2 \Omega}(E, \Omega) = \frac{\Theta(E_\nu^{\max} - E)}{(4\pi)^4 m_n} \int_{E_e^-}^{E_e^+} \overline{|\mathcal{M}|^2} \, \mathrm{d}E_e \ . \tag{C.173}$$

As expected, this result does not depend on the emission angle of the neutrino which is because there exists no preferred physical direction as we have averaged over the spin of the unpolarised neutrons.

Consequently, the differential decay width with respect to the neutrino energy reads

$$\frac{\partial \Gamma_{ne}}{\partial E}(E, \Omega) = \frac{\Theta(E_\nu^{\max} - E)}{(4\pi)^3 m_n} \int_{E_e^-}^{E_e^+} \overline{|\mathcal{M}|^2} \, \mathrm{d}E_e \ . \tag{C.174}$$

C.4.3 Final Form of the Beta Decay Matrix Element in the Neutron Rest Frame

Lastly, for completeness, we explicitly evaluate the scalar products appearing in the matrix element squared, i.e.

$$s_1 \coloneqq p_n \cdot p_\nu \,, \quad s_2 \coloneqq p_p \cdot p_e \,, \quad s_3 \coloneqq p_n \cdot p_e \,, \quad s_4 \coloneqq p_p \cdot p_\nu \,, \quad s_5 \coloneqq p_e \cdot p_\nu \,, \tag{C.175}$$

in terms of the neutrino and electron energies, E and E_e, respectively, in the rest frame of the decaying neutron. The first and third are trivial and yield

$$s_1 = E m_n \,, \qquad\qquad s_3 = E_e m_n \,. \tag{C.176}$$

For the second and fourth, we first exploit the relations

$$p_p \cdot p_e = \frac{(p_p + p_e)^2 - m_p^2 - m_e^2}{2} \,, \qquad p_p \cdot p_\nu = \frac{(p_p + p_\nu)^2 - m_p^2}{2} \,, \tag{C.177}$$

which in combination with energy and momentum conservation can be recast as

$$s_2 = \frac{m_n^2 - m_p^2 - m_e^2 - 2 m_n E}{2} \,, \qquad s_4 = \frac{m_n^2 - m_p^2 + m_e^2 - 2 m_n E_e}{2} \,. \tag{C.178}$$

The fifth is again trivial to express in terms of the electron and neutrino energies, i.e.

$$s_5 \coloneqq E \left(E_e - \sqrt{E_e^2 - m_e^2} \cos\theta^*(E, E_e) \right) \,, \tag{C.179}$$

but it still represents a special case as it contains the cosine of the angle between the electron and neutrino that we have already determined to be given by Equation (C.165).

In total, the squared matrix element then reads

$$\begin{aligned}\overline{|\mathcal{M}|^2} = 8G_F^2|V_{ud}|^2 m_n \Big\{ & (g_V + g_A)^2 E(\bar{m}_-^2 - 2m_n E) \\ & + (g_V - g_A)^2 E_e(\bar{m}_+^2 - 2m_n E_e) \\ & - (g_V^2 - g_A^2) m_p \left(4EE_e - (\bar{m}_+^2 + 2m_n(E_e + E))\right) \Big\},\end{aligned} \tag{C.180}$$

in terms of E and E_e with

$$\bar{m}_\pm^2 := m_n^2 - m_p^2 \pm m_e^2 \,. \tag{C.181}$$

D Appendix - Neutrino Oscillations in Curved Spacetime

This appendix chapter provides mathematical discussions for the consideration of strongly localised neutrino position space WPs in curved spacetime, cf. Section D.1. Furthermore in Section D.2, we present additional discussions and calculations for the neutrino oscillation probability in the scenario of linearised gravity. Here, we also focus on the explicit example of Gaussian neutrino WPs to be able to compare our results to those obtained in Section 2.3.2.

D.1 Parallel Transported Infinitesimal Coordinate Change

Consider a smooth curve $c : I \to \mathcal{M}$ on a smooth pseudo-Riemannian manifold $(\mathcal{M}, g)$ equipped with the unique, torsion free and metric compatible Levi–Civita connection ∇. We denote the parallel transport of tangent vectors rooted at $c(\tau_1)$ to $c(\tau_2)$ along the curve c by $P^c_{\tau_1\to\tau_2} : T_{c(\tau_1)}\mathcal{M} \to T_{c(\tau_2)}\mathcal{M}$. For an arbitrary point[1] $x_0 := c(\tau_0)$ on the curve, we consider another point y_0 in its vicinity. This point y_0 represents any point within the region U_ν, containing all neutrino WPs, intersected with the Cauchy surface Σ where we evaluate the scalar product of position space wave functions. Moreover, let $U_p \subset \mathcal{E}_p \subset T_p$ with $0 \in U_p$ be the region on that the exponential function at the point $p \in \mathcal{M}$,

$$\exp_p : \mathcal{E}_p \subset T_p\mathcal{M} \to \mathcal{M}\,, \tag{D.1}$$

is a diffeomorphism on its own image $V_p := \exp_p(U_p)$. Since per construction the neutrino WPs are sufficiently localised and close to each other, we have $y_0 \in V_{x_0}$. Let now $\varepsilon > 0$ such that $y_0 \in V_{c(\tau_0+\delta\tau)}$ for all $\delta\tau \in (-\varepsilon, \varepsilon)$, then the function

$$\zeta : (-\varepsilon, \varepsilon) \to U_0 \subset T_{x_0}\mathcal{M}\,, \qquad \zeta(\delta\tau) = P^c_{\tau_0+\delta\tau\to\tau_0} \exp^{-1}_{c(\tau_0+\delta\tau)}(y_0)\,, \tag{D.2}$$

is well-defined. Moreover, since ζ maps an open interval of $\mathbb{R}$ into $T_{x_0}\mathcal{M} \simeq \mathbb{R}^n$ also taking the difference quotients necessary to compute derivatives is well-defined. Furthermore, since c is smooth, $\exp_x$ and $\exp^{-1}_x$ smoothly depend on their foot point x and the parallel transport also smoothly depends on its starting point and vector-valued argument, all derivatives of ζ exist and its Taylor series is well-defined. Thus, for the Taylor expansion we obtain

$$\zeta(\delta\tau) = \zeta(0) + \left.\frac{\mathrm{d}\zeta}{\mathrm{d}\delta\tau}\right|_{\delta\tau=0} \delta\tau + \mathcal{O}(\delta\tau^2)\,, \tag{D.3}$$

[1] We choose a slightly different indexing than in the main text in order to streamline our notation.

on $(-\varepsilon, \varepsilon)$, as usual.

The zeroth order coefficient simply evaluates to

$$\zeta(0) = \underbrace{P^{c}_{\tau_0 \to \tau_0}}_{\mathrm{Id}_{T_{x_0}\mathcal{M}}} \underbrace{\exp^{-1}_{c(\tau_0)} \circ \exp_{c(\tau_0)}}_{\mathrm{Id}_{U_0}}(z_0) = z_0 \,, \tag{D.4}$$

and, hence, coincides with the tangent vector z_0 itself. Translated back to the actual physical setting of neutrino WPs considered in the main text, this means that at zeroth order in $\Delta\tau$ the normal coordinates at the next point of propagation along the geodesic coincide with those at the current point.

Next, the first derivative of ζ at $\delta\tau = 0$ can be rewritten as a covariant derivative, i.e.

$$\zeta(0) = \frac{\mathrm{d}}{\mathrm{d}\delta\tau}\bigg|_{\delta\tau=0} P^{c}_{\tau_0+\delta\tau\to\tau_0} \exp^{-1}_{c(\tau_0+\delta\tau)}(y_0) = \frac{\nabla}{\mathrm{d}\delta\tau}\bigg|_{\delta\tau=0} \exp^{-1}_{c(\tau_0+\delta\tau)}(y_0) \,. \tag{D.5}$$

Therefore, the task is now to determine the first covariant derivative at $\delta\tau = 0$ of the vector field

$$V \colon (-\varepsilon, \varepsilon) \to T\mathcal{M} \,, \qquad\qquad V(\delta\tau) \coloneqq \exp^{-1}_{c(\tau_0+\delta\tau)}(y_0) \,, \tag{D.6}$$

which is equivalent to asking the question: *How does the initial velocity vector of a (shortest) geodesic connecting $c(\tau_0 + \delta\tau)$ and y_0 change when nudging $\delta\tau$ away from zero?* To be able to do so, we first construct a geodesic variation

$$\sigma : [0,1] \times (-\varepsilon, \varepsilon) \to \mathcal{M} \,, \qquad\qquad \sigma(t, \delta\tau) \coloneqq \exp_{c(\tau_0+\delta\tau)}(tV(\delta\tau)) \,, \tag{D.7}$$

that exactly formalises the aforementioned procedure of nudging on $\delta\tau$. Consequently, $\delta\tau$ is the variational parameter and t is the affine parameter of the geodesic $t \mapsto \sigma(t, \delta\tau)$ for fixed $\delta\tau$. The geodesic variation is sketched in Figure D.1. That the curve $t \mapsto \sigma(t, \delta\tau)$ is indeed a geodesic trivially follows from the properties of the exponential function and we have

$$\sigma(0, \delta\tau) = \exp_{c(\tau_0+\delta\tau)}(0) = c(\tau_0 + \delta\tau) \,, \tag{D.8}$$

$$\sigma(1, \delta\tau) = \exp_{c(\tau_0+\delta\tau)}(V(\delta\tau)) = \exp_{c(\tau_0+\delta\tau)}(\exp^{-1}_{c(\tau_0+\delta\tau)}(y_0)) \equiv y_0 \,, \tag{D.9}$$

$$\frac{\partial\sigma}{\partial t} \equiv V(\delta\tau) \,. \tag{D.10}$$

In addition to that, because σ is a geodesic variation, the variational vector field

$$J : [0,1] \to T\mathcal{M} \,, \qquad\qquad J(t) \coloneqq \frac{\partial\sigma}{\partial\delta\tau}(t, 0) \,, \tag{D.11}$$

of σ fulfils the Jacobi equation

$$\frac{\nabla^2}{\mathrm{d}t^2} J(t) = -R\left(J(t), \frac{\partial\sigma}{\partial t}(t,0)\right) \frac{\partial\sigma}{\partial t}(t,0) \,. \tag{D.12}$$

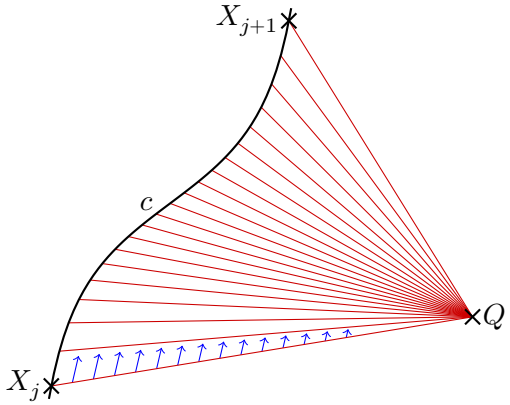

Figure D.1: Illustrated are the geodesic variation in red and its Jacobi vector field in blue. The variation of the geodesic is induced by varying its initial starting point along the curve c between $c(\tau_0)$ and $c(\tau_0 + \Delta\tau)$.

According to the explicit definition of σ, its first covariant derivative at $t = \delta\tau = 0$ reads

$$\frac{\nabla J}{\mathrm{d}t}(0) = \frac{\nabla}{\mathrm{d}t}\frac{\partial\sigma}{\partial\delta\tau}(0,0) = \frac{\nabla}{\mathrm{d}\delta\tau}\frac{\partial\sigma}{\partial t}(0,0) = \frac{\nabla V}{\mathrm{d}\delta\tau}(0)\,, \tag{D.13}$$

which is exactly the quantity we wish to evaluate. In switching the ordering of covariant and partial differentiation, we implicitly use that ∇ is torsion-free.

The detour we take by defining the geodesic variation σ, thus, enables us to compute the first derivative of V using the geometric properties of Jacobi vector fields. Jacobi fields, as solutions of Equation (D.12), are uniquely determined by their initial conditions, $J(0)$ and $\nabla J/\mathrm{d}t(0)$, or in our case by their boundary values, $J(0)$ and $J(1)$, as long as the corresponding foot points of the respective tangent spaces—x_0 and y_0 in our scenario—are in the diffeomorphic region V_{x_0} of $\exp_{x_0}$. Per construction, this is the case and the boundary values are given by

$$J(0) = \frac{\partial\sigma}{\partial\delta\tau}(0,0) = \frac{\mathrm{d}c}{\mathrm{d}\tau}\,, \qquad J(1) = \frac{\partial\sigma}{\partial\delta\tau}(1,0) = \frac{\partial}{\partial\delta\tau}[\delta\tau \mapsto y_0] \equiv 0\,. \tag{D.14}$$

Therefore, solving Equation (D.12) and evaluating $\nabla J/\mathrm{d}t$ at $t = 0$ would provide us with the desired quantity $\nabla V/\mathrm{d}\delta\tau$ at $\delta\tau = 0$ and concludes the Taylor expansion.

Unfortunately, this task is impossible to solve for general geometries and arbitrarily far separated boundary points, x_0 and y_0. However, we are primarily interested in x_0 and y_0 located closely to each other since the distance between x_0 and y_0 is bounded by the diameter σ_x of $U_\nu \cap \Sigma$. As already argued before, we assume σ_x to be small compared to the smallest curvature radius within $U_\nu \cap \Sigma$. To exploit this assumption, we express Equation (D.12) in an advantageous tangent basis along the curve $t \mapsto \sigma(t,0)$ and approximate the Riemann tensor by its value at x_0. For our basis, we choose a set of parallel vector fields E_μ along $t \mapsto \sigma(t,0)$—these are different from the E_μ in the main text—with initial conditions $E_\mu = \partial/\partial z_0^\mu$ making them orthonormal with respect to the metric g at every point along the curve, i.e. $g(E_\mu, E_\nu) = \eta_{\mu\nu}$.

Here, $\partial/\partial z_0^\mu$ is the local inertial tangent basis at x_0 that coincides with the same tangent basis chosen in the main text. Writing all required quantities in this basis yields

$$\frac{\nabla^2}{\mathrm{d}t^2}J(t) = \frac{\nabla^2}{\mathrm{d}t^2}J^\mu(t)E_\mu(t) = \frac{\nabla}{\mathrm{d}t}\frac{\mathrm{d}J^\mu(t)}{\mathrm{d}t}E_\mu(t) = \frac{\mathrm{d}^2J^\mu(t)}{\mathrm{d}t^2}E_\mu(t)\,, \tag{D.15}$$

$$\frac{\partial\sigma}{\partial t}(t,0) = z_0^\mu E_\mu(t)\,, \tag{D.16}$$

$$R\left(J(t),\frac{\partial\sigma}{\partial t}(t,0)\right)\frac{\partial\sigma}{\partial t}(t,0) = R^\mu{}_{\sigma\lambda\nu}(\sigma(t,0))z_0^\sigma z_0^\lambda J^\nu(t)E_\mu(t)\,, \tag{D.17}$$

where we make heavy use of the parallel property of the E_μ. Next, we use $R^\mu{}_{\nu\sigma\lambda}(\sigma(t,0)) \approx R^\mu{}_{\nu\sigma\lambda}(x_0)$ which leads to the approximated Jacobi equation in coordinate form, i.e.

$$\frac{\mathrm{d}^2J^\mu(t)}{\mathrm{d}t^2} = -R^\mu{}_{\sigma\lambda\nu}(x_0)z_0^\sigma z_0^\lambda J^\nu(t) =: A^\mu{}_\nu J^\nu(t)\,. \tag{D.18}$$

In order to solve this system of homogeneous, linear, ordinary differential equations with constant coefficients, we first note that the matrix A is symmetric within the Minkowski bilinear form, i.e.

$$A_{\mu\nu} := \eta_{\mu\sigma}A^\sigma{}_\nu = -R_{\mu\rho\lambda\nu}(x_0)z_0^\rho z_0^\lambda = -R_{\nu\lambda\rho\mu}(x_0)z_0^\rho z_0^\lambda = A_{\nu\mu}\,, \tag{D.19}$$

and can therefore be diagonalised via a Lorentz transformation $\Lambda \in O(1,3)$. The eigenvalues of A are then proportional to the sectional curvatures of the manifold at x_0 in terms of the eigenbasis of A:

$$E_\mu = \Lambda_\mu{}^\nu \tilde{E}_\nu\,, \tag{D.20}$$

$$\tilde{A}^\mu{}_\nu = \Lambda_\sigma{}^\mu A^\sigma{}_\rho \Lambda^\rho{}_\nu = -\eta^{\mu\sigma}g(\tilde{E}_\sigma, R(\tilde{E}_\nu, z_0)z_0)\,, \tag{D.21}$$

where $\tilde{A}^\mu{}_\nu$ is only different from zero for $\mu = \nu$.

Given the boundary conditions $J(0) = \mathrm{d}c(\tau_0)/\mathrm{d}\tau$ and $J(1) = 0$ Equation (D.18) is solved by

$$\tilde{J}^\mu(t) = \frac{\sinh\left(\sqrt{\tilde{A}_{[\mu]}}(1-t)\right)}{\sinh\left(\sqrt{\tilde{A}_{[\mu]}}\right)}\frac{\mathrm{d}\tilde{c}^\mu}{\mathrm{d}\tau}\,, \tag{D.22}$$

where $\tilde{A}_{[\mu]}$ denotes the μ-th eigenvalue of A and the brackets indicate that we do not sum over the index they enclose. For a zero eigenvalue we understand Equation (D.22) such that we

take the limit $\tilde{A}_{[\mu]} \to 0$. This finally enables us to compute the derivative of J at $t = 0$, i.e.

$$\frac{\nabla J}{\mathrm{d}t}(0) = [\Lambda^{-1}]^{\mu}{}_{\nu} \frac{\mathrm{d}\tilde{J}^{\nu}}{\mathrm{d}t} E_{\mu}(0) \tag{D.23}$$

$$= -[\Lambda^{-1}]^{\mu}{}_{\nu} \tilde{A}_{[\nu]} \coth\left(\tilde{A}_{[\nu]}\right) \frac{\mathrm{d}\tilde{c}^{\nu}}{\mathrm{d}\tau} E_{\mu}(0) \tag{D.24}$$

$$\approx -[\Lambda^{-1}]^{\mu}{}_{\nu} \left(\delta^{\nu}{}_{\rho} + \frac{\tilde{A}^{\nu}{}_{\rho}}{3}\right) \frac{\mathrm{d}\tilde{c}^{\rho}}{\mathrm{d}\tau} E_{\mu}(0) \tag{D.25}$$

$$= -\left(\delta^{\mu}{}_{\rho} + \frac{A^{\mu}{}_{\rho}}{3}\right) \frac{\mathrm{d}c^{\rho}}{\mathrm{d}\tau} E_{\mu}(0) \tag{D.26}$$

$$= -\frac{\mathrm{d}c}{\mathrm{d}\tau} + \frac{1}{3} R_{x_0}\left(\frac{\mathrm{d}c}{\mathrm{d}\tau}, z_0\right) z_0\,, \tag{D.27}$$

where we have used that $R(\cdot, z_0)z_0$ is a small quantity by construction.

In total, we get

$$\zeta(\delta\tau) \approx z_0 - \left(\frac{\mathrm{d}c}{\mathrm{d}\tau} - \frac{1}{3} R_{x_0}\left(\frac{\mathrm{d}c}{\mathrm{d}\tau}, z_0\right) z_0\right) \delta\tau, \tag{D.28}$$

and finally using the smallness of σ_x by also neglecting terms of quadratic order in the normal coordinates times the curvature tensor components yields

$$\zeta(\delta\tau) = z_0 - \frac{\mathrm{d}c}{\mathrm{d}\tau}\delta\tau + \mathcal{O}(R^{\max}\sigma_x^2, \delta\tau^2)\,, \tag{D.29}$$

which coincides with the flat spacetime result as expected by the equivalence principle.

D.2 Linear Gravity: Mean Propagation Time

To find the temporal peak of the envelope of the integrand of $\mathcal{I}_{jk}$, we define the exponent function

$$\Xi_{jk}(\Delta T, \varepsilon) = \mathrm{Re}(\Xi_{jk})(\Delta T, \varepsilon) + i\mathrm{Im}(\Xi_{jk})(\Delta T, \varepsilon)\,, \tag{D.30}$$

$$\begin{aligned}\mathrm{Re}(\Xi_{jk})(\Delta T, \varepsilon) = &-\frac{(\vec{\tilde{P}}_{\mathrm{S}j} - \vec{P}_{\mathrm{D}j})^2 + (\vec{\tilde{P}}_{\mathrm{S}k} - \vec{P}_{\mathrm{D}k})^2}{4(\sigma_{\mathrm{S}}^2 + \sigma_{\mathrm{D}}^2)} \\ &- \mathrm{Re}(\sigma_{\|j}^2)\frac{(\bar{v}_j L^0 - L)^2}{2|\sigma_{\|j}^2|^2} - \mathrm{Re}(\sigma_{\|k}^2)\frac{(\bar{v}_k L^0 - L)^2}{2|\sigma_{\|k}^2|^2}\,,\end{aligned} \tag{D.31}$$

$$\begin{aligned}\mathrm{Im}(\Xi_{jk})(\Delta T, \varepsilon) = &-(L^0 \Delta\bar{E}_{jk} - L\Delta\bar{p}_{jk}) \\ &+ \mathrm{Im}(\sigma_{\|j}^2)\frac{(\bar{v}_j L^0 - L)^2}{2|\sigma_{\|j}^2|^2} - \mathrm{Im}(\sigma_{\|k}^2)\frac{(\bar{v}_k L^0 - L)^2}{2|\sigma_{\|k}^2|^2}\,,\end{aligned} \tag{D.32}$$

and observe that the envelope of the integrand is exactly given by $\exp\big(\mathrm{Re}(\Xi_{jk})\big)$. Note that the exponent Ξ_{jk} may also depend on the detection time T_D, but we suppress this dependence on all quantities in the following. Finding the maximum of the envelope of the intgerand with respect to ΔT therefore amounts to finding the maximum of $\mathrm{Re}(\Xi_{jk})$ which we do order by order in ε, i.e. by using the ansatz

$$\Delta T^\star_{jk} = \Delta T^\star_{jk,0} + \varepsilon \Delta T^\star_{jk,1} + \mathcal{O}(\varepsilon^2)\,. \tag{D.33}$$

The zeroth order solution $\Delta T^\star_{jk,0}$ needs to fulfil

$$0 = \frac{\partial \mathrm{Re}(\Xi_{jk})}{\partial \Delta T}(\Delta T^\star_{jk,0}, 0)\,, \tag{D.34}$$

and the first order correction $\Delta T^\star_{jk,1}$ can be obtained explicitly as

$$\Delta T^\star_{jk,1} = -\left\{\frac{\partial^2 \mathrm{Re}(\Xi_{jk})}{\partial \Delta T^2}(\Delta T^\star_{jk,0}, 0)\right\}^{-1} \frac{\partial^2 \mathrm{Re}(\Xi_{jk})}{\partial \varepsilon \partial \Delta T}(T^\star_{jk,0}, 0)\,. \tag{D.35}$$

In the ultra-relativistic approximation, the $\mathcal{O}(\varepsilon^0)$ maximum yields

$$\begin{aligned}\Delta T^\star_{jk,0} = \Delta X \left(1 + \frac{m_j^2 + m_k^2}{4E^2} - \frac{\Delta p_j m_j^2 + \Delta p_k m_k^2}{2E^3} - \frac{(\Delta m^2_{jk})^2}{8E^4} - \frac{m_j^4 + m_k^4}{16E^4}\right) \\ + \mathcal{O}(\varepsilon^3_{\mathrm{UR}})\,.\end{aligned} \tag{D.36}$$

This is just the same result we have obtained in Section 2.3.2 plus higher order corrections.

To compute the higher order correction $\Delta T^\star_{jk,1}$, we first decompose all relevant quantities into a $\varepsilon = 0$ component and the respective first order ε correction, i.e.

$$\varepsilon \delta \Delta T(\Delta T) + \mathcal{O}(\varepsilon^2) := L^0(\Delta T) - \Delta T, \tag{D.37}$$

$$\varepsilon \delta \Delta X(\Delta T) + \mathcal{O}(\varepsilon^2) := L(\Delta T) - \Delta X\,, \tag{D.38}$$

$$\varepsilon \delta \vec{P}_{\mathrm{S}j}(\Delta T) + \mathcal{O}(\varepsilon^2) := \tilde{\bar{\vec{P}}}_{\mathrm{S}j}(\Delta T) - \vec{P}_{\mathrm{S}j}\,. \tag{D.39}$$

The decomposition of the mean momentum at the source also induces an associated ε-decomposition of the total mean momentum $\bar{\vec{p}}_j$ and the group velocity $\bar{\vec{v}}_j$, i.e.

$$\bar{\vec{p}}_j = \bar{\vec{p}}_{j0} + \varepsilon \delta \bar{\vec{p}}_j(\Delta T) + \mathcal{O}(\varepsilon^2)\,, \tag{D.40}$$

$$\bar{\vec{v}}_j = \bar{\vec{v}}_{j0} + \varepsilon \delta \bar{\vec{v}}_j(\Delta T) + \mathcal{O}(\varepsilon^2)\,, \tag{D.41}$$

with

$$\bar{\vec{p}}_{j0} := \frac{\sigma_{\mathrm{D}}^2 \vec{P}_{\mathrm{S}} + \sigma_{\mathrm{S}}^2 \vec{P}_{\mathrm{D}}}{\sigma_{\mathrm{S}}^2 + \sigma_{\mathrm{D}}^2}\,, \qquad \bar{E}_{j0} := \sqrt{\bar{\vec{p}}_{j0}^{\,2} + m_j^2}\,, \qquad \bar{\vec{v}}_{j0} := \frac{\bar{\vec{p}}_{j0}}{\bar{E}_{j0}}\,, \tag{D.42}$$

and

$$\delta\bar{\vec{p}}_j(\Delta T) = \frac{\sigma_{\rm D}^2}{\sigma_{\rm S}^2+\sigma_{\rm D}^2}\delta\vec{P}_{{\rm S}j}(\Delta T)\,, \qquad \delta\bar{\vec{v}}_j(\Delta T) = \left(\mathbb{1}-\bar{\vec{v}}_{j0}\bar{\vec{v}}_{j0}^T\right)\frac{\delta\bar{\vec{p}}_j(\Delta T)}{E_j^0}\,. \tag{D.43}$$

For simplicity, we drop the bar on all mean quantities from now on. As argued in the main text we approximate $\vec{\ell} \parallel \vec{p}_j, \vec{v}_j$ with $\vec{\ell} := \vec{L}/L$. Therefore, only the absolute values of the mean momentum and group velocities appear in all equations. The associated $\mathcal{O}(\varepsilon)$ corrections read

$$|\vec{p}_j| = |\vec{p}_{j0}| + \varepsilon\underbrace{\delta\vec{p}_j\cdot\vec{\ell}}_{\delta p_j} + \mathcal{O}(\varepsilon^2)\,, \qquad |\vec{v}_j| = |\vec{v}_{j0}| + \varepsilon\underbrace{\delta\vec{v}_j\cdot\vec{\ell}}_{\delta v_j} + \mathcal{O}(\varepsilon^2)\,, \tag{D.44}$$

respectively, where we have used that $\vec{p}_{j0}/|\vec{p}_{j0}| = \vec{v}_{j0}/|\vec{v}_{j0}| = \vec{\ell} + \mathcal{O}(\varepsilon)$. Finally, after employing the ultra-relativistic expansion we arrive at

$$\begin{aligned}\Delta T^\star_{jk,1} = -\delta\Delta T(\Delta T^\star_{jk,0}) + \left[1+\frac{m_j^2+m_k^2}{4E^2}\right]\delta\Delta X(\Delta T^\star_{jk,0}) \\ + \frac{\delta v_j(\Delta T^\star_{jk,0})+\delta v_k(\Delta T^\star_{jk,0})}{2}\Delta X\,.\end{aligned} \tag{D.45}$$

Substituting this result into the corrected neutrino propagation time L^0 yields

$$L^0(\Delta T^\star_{jk}) = \Delta T^\star_{jk} + \varepsilon\delta\Delta T(\Delta T^\star_{jk,0}) \tag{D.46}$$

$$\begin{aligned}&= \Delta X\left(1+\frac{m_j^2+m_k^2}{4E^2}-\frac{\Delta p_j m_j^2+\Delta p_k m_k^2}{2E^3}-\frac{(\Delta m^2_{jk})^2}{8E^4}-\frac{m_j^4+m_k^4}{16E^4}\right)\\ &\quad-\varepsilon\left(\delta\Delta T(\Delta T^\star_{jk,0})-\left[1+\frac{m_j^2+m_k^2}{4p^2}\right]\delta\Delta X(\Delta T^\star_{jk,0})\right.\\ &\qquad\left.-\frac{\delta v_j(\Delta T^\star_{jk,0})+\delta v_k(\Delta T^\star_{jk,0})}{2}\Delta X\right)\\ &\quad+\varepsilon\delta\Delta T(\Delta T^\star_{jk,0})+\mathcal{O}(\varepsilon^2,\varepsilon\varepsilon^2_{\rm UR},\varepsilon^3_{\rm UR})\end{aligned} \tag{D.47}$$

$$\begin{aligned}&= \left(1+\frac{m_j^2+m_k^2}{4E^2}+\frac{\delta v_j(\Delta T^\star_{jk,0})+\delta v_k(\Delta T^\star_{jk,0})}{2}\right.\\ &\quad\left.-\frac{\Delta p_j m_j^2+\Delta p_k m_k^2}{2E^3}-\frac{(\Delta m^2_{jk})^2}{8E^4}-\frac{m_j^4+m_k^4}{16E^4}\right)\\ &\quad\times\left(\Delta X+\varepsilon\delta\Delta X(\Delta T^\star_{jk,0})\right)+\mathcal{O}(\varepsilon^2,\varepsilon\varepsilon^2_{\rm UR},\varepsilon^3_{\rm UR})\,.\end{aligned} \tag{D.48}$$

In deriving the expression for $\Delta T^\star_{jk,1}$, we have used that the amplitude is only significantly different fro zero as long as the transported neutrino source momentum coincides with the detected mean momentum, i.e. when

$$\tilde{\vec{P}}_{{\rm S}j} \equiv \vec{P}_{{\rm D}j}\,, \tag{D.49}$$

holds. We enforce this relation *after* obtaining the solution for $\Delta T^\star_{jk,1}$, causing all contributions originating from the momentum deviation terms, present in $\mathrm{Re}(\Xi_{jk})$, to vanish. That this is the case can be easily seen by considering the expressions

$$\frac{\partial^2 \mathrm{Re}(\Xi_{jk})}{\partial \Delta T^2}(\Delta T^\star_{jk,0}, 0) \supset -\tilde{\vec{P}}''_{\mathrm{S}j} \cdot \frac{\left(\tilde{\vec{P}}_{\mathrm{S}j} - \vec{P}_{\mathrm{D}j}\right)}{\sigma_P^2}\bigg|_{\varepsilon=0} - \frac{\tilde{\vec{P}}'_{\mathrm{S}j} \cdot \tilde{\vec{P}}'_{\mathrm{S}j}}{\sigma_P^2}\bigg|_{\varepsilon=0} = 0\,, \tag{D.50}$$

$$\frac{\partial^2 \mathrm{Re}(\Xi_{jk})}{\partial \varepsilon \partial \Delta T}(\Delta T^\star_{jk,0}, 0) \supset -\frac{\partial \tilde{\vec{P}}'_{\mathrm{S}j}}{\partial \varepsilon} \cdot \frac{\left(\tilde{\vec{P}}_{\mathrm{S}j} - \vec{P}_{\mathrm{D}j}\right)}{\sigma_P^2}\bigg|_{\varepsilon=0} - \tilde{\vec{P}}'_{\mathrm{S}j} \cdot \frac{\partial \tilde{\vec{P}}_{\mathrm{S}j}}{\partial \varepsilon}\bigg|_{\varepsilon=0} = 0\,. \tag{D.51}$$

Here, we only need to enforce the equality (D.49) in the first term in the second quantity in order for it to vanish. All other terms are already zero in general. Moreover, we have introduced the effective momentum resolution $\sigma_P^2 := 2(\sigma_{\mathrm{S}}^2 + \sigma_{\mathrm{D}}^2)$.

Next, we evaluate the real and imaginary parts of Ξ_{jk} at the maximum $\Delta T^\star_{jk}$. To this end, we first evaluate the quantity

$$\begin{aligned} v_j L^0(\Delta T^\star_{jk}) - L(\Delta T^\star_{jk}) = \Bigg[&\left(1 - \frac{m_j^2}{2E^2} + \frac{3m_j^4}{8E^4} + \frac{\Delta p_j m_j^2}{E^3}\right) \\ &\times \left(1 + \frac{m_j^2 + m_k^2}{4E^2} + \varepsilon \frac{\delta v_j + \delta v_k}{2} - \frac{\Delta p_j m_j^2 + \Delta p_k m_k^2}{2E^3}\right. \\ &\left. - \frac{(\Delta m_{jk}^2)^2}{8E^4} - \frac{m_j^4 + m_k^4}{16E^4}\right) - 1 \Bigg] L(\Delta T^\star_{jk}) + \mathcal{O}(\varepsilon^2, \varepsilon\varepsilon_{\mathrm{UR}}^2, \varepsilon_{\mathrm{UR}}^3)\,, \end{aligned} \tag{D.52}$$

yielding

$$\begin{aligned} v_j L^0(\Delta T^\star_{jk}) - L(\Delta T^\star_{jk}) = \Bigg[&-\frac{\Delta m_{jk}^2}{4E^2} + \varepsilon \left(\frac{\delta v_j + \delta v_k}{2}\right) + \frac{\Delta p_j m_j^2 - \Delta p_k m_k^2}{2E^3} \\ &+ \frac{\Delta m_{jk}^4}{8E^4} - \left(\frac{\Delta m_{jk}^2}{4E^2}\right)^2 \Bigg] L + \mathcal{O}(\varepsilon^2, \varepsilon\varepsilon_{\mathrm{UR}}^2, \varepsilon_{\mathrm{UR}}^3)\,. \end{aligned} \tag{D.53}$$

$$=: \Delta v_{jk}^+ L(\Delta T^\star_{jk}) + \mathcal{O}(\varepsilon^2, \varepsilon\varepsilon_{\mathrm{UR}}^2, \varepsilon_{\mathrm{UR}}^3)\,, \tag{D.54}$$

and similarly for

$$\begin{aligned} v_k L^0(\Delta T^\star_{jk}) - L(\Delta T^\star_{jk}) = \Bigg[&+\frac{\Delta m_{jk}^2}{4E^2} + \varepsilon \left(\frac{\delta v_j + \delta v_k}{2}\right) - \frac{\Delta p_j m_j^2 - \Delta p_k m_k^2}{2E^3} \\ &- \frac{\Delta m_{jk}^4}{8E^4} + \left(\frac{\Delta m_{jk}^2}{4E^2}\right)^2 \Bigg] L + \mathcal{O}(\varepsilon^2, \varepsilon\varepsilon_{\mathrm{UR}}^2, \varepsilon_{\mathrm{UR}}^3)\,. \end{aligned} \tag{D.55}$$

$$=: \Delta v_{jk}^- L(\Delta T^\star_{jk}) + \mathcal{O}(\varepsilon^2, \varepsilon\varepsilon_{\mathrm{UR}}^2, \varepsilon_{\mathrm{UR}}^3)\,, \tag{D.56}$$

with

$$\Delta v^{\pm}_{jk} = \mp\frac{\Delta m^2_{jk}}{4E^2} + \varepsilon\left(\frac{\delta v_{j0}+\delta v_{k0}}{2}\right) \pm \frac{\Delta p_j m_j^2 - \Delta p_k m_k^2}{2E^3} \pm \frac{\Delta m^4_{jk}}{8E^4} \mp \left(\frac{\Delta m^2_{jk}}{4E^2}\right)^2 . \tag{D.57}$$

For the full real part, we obtain

$$\begin{aligned}\mathrm{Re}(\Xi_{jk})(\Delta T^{\star}_{jk}) = &-\left(\frac{(\Delta v^{+}_{jk})^2}{(1+\chi_j^2(L^0)^2)} + \frac{(\Delta v^{-}_{jk})^2}{(1+\chi_k^2(L^0)^2)}\right)\frac{L^2(\Delta T^{\star}_{jk})}{2\Theta^2} \\ &+ \mathcal{O}(\varepsilon^2, \varepsilon\varepsilon^2_{\mathrm{UR}}, \varepsilon^3_{\mathrm{UR}}) ,\end{aligned} \tag{D.58}$$

where we have used the explicit expressions for the effective neutrino WP widths

$$\sigma^2_{\parallel j} = \Theta^2\left(1 + i\chi_j L^0\right) , \qquad \Theta^2 = \frac{1}{2}\left(\frac{1}{\sigma^2_{\mathrm{S}}} + \frac{1}{\sigma^2_{\mathrm{D}}}\right) , \qquad \chi_j = \frac{(1-v_j^2)}{E_j\Theta^2} . \tag{D.59}$$

With $\Theta^2 = 2\sigma_X^2$, we arrive at

$$\mathrm{Re}(\Xi_{jk})(\Delta T^{\star}_{jk}) = -\left(\frac{L(\Delta T^{\star}_{jk})}{L^{\mathrm{coh}}_{jk}}\right)^2 + \mathcal{O}(\varepsilon^2, \varepsilon\varepsilon^2_{\mathrm{UR}}, \varepsilon^3_{\mathrm{UR}}) , \tag{D.60}$$

where the coherence length is given by

$$L^{\mathrm{coh}}_{jk} = 2\sqrt{2}\sigma_X\left[\frac{(\Delta v^{+}_{jk})^2}{(1+\chi_j^2(L^0)^2)} + \frac{(\Delta v^{-}_{jk})^2}{(1+\chi_k^2(L^0)^2)}\right]^{-\frac{1}{2}} . \tag{D.61}$$

Next, the imaginary part can be subdivided into the usual oscillation phase and a sub-leading part related to the WP spreading, i.e.

$$\mathrm{Im}(\Xi_{jk})(\Delta T^{\star}_{jk}, \varepsilon) \;= \Delta\Phi_{jk}(L) + \Delta\varphi_{jk}(L) , \tag{D.62}$$

$$\Delta\Phi_{jk}(L) := -L^0\Delta E_{jk} + L\Delta p_{jk} , \tag{D.63}$$

$$\Delta\varphi_{jk}(L) := \mathrm{Im}(\sigma^2_{\parallel j})\frac{(v_j L^0 - L)^2}{2|\sigma^2_{\parallel j}|^2} - \mathrm{Im}(\sigma^2_{\parallel k})\frac{(v_k L^0 - L)^2}{2|\sigma^2_{\parallel k}|^2} . \tag{D.64}$$

For completeness we now compute both appearing terms, but we only retain the main oscillation phase in the main text, as the other term $\Delta\varphi_{jk}$ is small compared to $\Delta\Phi_{jk}$. The energy difference at second order in the ultra-relativistic approximation is given by

$$\Delta E_{jk} = \Delta p_{jk} + \frac{\Delta m^2_{jk}}{2E} - \frac{\Delta m^4_{jk}}{8E^3} - \frac{\Delta p_j m_j^2 - \Delta p_k m_k^2}{2E^2} + \mathcal{O}(\varepsilon^2, \varepsilon\varepsilon^2_{\mathrm{UR}}, \varepsilon^3_{\mathrm{UR}}) , \tag{D.65}$$

and plugging it into the expression for the phase $\Delta\Phi_{jk}$ yields

$$\Delta\Phi_{jk}(L) = -\left(\Delta E_{jk}\left[1 + \frac{m_j^2 + m_k^2}{4E^2}\right] - \Delta p_{jk}\right) L + \mathcal{O}(\varepsilon^2, \varepsilon\varepsilon^2_{\mathrm{UR}}, \varepsilon^3_{\mathrm{UR}}) \tag{D.66}$$

$$= -\frac{\Delta m^2_{jk}}{2E}\left(1 - \frac{\Delta p_j + \Delta p_k}{2E}\right) L + \mathcal{O}(\varepsilon^2, \varepsilon\varepsilon^2_{\mathrm{UR}}, \varepsilon^3_{\mathrm{UR}}) , \tag{D.67}$$

where we have used that ΔE_{jk} already is of $\mathcal{O}(\varepsilon_{\mathrm{UR}})$. Lastly, the WP spreading correction yields

$$\Delta\varphi_{jk}(L) \approx \frac{L^2 L^0}{8\sigma_X^4}\left(\frac{\chi_j(\Delta v_{jk}^+)^2}{(1+\chi_j^2(L^0)^2)} - \frac{\chi_k(\Delta v_{jk}^-)^2}{(1+\chi_k^2(L^0)^2)}\right). \tag{D.68}$$

It is evident that the factor in parentheses is at least of order $\mathcal{O}(\varepsilon_{\mathrm{UR}}^3)$ and hence can be safely neglected.

Bibliography

[1] S. Weinberg, *The Quantum theory of fields. Vol. 1: Foundations*. Cambridge University Press, Jun. 2005, ISBN: 978-0-521-67053-1, 978-0-511-25204-4. DOI: 10.1017/CBO9781139644167.

[2] S. Weinberg, *The quantum theory of fields. Vol. 2: Modern applications*. Cambridge University Press, Aug. 2013, ISBN: 978-1-139-63247-8, 978-0-521-67054-8, 978-0-521-55002-4. DOI: 10.1017/CBO9781139644174.

[3] M. E. Peskin and D. V. Schroeder, *An Introduction to quantum field theory*. Reading, USA: Addison-Wesley, 1995, ISBN: 978-0-201-50397-5, 978-0-429-50355-9, 978-0-429-49417-8. DOI: 10.1201/9780429503559.

[4] M. Srednicki, *Quantum field theory*. Cambridge University Press, Jan. 2007, ISBN: 978-0-521-86449-7, 978-0-511-26720-8. DOI: 10.1017/CBO9780511813917.

[5] S. Weinberg, "Nonabelian Gauge Theories of the Strong Interactions," *Phys. Rev. Lett.*, vol. 31, pp. 494–497, 1973. DOI: 10.1103/PhysRevLett.31.494.

[6] H. D. Politzer, "Reliable Perturbative Results for Strong Interactions?" *Phys. Rev. Lett.*, vol. 30, J. C. Taylor, Ed., pp. 1346–1349, 1973. DOI: 10.1103/PhysRevLett.30.1346.

[7] D. J. Gross and F. Wilczek, "Ultraviolet Behavior of Nonabelian Gauge Theories," *Phys. Rev. Lett.*, vol. 30, J. C. Taylor, Ed., pp. 1343–1346, 1973. DOI: 10.1103/PhysRevLett.30.1343.

[8] H. Fritzsch, M. Gell-Mann, and H. Leutwyler, "Advantages of the Color Octet Gluon Picture," *Phys. Lett. B*, vol. 47, pp. 365–368, 1973. DOI: 10.1016/0370-2693(73)90625-4.

[9] A. Salam and J. C. Ward, "Weak and electromagnetic interactions," *Nuovo Cim.*, vol. 11, pp. 568–577, 1959. DOI: 10.1007/BF02726525.

[10] S. L. Glashow, "Partial Symmetries of Weak Interactions," *Nucl. Phys.*, vol. 22, pp. 579–588, 1961. DOI: 10.1016/0029-5582(61)90469-2.

[11] S. Weinberg, "A Model of Leptons," *Phys. Rev. Lett.*, vol. 19, pp. 1264–1266, 1967. DOI: 10.1103/PhysRevLett.19.1264.

[12] S. L. Glashow, J. Iliopoulos, and L. Maiani, "Weak Interactions with Lepton-Hadron Symmetry," *Phys. Rev. D*, vol. 2, pp. 1285–1292, 1970. DOI: 10.1103/PhysRevD.2.1285.

[13] J. Goldstone, A. Salam, and S. Weinberg, "Broken Symmetries," *Phys. Rev.*, vol. 127, pp. 965–970, 1962. DOI: 10.1103/PhysRev.127.965.

[14] F. Englert and R. Brout, "Broken Symmetry and the Mass of Gauge Vector Mesons," *Phys. Rev. Lett.*, vol. 13, J. C. Taylor, Ed., pp. 321–323, 1964. DOI: 10.1103/PhysRevLett.13.321.

[15] P. W. Higgs, "Spontaneous Symmetry Breakdown without Massless Bosons," *Phys. Rev.*, vol. 145, pp. 1156–1163, 1966. DOI: 10.1103/PhysRev.145.1156.

[16] G. S. Guralnik, C. R. Hagen, and T. W. B. Kibble, "Global Conservation Laws and Massless Particles," *Phys. Rev. Lett.*, vol. 13, J. C. Taylor, Ed., pp. 585–587, 1964. DOI: 10.1103/PhysRevLett.13.585.

[17] J. Goldstone, "Field Theories with Superconductor Solutions," *Nuovo Cim.*, vol. 19, pp. 154–164, 1961. DOI: 10.1007/BF02812722.

[18] N. Cabibbo, "Unitary Symmetry and Leptonic Decays," *Phys. Rev. Lett.*, vol. 10, pp. 531–533, 1963. DOI: 10.1103/PhysRevLett.10.531.

[19] M. Kobayashi and T. Maskawa, "CP Violation in the Renormalizable Theory of Weak Interaction," *Prog. Theor. Phys.*, vol. 49, pp. 652–657, 1973. DOI: 10.1143/PTP.49.652.

[20] A. Einstein, H. A. Lorentz, H. Weyl, and H. Minkowski, *The Principle of Relativity*, W. Perret and G. B. Jeffery, Eds. Dover Publications, Inc., 1924.

[21] S. Weinberg, *Gravitation and Cosmology: Principles and Applications of the General Theory of Relativity*. New York: John Wiley and Sons, 1972, ISBN: 978-0-471-92567-5, 978-0-471-92567-5.

[22] C. W. Misner, K. S. Thorne, and J. A. Wheeler, *Gravitation*. San Francisco: W. H. Freeman, 1973, ISBN: 978-0-7167-0344-0, 978-0-691-17779-3.

[23] S. M. Carroll, *Spacetime and Geometry: An Introduction to General Relativity*. Cambridge University Press, Jul. 2019, ISBN: 978-0-8053-8732-2, 978-1-108-48839-6, 978-1-108-77555-7. DOI: 10.1017/9781108770385.

[24] R. Alpher and R. Herman, "Evolution of the Universe," *Nature*, vol. 162, pp. 774–775, 1948. DOI: 10.1038/162774b0.

[25] A. A. Penzias and R. W. Wilson, "A Measurement of Excess Antenna Temperature at 4080 Mc/s," *Astrophysical Journal*, vol. 142, pp. 419–421, 1965. DOI: 10.1086/148307.

[26] C. L. Bennett *et al.*, "Nine-year wilkinson microwave anisotropy probe (wmap) observations: Final maps and results," *The Astrophysical Journal Supplement Series*, vol. 208, no. 2, p. 20, Sep. 2013. DOI: 10.1088/0067-0049/208/2/20. [Online]. Available: https://dx.doi.org/10.1088/0067-0049/208/2/20.

[27] N. Aghanim *et al.*, "Planck 2018 results. I. Overview and the cosmological legacy of Planck," *Astron. Astrophys.*, vol. 641, A1, 2020. DOI: 10.1051/0004-6361/201833880. arXiv: 1807.06205 [astro-ph.CO].

[28] D. N. Spergel *et al.*, "Wilkinson Microwave Anisotropy Probe (WMAP) three year results: implications for cosmology," *Astrophys. J. Suppl.*, vol. 170, p. 377, 2007. DOI: 10.1086/513700. arXiv: astro-ph/0603449.

[29] N. Aghanim *et al.*, "Planck 2018 results. VI. Cosmological parameters," *Astron. Astrophys.*, vol. 641, A6, 2020, [Erratum: Astron.Astrophys. 652, C4 (2021)]. DOI: 10.1051/0004-6361/201833910. arXiv: 1807.06209 [astro-ph.CO].

[30] S. Weinberg, "The Cosmological Constant Problem," *Rev. Mod. Phys.*, vol. 61, J.-P. Hsu and D. Fine, Eds., pp. 1–23, 1989. DOI: 10.1103/RevModPhys.61.1.

[31] E. W. Kolb and M. S. Turner, *The Early Universe*. Taylor and Francis, May 2019, vol. 69, ISBN: 978-0-429-49286-0, 978-0-201-62674-2. DOI: 10.1201/9780429492860.

[32] L. Husdal, "On Effective Degrees of Freedom in the Early Universe," *Galaxies*, vol. 4, no. 4, p. 78, 2016. DOI: 10.3390/galaxies4040078. arXiv: 1609.04979 [astro-ph.CO].

[33] N. D. Birrell and P. C. W. Davies, *Quantum Fields in Curved Space* (Cambridge Monographs on Mathematical Physics). Cambridge, UK: Cambridge University Press, 1982, ISBN: 978-0-521-27858-4, 978-0-521-27858-4. DOI: 10.1017/CBO9780511622632.

[34] R. M. Wald, *Quantum Field Theory in Curved Space-Time and Black Hole Thermodynamics* (Chicago Lectures in Physics). Chicago, IL: University of Chicago Press, 1995, ISBN: 978-0-226-87027-4.

[35] S. J. Avis, C. J. Isham, and D. Storey, "Quantum Field Theory in anti-De Sitter Space-Time," *Phys. Rev. D*, vol. 18, p. 3565, 1978. DOI: 10.1103/PhysRevD.18.3565.

[36] N. N. Bogolyubov, "A New method in the theory of superconductivity. I," *Sov. Phys. JETP*, vol. 7, pp. 41–46, 1958.

[37] S. A. Fulling, "Nonuniqueness of canonical field quantization in Riemannian space-time," *Phys. Rev. D*, vol. 7, pp. 2850–2862, 1973. DOI: 10.1103/PhysRevD.7.2850.

[38] P. C. W. Davies, "Scalar particle production in Schwarzschild and Rindler metrics," *J. Phys. A*, vol. 8, pp. 609–616, 1975. DOI: 10.1088/0305-4470/8/4/022.

[39] W. G. Unruh, "Notes on black hole evaporation," *Phys. Rev. D*, vol. 14, p. 870, 1976. DOI: 10.1103/PhysRevD.14.870.

[40] B. Pontecorvo, "Mesonium and anti-mesonium," *Sov. Phys. JETP*, vol. 6, p. 429, 1957.

[41] B. Pontecorvo, "Inverse beta processes and nonconservation of lepton charge," *Zh. Eksp. Teor. Fiz.*, vol. 34, p. 247, 1957.

[42] Z. Maki, M. Nakagawa, and S. Sakata, "Remarks on the unified model of elementary particles," *Prog. Theor. Phys.*, vol. 28, pp. 870–880, 1962. DOI: 10.1143/PTP.28.870.

[43] B. Pontecorvo, "Neutrino Experiments and the Problem of Conservation of Leptonic Charge," *Zh. Eksp. Teor. Fiz.*, vol. 53, pp. 1717–1725, 1967.

[44] R. Davis Jr., D. S. Harmer, and K. C. Hoffman, "Search for neutrinos from the sun," *Phys. Rev. Lett.*, vol. 20, pp. 1205–1209, 1968. DOI: 10.1103/PhysRevLett.20.1205.

[45] Y. Fukuda *et al.*, "Evidence for oscillation of atmospheric neutrinos," *Phys. Rev. Lett.*, vol. 81, pp. 1562–1567, 1998. DOI: 10.1103/PhysRevLett.81.1562. arXiv: hep-ex/9807003.

[46] Q. R. Ahmad *et al.*, "Direct evidence for neutrino flavor transformation from neutral current interactions in the Sudbury Neutrino Observatory," *Phys. Rev. Lett.*, vol. 89, p. 011 301, 2002. DOI: 10.1103/PhysRevLett.89.011301. arXiv: nucl-ex/0204008.

[47] P. Minkowski, "$\mu \to e\gamma$ at a Rate of One Out of 10^9 Muon Decays?" *Phys. Lett. B*, vol. 67, pp. 421–428, 1977. DOI: 10.1016/0370-2693(77)90435-X.

[48] M. Gell-Mann, P. Ramond, and R. Slansky, "Complex Spinors and Unified Theories," *Conf. Proc. C*, vol. 790927, pp. 315–321, 1979. arXiv: 1306.4669 [hep-th].

[49] T. Yanagida, "Horizontal gauge symmetry and masses of neutrinos," *Conf. Proc. C*, vol. 7902131, O. Sawada and A. Sugamoto, Eds., pp. 95–99, 1979.

[50] R. N. Mohapatra and G. Senjanovic, "Neutrino Mass and Spontaneous Parity Nonconservation," *Phys. Rev. Lett.*, vol. 44, p. 912, 1980. DOI: 10.1103/PhysRevLett.44.912.

[51] W. Grimus and P. Stockinger, "Real oscillations of virtual neutrinos," *Phys. Rev. D*, vol. 54, pp. 3414–3419, 1996. DOI: 10.1103/PhysRevD.54.3414. arXiv: hep-ph/9603430.

[52] M. Beuthe, "Oscillations of neutrinos and mesons in quantum field theory," *Phys. Rept.*, vol. 375, pp. 105–218, 2003. DOI: 10.1016/S0370-1573(02)00538-0. arXiv: hep-ph/0109119.

[53] E. K. Akhmedov and J. Kopp, "Neutrino Oscillations: Quantum Mechanics vs. Quantum Field Theory," *JHEP*, vol. 04, p. 008, 2010, [Erratum: JHEP 10, 052 (2013)]. DOI: 10.1007/JHEP04(2010)008. arXiv: 1001.4815 [hep-ph].

[54] D. V. Naumov and V. A. Naumov, "Quantum Field Theory of Neutrino Oscillations," *Phys. Part. Nucl.*, vol. 51, no. 1, pp. 1–106, 2020. DOI: 10.1134/S1063779620010050.

[55] V. A. Naumov and D. S. Shkirmanov, "Virtual neutrino propagation at short baselines," *Eur. Phys. J. C*, vol. 82, no. 8, p. 736, 2022. DOI: 10.1140/epjc/s10052-022-10670-w. arXiv: 2208.02621 [hep-ph].

[56] E. K. Akhmedov and A. Wilhelm, "Quantum field theoretic approach to neutrino oscillations in matter," *JHEP*, vol. 01, p. 165, 2013. DOI: 10.1007/JHEP01(2013)165. arXiv: 1205.6231 [hep-ph].

[57] C. Giunti, C. W. Kim, J. A. Lee, and U. W. Lee, "On the treatment of neutrino oscillations without resort to weak eigenstates," *Phys. Rev. D*, vol. 48, pp. 4310–4317, 1993. DOI: 10.1103/PhysRevD.48.4310. arXiv: hep-ph/9305276.

[58] C. Giunti, C. W. Kim, and U. W. Lee, "When do neutrinos cease to oscillate?" *Phys. Lett. B*, vol. 421, pp. 237–244, 1998. DOI: 10.1016/S0370-2693(98)00014-8. arXiv: hep-ph/9709494.

[59] E. K. Akhmedov and A. Y. Smirnov, "Paradoxes of neutrino oscillations," *Phys. Atom. Nucl.*, vol. 72, pp. 1363–1381, 2009. DOI: 10.1134/S1063778809080122. arXiv: 0905.1903 [hep-ph].

[60] E. Akhmedov, J. Kopp, and M. Lindner, "Collective neutrino oscillations and neutrino wave packets," *JCAP*, vol. 09, p. 017, 2017. DOI: 10.1088/1475-7516/2017/09/017. arXiv: 1702.08338 [hep-ph].

[61] J. F. Nieves and S. Sahu, "Neutrino effective potential in a fermion and scalar background," *Phys. Rev. D*, vol. 98, no. 6, p. 063 003, 2018. DOI: 10.1103/PhysRevD.98.063003. arXiv: 1808.01629 [hep-ph].

[62] H. D. Zeh, "On the interpretation of measurement in quantum theory," *Found. Phys.*, vol. 1, pp. 69–76, 1970. DOI: 10.1007/BF00708656.

[63] G. Lindblad, *Non-Equilibrium Entropy and Irreversibility*. Springer Netherlands, 1983, ISBN: 978-1-4020-0320-2.

[64] H. P. Breuer and F. Petruccione, *The theory of open quantum systems*. 2002.

[65] P. Strack and A. Burrows, "Generalized Boltzmann formalism for oscillating neutrinos," *Phys. Rev. D*, vol. 71, p. 093 004, 2005. DOI: 10.1103/PhysRevD.71.093004. arXiv: hep-ph/0504035.

[66] M. C. Gonzalez-Garcia, F. Halzen, and M. Maltoni, "Physics reach of high-energy and high-statistics icecube atmospheric neutrino data," *Phys. Rev. D*, vol. 71, p. 093 010, 2005. DOI: 10.1103/PhysRevD.71.093010. arXiv: hep-ph/0502223.

[67] M. Cirelli, N. Fornengo, T. Montaruli, I. A. Sokalski, A. Strumia, and F. Vissani, "Spectra of neutrinos from dark matter annihilations," *Nucl. Phys. B*, vol. 727, pp. 99–138, 2005, [Erratum: Nucl.Phys.B 790, 338–344 (2008)]. DOI: 10.1016/j.nuclphysb.2007.10.001. arXiv: hep-ph/0506298.

[68] M. Blennow, J. Edsjo, and T. Ohlsson, "Neutrinos from WIMP annihilations using a full three-flavor Monte Carlo," *JCAP*, vol. 01, p. 021, 2008. DOI: 10.1088/1475-7516/2008/01/021. arXiv: 0709.3898 [hep-ph].

[69] H. Duan, G. M. Fuller, and Y.-Z. Qian, "Collective Neutrino Oscillations," *Ann. Rev. Nucl. Part. Sci.*, vol. 60, pp. 569–594, 2010. DOI: 10.1146/annurev.nucl.012809.104524. arXiv: 1001.2799 [hep-ph].

[70] C. A. Arguelles and J. Kopp, "Sterile neutrinos and indirect dark matter searches in IceCube," *JCAP*, vol. 07, p. 016, 2012. DOI: 10.1088/1475-7516/2012/07/016. arXiv: 1202.3431 [hep-ph].

[71] Y. Zhang and A. Burrows, "Transport Equations for Oscillating Neutrinos," *Phys. Rev. D*, vol. 88, no. 10, p. 105 009, 2013. DOI: 10.1103/PhysRevD.88.105009. arXiv: 1310.2164 [hep-ph].

[72] C. A. Argüelles, J. Salvado, and C. N. Weaver, "nuSQuIDS: A toolbox for neutrino propagation," *Comput. Phys. Commun.*, vol. 277, p. 108 346, 2022. DOI: 10.1016/j.cpc.2022.108346. arXiv: 2112.13804 [hep-ph].

[73] D. Hellmann and H. Päs, "Light sterile neutrinos in the early universe: effects of altered dispersion relations and a coupling to axion-like dark matter," *JCAP*, vol. 11, p. 056, 2023. DOI: 10.1088/1475-7516/2023/11/056. arXiv: 2307.12118 [hep-ph].

[74] Päs, Heinrich and Pakvasa, Sandip and Weiler, Thomas J., "Sterile-active neutrino oscillations and shortcuts in the extra dimension," *Phys. Rev. D*, vol. 72, p. 095 017, 2005. DOI: 10.1103/PhysRevD.72.095017. arXiv: hep-ph/0504096.

[75] Marfatia, D. and Päs, H. and Pakvasa, S. and Weiler, T. J., "A model of superluminal neutrinos," *Phys. Lett. B*, vol. 707, pp. 553–557, 2012. DOI: 10.1016/j.physletb.2012.01.028. arXiv: 1112.0527 [hep-ph].

[76] E. Aeikens, H. Päs, S. Pakvasa, and P. Sicking, "Flavor ratios of extragalactic neutrinos and neutrino shortcuts in extra dimensions," *JCAP*, vol. 10, p. 005, 2015. DOI: 10.1088/1475-7516/2015/10/005. arXiv: 1410.0408 [hep-ph].

[77] E. Aeikens, H. Päs, S. Pakvasa, and T. J. Weiler, "Suppression of cosmological sterile neutrino production by altered dispersion relations," *Phys. Rev. D*, vol. 94, no. 11, p. 113 010, 2016. DOI: 10.1103/PhysRevD.94.113010. arXiv: 1606.06695 [hep-ph].

[78] D. Döring and H. Päs, "Sterile Neutrino Shortcuts in Asymmetrically Warped Extra Dimensions," *Eur. Phys. J. C*, vol. 79, no. 7, p. 604, 2019. DOI: 10.1140/epjc/s10052-019-7122-8. arXiv: 1808.07734 [hep-ph].

[79] D. Döring, H. Päs, P. Sicking, and T. J. Weiler, "Sterile neutrinos with altered dispersion relations as an explanation for neutrino anomalies," *Eur. Phys. J. C*, vol. 80, no. 12, p. 1202, 2020. DOI: 10.1140/epjc/s10052-020-08720-2. arXiv: 1808.07460 [hep-ph].

[80] G. A. Barenboim, P. Martínez-Miravé, C. A. Ternes, and M. A. Tórtola, "Sterile neutrinos with altered dispersion relations revisited," *JHEP*, vol. 03, p. 070, 2020. DOI: 10.1007/JHEP03(2020)070. arXiv: 1911.02329 [hep-ph].

[81] A. Aguilar *et al.*, "Evidence for neutrino oscillations from the observation of $\bar{\nu}_e$ appearance in a $\bar{\nu}_\mu$ beam," *Phys. Rev. D*, vol. 64, p. 112 007, 2001. DOI: 10.1103/PhysRevD.64.112007. arXiv: hep-ex/0104049.

[82] G. Mention *et al.*, "The Reactor Antineutrino Anomaly," *Phys. Rev. D*, vol. 83, p. 073 006, 2011. DOI: 10.1103/PhysRevD.83.073006. arXiv: 1101.2755 [hep-ex].

[83] C. Giunti and M. Laveder, "Statistical Significance of the Gallium Anomaly," *Phys. Rev. C*, vol. 83, p. 065 504, 2011. DOI: 10.1103/PhysRevC.83.065504. arXiv: 1006.3244 [hep-ph].

[84] A. A. Aguilar-Arevalo *et al.*, "Significant Excess of ElectronLike Events in the MiniBooNE Short-Baseline Neutrino Experiment," *Phys. Rev. Lett.*, vol. 121, no. 22, p. 221 801, 2018. DOI: 10.1103/PhysRevLett.121.221801. arXiv: 1805.12028 [hep-ex].

[85] A. A. Aguilar-Arevalo *et al.*, "Updated MiniBooNE neutrino oscillation results with increased data and new background studies," *Phys. Rev. D*, vol. 103, no. 5, p. 052 002, 2021. DOI: 10.1103/PhysRevD.103.052002. arXiv: 2006.16883 [hep-ex].

[86] M. G. Aartsen *et al.*, "Searches for Sterile Neutrinos with the IceCube Detector," *Phys. Rev. Lett.*, vol. 117, no. 7, p. 071 801, 2016. DOI: 10.1103/PhysRevLett.117.071801. arXiv: 1605.01990 [hep-ex].

[87] K. Abe *et al.*, "Limits on sterile neutrino mixing using atmospheric neutrinos in Super-Kamiokande," *Phys. Rev. D*, vol. 91, p. 052 019, 2015. DOI: 10.1103/PhysRevD.91.052019. arXiv: 1410.2008 [hep-ex].

[88] M. G. Aartsen *et al.*, "eV-Scale Sterile Neutrino Search Using Eight Years of Atmospheric Muon Neutrino Data from the IceCube Neutrino Observatory," *Phys. Rev. Lett.*, vol. 125, no. 14, p. 141 801, 2020. DOI: 10.1103/PhysRevLett.125.141801. arXiv: 2005.12942 [hep-ex].

[89] K. Abe *et al.*, "Search for short baseline ν_e disappearance with the T2K near detector," *Phys. Rev. D*, vol. 91, p. 051 102, 2015. DOI: 10.1103/PhysRevD.91.051102. arXiv: 1410.8811 [hep-ex].

[90] P. Adamson *et al.*, "Search for sterile neutrinos in MINOS and MINOS+ using a two-detector fit," *Phys. Rev. Lett.*, vol. 122, no. 9, p. 091 803, 2019. DOI: 10.1103/PhysRevLett.122.091803. arXiv: 1710.06488 [hep-ex].

[91] P. Adamson *et al.*, "Search for active-sterile neutrino mixing using neutral-current interactions in NOvA," *Phys. Rev. D*, vol. 96, no. 7, p. 072 006, 2017. DOI: 10.1103/PhysRevD.96.072006. arXiv: 1706.04592 [hep-ex].

[92] P. Abratenko *et al.*, "Search for an Excess of Electron Neutrino Interactions in MicroBooNE Using Multiple Final-State Topologies," *Phys. Rev. Lett.*, vol. 128, no. 24, p. 241 801, 2022. DOI: 10.1103/PhysRevLett.128.241801. arXiv: 2110.14054 [hep-ex].

[93] P. Abratenko *et al.*, "Search for an anomalous excess of charged-current quasielastic νe interactions with the MicroBooNE experiment using Deep-Learning-based reconstruction," *Phys. Rev. D*, vol. 105, no. 11, p. 112 003, 2022. DOI: 10.1103/PhysRevD.105.112003. arXiv: 2110.14080 [hep-ex].

[94] P. Abratenko *et al.*, "Search for an anomalous excess of charged-current νe interactions without pions in the final state with the MicroBooNE experiment," *Phys. Rev. D*, vol. 105, no. 11, p. 112 004, 2022. DOI: 10.1103/PhysRevD.105.112004. arXiv: 2110.14065 [hep-ex].

[95] P. Abratenko *et al.*, "Search for an anomalous excess of inclusive charged-current ν_e interactions in the MicroBooNE experiment using Wire-Cell reconstruction," *Phys. Rev. D*, vol. 105, no. 11, p. 112 005, 2022. DOI: 10.1103/PhysRevD.105.112005. arXiv: 2110.13978 [hep-ex].

[96] P. B. Denton, "Sterile Neutrino Search with MicroBooNE's Electron Neutrino Disappearance Data," *Phys. Rev. Lett.*, vol. 129, no. 6, p. 061 801, 2022. DOI: 10.1103/PhysRevLett.129.061801. arXiv: 2111.05793 [hep-ph].

[97] M. A. Acero *et al.*, "White paper on light sterile neutrino searches and related phenomenology," *J. Phys. G*, vol. 51, no. 12, p. 120 501, 2024. DOI: 10.1088/1361-6471/ad307f. arXiv: 2203.07323 [hep-ex].

[98] A. Addazi *et al.*, "Quantum gravity phenomenology at the dawn of the multi-messenger era—A review," *Prog. Part. Nucl. Phys.*, vol. 125, p. 103 948, 2022. DOI: 10.1016/j.ppnp.2022.103948. arXiv: 2111.05659 [hep-ph].

[99] D. Hellmann, "Cosmological implications of sterile Neutrinos taking shortcuts through extra dimensions in the primordial plasma," M.S. thesis, 2020.

[100] P. F. de Salas and S. Pastor, "Relic neutrino decoupling with flavour oscillations revisited," *JCAP*, vol. 07, p. 051, 2016. DOI: 10.1088/1475-7516/2016/07/051. arXiv: 1606.06986 [hep-ph].

[101] S. Gariazzo, P. F. de Salas, and S. Pastor, "Thermalisation of sterile neutrinos in the early Universe in the 3+1 scheme with full mixing matrix," *JCAP*, vol. 07, p. 014, 2019. DOI: 10.1088/1475-7516/2019/07/014. arXiv: 1905.11290 [astro-ph.CO].

[102] J. J. Bennett *et al.*, "Towards a precision calculation of $N_{\rm eff}$ in the Standard Model II: Neutrino decoupling in the presence of flavour oscillations and finite-temperature QED," *JCAP*, vol. 04, p. 073, 2021. DOI: 10.1088/1475-7516/2021/04/073. arXiv: 2012.02726 [hep-ph].

[103] S. Hannestad, R. S. Hansen, and T. Tram, "How Self-Interactions can Reconcile Sterile Neutrinos with Cosmology," *Phys. Rev. Lett.*, vol. 112, no. 3, p. 031 802, 2014. DOI: 10.1103/PhysRevLett.112.031802. arXiv: 1310.5926 [astro-ph.CO].

[104] B. Dasgupta and J. Kopp, "Cosmologically Safe eV-Scale Sterile Neutrinos and Improved Dark Matter Structure," *Phys. Rev. Lett.*, vol. 112, no. 3, p. 031 803, 2014. DOI: 10.1103/PhysRevLett.112.031803. arXiv: 1310.6337 [hep-ph].

[105] A. Mirizzi, G. Mangano, O. Pisanti, and N. Saviano, "Collisional production of sterile neutrinos via secret interactions and cosmological implications," *Phys. Rev. D*, vol. 91, no. 2, p. 025 019, 2015. DOI: 10.1103/PhysRevD.91.025019. arXiv: 1410.1385 [hep-ph].

[106] Y. Tang, "More Is Different: Reconciling eV Sterile Neutrinos with Cosmological Mass Bounds," *Phys. Lett. B*, vol. 750, pp. 201–208, 2015. DOI: 10.1016/j.physletb.2015.09.018. arXiv: 1501.00059 [hep-ph].

[107] F. Forastieri, M. Lattanzi, G. Mangano, A. Mirizzi, P. Natoli, and N. Saviano, "Cosmic microwave background constraints on secret interactions among sterile neutrinos," *JCAP*, vol. 07, p. 038, 2017. DOI: 10.1088/1475-7516/2017/07/038. arXiv: 1704.00626 [astro-ph.CO].

[108] M. Archidiacono, S. Gariazzo, C. Giunti, S. Hannestad, and T. Tram, "Sterile neutrino self-interactions: H_0 tension and short-baseline anomalies," *JCAP*, vol. 12, p. 029, 2020. DOI: 10.1088/1475-7516/2020/12/029. arXiv: 2006.12885 [astro-ph.CO].

[109] H. Davoudiasl and P. B. Denton, "Sterile neutrino shape shifting caused by dark matter," *Phys. Rev. D*, vol. 108, no. 3, p. 035 013, 2023. DOI: 10.1103/PhysRevD.108.035013. arXiv: 2301.09651 [hep-ph].

[110] A. Berlin, "Neutrino Oscillations as a Probe of Light Scalar Dark Matter," *Phys. Rev. Lett.*, vol. 117, no. 23, p. 231 801, 2016. DOI: 10.1103/PhysRevLett.117.231801. arXiv: 1608.01307 [hep-ph].

[111] Y. Zhao, "Cosmology and time dependent parameters induced by a misaligned light scalar," *Phys. Rev. D*, vol. 95, no. 11, p. 115 002, 2017. DOI: 10.1103/PhysRevD.95.115002. arXiv: 1701.02735 [hep-ph].

[112] Y. Farzan, "Ultra-light scalar saving the 3 + 1 neutrino scheme from the cosmological bounds," *Phys. Lett. B*, vol. 797, p. 134 911, 2019. DOI: 10.1016/j.physletb.2019.134911. arXiv: 1907.04271 [hep-ph].

[113] J. M. Cline, "Viable secret neutrino interactions with ultralight dark matter," *Phys. Lett. B*, vol. 802, p. 135 182, 2020. DOI: 10.1016/j.physletb.2019.135182. arXiv: 1908.02278 [hep-ph].

[114] G.-y. Huang and N. Nath, "Neutrino meets ultralight dark matter: $0\nu\beta\beta$ decay and cosmology," *JCAP*, vol. 05, no. 05, p. 034, 2022. DOI: 10.1088/1475-7516/2022/05/034. arXiv: 2111.08732 [hep-ph].

[115] G.-y. Huang, M. Lindner, P. Martínez-Miravé, and M. Sen, "Cosmology-friendly time-varying neutrino masses via the sterile neutrino portal," *Phys. Rev. D*, vol. 106, no. 3, p. 033 004, 2022. DOI: 10.1103/PhysRevD.106.033004. arXiv: 2205.08431 [hep-ph].

[116] G. Krnjaic, P. A. N. Machado, and L. Necib, "Distorted neutrino oscillations from time varying cosmic fields," *Phys. Rev. D*, vol. 97, no. 7, p. 075 017, 2018. DOI: 10.1103/PhysRevD.97.075017. arXiv: 1705.06740 [hep-ph].

[117] V. Brdar, J. Kopp, J. Liu, P. Prass, and X.-P. Wang, "Fuzzy dark matter and non-standard neutrino interactions," *Phys. Rev. D*, vol. 97, no. 4, p. 043 001, 2018. DOI: 10.1103/PhysRevD.97.043001. arXiv: 1705.09455 [hep-ph].

[118] J. Liao, D. Marfatia, and K. Whisnant, "Light scalar dark matter at neutrino oscillation experiments," *JHEP*, vol. 04, p. 136, 2018. DOI: 10.1007/JHEP04(2018)136. arXiv: 1803.01773 [hep-ph].

[119] F. Capozzi, I. M. Shoemaker, and L. Vecchi, "Neutrino Oscillations in Dark Backgrounds," *JCAP*, vol. 07, p. 004, 2018. DOI: 10.1088/1475-7516/2018/07/004. arXiv: 1804.05117 [hep-ph].

[120] M. M. Reynoso, O. A. Sampayo, and A. M. Carulli, "Neutrino interactions with ultralight axion-like dark matter," *Eur. Phys. J. C*, vol. 82, no. 3, p. 274, 2022. DOI: 10.1140/epjc/s10052-022-10228-w. arXiv: 2203.11642 [hep-ph].

[121] G. Sigl and G. Raffelt, "General kinetic description of relativistic mixed neutrinos," *Nucl. Phys. B*, vol. 406, pp. 423–451, 1993. DOI: 10.1016/0550-3213(93)90175-O.

[122] E. Aver, K. A. Olive, and E. D. Skillman, "The effects of He I λ10830 on helium abundance determinations," *JCAP*, vol. 07, p. 011, 2015. DOI: 10.1088/1475-7516/2015/07/011. arXiv: 1503.08146 [astro-ph.CO].

[123] S. Dodelson and L. M. Widrow, "Sterile-neutrinos as dark matter," *Phys. Rev. Lett.*, vol. 72, pp. 17–20, 1994. DOI: 10.1103/PhysRevLett.72.17. arXiv: hep-ph/9303287.

[124] A. Vlasenko, G. M. Fuller, and V. Cirigliano, "Neutrino Quantum Kinetics," *Phys. Rev. D*, vol. 89, no. 10, p. 105 004, 2014. DOI: 10.1103/PhysRevD.89.105004. arXiv: 1309.2628 [hep-ph].

[125] L. Stodolsky, "On the Treatment of Neutrino Oscillations in a Thermal Environment," *Phys. Rev. D*, vol. 36, p. 2273, 1987. DOI: 10.1103/PhysRevD.36.2273.

[126] D. N. Blaschke and V. Cirigliano, "Neutrino Quantum Kinetic Equations: The Collision Term," *Phys. Rev. D*, vol. 94, no. 3, p. 033 009, 2016. DOI: 10.1103/PhysRevD.94.033009. arXiv: 1605.09383 [hep-ph].

[127] J. Bernstein, *Kinetic Theory in the Expanding Universe* (Cambridge Monographs on Mathematical Physics). Cambridge University Press, 1988.

[128] P. A. R. Ade *et al.*, "Planck 2013 results. XVI. Cosmological parameters," *Astron. Astrophys.*, vol. 571, A16, 2014. DOI: 10.1051/0004-6361/201321591. arXiv: 1303.5076 [astro-ph.CO].

[129] D. Hellmann, H. Päs, and E. Rani, "Searching new particles at neutrino telescopes with quantum-gravitational decoherence," *Phys. Rev. D*, vol. 105, no. 5, p. 055 007, 2022. DOI: 10.1103/PhysRevD.105.055007. arXiv: 2103.11984 [hep-ph].

[130] D. Hellmann, H. Päs, and E. Rani, "Quantum gravitational decoherence in the three neutrino flavor scheme," *Phys. Rev. D*, vol. 106, no. 8, p. 083 013, 2022. DOI: 10.1103/PhysRevD.106.083013. arXiv: 2208.11754 [hep-ph].

[131] A. Domi, T. Eberl, D. Hellmann, S. Krieg, and H. Päs, "Potential of neutrino telescopes to detect quantum gravity-induced decoherence in the presence of dark fermions," *JCAP*, vol. 01, p. 063, 2025. DOI: 10.1088/1475-7516/2025/01/063. arXiv: 2409.12633 [hep-ph].

[132] J. A. Wheeler, "Geons," *Phys. Rev.*, vol. 97, pp. 511–536, 1955. DOI: 10.1103/PhysRev.97.511.

[133] J. A. Wheeler, "On the Nature of quantum geometrodynamics," *Annals Phys.*, vol. 2, pp. 604–614, 1957. DOI: 10.1016/0003-4916(57)90050-7.

[134] S. Carlip, "Spacetime foam: a review," *Rept. Prog. Phys.*, vol. 86, no. 6, p. 066 001, 2023. DOI: 10.1088/1361-6633/acceb4. arXiv: 2209.14282 [gr-qc].

[135] S. W. Hawking, "Virtual black holes," *Phys. Rev. D*, vol. 53, pp. 3099–3107, 1996. DOI: 10.1103/PhysRevD.53.3099. arXiv: hep-th/9510029.

[136] S. W. Hawking, "The Unpredictability of Quantum Gravity," *Commun. Math. Phys.*, vol. 87, pp. 395–415, 1982. DOI: 10.1007/BF01206031.

[137] J. R. Ellis, J. S. Hagelin, D. V. Nanopoulos, and M. Srednicki, "Search for Violations of Quantum Mechanics," *Nucl. Phys. B*, vol. 241, J. C. Allred, Ed., p. 381, 1984. DOI: 10.1016/0550-3213(84)90053-1.

[138] P. Huet and M. E. Peskin, "Violation of CPT and quantum mechanics in the K0 - anti-K0 system," *Nucl. Phys. B*, vol. 434, pp. 3–38, 1995. DOI: 10.1016/0550-3213(94)00390-Z. arXiv: hep-ph/9403257.

[139] J. R. Ellis, N. E. Mavromatos, and D. V. Nanopoulos, "Testing quantum mechanics in the neutral kaon system," *Phys. Lett. B*, vol. 293, pp. 142–148, 1992. DOI: 10.1016/0370-2693(92)91493-S. arXiv: hep-ph/9207268.

[140] Y. Liu, J.-L. Chen, and M.-L. Ge, "A Constraint on EHNS parameters from solar neutrino problem," *J. Phys. G*, vol. 24, pp. 2289–2296, 1998. DOI: 10.1088/0954-3899/24/12/014. arXiv: hep-ph/9711381.

[141] C.-H. Chang, W.-S. Dai, X.-Q. Li, Y. Liu, F.-C. Ma, and Z.-j. Tao, "Possible effects of quantum mechanics violation induced by certain quantum gravity on neutrino oscillations," *Phys. Rev. D*, vol. 60, p. 033 006, 1999. DOI: 10.1103/PhysRevD.60.033006. arXiv: hep-ph/9809371.

[142] F. Benatti and R. Floreanini, "Open system approach to neutrino oscillations," *JHEP*, vol. 02, p. 032, 2000. DOI: 10.1088/1126-6708/2000/02/032. arXiv: hep-ph/0002221.

[143] H. V. Klapdor-Kleingrothaus, H. Pas, and U. Sarkar, "Effects of quantum space-time foam in the neutrino sector," *Eur. Phys. J. A*, vol. 8, pp. 577–580, 2000. DOI: 10.1007/s100500070080. arXiv: hep-ph/0004123.

[144] A. M. Gago, E. M. Santos, W. J. C. Teves, and R. Zukanovich Funchal, "A Study on quantum decoherence phenomena with three generations of neutrinos," Aug. 2002. arXiv: hep-ph/0208166.

[145] D. Hooper, D. Morgan, and E. Winstanley, "Probing quantum decoherence with high-energy neutrinos," *Phys. Lett. B*, vol. 609, pp. 206–211, 2005. DOI: 10.1016/j.physletb.2005.01.034. arXiv: hep-ph/0410094.

[146] E. Lisi, A. Marrone, and D. Montanino, "Probing possible decoherence effects in atmospheric neutrino oscillations," *Phys. Rev. Lett.*, vol. 85, pp. 1166–1169, 2000. DOI: 10.1103/PhysRevLett.85.1166. arXiv: hep-ph/0002053.

[147] G. L. Fogli, E. Lisi, A. Marrone, D. Montanino, and A. Palazzo, "Probing non-standard decoherence effects with solar and KamLAND neutrinos," *Phys. Rev. D*, vol. 76, p. 033 006, 2007. DOI: 10.1103/PhysRevD.76.033006. arXiv: 0704.2568 [hep-ph].

[148] G. Balieiro Gomes, M. M. Guzzo, P. C. de Holanda, and R. L. N. Oliveira, "Parameter Limits for Neutrino Oscillation with Decoherence in KamLAND," *Phys. Rev. D*, vol. 95, no. 11, p. 113 005, 2017. DOI: 10.1103/PhysRevD.95.113005. arXiv: 1603.04126 [hep-ph].

[149] J. A. B. Coelho and W. A. Mann, "Decoherence, matter effect, and neutrino hierarchy signature in long baseline experiments," *Phys. Rev. D*, vol. 96, no. 9, p. 093 009, 2017. DOI: 10.1103/PhysRevD.96.093009. arXiv: 1708.05495 [hep-ph].

[150] IceCube Collaboration, "Search for decoherence from quantum gravity with atmospheric neutrinos," *Nature Phys.*, vol. 20, no. 6, pp. 913–920, 2024. DOI: 10.1038/s41567-024-02436-w.

[151] W. Israel, "Event horizons in static vacuum space-times," *Phys. Rev.*, vol. 164, pp. 1776–1779, 1967. DOI: 10.1103/PhysRev.164.1776.

[152] S. W. Hawking, "Particle Creation by Black Holes," *Commun. Math. Phys.*, vol. 43, G. W. Gibbons and S. W. Hawking, Eds., pp. 199–220, 1975, [Erratum: Commun. Math. Phys. 46, 206 (1976)]. DOI: 10.1007/BF02345020.

[153] D. N. Page, "Particle Transmutations in Quantum Gravity," *Phys. Lett. B*, vol. 95, pp. 244–246, 1980. DOI: 10.1016/0370-2693(80)90479-7.

[154] L. A. Anchordoqui, "Spacetime foam at a TeV," *J. Phys. Conf. Ser.*, vol. 60, F. Halzen, A. Karle, and T. Montaruli, Eds., pp. 191–194, 2007. DOI: 10.1088/1742-6596/60/1/039. arXiv: hep-ph/0610025.

[155] E. Witten, "Symmetry and Emergence," *Nature Phys.*, vol. 14, no. 2, pp. 116–119, 2018. DOI: 10.1038/nphys4348. arXiv: 1710.01791 [hep-th].

[156] D. Harlow and H. Ooguri, "Constraints on Symmetries from Holography," *Phys. Rev. Lett.*, vol. 122, no. 19, p. 191 601, 2019. DOI: 10.1103/PhysRevLett.122.191601. arXiv: 1810.05337 [hep-th].

[157] IceCube Collaboration, "Replication Data for: Searching for Decoherence from Quantum Gravity at the IceCube South Pole Neutrino Observatory," version V1, 2024. DOI: 10.7910/DVN/9WGYQN. [Online]. Available: https://doi.org/10.7910/DVN/9WGYQN.

[158] S. Antusch, C. Biggio, E. Fernandez-Martinez, M. B. Gavela, and J. Lopez-Pavon, "Unitarity of the Leptonic Mixing Matrix," *JHEP*, vol. 10, p. 084, 2006. DOI: 10.1088/1126-6708/2006/10/084. arXiv: hep-ph/0607020.

[159] S. Antusch and O. Fischer, "Non-unitarity of the leptonic mixing matrix: Present bounds and future sensitivities," *JHEP*, vol. 10, p. 094, 2014. DOI: 10.1007/JHEP10(2014)094. arXiv: 1407.6607 [hep-ph].

[160] L. A. Anchordoqui *et al.*, "Probing Planck scale physics with IceCube," *Phys. Rev. D*, vol. 72, p. 065 019, 2005. DOI: 10.1103/PhysRevD.72.065019. arXiv: hep-ph/0506168.

[161] Y. Farzan, T. Schwetz, and A. Y. Smirnov, "Reconciling results of LSND, MiniBooNE and other experiments with soft decoherence," *JHEP*, vol. 07, p. 067, 2008. DOI: 10.1088/1126-6708/2008/07/067. arXiv: 0805.2098 [hep-ph].

[162] J. C. Carrasco, F. N. Díaz, and A. M. Gago, "Probing CPT breaking induced by quantum decoherence at DUNE," *Phys. Rev. D*, vol. 99, no. 7, p. 075 022, 2019. DOI: 10.1103/PhysRevD.99.075022. arXiv: 1811.04982 [hep-ph].

[163] T. Stuttard and M. Jensen, "Neutrino decoherence from quantum gravitational stochastic perturbations," *Phys. Rev. D*, vol. 102, no. 11, p. 115 003, 2020. DOI: 10.1103/PhysRevD.102.115003. arXiv: 2007.00068 [hep-ph].

[164] V. De Romeri, C. Giunti, T. Stuttard, and C. A. Ternes, "Neutrino oscillation bounds on quantum decoherence," *JHEP*, vol. 09, p. 097, 2023. DOI: 10.1007/JHEP09(2023)097. arXiv: 2306.14699 [hep-ph].

[165] P. Coloma, J. Lopez-Pavon, I. Martinez-Soler, and H. Nunokawa, "Decoherence in Neutrino Propagation Through Matter, and Bounds from IceCube/DeepCore," *Eur. Phys. J. C*, vol. 78, no. 8, p. 614, 2018. DOI: 10.1140/epjc/s10052-018-6092-6. arXiv: 1803.04438 [hep-ph].

[166] A. L. G. Gomes, R. A. Gomes, and O. L. G. Peres, "Quantum decoherence and relaxation in long-baseline neutrino data," *JHEP*, vol. 10, p. 035, 2023. DOI: 10.1007/JHEP10(2023)035. arXiv: 2001.09250 [hep-ph].

[167] I. Esteban, M. C. Gonzalez-Garcia, M. Maltoni, T. Schwetz, and A. Zhou, "The fate of hints: updated global analysis of three-flavor neutrino oscillations," *JHEP*, vol. 09, p. 178, 2020. DOI: 10.1007/JHEP09(2020)178. arXiv: 2007.14792 [hep-ph].

[168] J. Kersten and A. Y. Smirnov, "Decoherence and oscillations of supernova neutrinos," *Eur. Phys. J. C*, vol. 76, no. 6, p. 339, 2016. DOI: 10.1140/epjc/s10052-016-4187-5. arXiv: 1512.09068 [hep-ph].

[169] M. Agostini *et al.*, "The Pacific Ocean Neutrino Experiment," *Nature Astron.*, vol. 4, no. 10, pp. 913–915, 2020. DOI: 10.1038/s41550-020-1182-4. arXiv: 2005.09493 [astro-ph.HE].

[170] M. G. Aartsen *et al.*, "First observation of PeV-energy neutrinos with IceCube," *Phys. Rev. Lett.*, vol. 111, p. 021 103, 2013. DOI: 10.1103/PhysRevLett.111.021103. arXiv: 1304.5356 [astro-ph.HE].

[171] M. G. Aartsen *et al.*, "Evidence for High-Energy Extraterrestrial Neutrinos at the IceCube Detector," *Science*, vol. 342, p. 1 242 856, 2013. DOI: 10.1126/science.1242856. arXiv: 1311.5238 [astro-ph.HE].

[172] M. G. Aartsen *et al.*, "Observation of High-Energy Astrophysical Neutrinos in Three Years of IceCube Data," *Phys. Rev. Lett.*, vol. 113, p. 101 101, 2014. DOI: 10.1103/PhysRevLett.113.101101. arXiv: 1405.5303 [astro-ph.HE].

[173] M. G. Aartsen *et al.*, "Flavor Ratio of Astrophysical Neutrinos above 35 TeV in IceCube," *Phys. Rev. Lett.*, vol. 114, no. 17, p. 171 102, 2015. DOI: 10.1103/PhysRevLett.114.171102. arXiv: 1502.03376 [astro-ph.HE].

[174] M. G. Aartsen *et al.*, "Characteristics of the diffuse astrophysical electron and tau neutrino flux with six years of IceCube high energy cascade data," *Phys. Rev. Lett.*, vol. 125, no. 12, p. 121 104, 2020. DOI: 10.1103/PhysRevLett.125.121104. arXiv: 2001.09520 [astro-ph.HE].

[175] S. Pakvasa, W. Rodejohann, and T. J. Weiler, "Flavor Ratios of Astrophysical Neutrinos: Implications for Precision Measurements," *JHEP*, vol. 02, p. 005, 2008. DOI: 10.1088/1126-6708/2008/02/005. arXiv: 0711.4517 [hep-ph].

[176] L. A. Anchordoqui, H. Goldberg, F. Halzen, and T. J. Weiler, "Galactic point sources of TeV antineutrinos," *Phys. Lett. B*, vol. 593, p. 42, 2004. DOI: 10.1016/j.physletb.2004.04.054. arXiv: astro-ph/0311002.

[177] J. R. Ellis, N. E. Mavromatos, D. V. Nanopoulos, and E. Winstanley, "Quantum decoherence in a four-dimensional black hole background," *Mod. Phys. Lett. A*, vol. 12, pp. 243–256, 1997. DOI: 10.1142/S0217732397000248. arXiv: gr-qc/9602011.

[178] J. R. Ellis, N. E. Mavromatos, and D. V. Nanopoulos, "Quantum decoherence in a D foam background," *Mod. Phys. Lett. A*, vol. 12, pp. 1759–1773, 1997. DOI: 10.1142/S0217732397001795. arXiv: hep-th/9704169.

[179] F. Benatti and R. Floreanini, "Non-standard Neutral Kaon Dynamics from Infinite Statistics," *Annals Phys.*, vol. 273, pp. 58–71, 1999. DOI: 10.1006/aphy.1998.5896. arXiv: hep-th/9811196.

[180] R. Abbasi *et al.*, "Detection of astrophysical tau neutrino candidates in IceCube," *Eur. Phys. J. C*, vol. 82, no. 11, p. 1031, 2022. DOI: 10.1140/epjc/s10052-022-10795-y. arXiv: 2011.03561 [hep-ex].

[181] IceCube Collaboration, "Evidence for neutrino emission from the nearby active galaxy NGC 1068," *Science*, vol. 378, no. 6619, pp. 538–543, Nov. 2022, ISSN: 1095-9203. DOI: 10.1126/science.abg3395. [Online]. Available: http://dx.doi.org/10.1126/science.abg3395.

[182] I. Collaboration, *Nuflux: A library for calculating atmospheric neutrino fluxes*, version 2.0.7, Jul. 3, 2024. DOI: 10.5281/zenodo.5874708. [Online]. Available: https://doi.org/10.5281/zenodo.5874708.

[183] IceCube Collaboration, "Characteristics of the diffuse astrophysical electron and tau neutrino flux with six years of IceCube high energy cascade data," *Phys. Rev. Lett.*, vol. 125, no. 12, p. 121 104, 2020. DOI: 10.1103/PhysRevLett.125.121104. arXiv: 2001.09520 [astro-ph.HE].

[184] IceCube Collaboration, "Searching for eV-scale sterile neutrinos with eight years of atmospheric neutrinos at the IceCube Neutrino Telescope," *Phys. Rev. D*, vol. 102, no. 5, p. 052 009, 2020. DOI: 10.1103/PhysRevD.102.052009. arXiv: 2005.12943 [hep-ex].

[185] C. A. Argüelles, A. Schneider, and T. Yuan, "A binned likelihood for stochastic models," *JHEP*, vol. 06, p. 030, 2019. DOI: 10.1007/JHEP06(2019)030. arXiv: 1901.04645 [physics.data-an].

[186] B. Dasgupta and J. Kopp, "Sterile Neutrinos," *Phys. Rept.*, vol. 928, pp. 1–63, 2021. DOI: 10.1016/j.physrep.2021.06.002. arXiv: 2106.05913 [hep-ph].

[187] L. Roszkowski, E. M. Sessolo, and S. Trojanowski, "WIMP dark matter candidates and searches—current status and future prospects," *Rept. Prog. Phys.*, vol. 81, no. 6, p. 066 201, 2018. DOI: 10.1088/1361-6633/aab913. arXiv: 1707.06277 [hep-ph].

[188] S. Westhoff, "FIMP Dark Matter at the LHC," *PoS*, vol. LHCP2023, p. 221, 2024. DOI: 10.22323/1.450.0221. arXiv: 2312.13373 [hep-ph].

[189] D. Hellmann, S. Krieg, H. Päs, and M. Tabet, "Neutrino oscillations as a gravitational wave detector?" *JCAP*, vol. 05, p. 075, 2025. DOI: 10.1088/1475-7516/2025/05/075. arXiv: 2405.05000 [hep-ph].

[190] P. Mészáros, D. B. Fox, C. Hanna, and K. Murase, "Multi-Messenger Astrophysics," *Nature Rev. Phys.*, vol. 1, pp. 585–599, 2019. DOI: 10.1038/s42254-019-0101-z. arXiv: 1906.10212 [astro-ph.HE].

[191] L. Stodolsky, "Matter and Light Wave Interferometry in Gravitational Fields," *Gen. Rel. Grav.*, vol. 11, pp. 391–405, 1979. DOI: 10.1007/BF00759302.

[192] C. Y. Cardall and G. M. Fuller, "Neutrino oscillations in curved space-time: An Heuristic treatment," *Phys. Rev. D*, vol. 55, pp. 7960–7966, 1997. DOI: 10.1103/PhysRevD.55.7960. arXiv: hep-ph/9610494.

[193] N. Fornengo, C. Giunti, C. W. Kim, and J. Song, "Gravitational effects on the neutrino oscillation," *Phys. Rev. D*, vol. 56, pp. 1895–1902, 1997. DOI: 10.1103/PhysRevD.56.1895. arXiv: hep-ph/9611231.

[194] N. Fornengo, C. Giunti, C. W. Kim, and J. Song, "Gravitational effects on the neutrino oscillation in vacuum," *Nucl. Phys. B Proc. Suppl.*, vol. 70, A. Bottino, A. Di Credico, and P. Monacelli, Eds., pp. 264–266, 1999. DOI: 10.1016/S0920-5632(98)00435-6. arXiv: hep-ph/9711494.

[195] K. Konno and M. Kasai, "General relativistic effects of gravity in quantum mechanics: A Case of ultrarelativistic, spin 1/2 particles," *Prog. Theor. Phys.*, vol. 100, pp. 1145–1157, 1998. DOI: 10.1143/PTP.100.1145. arXiv: gr-qc/0603035.

[196] M. Alimohammadi and A. Shariati, "Neutrino oscillation in a space-time with torsion," *Mod. Phys. Lett. A*, vol. 14, pp. 267–274, 1999. DOI: 10.1142/S0217732399000316. arXiv: gr-qc/9808066.

[197] T. Bhattacharya, S. Habib, and E. Mottola, "Gravitationally induced neutrino oscillation phases in static space-times," *Phys. Rev. D*, vol. 59, p. 067 301, 1999. DOI: 10.1103/PhysRevD.59.067301.

[198] H. Maiwa and S. Naka, "Neutrino oscillations in gravitational fields," Jan. 2004. arXiv: hep-ph/0401143.

[199] M. Gozdz and M. Rogatko, "Neutrino oscillations in strong gravitational fields," *Int. J. Mod. Phys. E*, vol. 20, A. Baran, K. Pomorski, J. Bartel, and M. Gozdz, Eds., pp. 507–513, 2011. DOI: 10.1142/S0218301311017922. arXiv: 1201.1249 [hep-ph].

[200] A. Chatelain and M. C. Volpe, "Neutrino decoherence in presence of strong gravitational fields," *Phys. Lett. B*, vol. 801, p. 135 150, 2020. DOI: 10.1016/j.physletb.2019.135150. arXiv: 1906.12152 [hep-ph].

[201] G. G. Luciano, "Inertial effects on neutrino oscillations and decoherence: A wave packet approach," *Phys. Lett. B*, vol. 823, p. 136 772, 2021. DOI: 10.1016/j.physletb.2021.136772.

[202] A. Capolupo, G. Lambiase, and A. Quaranta, "Neutrinos in curved spacetime: Particle mixing and flavor oscillations," *Phys. Rev. D*, vol. 101, no. 9, p. 095 022, 2020. DOI: 10.1103/PhysRevD.101.095022. arXiv: 2003.00516 [hep-th].

[203] A. Capolupo, A. Quaranta, and R. Serao, "Field Mixing in Curved Spacetime and Dark Matter," *Symmetry*, vol. 15, no. 4, p. 807, 2023. DOI: 10.3390/sym15040807.

[204] S. W. Hawking, "Black hole explosions," *Nature*, vol. 248, pp. 30–31, 1974. DOI: 10.1038/248030a0.

[205] B. S. DeWitt, "QUANTUM GRAVITY: THE NEW SYNTHESIS," in *General Relativity: An Einstein Centenary Survey*. 1980, pp. 680–745.

[206] B. S. DeWitt, "Quantum Field Theory in Curved Space-Time," *Phys. Rept.*, vol. 19, pp. 295–357, 1975. DOI: 10.1016/0370-1573(75)90051-4.

[207] M. D. Raschke, "Neutrinooszillationen im Gravitationsfeld," Contact dekanat.physik@tu-dortmund.de to gain access to this thesis., Bachelor's Thesis, 2023.

[208] B. P. Abbott *et al.*, "Observation of Gravitational Waves from a Binary Black Hole Merger," *Phys. Rev. Lett.*, vol. 116, no. 6, p. 061 102, 2016. DOI: 10.1103/PhysRevLett.116.061102. arXiv: 1602.03837 [gr-qc].

[209] B. P. Abbott *et al.*, "GWTC-1: A Gravitational-Wave Transient Catalog of Compact Binary Mergers Observed by LIGO and Virgo during the First and Second Observing Runs," *Phys. Rev. X*, vol. 9, no. 3, p. 031 040, 2019. DOI: 10.1103/PhysRevX.9.031040. arXiv: 1811.12907 [astro-ph.HE].

[210] B. P. Abbott *et al.*, "GW170817: Observation of Gravitational Waves from a Binary Neutron Star Inspiral," *Phys. Rev. Lett.*, vol. 119, no. 16, p. 161 101, 2017. DOI: 10.1103/PhysRevLett.119.161101. arXiv: 1710.05832 [gr-qc].

[211] J. Casalderrey-Solana, D. Mateos, and M. Sanchez-Garitaonandia, "Mega-Hertz Gravitational Waves from Neutron Star Mergers," Oct. 2022. arXiv: 2210.03171 [hep-th].

[212] M. Sasaki, T. Suyama, T. Tanaka, and S. Yokoyama, "Primordial Black Hole Scenario for the Gravitational-Wave Event GW150914," *Phys. Rev. Lett.*, vol. 117, no. 6, p. 061 101, 2016, [Erratum: Phys.Rev.Lett. 121, 059901 (2018)]. DOI: 10.1103/PhysRevLett.117.061101. arXiv: 1603.08338 [astro-ph.CO].

[213] Y. Eroshenko and V. Stasenko, "Gravitational Waves from the Merger of Two Primordial Black Hole Clusters," *Symmetry*, vol. 15, no. 3, p. 637, 2023. DOI: 10.3390/sym15030637. arXiv: 2302.05167 [astro-ph.CO].

[214] S. Rahvar, "Primordial black hole collision with neutron stars and astrophysical black holes and the observational signatures," *Int. J. Mod. Phys. D*, vol. 32, no. 16, p. 2 350 103, 2023. DOI: 10.1142/S0218271823501031. arXiv: 2304.00348 [gr-qc].

[215] E. Bagui *et al.*, "Primordial black holes and their gravitational-wave signatures," *Living Rev. Rel.*, vol. 28, no. 1, p. 1, 2025. DOI: 10.1007/s41114-024-00053-w. arXiv: 2310.19857 [astro-ph.CO].

[216] P. Auclair *et al.*, "Probing the gravitational wave background from cosmic strings with LISA," *JCAP*, vol. 04, p. 034, 2020. DOI: 10.1088/1475-7516/2020/04/034. arXiv: 1909.00819 [astro-ph.CO].

[217] A. Eichhorn, R. R. Lino dos Santos, and J. L. Miqueleto, "From quantum gravity to gravitational waves through cosmic strings," *Phys. Rev. D*, vol. 109, no. 2, p. 026 013, 2024. DOI: 10.1103/PhysRevD.109.026013. arXiv: 2306.17718 [gr-qc].

[218] M. C. Guzzetti, N. Bartolo, M. Liguori, and S. Matarrese, "Gravitational waves from inflation," *Riv. Nuovo Cim.*, vol. 39, no. 9, pp. 399–495, 2016. DOI: 10.1393/ncr/i2016-10127-1. arXiv: 1605.01615 [astro-ph.CO].

[219] G. Agazie *et al.*, "The NANOGrav 15 yr Data Set: Evidence for a Gravitational-wave Background," *Astrophys. J. Lett.*, vol. 951, no. 1, p. L8, 2023. DOI: 10.3847/2041-8213/acdac6. arXiv: 2306.16213 [astro-ph.HE].

[220] M. Dvornikov, "Neutrino flavor oscillations in stochastic gravitational waves," *Phys. Rev. D*, vol. 100, no. 9, p. 096 014, 2019. DOI: 10.1103/PhysRevD.100.096014. arXiv: 1906.06167 [hep-ph].

[221] G. Koutsoumbas and D. Metaxas, "Neutrino oscillations in gravitational and cosmological backgrounds," *Gen. Rel. Grav.*, vol. 52, no. 10, p. 102, 2020. DOI: 10.1007/s10714-020-02758-z. arXiv: 1909.02735 [hep-ph].

[222] M. Dvornikov, "Neutrino oscillations in gravitational waves," *J. Phys. Conf. Ser.*, vol. 1435, no. 1, p. 012 005, 2020. DOI: 10.1088/1742-6596/1435/1/012005. arXiv: 1910.01415 [hep-ph].

[223] M. Dvornikov, "Flavor ratios of astrophysical neutrinos interacting with stochastic gravitational waves having arbitrary spectra," *JCAP*, vol. 12, p. 022, 2020. DOI: 10.1088/1475-7516/2020/12/022. arXiv: 2009.02195 [astro-ph.HE].

[224] M. Dvornikov, "Interaction of supernova neutrinos with stochastic gravitational waves," *Phys. Rev. D*, vol. 104, no. 4, p. 043 018, 2021. DOI: 10.1103/PhysRevD.104.043018. arXiv: 2103.15464 [hep-ph].

[225] M. Dvornikov, "Neutrino Oscillations in Gravitational Fields and Astrophysical Applications," *Moscow Univ. Phys. Bull.*, vol. 77, no. 2, pp. 439–441, 2022. DOI: 10.3103/S002713492202031X. arXiv: 2207.03937 [hep-ph].

[226] G. Lambiase, L. Mastrototaro, and L. Visinelli, "Gravitational waves and neutrino oscillations in Chern-Simons axion gravity," *JCAP*, vol. 01, p. 011, 2023. DOI: 10.1088/1475-7516/2023/01/011. arXiv: 2207.08067 [hep-ph].

[227] G. Lambiase, L. Mastrototaro, and L. Visinelli, "Astrophysical neutrino oscillations after pulsar timing array analyses," *Phys. Rev. D*, vol. 108, no. 12, p. 123 028, 2023. DOI: 10.1103/PhysRevD.108.123028. arXiv: 2306.16977 [astro-ph.HE].

[228] A. Domi *et al.*, "Understanding gravitationally induced decoherence parameters in neutrino oscillations using a microscopic quantum mechanical model," *JCAP*, vol. 11, p. 006, 2024. DOI: 10.1088/1475-7516/2024/11/006. arXiv: 2403.03106 [gr-qc].

[229] A. Abusleme *et al.*, "Calibration Strategy of the JUNO Experiment," *JHEP*, vol. 03, p. 004, 2021. DOI: 10.1007/JHEP03(2021)004. arXiv: 2011.06405 [physics.ins-det].

[230] C. J. Moore, R. H. Cole, and C. P. L. Berry, "Gravitational-wave sensitivity curves," *Class. Quant. Grav.*, vol. 32, no. 1, p. 015 014, 2015. DOI: 10.1088/0264-9381/32/1/015014. arXiv: 1408.0740 [gr-qc].

[231] K. Hirata *et al.*, "Observation of a Neutrino Burst from the Supernova SN 1987a," *Phys. Rev. Lett.*, vol. 58, K. C. Wali, Ed., pp. 1490–1493, 1987. DOI: 10.1103/PhysRevLett.58.1490.

[232] R. M. Bionta *et al.*, "Observation of a Neutrino Burst in Coincidence with Supernova SN 1987a in the Large Magellanic Cloud," *Phys. Rev. Lett.*, vol. 58, p. 1494, 1987. DOI: 10.1103/PhysRevLett.58.1494.

[233] H. Duan, G. M. Fuller, and Y.-Z. Qian, "Collective neutrino flavor transformation in supernovae," *Phys. Rev. D*, vol. 74, p. 123 004, 2006. DOI: 10.1103/PhysRevD.74.123004. arXiv: astro-ph/0511275.

[234] H. Duan, G. M. Fuller, J. Carlson, and Y.-Z. Qian, "Simulation of Coherent Non-Linear Neutrino Flavor Transformation in the Supernova Environment. 1. Correlated Neutrino Trajectories," *Phys. Rev. D*, vol. 74, p. 105 014, 2006. DOI: 10.1103/PhysRevD.74.105014. arXiv: astro-ph/0606616.

[235] H. Duan, G. M. Fuller, J. Carlson, and Y.-Z. Qian, "Coherent Development of Neutrino Flavor in the Supernova Environment," *Phys. Rev. Lett.*, vol. 97, p. 241 101, 2006. DOI: 10.1103/PhysRevLett.97.241101. arXiv: astro-ph/0608050.

[236] S. Hannestad, G. G. Raffelt, G. Sigl, and Y. Y. Y. Wong, "Self-induced conversion in dense neutrino gases: Pendulum in flavour space," *Phys. Rev. D*, vol. 74, p. 105 010, 2006, [Erratum: Phys.Rev.D 76, 029901 (2007)]. DOI: 10.1103/PhysRevD.74.105010. arXiv: astro-ph/0608695.

[237] G. L. Fogli, E. Lisi, A. Marrone, and A. Mirizzi, "Collective neutrino flavor transitions in supernovae and the role of trajectory averaging," *JCAP*, vol. 12, p. 010, 2007. DOI: 10.1088/1475-7516/2007/12/010. arXiv: 0707.1998 [hep-ph].

[238] H. Duan, G. M. Fuller, J. Carlson, and Y.-Z. Qian, "Analysis of Collective Neutrino Flavor Transformation in Supernovae," *Phys. Rev. D*, vol. 75, p. 125 005, 2007. DOI: 10.1103/PhysRevD.75.125005. arXiv: astro-ph/0703776.

[239] A. Mirizzi *et al.*, "Supernova Neutrinos: Production, Oscillations and Detection," *Riv. Nuovo Cim.*, vol. 39, no. 1-2, pp. 1–112, 2016. DOI: 10.1393/ncr/i2016-10120-8. arXiv: 1508.00785 [astro-ph.HE].

[240] D. Eichler, "Neutrinos from Binary Pulsars," *Nature*, vol. 275, pp. 725–726, 1978. DOI: 10.1038/275725b0.

[241] T. K. Gaisser, F. Halzen, and T. Stanev, "Particle astrophysics with high-energy neutrinos," *Phys. Rept.*, vol. 258, pp. 173–236, 1995, [Erratum: Phys.Rept. 271, 355–356 (1996)]. DOI: 10.1016/0370-1573(95)00003-Y. arXiv: hep-ph/9410384.

[242] R. J. Protheroe, W. Bednarek, and Q. Luo, "Gamma-rays and neutrinos from very young supernova remnants," *Astropart. Phys.*, vol. 9, pp. 1–14, 1998. DOI: 10.1016/S0927-6505(98)00014-0. arXiv: astro-ph/9703045.

[243] B. Link and F. Burgio, "TeV mu neutrinos from young neutron stars," *Phys. Rev. Lett.*, vol. 94, p. 181 101, 2005. DOI: 10.1103/PhysRevLett.94.181101. arXiv: astro-ph/0412520.

[244] B. Link and F. Burgio, "Flux predictions of high-energy neutrinos from pulsars," *Mon. Not. Roy. Astron. Soc.*, vol. 371, pp. 375–379, 2006. DOI: 10.1111/j.1365-2966.2006.10665.x. arXiv: astro-ph/0604379.

[245] A. Bhadra and R. K. Dey, "TeV neutrinos and gamma rays from pulsars," *Mon. Not. Roy. Astron. Soc.*, vol. 395, p. 1371, 2009. DOI: 10.1111/j.1365-2966.2008.14345.x. arXiv: 0812.1845 [astro-ph].

[246] Z.-X. Li, G.-F. Lin, and W.-W. Na, "Diffuse emission of TeV Neutrinos and Gamma-rays from young pulsars by Photo-meson interaction in the galaxy," *Res. Astron. Astrophys.*, vol. 13, p. 1097, 2013. DOI: 10.1088/1674-4527/13/9/008. arXiv: 1304.3895 [astro-ph.HE].

[247] F. W. Stecker, "Diffuse Fluxes of Cosmic High-Energy Neutrinos," *Astrophys. J.*, vol. 228, pp. 919–927, 1979. DOI: 10.1086/156919.

[248] V. S. Berezinsky, T. K. Gaisser, F. Halzen, and T. Stanev, "Diffuse radiation from cosmic ray interactions in the galaxy," *Astropart. Phys.*, vol. 1, pp. 281–288, 1993. DOI: 10.1016/0927-6505(93)90014-5.

[249] F. W. Stecker, C. Done, M. H. Salamon, and P. Sommers, "High-energy neutrinos from active galactic nuclei," *Phys. Rev. Lett.*, vol. 66, pp. 2697–2700, 1991, [Erratum: Phys.Rev.Lett. 69, 2738 (1992)]. DOI: 10.1103/PhysRevLett.66.2697.

[250] P. Meszaros and E. Waxman, "TeV neutrinos from successful and choked gamma-ray bursts," *Phys. Rev. Lett.*, vol. 87, p. 171 102, 2001. DOI: 10.1103/PhysRevLett.87.171102. arXiv: astro-ph/0103275.

[251] A. Loeb and E. Waxman, "The Cumulative background of high energy neutrinos from starburst galaxies," *JCAP*, vol. 05, p. 003, 2006. DOI: 10.1088/1475-7516/2006/05/003. arXiv: astro-ph/0601695.

[252] F. Oikonomou, K. Murase, P. Padovani, E. Resconi, and P. Mészáros, "High energy neutrino flux from individual blazar flares," *Mon. Not. Roy. Astron. Soc.*, vol. 489, no. 3, pp. 4347–4366, 2019. DOI: 10.1093/mnras/stz2246. arXiv: 1906.05302 [astro-ph.HE].

[253] F. Oikonomou, "High-energy neutrino emission from blazars," *PoS*, vol. ICRC2021, p. 030, 2022. DOI: 10.22323/1.395.0030. arXiv: 2201.05623 [astro-ph.HE].

[254] M. Boettcher, M. Fu, T. Govenor, Q. King, and P. Roustazadeh, "Multiwavelength and Multimessenger Observations of Blazars and Theoretical Modeling: Blazars as Astrophysical Neutrino Sources," *Acta Phys. Polon. Supp.*, vol. 15, no. 3, p. 8, 2022. DOI: 10.5506/APhysPolBSupp.15.3-A8. arXiv: 2204.12242 [astro-ph.HE].

[255] S. Paiano, R. Falomo, A. Treves, and R. Scarpa, "The redshift of the BL Lac object TXS 0506+056," *Astrophys. J. Lett.*, vol. 854, no. 2, p. L32, 2018. DOI: 10.3847/2041-8213/aaad5e. arXiv: 1802.01939 [astro-ph.GA].

[256] M. G. Aartsen *et al.*, "Neutrino emission from the direction of the blazar TXS 0506+056 prior to the IceCube-170922A alert," *Science*, vol. 361, no. 6398, pp. 147–151, 2018. DOI: 10.1126/science.aat2890. arXiv: 1807.08794 [astro-ph.HE].

[257] G. G. Pavlov, D. Sanwal, and M. A. Teter, "Central compact objects in supernova remnants," *IAU Symp.*, vol. 218, p. 239, 2004. arXiv: astro-ph/0311526.

[258] R. Lin, M. H. van Kerkwijk, F. Kirsten, U.-L. Pen, and A. T. Deller, "The Radio Parallax of the Crab Pulsar: A First VLBI Measurement Calibrated with Giant Pulses," *Astrophys. J.*, vol. 952, no. 2, p. 161, 2023. DOI: 10.3847/1538-4357/acdc98. arXiv: 2306.01617 [astro-ph.HE].

[259] P. A. Caraveo, A. De Luca, R. P. Mignani, and G. F. Bignami, "The distance to the vela pulsar gauged with hst parallax oservations," *Astrophys. J.*, vol. 561, p. 930, 2001. DOI: 10.1086/323377. arXiv: astro-ph/0107282.

[260] C. Guépin, B. Cerutti, and K. Kotera, "Proton acceleration in pulsar magnetospheres," *Astron. Astrophys.*, vol. 635, A138, 2020. DOI: 10.1051/0004-6361/201936816. arXiv: 1910.11387 [astro-ph.HE].

[261] R. Abbasi *et al.*, "Evidence for neutrino emission from the nearby active galaxy NGC 1068," *Science*, vol. 378, no. 6619, pp. 538–543, 2022. DOI: 10.1126/science.abg3395. arXiv: 2211.09972 [astro-ph.HE].

[262] T. Namikawa, S. Saga, D. Yamauchi, and A. Taruya, "CMB Constraints on the Stochastic Gravitational-Wave Background at Mpc scales," *Phys. Rev. D*, vol. 100, no. 2, p. 021 303, 2019. DOI: 10.1103/PhysRevD.100.021303. arXiv: 1904.02115 [astro-ph.CO].

[263] B. J. P. Jones, "Dynamical pion collapse and the coherence of conventional neutrino beams," *Phys. Rev. D*, vol. 91, no. 5, p. 053 002, 2015. DOI: 10.1103/PhysRevD.91.053002. arXiv: 1412.2264 [hep-ph].

[264] K. M. Groth and M. Ahlers, "Deciphering the Sources of Cosmic Neutrinos," Mar. 2025. arXiv: 2503.07718 [astro-ph.HE].

[265] A. Sicilia *et al.*, "The Black Hole Mass Function Across Cosmic Times. I. Stellar Black Holes and Light Seed Distribution," *Astrophys. J.*, vol. 924, no. 2, p. 56, 2022. DOI: 10.3847/1538-4357/ac34fb. arXiv: 2110.15607 [astro-ph.GA].

[266] M. Abdul Karim *et al.*, "DESI DR2 Results I: Baryon Acoustic Oscillations from the Lyman Alpha Forest," Mar. 2025. arXiv: 2503.14739 [astro-ph.CO].

[267] M. Abdul Karim *et al.*, "DESI DR2 Results II: Measurements of Baryon Acoustic Oscillations and Cosmological Constraints," Mar. 2025. arXiv: 2503.14738 [astro-ph.CO].

[268] W. Elbers *et al.*, "Constraints on Neutrino Physics from DESI DR2 BAO and DR1 Full Shape," Mar. 2025. arXiv: 2503.14744 [astro-ph.CO].

[269] L. Feng, J.-F. Zhang, and X. Zhang, "Searching for sterile neutrinos in dynamical dark energy cosmologies," *Sci. China Phys. Mech. Astron.*, vol. 61, no. 5, p. 050 411, 2018. DOI: 10.1007/s11433-017-9150-3. arXiv: 1706.06913 [astro-ph.CO].

[270] G.-H. Du *et al.*, "Cosmological search for sterile neutrinos after DESI 2024," Jan. 2025. arXiv: 2501.10785 [astro-ph.CO].

[271] C. Weinheimer, "KATRIN, a next generation tritium beta decay experiment in search for the absolute neutrino mass scale," *Prog. Part. Nucl. Phys.*, vol. 48, A. Faessler, Ed., pp. 141–150, 2002. DOI: 10.1016/S0146-6410(02)00120-5.

[272] M. Aker *et al.*, "Direct neutrino-mass measurement based on 259 days of KATRIN data," Jun. 2024. arXiv: 2406.13516 [nucl-ex].

[273] M. G. Betti *et al.*, "Neutrino physics with the PTOLEMY project: active neutrino properties and the light sterile case," *JCAP*, vol. 07, p. 047, 2019. DOI: 10.1088/1475-7516/2019/07/047. arXiv: 1902.05508 [astro-ph.CO].

[274] C. G. Tully and G. Zhang, "Multi-messenger astrophysics with the cosmic neutrino background," *JCAP*, vol. 06, p. 053, 2021. DOI: 10.1088/1475-7516/2021/06/053. arXiv: 2103.01274 [astro-ph.CO].

[275] S. Aiello *et al.*, "Observation of an ultra-high-energy cosmic neutrino with KM3NeT," *Nature*, vol. 638, no. 8050, pp. 376–382, 2025, [Erratum: Nature 640, E3 (2025)]. DOI: 10.1038/s41586-024-08543-1.

[276] H. Abreu *et al.*, "First Direct Observation of Collider Neutrinos with FASER at the LHC," *Phys. Rev. Lett.*, vol. 131, no. 3, p. 031 801, 2023. DOI: 10.1103/PhysRevLett.131.031801. arXiv: 2303.14185 [hep-ex].

[277] F. Kling, "Neutrino Physics at the LHC: Status and Prospects," in *29th International Symposium on Particles, String and Cosmology*, Jan. 2025. arXiv: 2501.07152 [hep-ph].

[278] R. Albanese *et al.*, "Observation of Collider Muon Neutrinos with the SND@LHC Experiment," *Phys. Rev. Lett.*, vol. 131, no. 3, p. 031 802, 2023. DOI: 10.1103/PhysRevLett.131.031802. arXiv: 2305.09383 [hep-ex].

[279] J. A. Formaggio and G. P. Zeller, "From eV to EeV: Neutrino Cross Sections Across Energy Scales," *Rev. Mod. Phys.*, vol. 84, pp. 1307–1341, 2012. DOI: 10.1103/RevModPhys.84.1307. arXiv: 1305.7513 [hep-ex].

[280] R. Gandhi, C. Quigg, M. H. Reno, and I. Sarcevic, "Neutrino interactions at ultrahigh-energies," *Phys. Rev. D*, vol. 58, p. 093 009, 1998. DOI: 10.1103/PhysRevD.58.093009. arXiv: hep-ph/9807264.

[281] B. Zhou and J. F. Beacom, "W-boson and trident production in TeV–PeV neutrino observatories," *Phys. Rev. D*, vol. 101, no. 3, p. 036 010, 2020. DOI: 10.1103/PhysRevD.101.036010. arXiv: 1910.10720 [hep-ph].

[282] B. Zhou and J. F. Beacom, "Neutrino-nucleus cross sections for W-boson and trident production," *Phys. Rev. D*, vol. 101, no. 3, p. 036 011, 2020. DOI: 10.1103/PhysRevD.101.036011. arXiv: 1910.08090 [hep-ph].

[283] A. Cooper-Sarkar, P. Mertsch, and S. Sarkar, "The high energy neutrino cross-section in the Standard Model and its uncertainty," *JHEP*, vol. 08, p. 042, 2011. DOI: 10.1007/JHEP08(2011)042. arXiv: 1106.3723 [hep-ph].

[284] S. I. Dutta, M. H. Reno, and I. Sarcevic, "Tau neutrinos underground: Signals of muon-neutrino —> tau neutrino oscillations with extragalactic neutrinos," *Phys. Rev. D*, vol. 62, p. 123 001, 2000. DOI: 10.1103/PhysRevD.62.123001. arXiv: hep-ph/0005310.

[285] M. Galassi and et al., *GNU Scientific Library Reference Manual*. Network Theory Ltd., 2009, ISBN: 978-0954612078.

[286] M. Steffen, "A simple method for monotonic interpolation in one dimension.," *Astronomy and Astrophysics*, vol. 239, pp. 443–450, 1990. [Online]. Available: https://api.semanticscholar.org/CorpusID:116703131.

[287] A. D. Dolgov, S. H. Hansen, and D. V. Semikoz, "Nonequilibrium corrections to the spectra of massless neutrinos in the early universe," *Nucl. Phys. B*, vol. 503, pp. 426–444, 1997. DOI: 10.1016/S0550-3213(97)00479-3. arXiv: hep-ph/9703315.